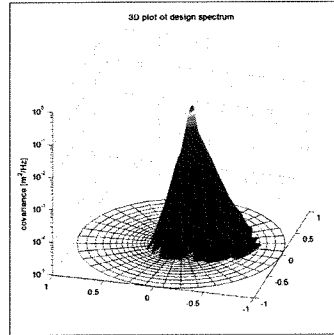
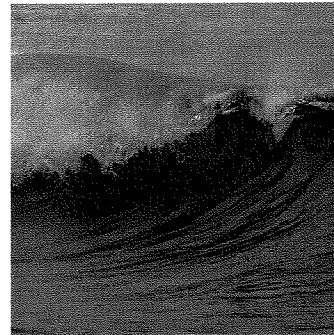
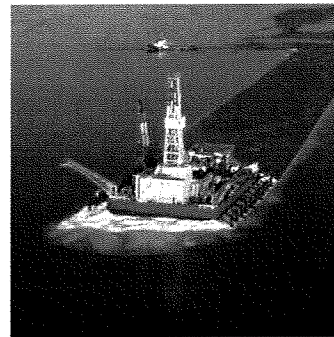
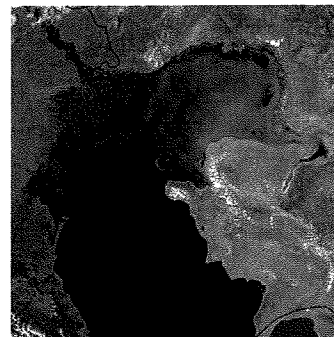


Analysis and modelling of wave spectra on the Caspian Sea

Report

**P.E. Hartgerink, M.Sc. Thesis
9308358**



Analysis and modelling of wave spectra on the Caspian Sea

Report
P.E. Hartgerink, M.Sc. Thesis
9308358

reference	projectcode	status
ZZWI5039/rijm3/001	ZZWI5039	Final Report
project manager	project director	date
S.C. van der Biezen	H.E. Nieboer	January 24, 2005

authorisation	name	initials
approved	A.J. Smale	(A.J.) SB



	P.
INDEX	P.
PREFACE	I
EXECUTIVE SUMMARY	II
SUMMARY	V
LIST OF FIGURES	VI
LIST OF TABLES	VIII
LIST OF SYMBOLS AND ACRONYMS	IX
1 INTRODUCTION	1
1.1 Background	1
1.2 Objectives	2
1.3 Outline	2
2 INVENTORY OF MEASUREMENTS	4
2.1 Introduction	4
2.2 Data requirements and availability	5
2.3 Summary	14
3 CONVERSION OF PRESSURE MEASUREMENTS TO SPECTRAL WAVE DATA	16
3.1 Introduction	16
3.2 Theory	16
3.3 Possible conversion methods	18
3.4 Choice of conversion method	21
3.5 Summary	22
4 ANALYSIS OF THE WAVE DATA	24
4.1 Introduction	24
4.2 Quality of the wave measurements	24
4.3 Characteristics of the wave measurements	25
4.4 Comparison of the spectral shape with theoretical spectra	28
4.5 Summary	30
5 SWAN MODEL DESCRIPTION AND SET-UP	31
5.1 Introduction	31
5.2 Description of SWAN	31
5.3 The base model, by Van Thiel de Vries (2003)	31
5.4 Wind input	32
5.5 Wind-driven surges, water depth and water levels	33
5.6 Numerical issues	37
5.7 Summary	38
6 CALIBRATION AND VALIDATION OF THE SWAN MODEL	40
6.1 Introduction	40
6.2 Calibration method	40
6.3 Calibration process	45
6.4 Validation	54
6.5 Summary	55

7 SENSITIVITY ANALYSIS	56
7.1 Introduction	56
7.2 The design storm and the resulting waves	58
7.3 Sensitivity to choices regarding numerics	65
7.4 Sensitivity to choices regarding physics; one-dimensional analysis	70
7.5 Sensitivity to choices regarding physics; multi-dimensional analysis	76
7.6 The model's performance quantified	80
7.7 Recommended activities to increase the model's performance	81
7.8 Summary	83
8 CONCLUSIONS AND RECOMMENDATIONS	84
8.1 Conclusions	84
8.2 Recommendations	86
REFERENCES	88
last page	90

PREFACE

This report, written as a Master Thesis at the Faculty of Civil Engineering and Geosciences of Delft University of Technology, would not have been completed without the help of all those people who supported me.

Particularly, I would like to thank the people of Witteveen+Bos for giving me the opportunity to work at their office in Rotterdam. It has been great to work in such a stimulating and pleasant atmosphere, surrounded by excellent engineers who really enjoy the work they do together. I owe many thanks to Alfon Smale, who was always there to help and who was full of interesting ideas.

During my study of the conversion of burst pressure measurements to wave spectra, I could not have progressed without the expert advice of Bram Roskam of RIKZ and of Luigi Cavalieri of ISMAR (Venice); many thanks to them.

I also thank Chris Graham of Shell for the interesting discussions and for all his useful comments.

And of course, I want to thank my supervisors at Delft University of Technology: Pieter van Gelder, for helping me with the statistical analyses, and André van der Westhuysen, for sharing his knowledge of wind waves and experience on the use of SWAN. Furthermore I like to thank Guus Stelling and Marcel Stive for their constructive comments on my work.

Finally I would like to thank the NWO for enabling me to participate in the XCASP workshop in Moscow on research regarding the Caspian Sea and the field trip to the Volga Delta area in May 2004 (NWO project number 047.014.015).

Pieter Hartgerink

January 2005

EXECUTIVE SUMMARY

The discovery of great oil reserves located under the northern part of the Caspian Sea has lead to an increased interest in the wave climate in this area. Statistical analysis of wave measurements is insufficient to determine reliable design wave conditions on the northern part of the Caspian Sea, because the amount of available wave measurements is insufficient and the available wave measurements do not contain events with design water levels. Wind and water level statistics, however, are available. Wave statistics can now be obtained by means of a wave generation model.

At Delft University of Technology a wave generation model has been developed, named SWAN (Simulating WAves Nearshore). The model calculates the evolution of wind wave spectra. Test cases are needed in order to obtain an insight in the performance of this model. The northern part of the Caspian Sea could be an interesting test case. Water depths are small (3 to 4 meters at the Kashagan oil fields) and therefore many physical processes influence the wave spectra in this area. The commercial interest in the area has lead to the initiation of measurement campaigns, leading to the availability of wind and spectral wave measurements.

This project therefore serves two main objectives. Firstly, Witteveen+Bos gains insight in the hydraulic boundary conditions on the northern part of the Caspian Sea. Secondly, SWAN in its current state of development is tested thoroughly on an interesting case. This can ultimately contribute to improvements of SWAN itself. Note that many hydraulic engineers follow the developments around SWAN with great interest, as it can be a valuable tool during various projects.

This study is a succession of the MSc project by Van Thiel de Vries (2003). He calibrated SWAN on integral wave parameters, such as H_m0 and T_p . The underlying burst pressure measurements of these wave parameters have now become available.

In this project the model is re-calibrated with the use of spectral wave measurements. Furthermore its performance is studied quantitatively. The following approach was used:

- an inventory was made of the requirements and the availability of measurements;
- the burst pressure measurements were converted to wave spectra;
- the wave spectra were analysed qualitatively; typical events were selected for calibration;
- the SWAN model was setup and re-calibrated;
- the SWAN model's ability to determine the design wave spectrum was tested and quantified.

An analysis of various methods for the conversion of burst pressure measurements to wave spectra showed some interesting results. Much controversy exists around the cut-off frequency of the so-called gain correction factor. This is the multiplying factor, applied to transform pressure variation spectra to sea level elevation spectra. This factor has its origin in linear wave theory. The factor must be cut-off at a certain value in order to prevent the introduction of instrument noise in the wave spectrum. The method, chosen at the end of the study, resulted in an increase in significant wave heights and a decrease in integral wave periods compared to those used by Van Thiel de Vries (2003) (although he used the same raw measurements). Contrary to his conclusions that a default configuration of SWAN overestimates wave heights and underestimates wave periods, SWAN had actually performed rather well. The mismatch proved to be due to an inaccuracy in the conversion of the raw data.

The SWAN model created by Van Thiel de Vries (2003) was used as a basis. For this research the bathymetric map of this model was raised by 70 cm, after a comparison of the map with recent surveys and pressure measurements. The discrepancy was probably caused by an inconsistency in the definition of the reference levels in the old Russian bathymetric maps, on which it was based. The change in the map led to an improved auto-calibration of the Delft3D model, used for the calculation of wind-driven surges.

NCEP wind data proved not to be adequate for calibration of the SWAN model, contrary to what was expected previously (Smale, 2004). This dataset proved to have an insufficient resolution of short time

scale variations necessary to provide detailed wave time series. Only the ADL wind data was sufficiently accurate. Therefore, many of the spectral wave measurements could not be used for the calibration, as no simultaneous wind measurements were available. The NCEP data, however, was useful to prove that the assumption that wind is uniform on the northern part of the Caspian Sea is acceptable. Wind speeds and wind directions on various grid points of the NCEP data on the northern part of the Caspian Sea do not differ much.

The calibration of the model per source term led to the following changes to the base model of Van Thiel de Vries:

- 1 The calibration of the source term for the generation of wave energy by wind led to the decision to use the default Komen et al (1984) expression.
- 2 The bottom friction coefficient cfjon was set to $0.04 \text{ m}^2/\text{s}^3$.
- 3 The calibration for whitecapping and quadruplets had to be performed simultaneously. A default configuration of the DIA is used for the quadruplets. An attempt was made to use the exact XNL method instead (Van Vledder and Bottema, 2003). This, however, was met by model errors. A study of the causes of this erroneous behaviour is beyond the scope of this project. The whitecapping source term gave the best calibration after setting delta to 1 (instead of the default value 0; increasing delta shifted the activity of whitecapping to higher frequencies). Rogers et al (2002) had already shown that this setting can provide good results in many cases. It is however frequently stated that such a setting only compensates the errors generated by the schematisation applied by the DIA method for quadruplets. Physically a value of 1 is incorrect.
- 4 A calibration of breaker parameter gamma proved to be impossible, as the wave measurements did not represent conditions during which the waves were sufficiently depth limited. The default value is therefore applied.
- 5 Triads do not play a role of importance on the northern part of the Caspian Sea.

Two validation runs proved that the model was calibrated satisfactorily.

With the validated model the design spectrum was calculated (design wave parameters are shown in Table 1.1; row *calibrated model*). The SWL during this event was set at CD +2.4 m. A stationary SWAN run was used for this purpose, as conditions during extreme events proved not to be time-dependent (the waves are depth-limited).

The performance of the validated model mainly depends on three factors:

- the quality of the calibration;
- numerical settings;
- the accuracy of physical coefficients and physical input data.

Monte Carlo simulations have been made to study the uncertainty around the model's output (Table 1.1; statistical parameters: *mean*, *standard deviation*, *skewness*, *kurtosis* and *the 95%-reliability interval*) and which of eight random variables contribute most to this uncertainty (Table 1.2; based on the influence factors α_i^2). It appears that gamma, delta and cfjon contribute most to the uncertainty around the model's output.

The following recommendations could therefore be made to improve the SWAN model's accuracy in modelling design spectra on the northern part of the Caspian Sea.

- More spectral wave measurements and wind measurements should be collected. The availability of measurements carried out during more extreme events, would allow a better calibration of the depth-induced wave breaking source term, which could reduce the uncertainty around the model's output significantly.
- Research on the modelling of quadruplets and whitecapping must be a main priority. These source terms cause a significant uncertainty around the model's output. The significant influence of the uncertainty around delta on the uncertainty around the model's output illustrates this.
- The uncertainty around the bottom friction coefficient appeared to have a significant influence on the model's performance. The bottom friction source term, however, in practice is a closing term during the calibration process, which can be tuned with coefficient cfjon. Improvements of the proc-

ess descriptions of the other source terms are needed, before a better estimate can be made of this coefficient by means of a re-calibration.

The percentages in Table 1.2. can also be interpreted as the percentile decrease of the uncertainty around the model output that can be obtained by means of a reduction of uncertainty around the random variables to zero. The contributions of the other random variables to the remaining uncertainty would then keep the same proportions relative to each other.

A linear regression analysis was made with the data resulting from the Monte Carlo analysis to study whether a simplified mathematical linear model can be made for the SWAN model of design conditions on the northern part of the Caspian Sea. This appeared to be feasible. This model showed that the linear wind growth coefficient agrow and quadruplets coefficient cnl4 are of insignificant importance on the value of H_{m0} and that quadruplets coefficient cnl4 has no influence on Q_b (when simulating design waves) (Q_b is the fraction of broken waves).

Table 1.1. Design wave parameters, their 95%-reliability interval and shape parameters of their distributions

	H_{m0} [m]	T_p [s]	T_{m02} [s]	Q_b [-]	L [m]
Calibrated model	2.80	5.46	5.03	1.24e-4	34.39
Revised calibrated model	3.10	5.89	5.42	0.93e-4	38.70
Lower limit 95%-rel.interv.	2.37	4.25	3.58	0.17e-4	18.87
Upper limit 95%-rel.interv.	3.64	6.48	5.92	1.88e-4	44.26
Mean	3.08	5.41	4.83	0.88e-4	32.19
Standard deviation	0.33	0.58	0.62	0.45e-4	6.73
Skewness	-0.37	-0.10	-0.17	+0.53	-0.10
Kurtosis	2.54	2.58	2.49	2.88	2.42

Table 1.2. Contribution of the random variables to the uncertainty around the model's output

Random variables	Coefficient of source term:	Output variables				
		H_{m0}	T_p	T_{m02}	Q_b	L
cds2	Whitecapping	0.3%	6.3%	7.0%	10.3%	7.0%
cfjon	Bottom friction	3.6%	3.8%	1.9%	35.3%	1.9%
cnl4	Quadruplets	0.2%	0.0%	0.2%	0.0%	0.2%
delta	Whitecapping	0.2%	32.7%	49.1%	4.7%	50.2%
bathymetry	Physical input	1.8%	0.8%	0.6%	0.0%	0.9%
gamma	Breaker parameter	91.7%	55.5%	40.3%	49.5%	38.7%
agrow	Wind input (linear)	0.1%	0.0%	0.0%	0.1%	0.0%
surges	Physical input	2.2%	1.1%	0.9%	0.2%	1.2%

During the sensitivity analysis it became clear that the most probable wave spectrum represented higher waves than the wave spectrum as calculated by the calibrated model. This is caused by the fact that the chosen probability distribution for the breaker parameter gamma has a higher expected value than the default value used in SWAN (Smale 2004). On the basis of the available measurements, however, a deviation from the default value of breaker parameter gamma could not be justified. On the basis of the sensitivity analysis it was decided to revise the calibrated model by changing breaker parameter gamma to 0.82.

On the basis of this study the wave parameters, as stated in row *revised calibrated model* in Table 1.1, should be applied for design purposes, keeping in mind the confidence limits, also presented in this table. These values are not equal to the *mean* values (expected values), as the chosen model uses a value for delta of 1, which is not its expected value (mean of uniform distribution from 0 to 1).

SUMMARY

The discovery of great oil reserves located under the northern part of the Caspian Sea has lead to an increased interest in the wave climate in this area. Statistical analysis of wave measurements is insufficient to determine reliable design wave conditions on the northern part of the Caspian Sea, because the amount of available wave measurements is insufficient and the available wave measurements do not contain events with design water levels. Wind and water level statistics, however, are available. Wave statistics can now be obtained by means of a wave generation model.

At Delft University of Technology a wave generation model has been developed, named SWAN (Simulating WAves Nearshore). The model calculates the evolution of wind wave spectra. Test cases are needed in order to obtain an insight in the performance of this model. The northern part of the Caspian Sea could be an interesting test case. Water depths are small (3 to 4 meters at the Kashagan oil fields) and therefore many physical processes influence the wave spectra in this area. The commercial interest in the area has lead to the initiation of measurement campaigns, leading to the availability of wind and spectral wave measurements.

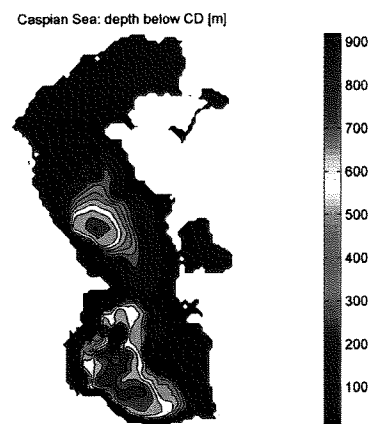
This project therefore serves two main objectives. Firstly, Witteveen+Bos gains insight in the hydraulic boundary conditions on the northern part of the Caspian Sea. Secondly, SWAN in its current state of development is tested thoroughly on an interesting case. This can ultimately contribute to improvements of SWAN itself. Note that many hydraulic engineers follow the developments around SWAN with great interest, as it can be a valuable tool during various projects.

Burst pressure measurements carried out at the project sites were converted to wave spectra. The model consisted of the complete Caspian Sea and was calibrated on these measured wave spectra. The spatially defined surge input for the SWAN model was calculated with a Delft3D model. The calibration of the SWAN model of the Caspian Sea was performed per source term.

The calibrated SWAN model was used to calculate the wave spectrum, which occurs during design conditions. A sensitivity analysis was performed to study the influence of the various uncertainties (caused by either numerics or physics) on the confidence limits of the model's output. Therefore some physical parameters were defined as random variables, described by probability density functions. With the use of an extensive Monte Carlo analysis (2000 model runs), the sensitivities were calculated.

The two main objectives of the study were met:

- the design spectrum was calculated and the confidence bounds around it were defined;
- insight was gained into the performance of SWAN in its current state of development.



LIST OF FIGURES

Figure 1.1. The Caspian Sea.....	1
Figure 2.1. Northern part of the Caspian Sea. Deployment locations of measuring instruments.....	4
Figure 2.2. Flow chart of the modelling process, illustrating the data requirements	5
Figure 2.3. Water level variations caused by wind-driven surges and its spectrum.....	6
Figure 2.4. Variations of H_{m0} (from integral wave dataset of ADL) and its spectrum	7
Figure 2.5. Comparison of NCEP and ADL wind (NCEP shifted to local time)	9
Figure 2.6. Comparison of KazAviaMet and ADL wind.....	10
Figure 2.7. Long term sea level variations (annual sea level related to Baltic Datum).....	11
Figure 2.8. Monthly mean water levels 1995-2002	11
Figure 2.9. Bathymetry of the Caspian Sea.....	13
Figure 2.10. Minimal measurable pressure variation visualised	14
Figure 3.1. Tapering function.....	17
Figure 3.2. H_{m0} of integrated ADL data compared with H_{m0} of ADL method.....	20
Figure 3.3. K_p for ADL method.....	20
Figure 3.4. H_{m0} of integrated ADL data compared with H_{m0} of RIKZ method.....	20
Figure 3.5. K_p for RIKZ method	20
Figure 3.6. Double peaked spectrum obtained through Cavalieri method.....	22
Figure 3.7. H_{m0} integrated ADL data compared with H_{m0} of chosen method	22
Figure 4.1. Increasing registered depth at E.....	24
Figure 4.2. Spectrum at E3.....	24
Figure 4.3. Filtering of ice dates	25
Figure 4.4. Minimum wave period.....	26
Figure 4.5. Histogram of d/L_{op}	26
Figure 4.6. Wave ages in deployment C3.....	27
Figure 4.7. Spectrum with large wave age and H_{m0}	27
Figure 4.8. Relative wave height against dimensionless depth	27
Figure 4.9. Spectral moments of measurements compared with JONSWAP (black) and TMA (red)	29
Figure 4.10. Measured spectrum compared with JONSWAP and TMA	29
Figure 5.1. H_{m0} simulated (with NCEP wind) and measured	33
Figure 5.2. H_{m0} simulated (with ADL wind) and measured	33
Figure 5.3. Wind speed (NCEP) and measured H_{m0}	33
Figure 5.4. Wind speed (ADL) and measured H_{m0}	33
Figure 5.5. Wind speed (NCEP) and simulated H_{m0}	33
Figure 5.6. Wind speed (ADL) and simulated H_{m0}	33
Figure 5.7. Comparison measured water levels and calculated water levels (Delft3D)	34
Figure 5.8. Comparison depths SWAN and ADL in C3	35
Figure 5.9. Comparison of depths from various sources	36
Figure 5.10. Depths after change in bathymetric map	36
Figure 5.11. No convergence in solver causing minimum H_{m0} (Van Thiel de Vries, 2003)	37
Figure 5.12. Convergence behaviour	38
Figure 6.1. Comparison calculations with and without friction for "deep" water conditions	41
Figure 6.2. Conflicting definitions of the spectral tail.....	43
Figure 7.1. Occurrence of wind speed exceedance; extrapolation was made using this graph.....	59
Figure 7.2. Wind speed during the design storm	59
Figure 7.3. Wind speeds and the resulting surges at Kashagan East during a design storm from WSW	60
Figure 7.4 H_{m0} , wind speed, depth and H_{m0}/d during design storm from WSW	61
Figure 7.5. Revised Bretschneider curve for Kashagan East	62
Figure 7.6. H_{m0} and H_{m0}/d during a linearly increasing storm (5-50 m/s)	63
Figure 7.7. Surges during design storm, at the moment when the maximum wave height occurs	64
Figure 7.8. The design wave spectrum	64
Figure 7.9. H_{m0} using Janssen with strict criteria, compared with H_{m0} of calibration run Som 002	66
Figure 7.10. H_{m0} , T_p , T_{m02} , Q_b and L as function of computational grid spacing; storm from N.....	67

Figure 7.11. H_{m0} , T_p , T_{m02} , Q_b and L as function of computational grid spacing; storm from WSW	68
Figure 7.12. Comparison of SWAN output of runs with time steps 15 minutes and 3 hours.....	68
Figure 7.13. Probability density functions of the stochastically defined physical parameters	72
Figure 7.14. Linearity of the model's output as a function of the stochastically defined physical parameters visualised using the results of the one-dimensional Monte Carlo analysis	75
Figure 7.15. Result of multi-dimensional Monte Carlo Simulation	77
Figure 7.16. The design spectrum, revised.....	78
Figure 7.17. Relative integral values of the various source terms during design conditions.....	78
Figure 7.18. Relative contribution of physical coefficients/variables on the model's error margin	82

Copyrights:

Photo of the Kashagan field on the cover of this report: *Photo courtesy of ConocoPhillips*
 Satellite image of the Caspian Sea on the cover and in Figure 1.1: *Photo courtesy of NASA*

LIST OF TABLES

Table 1.1. Design wave parameters, their 95%-reliability interval and shape parameters of their distributions	IV
Table 1.2. Contribution of the random variables to the uncertainty around the model's output	IV
Table 2.1. Deployment periods of pressure transducers	14
Table 5.1. Availability of wind and wave data	32
Table 5.2. Overview of plots made to compare the performance of a model using NCEP wind and ADL wind	32
Table 6.1. Calibration scheme	45
Table 6.2. bias and RMSE; calibration of S_{wind} (best results are highlighted)	47
Table 6.3. bias and RMSE; calibration of S_{fric} (best results for m_0 are highlighted)	48
Table 6.4. bias and RMSE; calibration of S_{nl4} and S_{wcap} for the deep water time series	51
Table 6.5. bias and RMSE; calibration of S_{nl4} and S_{wcap} for the shallow water time series	51
Table 6.6. bias and RMSE; calibration of S_{surf} (best results are highlighted)	53
Table 6.7. bias and RMSE; final calibration run compared with validation run	55
Table 7.1. Duration per year of continuous wind speed exceedance during at least a certain time.....	58
Table 7.2. Duration of continuous exceedance with an occurrence of once every 10 years (result of extrapolation).....	59
Table 7.3. bias and RMSE; S_{nl4} and S_{wcap} calibration with stricter convergence criteria.....	66
Table 7.4. Ratio of σ/μ of the output parameters to σ/μ of the input parameters	74
Table 7.5. Influence factors α_i resulting from multi-dimensional Monte Carlo simulation.....	76
Table 7.6. Design wave parameters, their 95%-reliability interval and shape parameters of their distributions	80
Table 7.7. Contribution of the random variables to the uncertainty around the model's output	81
Table 8.1. The design wave parameters and their statistical characteristics, resulting from the sensitivity analysis	85
Table 8.2. Relative contributions of the most important physical input variables on the model's output	85

LIST OF SYMBOLS AND ACRONYMS

Roman letters

agrow	wind input coefficient (linear growth term) in SWAN	[-]
cds2	whitecapping coefficient in SWAN	[-]
cfjon	bottom friction coefficient c_f of the JONSWAP model in SWAN	[m ² /s ³]
c_{ph}	phase speed	[m/s]
cnl4	quadruplets coefficient in the DIA in SWAN	[-]
d	depth	[m below CD]
delta	whitecapping coefficient in SWAN	[-]
f	wave frequency	[Hz]
g	gravitational acceleration (9.81 m/s ²)	[m/s ²]
gamma	breaker parameter in SWAN	[-]
E	variance density spectrum	[m ² /Hz]
E_{tot}	total variance	[m ²]
H _{max}	maximum possible wave height	[m]
H _{m0}	significant wave height defined as $4 m_0^{1/2}$	[m]
H _s	significant wave height defined as mean of 1/3 highest waves	[m]
k	wave number	[m ⁻¹]
K _p	gain correction factor	[-]
m_0	zeroth moment of spectrum = E_{tot}	[m ²]
m_n	n th moment of spectrum	[m ² /s ⁻ⁿ]
m_{-n}	n th negative moment of spectrum	[m ² /s ⁿ]
p_z	pressure at height z above the sea bed	[m]
Q _b	fraction of broken waves	[-]
S _{wind}	wind source term	[m ² /Hz/s]
S _{wcap}	whitecapping source term	[m ² /Hz/s]
S _{fric}	bottom friction source term	[m ² /Hz/s]
S _{surf}	depth induced wave breaking source term	[m ² /Hz/s]
S _{nl4}	quadruplet (four wave) interactions source term	[m ² /Hz/s]
S _{nl3}	triads (three wave) interactions source term	[m ² /Hz/s]
T _{m-10}	period corresponding to mean frequency of the spectrum, m_{-1}/m_0	[s]
T _{m01}	period corresponding to mean frequency of the spectrum, m_0/m_1	[s]
T _{m02}	period corresponding to mean frequency of the spectrum, $(m_0/m_2)^{0.5}$	[s]
T _p	peak wave period	[s]
Ur	Ursell's number	[-]
u·	friction velocity	[m/s]
U ₁₀	wind speed at 10 meters height	[m/s]

Greek letters

γ	breaker parameter	[-]
η	sea level elevation	[m]
ω	radial wave frequency (= $2 \pi f$)	[Hz]

Acronyms

ADL	Arthur D. Little
AgipKCO	Agip Kazakhstan North Caspian Operating Company
CD	Caspian Datum
NCEP	National Centers for Environmental Prediction
OKIOC	Offshore Kazakhstan International Operating Company (now AGIP KCO)
ORL	OKIOC Reference Level
RIKZ	RijksInstituut voor Kust en Zee
SWL	Still Water Level
SWAN	Simulating WAves Nearshore

1 INTRODUCTION

1.1 Background

After the discovery of great oil reserves under the northern part of the Caspian Sea (Figure 1.1), a consortium of oil companies has created a strategy for the exploitation of these reserves. This consortium awarded the Dutch civil engineering consultant Witteveen+Bos contracts for the design of several hydraulic structures, such as breakwaters and artificial islands. The design of these structures requires insight in the hydraulic boundary conditions. Statistical analysis of wave measurements is insufficient to determine reliable design wave conditions on the northern part of the Caspian Sea, because the amount of available wave measurements is insufficient and the available wave measurements do not contain events with design water levels. Wind and water level statistics, however, are available. Wave statistics can now be obtained by means of a wave generation model. A powerful and state-of-the-art tool to perform these calculations is SWAN (Simulating WAves Nearshore) (Booij et al, 1999), developed at Delft University of Technology.

SWAN is a spectral wave model that calculates the evolution of wave spectra by means of source terms. These source terms describe the relevant physical processes that influence these wave spectra. Many researchers are currently working on improvements of SWAN, as in particular the non-linear source terms (quadruplets and triads) cause significant uncertainty in the computed wave conditions. Test cases are needed, to test the reliability and accuracy of new versions of SWAN. Cases with shallow water depth, where simultaneous wind, water level and wave measurements are available, are scarce but of special interest (in deep water areas many source terms, such as bottom friction, are inactive and cannot be tested). The northern part of the Caspian Sea has a large shallow area (depths are about 4 meters). Measuring campaigns have been initiated since the discovery of the oil reserves, making the northern part of the Caspian Sea an interesting test case.

MSc student Jaap van Thiel de Vries graduated in December 2003 on an MSc thesis, written at and for Witteveen+Bos, titled "Wave fields in transitional water depths", subtitled "A study of wave spectra and wave height distributions in the North Caspian Sea" (van Thiel de Vries, 2003). He calibrated and validated a SWAN model of the Caspian Sea. He hindcasted the 100 most severe storms over the period 1948 to 2000. The results of these hindcasts enabled him to verify the design conditions as applied by Witteveen+Bos.

The two main reasons for a review of the SWAN model of the Caspian Sea, as created by Van Thiel de Vries, are:

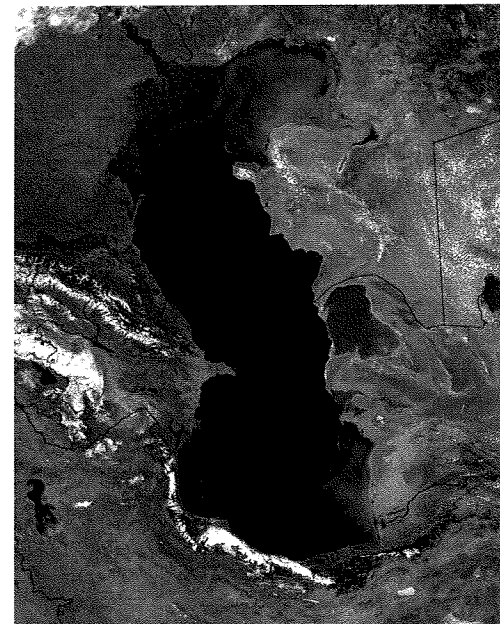
1. Spectral wave data has become available.
2. New process descriptions have been implemented in SWAN.

add 1

- Witteveen+Bos has recently obtained permission to use the complete datasets of burst pressure measurements, on which the integral wave parameters Van Thiel de Vries used were based.
- A great part of the Arthur D. Little wave database could not be used during Van Thiel de Vries' project, as no simultaneous local wind measurements were available. Subsequently a brief desk study performed by Witteveen+Bos (Smale, 2004) showed that wind data obtained from NCEP/NCAR may have sufficient accuracy for this purpose. This potentially means that wind data anywhere on

Figure 1.1. The Caspian Sea

(from: <http://www.parstimes.com/caspian/>)



the Caspian Sea now is available, making wave measurements obtained anywhere on the Caspian Sea usable.

- More wave measurements are expected to become available during this project. This dataset may contain measurements of more extreme conditions.

add 2

- New formulations for wind (Yan, 1987) and whitecapping (Cumulative Steepness Method; Hurdle and Van Vledder, 2004) have been implemented in SWAN since Van Thiel de Vries' study (2003) (SWAN 40.31ABCDEFG). The FD-RIAM-formulation (Hashimoto, 2003) and XNL-method for quadruplets have also been implemented. These two methods yield the complete solution of the Boltzmann integral for non-linear quadruplet interactions (referred to as exact methods), but are time-consuming.
- More research on the deep water source terms (wind, whitecapping and quadruplets) is being carried out by A.J. van der Westhuysen.

1.2 Objectives

This project serves two main interests. Witteveen+Bos has a commercial interest. The SWAN model that will result from this study can be used to calculate the design wave conditions on the northern part of the Caspian Sea. These can be used to verify the design conditions as applied by Witteveen+Bos. Delft University of Technology has a scientific interest in the project. SWAN in its current state of development will be tested on an interesting case. This study can show where SWAN still needs improvement.

The objectives of this project therefore are:

- to increase the understanding of the shape and the evolution of wave spectra in the shallow waters of the northern part of the Caspian Sea;
- to increase the performance of the Caspian Sea SWAN model by means of a re-calibration;
- to quantify the reliability of wave predictions made by SWAN, if possible per responsible source term;
- to re-determine the design conditions, by simulating extreme events, including a quantification of the accuracy of this prediction.

1.3 Outline

Section 2 of this report describes the need and availability of data for this study. Measurements of wind, water levels, bathymetry and waves are needed. The demands on the quality of these measurements are described, depending of course on the purpose for which the measurements will be used. The available measurements are described. It is stated which available measurements comply with the qualitative demands and therefore can be usable during the project.

Spectral wave data appears to be available in the form of burst pressure measurements. The conversion of these burst pressure measurements to variance density spectra of sea level elevations is described in Section 3. Most attention is given to the determination of the so-called gain correction factor. This is the multiplying factor, applied to transform pressure variation spectra to sea level elevation spectra.

In Section 4 the wave spectra, resulting from the conversion, are analysed. A quality check is performed. Some characteristics of the spectra are studied. And the spectra are compared with wave spectra, as they are described in theory.

Section 5 describes how the SWAN model of the Caspian Sea is set-up. The model, created by Van Thiel de Vries served as a base model. A final decision is made on which wind data can be used. Some changes are made regarding the bathymetric map.

The procedure and results of the calibration and validation of the model are presented in Section 6.

In Section 7 the model's ability to calculate the design conditions is studied. First a design spectrum is calculated with the validated model. Then the reliability of this wave prediction is quantitatively described. The various sources of uncertainty are studied and their relative importance quantified.

2 INVENTORY OF MEASUREMENTS

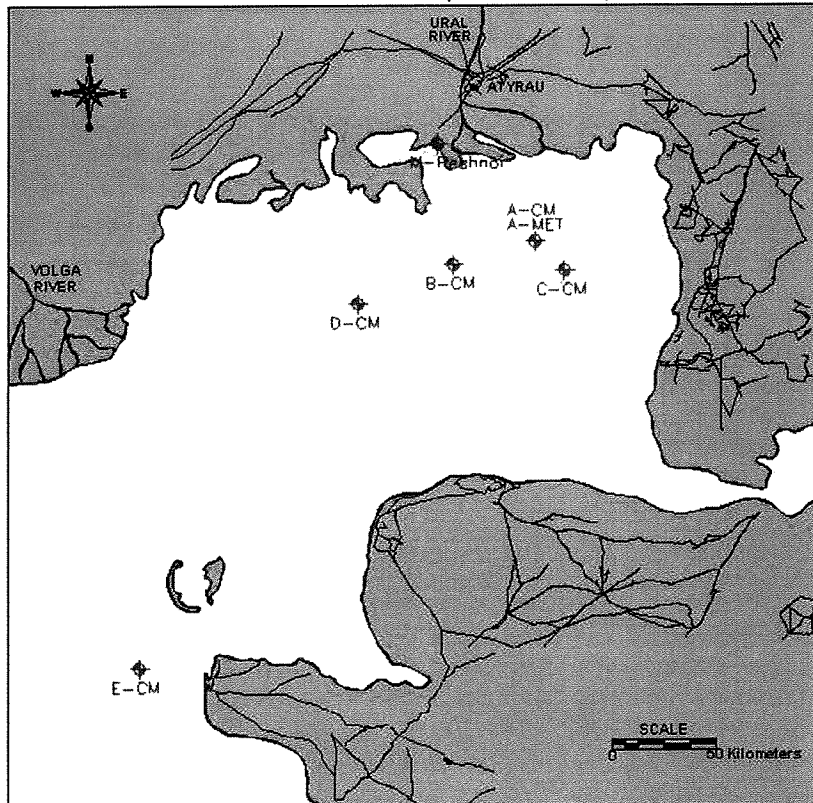
2.1 Introduction

Measurements are needed to setup, calibrate and validate the SWAN model of the Caspian Sea. Such measurements of wind, water levels and wave spectra have recently become available. These measurements have to be used with great caution, because errors can be induced through an incorrect usage of the measuring instruments or a false interpretation of the results.

The SWAN model that was setup in this project covers the entire Caspian Sea. The advantage is that no boundary conditions have to be defined, because the Caspian Sea is enclosed by land boundaries. These boundaries are not very well fixed, due to regular coastal flooding and sea level variations. The movement of the boundaries is however not deemed to have an impact on the evolution of wave spectra in the area of interest (more in Section 5.5). The area of interest is located in the northern part of the Caspian Sea, where Witteveen+Bos requires wave conditions. The map in Figure 2.1 shows the northern part of the Caspian Sea. In this map the measuring locations of the Arthur D. Little measuring campaign are shown. The Kashagan oil fields are located near A-CM and C-CM. The SWAN model was calibrated with these measurements in order to be able to simulate wave spectra at these locations as accurately as possible.

A model is often a simplification of reality. A difference will then exist between the model's output (in this case computed wave spectra) and the behaviour of the system in practice. Some models need calibration and validation based on measurements. The performance of the validated model does not only depend on the model itself, but also on the quality of the measurements used for calibration and validation. A quantification of the performance of the constructed model requires insight into the quality of the measurements. The flow chart in Figure 2.2 gives insight in the data requirements for this study.

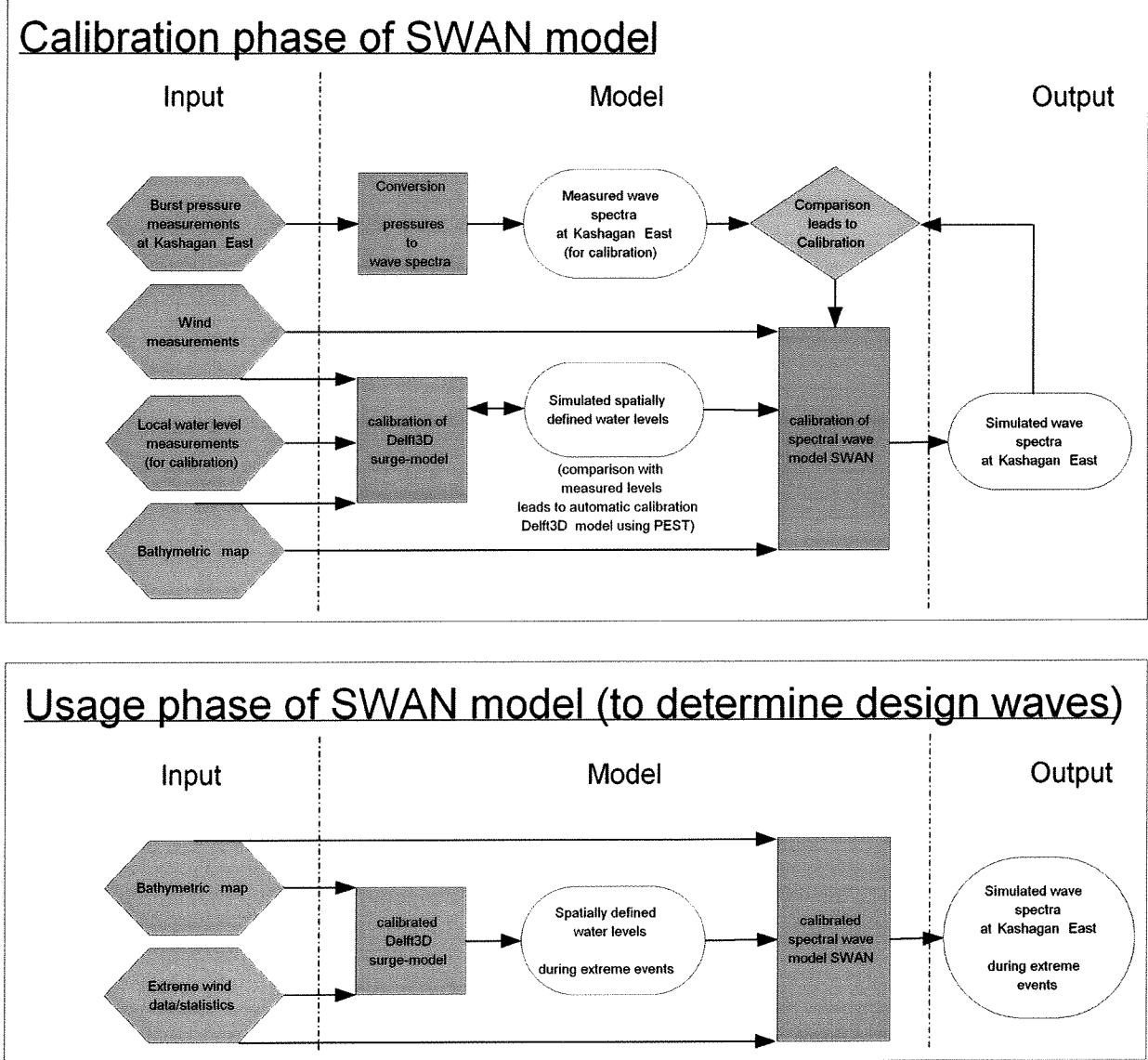
Figure 2.1. Northern part of the Caspian Sea. Deployment locations of measuring instruments
extracted from the MetOcean Data representation (Arthur D. Little, 1999)



2.2 Data requirements and availability

The construction of a SWAN model of the northern part of the Caspian Sea, calibrated for the northern part of the Caspian Sea, requires various types of measurements. The required quality of the measurements depends on the purpose the measurements (Figure 2.2). A description of the required quantity and quality of measurements is presented in this Section.

Figure 2.2. Flow chart of the modelling process, illustrating the data requirements



2.2.1 Wind data

requirements

Wind data is needed for:

1. Calculation of the wind-driven surges

Wind-driven surges play a significant role in the Caspian Sea. The water levels can change as much as 1 meter within days (Figure 2.3), while the water depth in the area is on average about

3.5 meters. The wind-driven surges have a significant influence on the evolution of wave spectra on the northern part of the Caspian Sea, because of:

- the short time frame in which these water level changes take place
- the relatively small area in space in which these water level variations are concentrated
- the size of these water level changes relative to the absolute depth

A Delft3D model was created and calibrated to calculate the surge levels. Therefore simultaneous wind and water level measurements were necessary.

The quality of wind measurements mainly depends on three factors:

1 The reliability of the measuring device

Measuring devices for wind are often mechanical (swinging plates) and therefore easily susceptible to damage, reducing the reliability of the measurements. Measurements therefore need to be used with great caution.

2 The spatial resolution

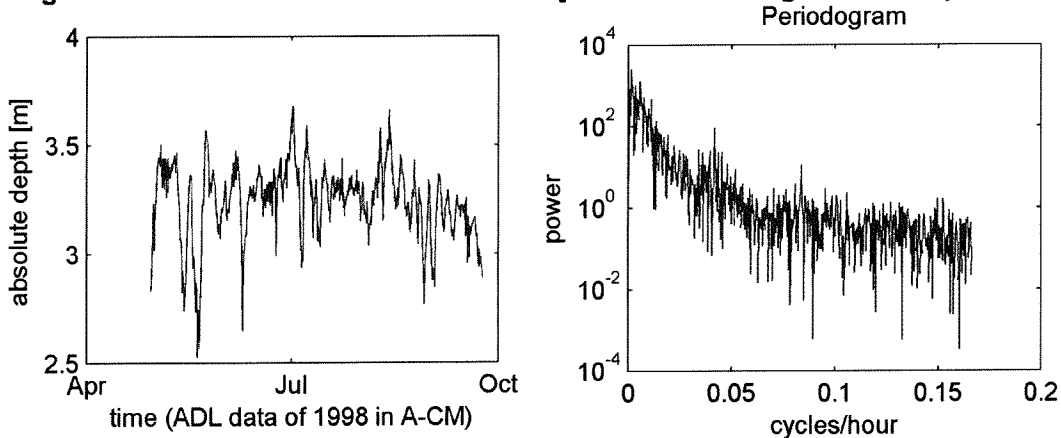
The required spatial resolution depends on the non-uniformity of wind speeds and directions on the Caspian Sea. The wind field can be modelled as spatially uniform, if wind speeds and wind directions do not vary much over the North of the Caspian Sea. In Appendix II it is proven that wind speeds and directions of the NCEP database on the northern part of the Caspian Sea can be schematised as uniform. The wind speeds and directions at various grid points of the NCEP database on the northern part of the Caspian Sea were compared. The differences are relatively small. Therefore, it can be stated that at least wind measurements near the area of interest are required for the modelling of wind driven surges.

3 The sampling interval

The sampling interval should be several times the timescale of the process to be modelled. A spectrum was calculated of the wind-driven surges to determine which sampling frequency is necessary to cover all significant variations. From this spectrum (Figure 2.3) it can be noticed that very little energy is present at frequencies greater than 0.1 cycles per hour. A sampling interval of wind speeds and directions smaller than 10 hours would therefore give sufficiently reliable results for the water level calculations.

An inaccuracy of water level input to SWAN of a few centimetres is not expected to influence the calculation of the evolution of wave spectra significantly as long as depth induced breaking is not significant.

Figure 2.3. Water level variations caused by wind-driven surges and its spectrum



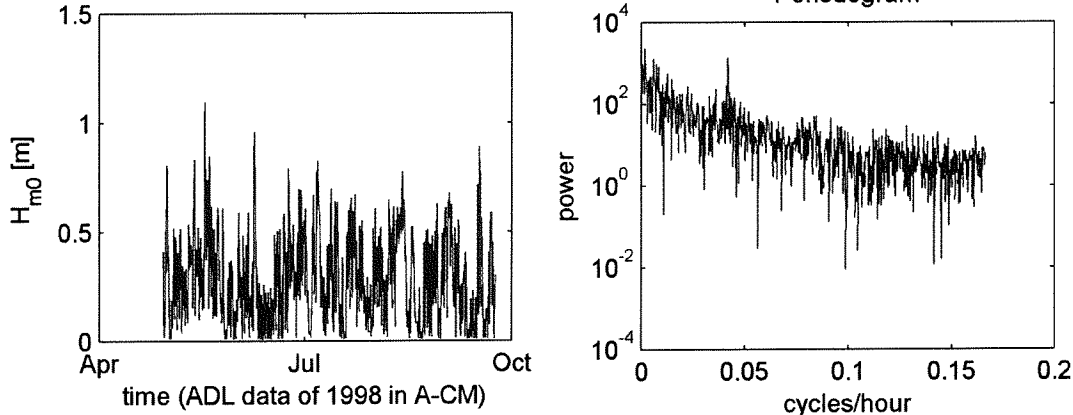
2. SWAN calibration and validation

SWAN requires an input wind speed, wind direction and the corresponding water levels (surges) and produces wave spectra. During the calibration phase a comparison of calculated spectra and measured spectra is made in order to calibrate SWAN. Inaccurate wind input data will result in an inaccurate calibration of the model.

Due to the shallowness of the northern part of the Caspian Sea, waves are not expected to propagate very far and are therefore not very much influenced by non-local wind speeds and directions. In addition, it was proven in Appendix IV that wind fields on the northern part of the Caspian Sea are relatively uniform. As a result it can be stated that measurements of wind speeds and directions near the project sites are needed. These can then be applied uniformly on the northern part of the Caspian Sea.

The reaction of wave spectra to variations in wind speed and direction is much faster than the reaction of wind-driven surges (Figure 2.4). A spectrum of the variations of H_{m0} is presented (from the same dataset as Figure 2.3). Much more energy can still be found at the higher frequencies than in Figure 2.3. The dataset of H_{m0} had a sampling interval of 3 hours. Therefore the highest frequency visible in the spectrum is 1/6 cycles per hour. A sampling interval of wind measurements smaller than 3 hours is required in order to also correctly simulate these high (and higher) frequency components. A peak can be observed at approximately 0.04 cycles per hour. A physical explanation for this peak could not be found.

Figure 2.4. Variations of H_{m0} (from integral wave dataset of ADL) and its spectrum Periodogram



3. SWAN simulations of extreme events

The calibrated model can be used to simulate extreme events. Wind inputfiles, describing these extreme storms, can be used as input to the SWAN model. The resulting wave spectra will be calculated.

During the calibration phase it is important that the high frequency components of the wave height variations are hindcasted accurately in order to make a comparison with the measured waves. During the simulation of design conditions these high frequency components are less important. Witteveen+Bos is not that much interested in the exact variations of the wave spectra within the extreme event. They are much more interested in the long term statistics of the wave spectra and the extremes that occur within the extreme events, as they are needed for design purposes. Furthermore the waves during design conditions are expected to be depth-limited and therefore time-independent. At least accurate wind statistics are needed.

availability

There are three relevant sources of wind data (wind speeds were defined at 10 meters above the surface (U_{10})):

1. Arthur D. Little (referred to as ADL)

This dataset is the most accurate dataset available. Wind was measured at location A-MET and Peshnoi (Figure 2.1). The sampling interval of this dataset is 20 minutes. In Appendix I an overview is given of the ADL measuring campaign, including information on the types of instruments, locations and deployment periods. A disadvantage of this dataset is that the period during which measurements were taken is relatively short. Only between 10/10/1997 and 30/10/1997 (A-MET), between 11/11/1997 and 23/04/1998 (Peshnoi) and between 29/04/1998 and 17/06/1998 (A-MET) measurements were carried out. The second subset is not sufficiently accurate, as it was taken on land (at Peshnoi) and relatively far from the area of interest. Furthermore the measuring instrument at Peshnoi may have been subject to sheltering from various directions.

2. NCEP database

In the NCEP Reanalysis Project a state-of-the-art data assimilation model was used to hindcast wind speeds and directions on a global scale, using various sources of measurements. This resulted in a database of one-hourly averaged wind speeds and directions, covering a period from 1948 to present, with a spatial interval of approximately 2.0° by 2.0° and with a time interval of 6 hours. One must pay attention to the fact that the time domain in the NCEP database is stated in GMT (local time at the project site is GMT +5 hours).

A great advantage of this dataset is that it contains wind speeds of a much longer period in time than the ADL dataset. A disadvantage is the fact that the sampling interval is 6 hours, which is much greater than the sampling interval of 20 minutes of the ADL winds.

Witteveen+Bos states in an internal Technical Note (Smale 2004) that the NCEP wind data can be used for feasibility studies and conceptual designs (Smale, 2004). For detailed designs, a verification of the NCEP data with actual measurements is recommended. Although the correlation with simultaneous measurements is not very high, the probability density function is rather accurate.

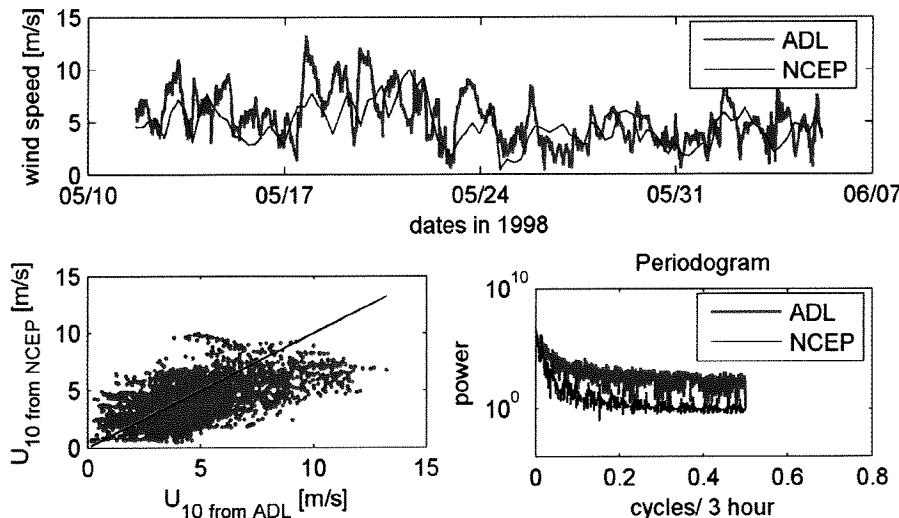
For the SWAN simulations of extreme events, the NCEP database will probably be accurate enough, as the probability density function is fairly accurate (Smale, 2004). For the Caspian Sea data, this is visualised with the scatter diagram in Figure 2.5. The spreading is rather great (RMSE = 0.0348), and R^2 has a value 0.326, which is a measure for how well a linear trendline can be applied. The question whether the dataset contains events that are sufficiently extreme is more important.

It is much more difficult to determine whether the database will be sufficiently accurate for calibration and validation of the SWAN model. It can be seen that the trend is described quite well by the NCEP database, when comparing the wind speeds of ADL and NCEP (Figure 2.5). However, not every individual peak found in the ADL dataset can be observed in the NCEP database. The periodogram shows that the NCEP dataset contains less energy at the higher frequencies than the ADL dataset. This is partly caused by the fact that the sampling interval of the NCEP dataset is 6 hours, compared to 3 hours in the ADL dataset. An attempt will be made to apply NCEP winds for calibration in Section 5. If the accuracy turns out to be insufficient, the ADL winds have to be used. This however would imply that part of the wave measurements will have to be rejected for calibration, as no simultaneous wind measurements of sufficient quality would then exist (see Table 2.1).

For the calculation of wind-driven surges with the Delft3D model the NCEP wind dataset is considered to be sufficiently accurate for the purpose. The sampling interval of 6 hours is sufficiently small relative to the time scale of the surges.

The fact that the trend is described rather well by the NCEP wind dataset (Figure 2.5) increased confidence that the NCEP wind dataset may be used to prove that wind speeds and direction can be schematised as uniform on the northern part of the Caspian Sea (Appendix II). Later during this project (in Section 5) good results were obtained when simulating wind-driven surges with Delft3D and wave spectra with SWAN using spatially uniform wind speeds. This also suggested that the assumption of uniformity had been acceptable.

Figure 2.5. Comparison of NCEP and ADL wind (NCEP shifted to local time)



3. KazAviaMet

The third source of wind data is the KazAviaMet database, consisting of measurements taken at the airport of Atyrau, north of the Kashagan oil fields. The distance between this measuring location and the point of interest may be too great. Furthermore these measurements were taken on land. It can be seen that the correlation is smaller than between the ADL and the NCEP data (Figure 2.6). The spreading around the centreline is greater ($RMSE = 0.0443$) and R^2 of a linear trendline is smaller ($R^2 = 0.091$). It was decided not to use the KazAviaMet data, although it better describes the higher frequency wind speed variations than the NCEP database. The sudden dip in energy at approximately 0.33 cycles per 3 hours could not be explained.

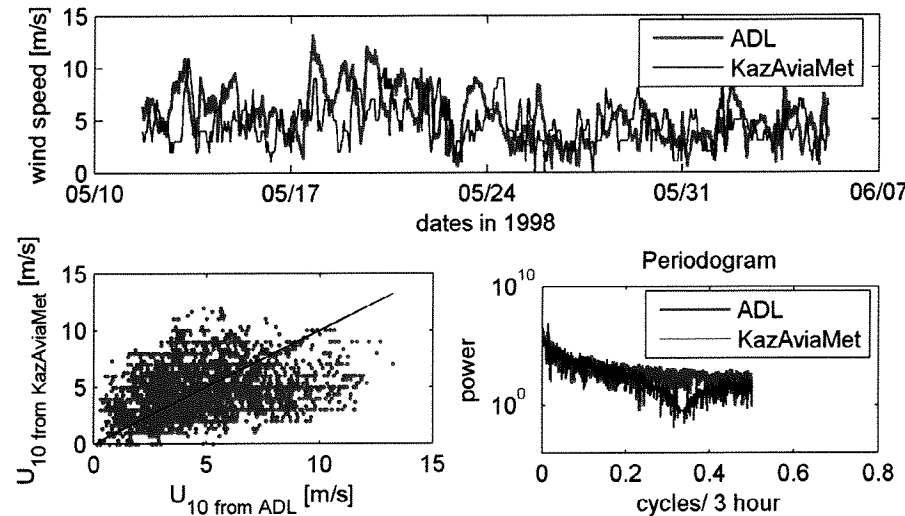
conclusions

For the calculation of wind-driven surges, both the NCEP and ADL wind data are sufficiently accurate.

The calibration and validation of the SWAN model require a higher quality level. Although it is doubted whether the NCEP data is sufficiently accurate, an attempt will be made to use the wind speeds for this purpose in Section 5. The ADL wind must be applied, if the results are not satisfactory. This however would imply that part of the wave measurements will have to be rejected for calibration, as no simultaneous wind measurements of sufficient quality would then exist (Table 2.1).

For the purpose of simulation of extreme events the ADL wind data is too small to contain sufficiently extreme events. The NCEP data may prove to be usable for this purpose.

Figure 2.6. Comparison of KazAviaMet and ADL wind



2.2.2 Water level data

requirements

Spatially defined water level input is necessary for the SWAN model of the Caspian Sea, as water levels vary significantly (Figure 2.3), both in time and in space.

Water level data is required for:

- 1 The calculation of wind-driven surges

As stated in Section 2.2.1, a Delft3D model is created to calculate the spatial and time dependent variations of water level variations caused by wind-driven surges. This Delft3D model needs calibration on measurements of water level variations. A best fit of the measured water levels with the water levels calculated by Delft3D will be made.

- 2 The determination of water levels during future extreme events

Statistical information is needed on both wind and water levels in order to determine a design value of wave heights and wave periods.

availability

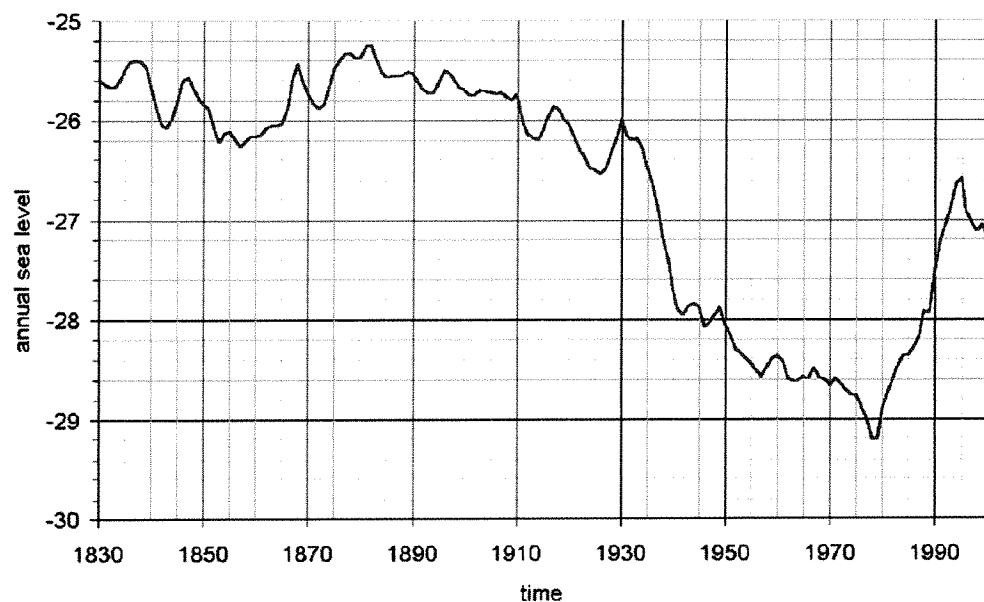
The variations in water level on the Caspian Sea have various causes:

- 1 Long term variations

The annual water level of the Caspian Sea has varied enormously in the past. This is illustrated by Figure 2.7. Expected long term water level changes must be taken into account, when using SWAN to predict wave spectra during future extreme events. Many researchers have attempted to stochastically describe the expected future sea level changes (Probabilitas, 2002).

Van Thiel de Vries (2003) simulated extreme events for five different water levels, in order to provide Witteveen+Bos with an insight into the correlation between these water levels and the spectra. How these long term variations will be dealt with in this project, is described in Section 7.

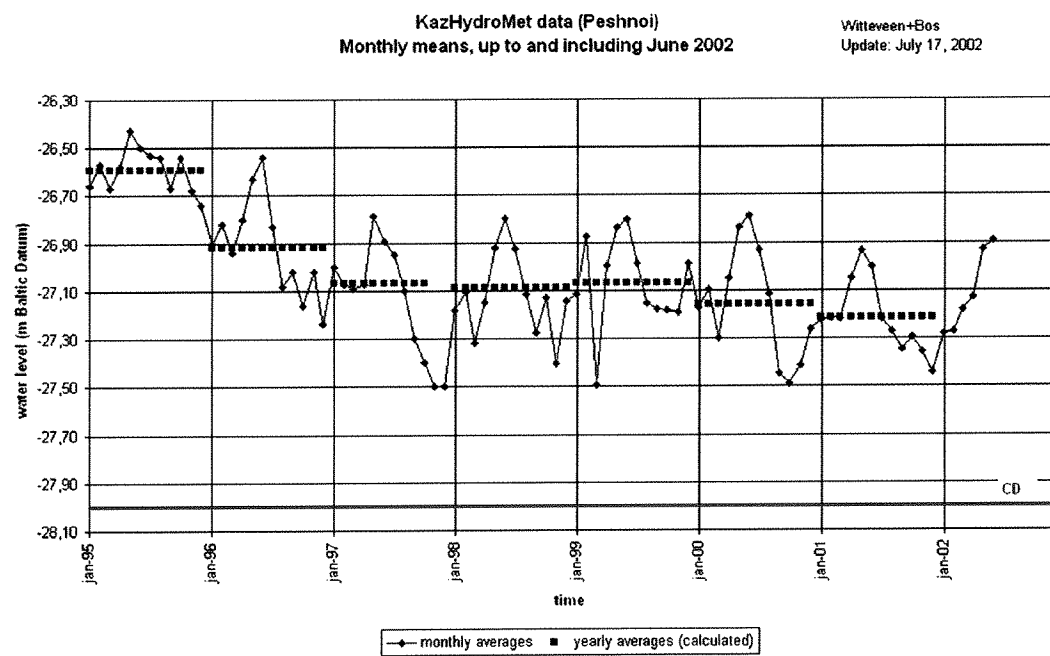
Figure 2.7. Long term sea level variations (annual sea level related to Baltic Datum)



2 Seasonal variations

The seasonal variations in water level on the Caspian Sea are significant, as can be seen in Figure 2.8. This figure is based on the KazHydroMet dataset, which contains water level measurements from 1977 to present, carried out at Peshnoi. The monthly means can be interpreted as the SWL in that month. It is seen that water levels are higher during the summer months than during winter months.

Figure 2.8. Monthly mean water levels 1995-2002



3 Tidal variations

Tide does not play a significant role, because the Caspian Sea is enclosed by land boundaries. The tidal difference is approximately 10 centimetres.

4 Wind driven surges

In Section 2.2.1 it was stated that wind-driven surges play a significant role on the Caspian Sea. Water level measurements are available in the ADL dataset. The pressure measurements used to measure wave heights (Section 2.2.4) can also be used as water level variation measurements. A dataset of three-hourly averaged absolute depths is obtained, by adding the distance between the seabed and the measuring device to the average of the pressures of every burst (17 minutes of 2 Hz measurements, carried out with an interval of 3 hours). The variations around the monthly mean value of these depths can be interpreted as water level variations around SWL.

conclusions

The pressure measurements of the ADL dataset can be applied as measurements of wind-driven surges. These will be used for the calibration of a Delft3D surge model. The SWL, as it was during the ADL measurement campaign, can be taken from the KazHydroMet dataset.

Statistics on long term sea level variations can be obtained from the Probabilitas report (Probabilitas, 2002). These can be used for the determination of the SWL in design conditions. The spatial variations of the surges during these extreme events can then be calculated with the calibrated Delft3D model.

2.2.3 Bathymetric data

requirements

Bathymetric data of the Caspian Sea is needed for:

1 Calculation of the wind-driven surges

As stated earlier, the wind-driven surges will be calculated using the Delft3D software package. These calculations require a bathymetric map of the Caspian Sea as input. The quality of such data depends on the resolution of the map and the age of the data.

The resolution of the bathymetric map must cover variations in depth, as far as of influence to the generation of wind-driven surges. A grid spacing of 10 km should be sufficiently accurate, as the sea bed of the northern part of the Caspian Sea is relatively flat.

2 SWAN runs

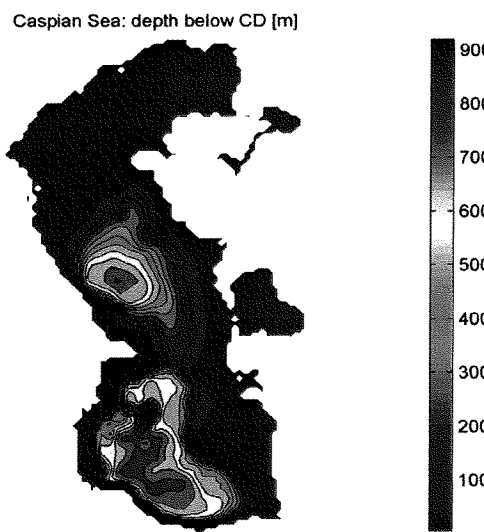
The SWAN model itself also needs a bathymetric map as input. The accuracy of the data is important for the SWAN model, particularly near the area of interest on the northern part of the Caspian Sea.

Wave spectra are more influenced by local variations in depth than the wind-driven surges. These variations can be of importance and should be covered by the bathymetric map. An accurate bathymetric map is particularly important during the simulation of extreme events. Shallow water depth processes then are very important.

availability

The bathymetric map, as used in Van Thiel de Vries (2003) to create his SWAN model, is used as a starting point for this study. The Section of Van Thiel de Vries (2003) in which the source of this map is described, is added as Appendix III. The map is shown in Figure 2.9. The bathymetric map has a grid spacing of 10 km. Levels are related to Caspian Datum (CD).

Figure 2.9. Bathymetry of the Caspian Sea



Other bathymetric data is available through survey data, retrieved by Boskalis International Kazakhstan BV and Thales in 2001. These surveys only cover a small area (near the oil Kashagan fields), but have a much higher resolution. The seabed level is related to OKIOC reference level (ORL), which is at approximately CD +0.9 m. The survey data is used to verify the bathymetric map, as described in Section 5.

Lastly the pressure measurements, from which wave spectra are distilled, are also a source of data on the local depths. The average pressure of one burst measurement added to the distance between the sensor and the sea bed can be interpreted as the total of the depth at that location and the water level at that moment.

conclusions

The bathymetric map, as presented in Figure 2.9, is the only available map of the complete Caspian Sea and is therefore used, both for the Delft3D model as for the SWAN model. The reference level can be verified with the available local water level measurements in Section 5.

2.2.4 Wave data

requirements

Wave measurements are needed to calibrate and validate the SWAN model. SWAN is a spectral wave model. Therefore spectral wave measurements are preferred to integral wave measurements. Furthermore it is of great importance that simultaneous wind and water level measurements are available.

availability

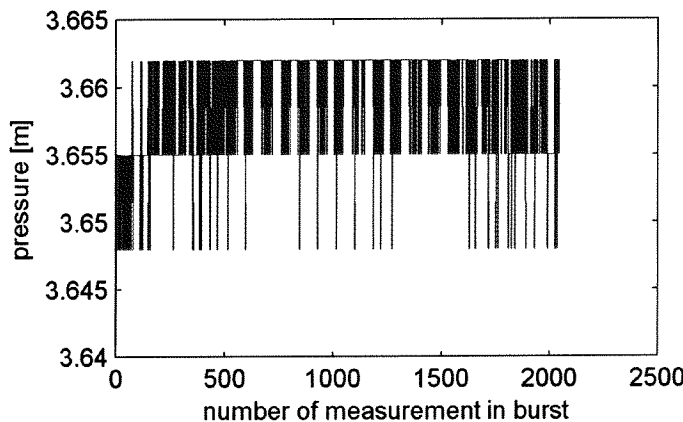
Arthur D. Little (1999) collected measurements in the northern part of the Caspian Sea with pressure transducers (two Coastal Leasing, Inc. Microspec current meters and one InterOcean S4 current meter). They were deployed at three locations from 29 October 1997 to 27 September 1998. Measurements collected from 19 December 1997 to 6 March 1998 were already removed from the datasets, as the locations were covered with ice at these times. More details about this measuring campaign can be found in Appendix I (Arthur D. Little, 1999), which is summarized in Table 2.1. The locations of the stations are shown in Figure 2.1.

Table 2.1. Deployment periods of pressure transducers

Station name	Deployment Name	Deployment Period	Start of Deployment	End of Deployment
A-CM	A2	2	31Oct97	28Apr98
A-CM	A3	3	29Apr98	24Sep98
C-CM	C2	2	29Oct97	28Apr98
C-CM	C3	3	29Apr98	25Sep98
E-CM	E3	3	01May98	27Sep98

Burst pressurehead measurements were collected with a frequency of 2 Hz, every three hours for 17 minutes (one burst). Every burst was checked for coverage. It appeared that the datasets were very complete. A scan for unrealistic values of pressures also resulted in no errors at all. Arthur D. Little (1999) already performed similar checks.

The accuracy of the instruments was investigated. A burst containing hardly any wave energy was studied. In this burst it could clearly be seen that the minimum variation in pressurehead measurable by the instruments was 7 mm. An example of such data can be seen in Figure 2.10. It is expected that this discretisation will not have a noticeable impact during the conversion of pressure measurements to wave spectra.

Figure 2.10. Minimal measurable pressure variation visualised

The pressure measurements can be converted into wave spectra. This process is described in Section 3.

conclusions

For the calibration of the SWAN model it is preferred to use spectral wave measurements carried out at the project location. These are available as burst pressure measurements. These have to be converted into wave spectra. This will be dealt with in Section 3.

2.3 Summary

In this Section the data requirements and availability of this study are described. Various purposes demand various quality levels of the measurements. Per purpose the requirements are defined, mainly in terms of resolution in time and space. The available measurements are described. Finally a decision is made on which measurements to use.

wind

Wind measurements are needed for three purposes:

- 1 the calculation of wind-driven surges with a Delft3D model;
- 2 the calibration and validation of the SWAN model of the Caspian Sea;
- 3 the simulation of extreme events with the SWAN model of the Caspian Sea.

Three sources of wind measurements are available:

The ADL dataset

- not usable for the simulation of extreme events;
- adequate for the purpose of calibration of both the SWAN wave model and the Delft3D surge model.

The NCEP dataset:

- adequate for the purpose of calibration of the Delft3D model;
- potentially adequate for the purpose of calibration of the SWAN model;
- statistics potentially usable for the simulation of extreme events.

KazAviaMet dataset

- insufficiently accurate for all three purposes.

water levels

Water level measurements are needed for:

- 1 the determination of the SWL during design conditions;
- 2 the calibration of the Delft3D surge model.

Water levels vary on four time scales. Long term statistics are available in a report by Probabilitas (2002). Seasonal variations are available in the KazHydroMet dataset. Tides don't play a role of importance. Wind driven surges can cause great variations within days and were measured in the ADL measuring campaign.

The long term water level statistics in the Probabilitas report (2002) can be applied for the determination of the SWL during design conditions. The pressure measurements of the ADL dataset can be used for the calibration of a Delft3D surge model. The SWL, as during the ADL measurement campaign, can be taken from the KazHydroMet dataset.

bathymetry

A bathymetric map of the complete Caspian Sea is needed for calculations with the Delft3D surge model and with the SWAN wave model.

The bathymetric map, applied by Van Thiel de Vries during his project (2003), will be used as a basis. The reference level of the map will be checked in Section 4 with the use of the ADL pressure measurements and with recent bathymetric surveys, carried out by Boskalis International Kazakhstan BV and by Thales.

waves

Wave measurements, preferably spectral wave measurements, carried out near the project sites, are needed to calibrate and validate the SWAN model of the Caspian Sea. These are available as the ADL burst pressure measurements. These burst pressure measurements have to be converted to wave spectra. This conversion will be treated in the following Section.

3 CONVERSION OF PRESSURE MEASUREMENTS TO SPECTRAL WAVE DATA

3.1 Introduction

Arthur D. Little (1999) has taken burst pressure measurements in the northern part of the Caspian Sea (Figure 2.1). The actual burst datasets have recently become available to Witteveen+Bos. Such burst pressure measurements can be converted to wave spectra. Subsequently integral wave parameters like H_{m0} and T_{m01} can be calculated. Arthur D. Little once performed such a conversion. The resulting integral wave parameters are also available to Witteveen+Bos and were used by Van Thiel de Vries (2003). The wave spectra on which these integral wave parameters were based are not available.

Unfortunately the conversion method, used by Arthur D. Little (1999), was not well documented. Furthermore the department of Arthur D. Little which performed the measuring campaign no longer exists, making it difficult to reproduce their methods.

Spectral wave data is required to recalibrate SWAN. In this Section the conversion of the burst pressure measurements to wave spectra is described.

3.2 Theory

The conversion of burst pressure measurements to variance density spectra (or energy density spectra) of sea level elevations requires the following steps (Roskam, 2004; Cavaleri, 2004; Gaikwad et al, 1996; Oelerich et al, 2003):

1. Split the burst into subseries of 100 seconds and calculate the difference between the instantaneous pressures and the mean burst pressure.
2. Apply a cosine tapering on the pressure variations time-records.
3. Calculate the power spectrum of the pressure variations for these 100-second series.
4. Calculate the mean power spectrum for each burst.
5. Convert the power spectra of the pressure variations to power spectra of sea level elevations, by multiplying by a factor, varying with wave-frequency.

Some considerations regarding these steps are described below:

add 1

There are two main reasons why every burst is split into subseries of 100 seconds:

- a. A Fast Fourier Transform of the complete burst would result in a very grassy spectrum with very small frequency bins. Information is lost by splitting the burst in subseries and calculating the average spectrum, but the resulting spectrum will be less grassy. From previous conversion studies it has become clear that splitting the burst into series of 100 seconds will give the most useful results. The spectrum will have a range of 0 to 1 Hz and a frequency bin of 0.01 Hz.
- b. A burst is assumed to contain a stationary Gaussian process. Spectral components caused by non-stationarity, will be averaged out of the spectrum, by splitting the burst into 100 second subseries and calculating the average spectrum,

add 2

Fast Fourier Transforms can best be performed on periodical functions. Therefore zero pressure at T_0 and T_{100} is required. The pressure burst then seems periodical with $T = 200$ seconds. This produces the best results, as components with periods greater than 200 seconds are filtered out.

T_0 and T_{100} become equal to zero through multiplication of the 100 seconds-time series by a tapering function. In Figure 3.1 the tapering function is plotted. The mathematical description of the tapering function is as follows:

$$tap_1(t) = \frac{1}{2} \left[1 - \cos\left(\pi \frac{t}{x}\right) \right] \quad 3.1$$

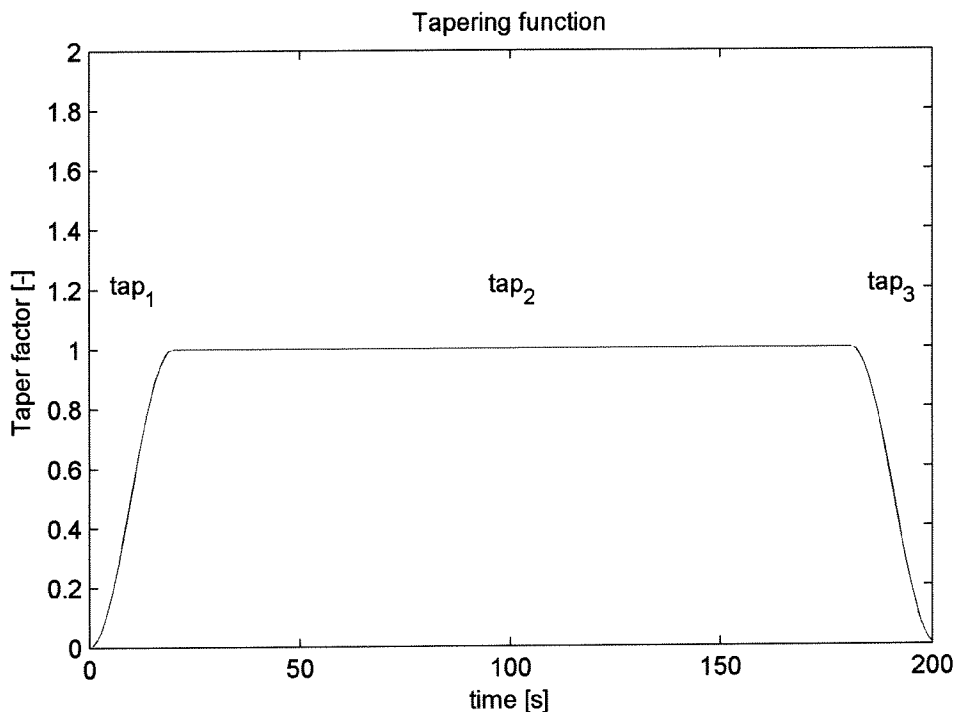
$$tap_2(t) = 1 \quad 3.2$$

$$tap_3(t) = tap_1(t) \text{ mirrored} \quad 3.3$$

$$r = \int tap_1^2 + \int tap_2^2 + \int tap_3^2 = 1 - \frac{5x}{4} \quad 3.4$$

where $x = 10\%$ of the length of the time series.

Figure 3.1. Tapering function



Energy is lost through the multiplication of the time series by the tapering function. Factor r describes the amount of energy which was lost. The time series after tapering are scaled with a factor $\sqrt(1/r)$, in order to compensate for this energy loss

add 3

Matlab contains a routine called *fft* (*Fast Fourier Transform*) making this calculation easy to perform. The Fast Fourier Transform results in power spectra of pressure variations with range 0 to 1 Hz, with frequency bins of 0.01 Hz.

add 4

A number of power spectra, equal to the number of 100-seconds time series, is obtained for every burst. The average of these spectra is calculated by adding up the power of all corresponding frequency bins and dividing these sums by the number of 100-seconds time series per burst.

add 5

A power spectrum of pressure variations can be converted to a variance density spectrum of sea level elevations by multiplying the spectrum with a frequency dependent factor, known as gain correction factor.

In linear wave theory pressures at a certain depth are described by the following formula.

$$p_z(x,t) = d - z + \frac{\cosh(kz)}{\cosh(kd)} \eta(x,t) \quad 3.5$$

where:

p_z = pressure (meters water column), at height z above the seabed

k = wave number

d = depth

η = surface elevation

The gain correction factor K_p can be derived from this function. This factor is:

$$K_p = \left(\frac{\cosh kd}{\cosh kz} \right)^2 \quad 3.6$$

The wave number k can be calculated for every frequency using the dispersion relation:

$$\omega^2 = gk \tanh kd \quad 3.7$$

Many have doubts whether linear wave theory is a good enough approximation to base the gain correction factor on. Cavaleri (2004) however stated in a personal communication:

"All above arguments are based on the assumption that the linear theory is true. Unluckily we found this is not the case. This is what we were actually looking for with our measurements on the tower. However, this is the good news for you, the non-linearity becomes more and more serious when we move away from the surface in relationship with the present wave length ... In any case I would tend to think that on 4-meters depth you could reasonably apply the linear theory, at the least with the serious events".

Therefore the results are expected to be trustworthy.

This gain correction factor increases with increasing frequency f . The amount of wave energy at the high frequency end and at the low frequency end of the wave spectrum is limited. In case of low wave energy the influence of instrument noise is significant. The signal to noise ratio is very small. Therefore the gain correction factor must be cut-off.

- At the high frequency end the gain correction factor is cut-off in order to reduce the influence of instrument noise.
- At the low frequency end the gain correction factor is cut-off to prevent the introduction of long waves (> 20 seconds), caused by the effects of non-stationarity in bursts with very small amounts of wave energy. The process in a burst is never exactly a stationary Gaussian process.

3.3 Possible conversion methods

Three methods for the determination of the gain correction factor were investigated. Firstly the method used by Arthur D. Little (1999), further referred to as the ADL method, was investigated. Secondly the method used by RIKZ (Roskam, 2004), for the purpose of this project called the RIKZ method, was

studied. Finally the method, as described by Cavaleri (Cavaleri, 1980; Cavaleri, 2004; McKee, 2002), was investigated.

the ADL method

The ADL wave measurements are available as burst pressure measurements and as integral wave parameters. Through trial and error the ADL conversion method was reproduced. The H_{m0} as given by Arthur D. Little can be calculated by applying the following method:

- 1 The time series of 17 minutes were not split into subseries, but immediately subjected to a Fast Fourier Transform.
- 2 No cosine tapering function was used.
- 3 For frequencies smaller than 0.05 Hz and greater than 0.42 Hz the gain correction factor was reduced to zero. These cut off frequencies were determined empirically in order to prevent the low signal-to-noise ratio at the higher frequencies to dominate the lower frequency regions of the spectrum with greater signal-to-noise ratios (Arthur D. Little, 1999). The low frequency limit was applied to remove physically unreasonable low frequency variations, observed in some bursts with very small energy contents. Figure 3.3 shows the gain correction factor as a function of the wave frequency. The value of the gain correction factor at cut-off frequency 0.42 Hz reaches values as high as 187.

Figure 3.2 shows a comparison of the integral wave heights, as provided by ADL, with the integral wave parameters, as determined by the above method. This method results in very unrealistically looking spectra, as the spectra end very abruptly at 0.42 Hz. Wave parameters obtained with this method will not be used in this project.

the RIKZ method (Roskam, 2004)

RIKZ splits the bursts in subseries of 100 seconds and uses a tapering function to guarantee a correct functioning of the Fast Fourier Transform. The determination of the gain correction factor deviates significantly from the ADL method.

RIKZ does not cut off the factor at a certain frequency, but cuts off the factor at a certain value. In the past their best results were obtained by cutting of the gain correction factor at value 2.5. A value of 2.5 is used (instead of reducing K_p to 0) for frequencies with K_p -values higher than 2.5 (Figure 3.5).

The gain correction factor increases very rapidly, because the measurements on the northern part of the Caspian Sea were collected very near the seabed (mostly about 20 cm above the sea bed). Cutting off at value 2.5 would mean that the gain correction factor would already be cut-off at a frequency lower than the peak frequency of the spectrum. A higher value of the cut-off is therefore desirable. The method is applied with cut-off values of 10 (maximum advised by Roskam (2004); Figure 3.5). The resulting H_{m0} was again compared with the integrated data as supplied by Arthur D. Little (1999) (Figure 3.4). The H_{m0} obtained with this method are structurally smaller.

the Cavaleri method

Like RIKZ, Cavaleri (Cavaleri 2004 and McKee, 2002) suggests to split the bursts into subseries of 100 seconds and to use a cosine tapering function to guarantee a correct functioning of the Fast Fourier Transform. The main difference with the RIKZ method lies in the definition of the cut-off value of the gain correction factor. Cavaleri and McKee recommend to cut-off the gain correction factor at a value 100 or 1000 (depending on the situation) and to attach a theoretical f^5 or f^4 tail to the spectrum for the higher frequencies. Both Cavaleri (1980) and McKee (2002) have compared measured spectra using wave buoys with spectra obtained with pressure measurements. The choice for cut-off values of 100 or 1000 is based on these studies. In a personal communication (2004) Cavaleri recommended to use a f^5 tail for the waves on the northern part of the Caspian Sea.

Hashimoto et al (1997) also determined the gain correction factor, by comparing converted spectra with sea level elevation spectra directly measured by means of wave buoys. These pressure measurements were collected 2 meters above the seabed, where the depth was 30 meters. This situation is compara-

ble to the northern part of the Caspian Sea (measurements collected 20 cm above the seabed, while depths were 4 meters). In this study the gain correction factor reaches very high values. This also suggests that a strict usage of the rule-of-thumb to cut off at values like 2.5 or 10 is not strictly necessary to obtain reliable results.

Figure 3.2. H_{m0} of integrated ADL data compared with H_{m0} of ADL method

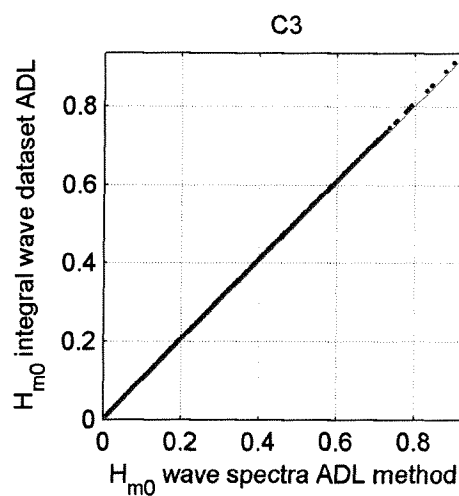


Figure 3.3. K_p for ADL method

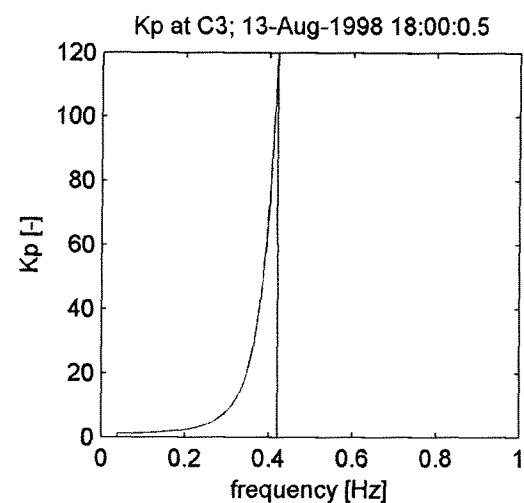


Figure 3.4. H_{m0} of integrated ADL data compared with H_{m0} of RIKZ method

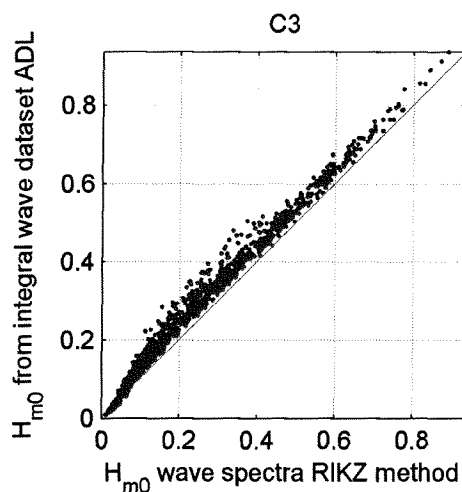
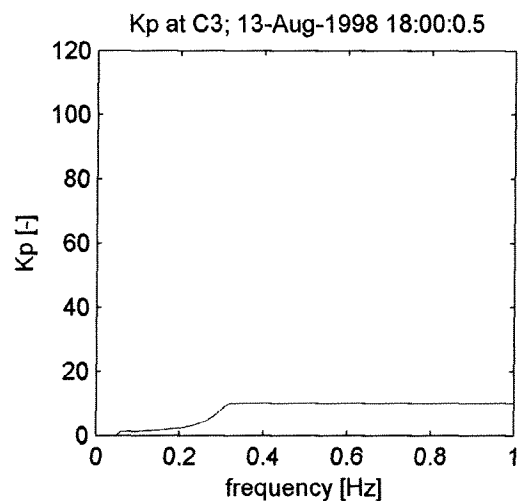


Figure 3.5. K_p for RIKZ method



3.4 Choice of conversion method

splitting in part time series

In most literature the splitting of the burst in subseries of 100 seconds is recommended. This recommendation will be followed in this conversion study.

tapering

A Fast Fourier Transform produces the best results if the time series is periodical. A 100 seconds time series becomes quasi-periodical with period $T = 200$ seconds, by multiplying the part time series with a tapering function as described in the preceding Section. This recommendation will also be followed.

gain correction factor

The reasoning behind the cut off frequencies based on signal-to-noise ratios, suggested by Arthur D Little (1999), seems trustworthy. However, the decision to abruptly reduce the K_p -factor to 0 at frequencies higher than the cut-off frequency, results in unrealistically shaped spectra.

The method described by Cavaleri (2004) seems to be well-accepted. In the articles by McKee (2002) and Hashimoto (1997) the methods proved to be accurate.

The application of this method results in some double peaked spectra. An example can be seen in Figure 3.6. There are a few reasons to believe that these double peaked spectra are not based on the true physical process.

- 1 The high-frequency peak had a frequency, which was twice the frequency of the low-frequency peak, suggesting that this might be a numerical result of the Fourier Transform.
- 2 Shoaling waves sometimes show a second peak at a higher harmonic of the peak frequency. However, the peak as shown in Figure 3.6 certainly is much too high for such an explanation.
- 2 Double-peaked spectra are often caused by the combination of sea waves and swell waves. The high-frequency peak corresponds with the sea wave peak. The frequency of this high-frequency peak is very different from the peak frequencies of single-peaked spectra in this dataset, containing sea-waves only. Therefore this peak is probably false.
- 3 The frequency of the high frequency peak lies at a frequency greater than 0.42 Hz. Arthur D. Little's report (1999) suggests that at such frequencies the signal-to-noise-ratio is smaller than 1. This suggests that these high frequency peaks are blown-up instrument noise.

It is recommended to cut off the gain correction factor at frequency 0.42 Hz (as Arthur D. Little (1999) suggests). Instead of reducing K_p (and through this the resulting spectrum) to 0 for higher frequencies, a theoretical high frequency tail of the f^5 -shape is added (as Cavaleri recommends (2004)). The H_m0 resulting from these spectra tend to be greater than when using the ADL method (Figure 3.7). This is logical as more energy was added at the high frequency end of the spectrum through this theoretical f^5 -tail.

This chosen method combines the results of Cavaleri's extensive research on the conversion of pressure measurements to wave spectra in general, with the study of the signal-to-noise ratio of the actual measurements taken at the northern part of the Caspian Sea by Arthur D. Little (1999).

The spectra resulting from this method look very realistic and will be used for this study. Most interesting is the fact that the resulting significant wave heights are on average 5 cm higher than was first thought, due to the use of this new method.

Figure 3.6. Double peaked spectrum obtained through Cavalieri method
Double peaked spectrum Cavalieri method

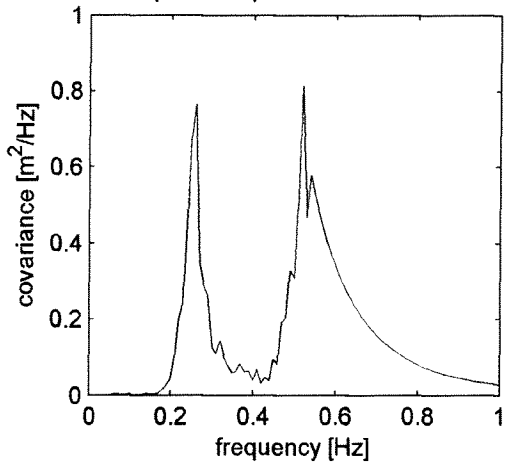
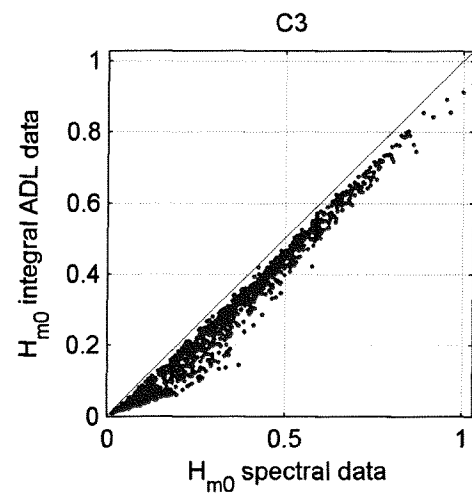


Figure 3.7. H_{m0} integrated ADL data compared with H_{m0} of chosen method



3.5 Summary

The conversion of burst pressure measurements to variance density spectra of sea level elevation is treated in this Section. Various methods have been developed for this conversion. All are based on linear wave theory. Formulae are available which describe pressure variations at a certain depth resulting from wave motion at the surface. From these formulae a so-called gain correction factor was derived. This is the multiplying factor, applied to transform pressure variation spectra to sea level elevation spectra.

Three conversion methods were compared. These differ in four aspects:

- The splitting of the bursts into sub-series
By splitting every burst in sub-series, calculating the spectra of these sub-series and then averaging these spectra, a less grassy spectrum is obtained having greater frequency bins.
- The application of a so-called tapering function
A tapering function can be used to make a time series quasi-periodical, which can result in a better performance of the Fast Fourier Transform, used for the calculation of the spectrum.
- The determination of a cut-off for the gain correction factor
The gain correction factor is an increasing function of the wave frequency. At high frequencies this could result in the multiplication of instrument-noise with a very high factor. Therefore the gain correction factor must be cut-off, either at a certain frequency or a certain value.
- The determination of the high frequency tail of the wave spectrum
The gain correction factor is cut-off at a certain value of frequency. The high frequency tail can now be determined in various ways.

The chosen method is as follows:

- 1 Every burst is split into time series of 100 seconds.
- 2 A tapering function is applied on every subseries.
- 3 A Fast Fourier Transform is applied on every tapered subseries and an average spectrum is calculated.
- 4 The gain correction factor is cut-off at 0.42 Hz and multiplied with the pressure spectrum.
- 5 A theoretical f^{-5} -tail is added, starting from 0.42 Hz.

Most interesting is the fact that the resulting significant wave heights are on average 5 cm higher than was first thought, due to the use of this new method.

It must be noted that the method, which was presumably applied by Arthur D. Little (1999), implies neglecting all wave energy at frequencies above 0.42 Hz. Therefore the ADL method resulted in too small significant wave heights and average wave frequencies. It is expected that this has seriously influenced the calibration study, performed by Van Thiel de Vries (2003).

In the following Section a closer look is given to the spectra that resulted from this conversion study.

4 ANALYSIS OF THE WAVE DATA

4.1 Introduction

Much can be learnt about the waves on the Caspian Sea by taking a closer look at the wave spectra. In this Section the results of the analysis of the spectra are presented. First the quality of the spectral wave data is studied. Some of the data may not be usable for the calibration and validation of the SWAN model. Also some characteristics of the spectra are highlighted. Finally the spectra are compared with theoretical spectra.

4.2 Quality of the wave measurements

location E

It is decided not to use the data collected in E-CM (see Figure 2.1), because of the following reasons:

- 1 The instrument moved during deployment (Arthur D. Little, 1999). This can also be seen from the recorded depths, which increase abnormally (Figure 4.1).
- 2 The pressures were collected at a very large depth, resulting in great uncertainties in the spectra. A large gain correction factor is needed, as the surface waves are hardly registered at such large depths. This introduces a great error margin.
- 3 The uncertainty introduced by the choice of a conversion method is not acceptable. An example of a resulting spectrum is given in Figure 4.2. It is not hard to imagine that the choice of the cut-off frequency will greatly influence the shape of this spectrum. The resulting spectrum becomes very doubtful, when adding the theoretical f^{-5} tail starting from a frequency of 0.42 Hz. Furthermore the resulting H_{m0} reaches an unrealistically high value. No reasonable reference exists on which a decision can be based, as no comparison can be made with directly measured sea level elevation spectra. The spectrum in Figure 4.2 was measured in May 1998, when the measuring instrument was not moving yet, as can be seen in Figure 4.1. Therefore it can be concluded that also the spectra measured before the movement of the instrument (starting in July 1998), should not be used.
- 4 Significant wave heights at location E reach unrealistically great values (17 meters), when applying the conversion method chosen in Section 3.

The use of this data would introduce great uncertainty. It is therefore decided not to use the data collected in deployment E3.

Figure 4.1. Increasing registered depth at E

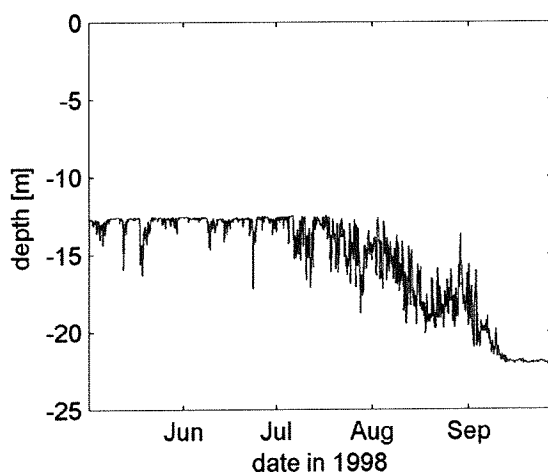
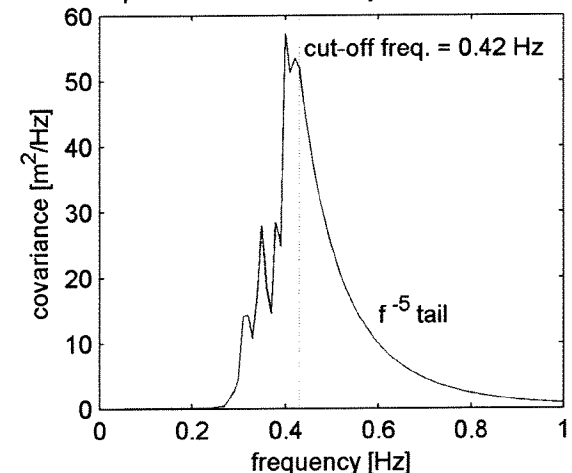


Figure 4.2. Spectrum at E3
spectrum in E at 02-May-1998 18:02:0.5

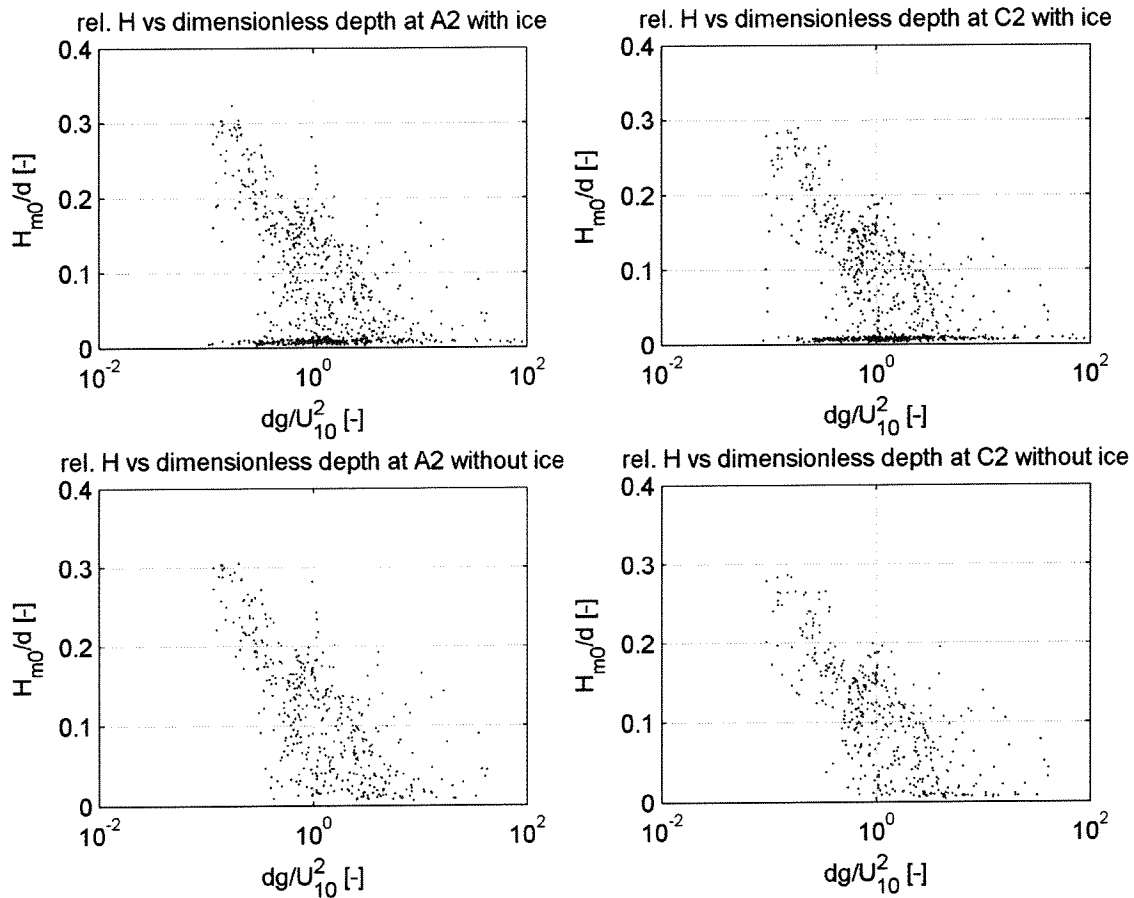


removal of measurements influenced by the nearby presence of ice-coverage

Arthur D. Little (1999) had already filtered out the measurements that were carried out while the measuring locations were covered with ice. Plots were made of the relative wave height versus the dimensionless depth for deployments A2 and C2, in order to see whether the influence of ice coverage at nearby locations was also filtered out (SWAN would not be able to hindcast those spectra without added programming, as the fetch lengths would be influenced). These plots are shown in Figure 4.3.

Figure 4.3 (top row) shows that some spectra contain very little wave energy, while the wind speed at those times was significant (visualised by the dots with values of H_{m0}/d near 0, but with small values of the dg/U_{10}^2 (significant wind speeds)). This combination is very unlikely. The nearby presence of ice is considered to be the explanation for these conditions, given the fact that these conditions were observed during the winter period. It was decided to only use the data obtained from 1 to 21 November 1997 and from 26 March to 27 April 1998 of deployments A2 and C2. Most measurements collected in 1997 were removed from the datasets.

Figure 4.3. Filtering of ice dates



4.3 Characteristics of the wave measurements

minimum period

Plots of T_p against H_{m0} show the existence of a lower limit of T_p . This limit was already observed by Van Thiel de Vries (2003), but could not be explained. It has now become clear that this limit is caused by the determination of the cut-off frequency. Arthur D. Little (1999) used a cut-off frequency for K_p of 0.42 Hz. In situations with small amounts of wave energy, the peak frequency of the spectrum always ap-

proaches the value of 0.42 Hz (a period of 2.38 seconds), as at this frequency K_p reaches its maximum (see Figure 3.3). A similar phenomenon occurs when applying the conversion method, chosen in this study (Figure 4.4). It is expected that this limit will not cause significant problems during the calibration of the model. For spectra with small amounts of wave energy SWAN is expected to reach similar values of T_p .

depths

Most data suggests the presence of transitional water depth (Figure 4.5). This could create difficulties in the choice of time series needed for the calibration of the model. It would be favourable if a subseries existed in which deep water conditions are prevailing (see Section 6.2). Unfortunately the data collected in E, where deep water conditions are present, is not considered sufficiently accurate.

**Figure 4.4. Minimum wave period
C3**

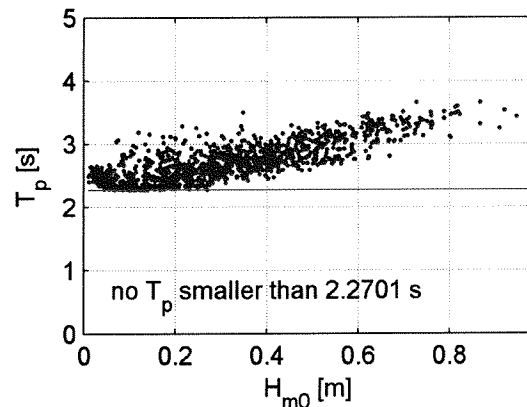
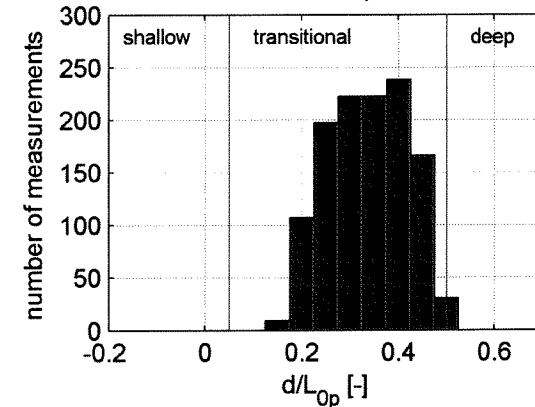


**Figure 4.5. Histogram of d/L_{Op}
relative waterdepth at C3**



the presence of swell

The wave age is an indicator for the presence of swell waves. Wave age is defined as the ratio of wave propagation speed to wind speed (the NCEP winds were used, as the ADL dataset does not contain simultaneous wind data for every available wave spectrum). In cases where the wave age is greater than 1, swell could be present. The waves then travel at a greater speed than the wind velocity. It is suggested that swell might be present, when studying Figure 4.6. A better insight into the presence of swell can be obtained by studying the wave spectra. Therefore plots were made of all wave spectra, with wave ages greater than 1. No double peaked spectra of importance were found. Most of the spectra appeared to have very small energy contents. Figure 4.7 shows a (rare) example of a spectrum with a significant value of H_{m0} and a wave age greater than 1. This spectrum does not show any presence of swell. It is speculated that the data points with wave ages greater than 1 were caused by inaccuracies in the NCEP wind data. At wave heights greater than 0.8 meter no wave ages greater than 1 were observed. Witteveen+Bos is most interested in more extreme wave conditions. It was therefore concluded that swell is not a factor of great importance in the northern part of the Caspian Sea.

Non-locally generated waves would have to travel a great distance over the shallow northern part of the Caspian Sea, in order to have swell waves at locations A-CM and C-CM (Figure 2.1). Furthermore a shallow sill across the width of the Caspian Sea exists at the entrance to the northern part of the Caspian Sea. This sill could prevent low frequency waves, generated by storms in the South, to propagate into the northern part of the Caspian Sea (Graham, 2002). Many researchers have already assumed that swell waves would already be dissipated by the time they reach these locations. These assumptions are now proven to be correct.

Figure 4.6. Wave ages in deployment C3

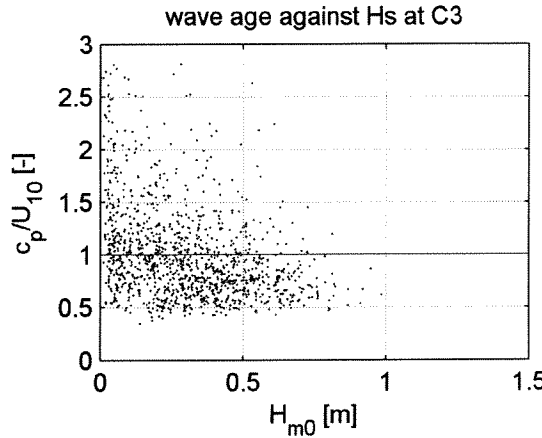
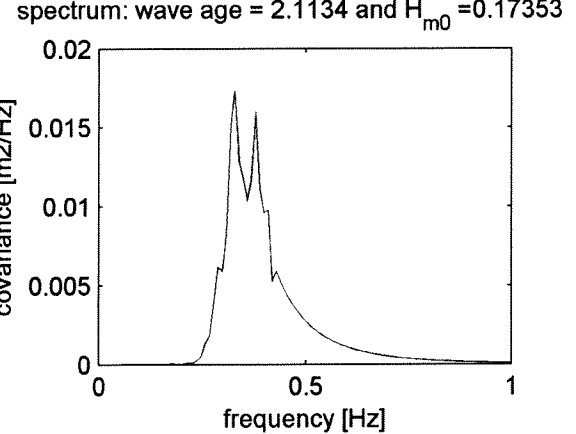


Figure 4.7. Spectrum with large wave age and H_{m0}



wave breaking

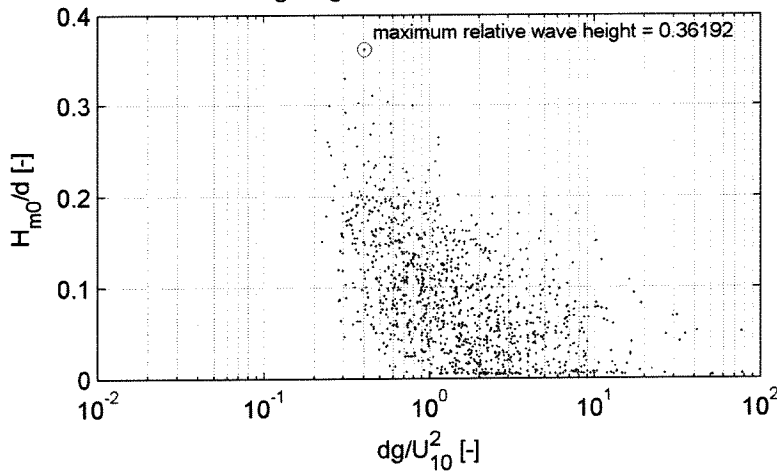
During the ADL measuring campaign H_{m0}/d did not reach values higher than 0.36 (Figure 4.8). As individual waves break at relative wave heights H_{max}/d of about 0.78 (Tanaka, 1986), it is expected to be difficult to calibrate the source term for depth-induced wave breaking with the available measurements. SWAN uses a breaker parameter of 0.73 by default.

This does not imply that wave breaking will not occur at all. The fraction of breaking waves Q_b can be estimated from the Battjes and Janssen (1978) breaker model:

$$\frac{1 - Q_b}{\ln Q_b} = -8 \frac{E_{tot}}{H_{max}^2} \quad 4.1$$

The measurement with maximum $H_{m0}/d = 0.36$ had a H_{m0} of 1.15 m and depth of 3.19 m. The maximum possible individual wave height H_{max} at that moment was 2.49 m ($0.78 * 3.19$). Therefore Q_b had a value of 8.6e-5. Only a very small fraction of the waves were breaking during these most extreme conditions represented in the measurements (although this fraction does represent the highest and therefore most energetic waves in the wave field).

Figure 4.8. Relative wave height against dimensionless depth
relative waveheight against dimensionless water depth at A3



4.4 Comparison of the spectral shape with theoretical spectra

In this Section an attempt is made to relate the measured spectra to known theoretical spectra. From theory not much is known about the shape of wave spectra on transitional water depth. Spectra in deep water conditions are well described by the JONSWAP spectrum. Its high frequency tail is described by an f^{-5} shape. This spectrum is described by the following formula:

$$E_{JONSWAP}(f) = \alpha g^2 (2\pi)^{-4} f^{-5} \exp \left\{ -\frac{5}{4} \left(\frac{f}{f_p} \right)^{-4} \right\} \cdot \gamma \exp \left[-\frac{1}{2} \left(\frac{f-f_p}{\sigma_a f_p} \right)^2 \right] \quad 4.2$$

All coefficients in expression 4.2 are free coefficients, which depend on the stage of wave development, where α is a scale parameter and γ , σ_a and σ_b are shape parameters.

Spectra on shallow water can be described by a TMA spectrum (Bouws et al, 1985; Bouws et al, 1986). This spectrum is described as follows:

$$E_{TMA}(f, d) = E_{JONSWAP}(f) \Phi(\omega_d) \quad 4.3$$

$$\text{With } \Phi(\omega_d) = \frac{k(\omega, d)^{-3} \frac{\partial k(\omega, d)}{\partial f}}{k(\omega, \infty)^{-3} \frac{\partial k(\omega, \infty)}{\partial f}} \quad 4.4$$

The TMA spectrum is equal to the JONSWAP spectrum times a depth dependent factor Φ_d . For deep water conditions the TMA spectrum and JONSWAP spectrum are equal. In shallow water conditions the TMA spectrum is wider and the exponent of the tail shifts from -5 towards -4 . Unfortunately it is difficult to check whether the measurements correspond well with this theory, as the measured spectra by definition all have f^{-5} tails, from 0.42 Hz to 1 Hz, as a result of the chosen conversion method.

Lewis and Allos (1990) have described a method to calculate the shape of theoretical TMA and JONSWAP spectra with given H_{m0} and T_p . With this method theoretical TMA and JONSWAP spectra were calculated with equivalent H_{m0} and T_p to the measured spectra. Figure 4.9 compares the spectral moments of the measured spectra with that of the JONSWAP and TMA spectrum (calculated according to Lewis and Allos (1990)). It can be observed that indeed for the larger spectral moment (bigger waves, greater H_{m0}/d , relatively shallow conditions) the measured spectral moments are closest to spectral moments of the TMA spectrum (even though an f^{-5} tail was attached at the high frequency end of the measured spectra during the conversion from pressures to spectra). This is also illustrated by the fact that the RMSEs of the spectral moments of the TMA spectra are smaller than those of the JONSWAP spectra.

An example of a spectrum containing relatively much energy plotted in one figure with a theoretical JONSWAP and TMA spectrum is shown in Figure 4.10. It can be observed that the measured spectrum better corresponds with a TMA spectrum than to a JONSWAP spectrum. The fact that the similarities between theory and measurements are clearly visible increases confidence in the conversion method used in Section 3.

Figure 4.9. Spectral moments of measurements compared with JONSWAP (black) and TMA (red)

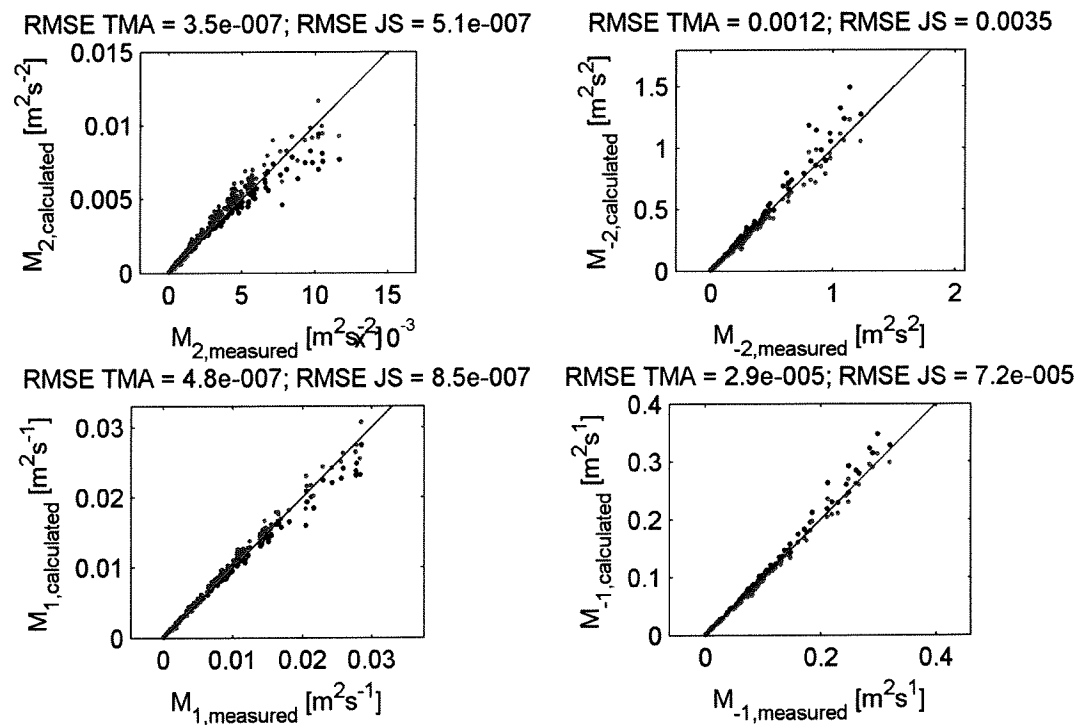
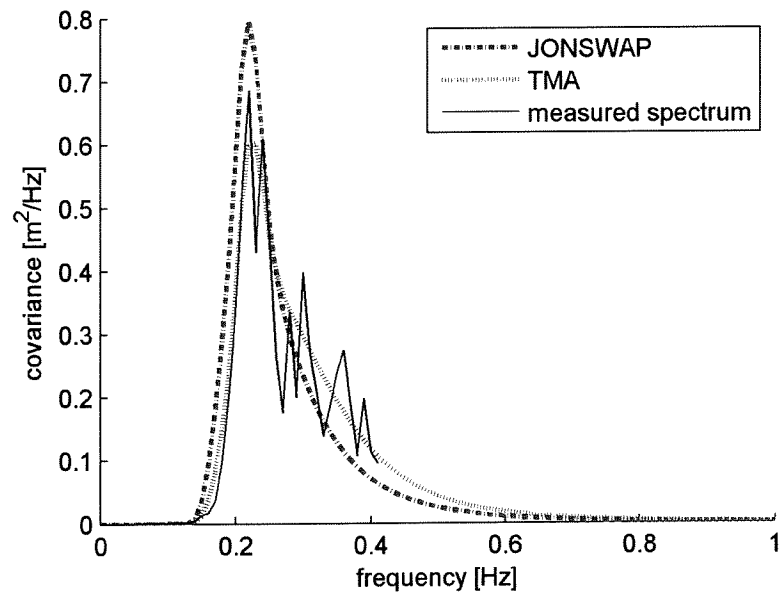


Figure 4.10. Measured spectrum compared with JONSWAP and TMA



4.5 Summary

In this Section the wave measurements, as obtained in Section 3, were analysed.

A quality check of the wave measurements resulted in two main decisions:

- 1 The spectra obtained from deployment E-CM are rejected for use in the calibration phase, due to a too great error margin.
- 2 The spectra measured between 21 November 1997 and 26 March 1998 are also rejected, due to a probable nearby influence of ice coverage. This decision was made after an analysis of relative wave heights and dimensionless depths.

Some characteristics of the waves were studied, which led to the following conclusions:

- 1 The minimum measured wave peak period of 2.38 seconds, already mentioned but not explained by Van Thiel de Vries (2003), appears to be caused by the conversion method of burst pressure measurements to wave spectra.
- 2 The measurements only contain transitional water depths.
- 3 Swell waves are not present. Wave spectra with wave ages greater than one were plotted, but none had clear peaks that could be interpreted as swell waves.
- 4 No significant depth-induced wave breaking occurred during the measuring campaign. The maximum measured fraction of breaking waves in a wave field was 8.6e-5

Finally, a comparison of the measured wave spectra with the theoretically defined JONSWAP and TMA spectrum was made. The similarities between the measured spectra and the theoretical spectra, analysed in terms of spectral moments, were clearly visible. This increases confidence in the conversion method used in Section 3.

5 SWAN MODEL DESCRIPTION AND SET-UP

5.1 Introduction

After a brief description of SWAN in general and the base model created by Van Thiel de Vries (2003), decisions are described regarding the wind input, surge input and bathymetric input to the SWAN model of the Caspian Sea. Some numerical settings are also dealt with.

5.2 Description of SWAN

SWAN is a third-generation wave action model. It was designed to overcome the difficulties, faced by other wave action models in coastal regions. For this study version 40.31ABCDEFG was used (Holt-huijsen et al, 2004). The governing equation in the SWAN model is as follows:

$$\frac{\partial N}{\partial t} + \frac{\partial C_{g,x}N}{\partial x} + \frac{\partial C_{g,y}N}{\partial y} + \frac{\partial C_{g,\sigma}N}{\partial \sigma} + \frac{\partial C_{g,\theta}N}{\partial \theta} = \frac{S}{\sigma} \quad 5.1$$

SWAN calculates the development of a sea state by means of action density $N(\sigma, \theta)$ rather than by means of energy density $E(\sigma, \theta)$, as in the presence of currents action density is conserved whereas energy density is not. Action density is equal to energy density divided by relative frequency ($N=E/\sigma$). The terms on the left hand side of expression 5.1 describe the evolution of the action density spectrum (N) of a sea state in time (t), space (x and y), relative wave frequency (σ) and direction (θ). In expression 4.1 C_g is the wave propagation speed in (x, y, σ, θ) space. In case of stationary SWAN runs the first term equals zero. During the calibration phase of this project SWAN was applied in non-stationary mode, as time series needed to be hindcasted.

The evolution of the action density spectrum N is forced by the so-called source terms S . In SWAN six source terms are defined, summarised by the following expression:

$$S = S_{wind} + S_{wcap} + S_{nl4} + S_{fric} + S_{surf} + S_{nl3} \quad 5.2$$

The first three source terms are the deep water source terms; the last three source terms are the shallow water source terms:

S_{wind}	describes the addition of wave energy by wind
S_{wcap}	describes the dissipation of wave energy by whitecapping
S_{nl4}	describes the spectral redistribution of wave energy by quadruplet interactions
S_{fric}	describes the dissipation of wave energy by bottom friction
S_{surf}	describes the dissipation of wave energy by depth-induced wave breaking
S_{nl3}	describes the spectral redistribution of wave energy by triad interaction

Ideally the deep water source terms are calibrated first on a timeseries of measurements in which deep water conditions are represented. In such timeseries the shallow water processes do not play a role and therefore will not influence the calibration process. After calibration of the deep water source terms the shallow water source terms can then be calibrated on a timeseries of measurements representing shallow water conditions.

5.3 The base model, by Van Thiel de Vries (2003)

The model set-up created by Van Thiel de Vries (2003) is applied as a base model for this project. The following settings characterise his model set-up:

- a time-step of 3 hours is applied;
- the computational grid has a grid spacing of 10 km;
- the computational frequency domain was set at 0.15-1.00 Hz with 30 frequency bins;
- the directional domain covers all directions and contains 36 bins (default);
- the density of the water is set to 1013 kg/m³ (salinity levels are lower than in the oceans).

The bathymetric map, used by Van Thiel de Vries (2003), is the only one available. It was described in Section 2.2.3. Depths are defined at grid spacings of 10 km and are related to Caspian Datum (CD).

No boundary conditions need to be imposed on the model, as the system of the model contains the complete Caspian Sea, which is surrounded by land boundaries.

5.4 Wind input

As was stated in Section 2, a choice can be made between the use of the ADL wind dataset and the NCEP wind dataset. The use of the ADL wind dataset has one great disadvantage. Not for every measured wave spectrum a simultaneously measured wind speed and direction are available (Table 5.1). This implies that when the ADL wind dataset is used, a great part of the ADL wave data becomes unusable for this study. Only the NCEP dataset does not have this disadvantage. The great advantage of the ADL data is that it contains more information on the high frequency variations of the wind speed.

Table 5.1. Availability of wind and wave data

Month	10-97	11-97	12-97	01-98	02-98	03-98	04-98	05-98	06-98	07-98	08-98	09-98
ADL waves												
ADL wind												
NCEP wind												

attempt to use the NCEP data

Before running SWAN with the NCEP wind, the wind driven surges were calculated. This was done using a Delft3D model (see Section 5.5). Then a first SWAN calculation using a default configuration was run. The same was performed using ADL wind. The following plots were made (Table 5.2):

Table 5.2. Overview of plots made to compare the performance of a model using NCEP wind and ADL wind

	NCEP wind	ADL wind
simulated and measured H_{m0}	Figure 5.1	Figure 5.2
wind speed and measured H_{m0}	Figure 5.3	Figure 5.4
wind speed and simulated H_{m0}	Figure 5.5	Figure 5.6

From these plots the following can be concluded:

- the ADL wind results in the best hindcast of the measured wave heights, although the model was not calibrated yet;
- the trend in measured wave heights much better follow the trend of the ADL wind than the trend of the NCEP wind;
- it appears to be reasonable that the wind input given to the SWAN model would result in the simulated wave heights, both for the NCEP wind as for the ADL wind.

A calibration of the model, using other formulations or coefficients, is not expected to give much improved results with the NCEP wind. It is doubtful that a simulation better corresponding with the measurements (in terms of e.g. the Root Mean Square Error of the H_{m0}), would represent a better configuration. The error in the input would be greater than the error in the output.

Summarising it can be stated that:

- the NCEP dataset contains too little information on the high frequency wind speed variations for calibration purposes;
- wave spectra calculated with SWAN runs using NCEP wind correlate too little with the measured wave spectra.

It is concluded that the NCEP wind data cannot be used for the calibration of SWAN. From this point onwards only the ADL wind data and the simultaneously measured wave data are used. The

black cells in Table 5.1 indicate the data, usable for this study. Of these months simultaneous ADL wind measurements and ADL wave measurements are available.

Figure 5.1. H_{m0} simulated (with NCEP wind) and measured

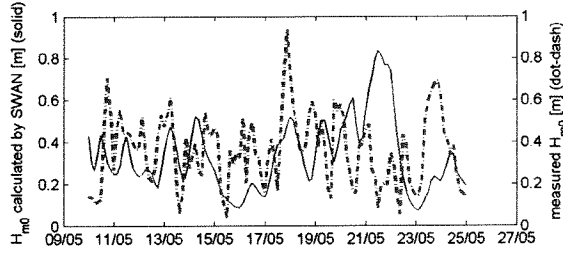


Figure 5.2. H_{m0} simulated (with ADL wind) and measured

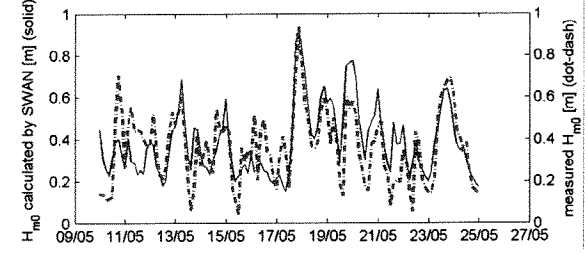


Figure 5.3. Wind speed (NCEP) and measured H_{m0}

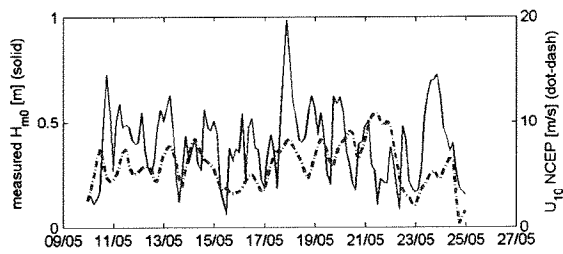


Figure 5.4. Wind speed (ADL) and measured H_{m0}

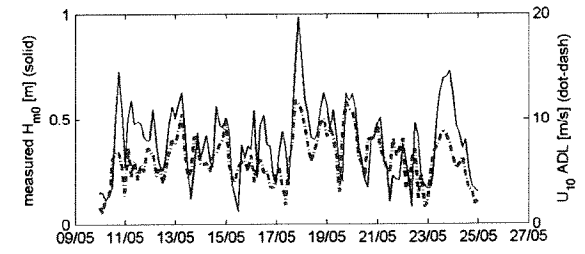


Figure 5.5. Wind speed (NCEP) and simulated H_{m0}

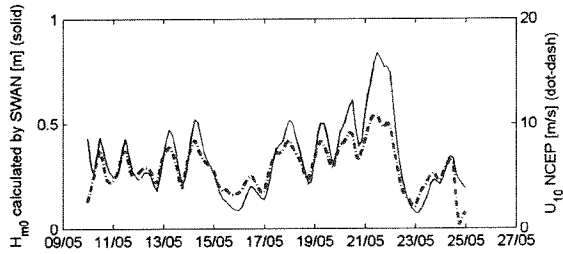
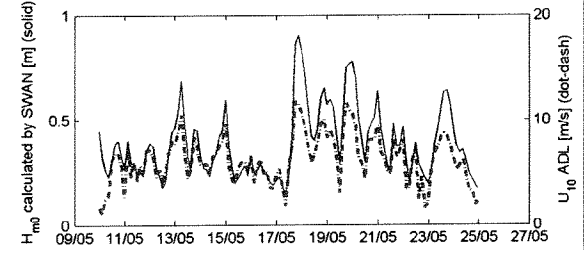


Figure 5.6. Wind speed (ADL) and simulated H_{m0}



5.5 Wind-driven surges, water depth and water levels

5.5.1 Introduction

Spatially defined wind-driven surges were calculated by Van Thiel de Vries (2003) with a Delft3D model, auto-calibrated on measured local water levels. In this Section this surge model is more elaborately described. After a further analysis of the resulting wind driven surges and the used bathymetric map, the surge and depth input for this project are defined.

5.5.2 Calculation method of the wind-driven surges

The surge input, which Van Thiel de Vries (2003) used, was calculated using a Delft3D model created by Witteveen+Bos. This model was auto-calibrated with a tool called PEST (Parameter ESTimation). The ADL wind dataset was used as wind input.

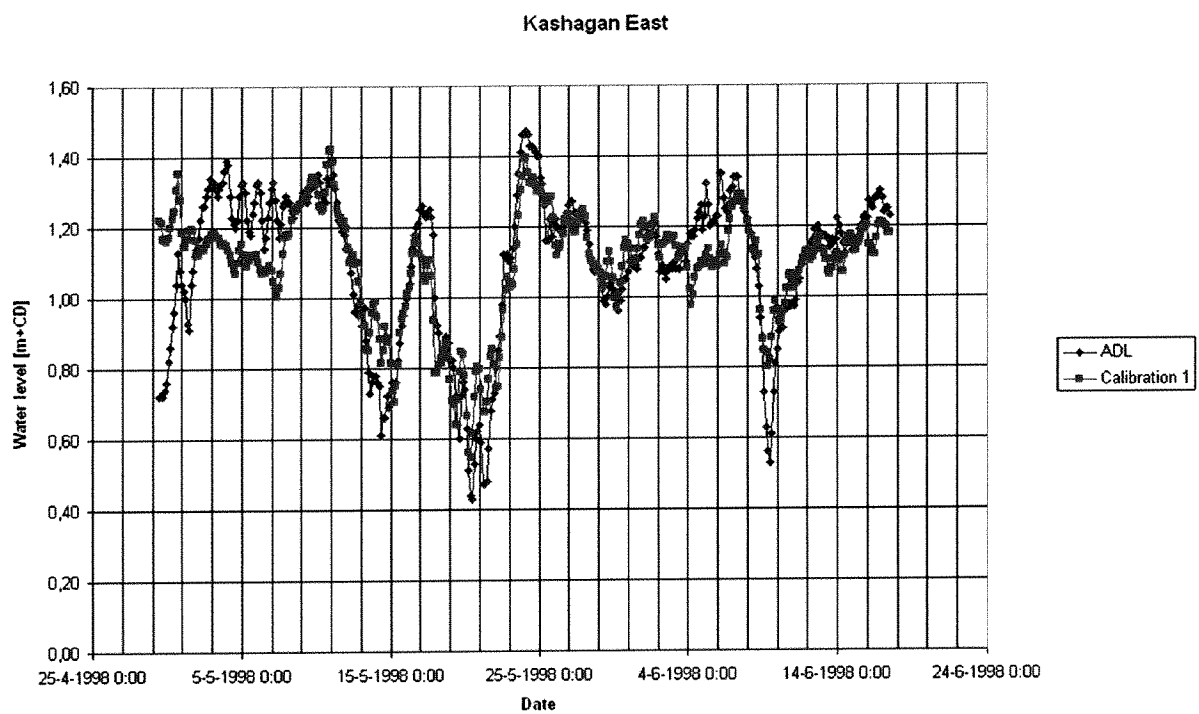
This wind speed was applied uniformly across the whole of the Caspian Sea. The NCEP wind dataset is the only dataset containing wind speeds at various grid point on the Caspian Sea. The dataset was assumed to be accurate enough for the purpose of proving the acceptability of a spatially uniform wind schematisation, as at least the trends in wind speeds and directions match rather well with the more accurate ADL wind (Appendix II). The fact that the Delft3D model performs as well as it does also suggests the viability of the assumption (see Figure 5.7).

The measured surges are provided by the burst pressure measurements of ADL, taken from the 29th of April until the 17th of June 1998. The average of the 2 Hz pressure measurements of one burst (17 minutes) is equal to the depth in that burst minus the distance between the seabed and the instrument. These averages result in a record of one depth registration per three hours. By subtracting the average of these depths from this record, the depth fluctuations around the SWL are obtained (the chosen calibration period is sufficiently short to minimise the influence of seasonal variation of SWL). The value of SWL, related to Caspian Datum, is taken from KazHydroMet data, provided by Witteveen+Bos. In the calibration period SWL was CD + 1.1 meter (see Figure 2.8).

The calibration of the Delft3D model was performed by tuning the roughness coefficient and the wind drag coefficients. After calibration, Delft3D was able to produce the wind-driven surges rather accurately, as can be observed in Figure 5.7. In the first time steps of the calibration run the match is less accurate, which is caused by the spin-up time of the model. The wind direction varied during the calibration timeseries, as can be observed in Appendix IV. The Delft3D output was converted into water level files (one file for every 3-hour time step), accessible by SWAN.

The Delft3D model takes coastal flooding into account. This can be of significant importance in the northern part of the Caspian Sea, in particular during extreme upsurges. Downsurges, however, can be very significant too, leaving part of the North Caspian Sea dry. These are also correctly modelled. In particular the surge levels at the area of interest are well represented by the Delft3D model, as the model was calibrated on measured surge levels at this location.

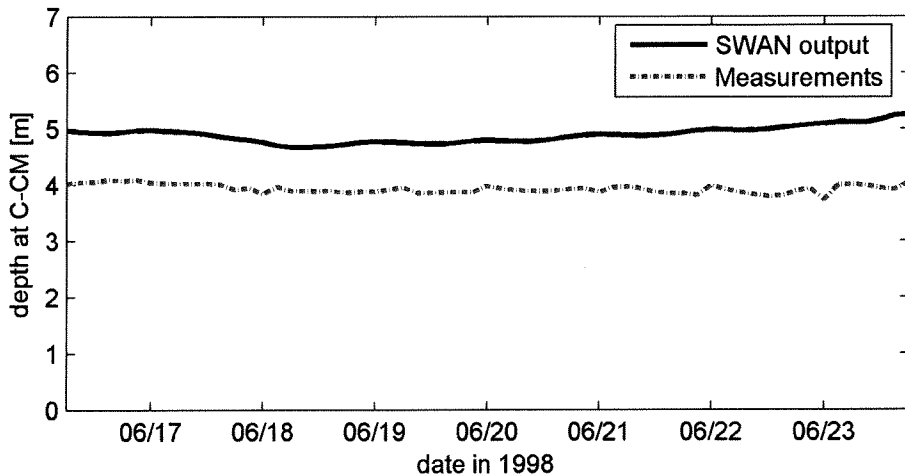
Figure 5.7. Comparison measured water levels and calculated water levels (Delft3D)



5.5.3 Definition of the depths and water level input

A SWAN run was made to test whether SWAN reads the inputfiles correctly, after calculating the wind-driven surges using the method described above. As output the total depth was requested for every time step at locations A-CM and C-CM. When comparing these depths with the measured depth of ADL, an inconsistency can be observed (Figure 5.8).

Figure 5.8. Comparison depths SWAN and ADL in C3

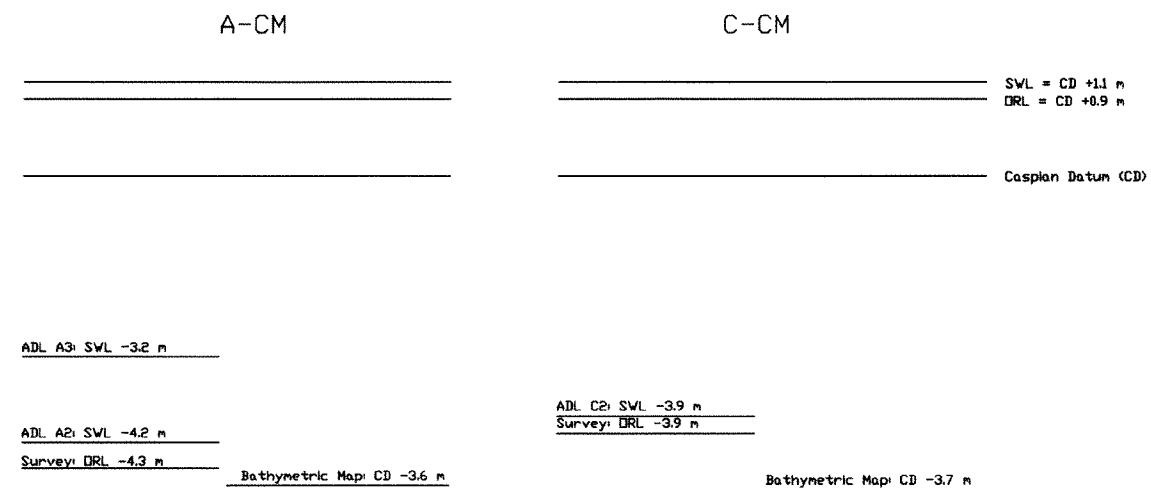


The available survey data was studied more closely, to determine whether this inconsistency was due to a local variation within the 10×10 km grid cells of the bathymetric map, due to an erroneous bathymetric map itself or due to an incorrect SWL.

In Figure 5.9 the various sources for bathymetric data were compared. These are:

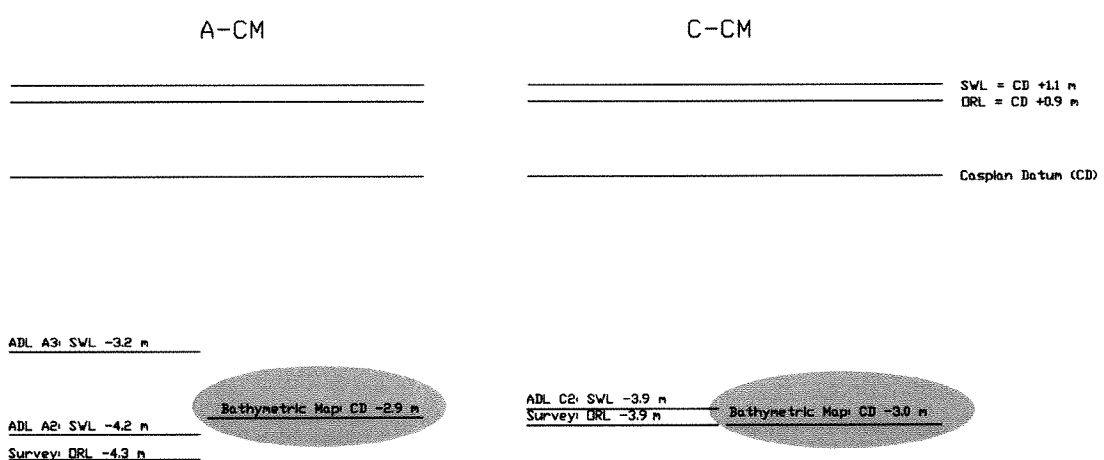
- 1 The survey data
The survey data states that the seabed at A-CM lies at ORL -4.3 m and the sea bed at C-CM lies at ORL -3.9 m. ORL is approximately CD +0.9 m (Agip KCO 2001).
- 2 The bathymetric map
According to the bathymetric map the seabed lies at CD -3.6 m at A-CM and CD -3.7 m at C-CM.
- 3 The burst pressure measurements
The instruments of ADL registered a depth of 4.2 m at A-CM in deployment A2, a depth of 3.2 m at A-CM in deployment A3, a depth of 3.9 m at C-CM in deployment C2 and a depth of 4.0 m in deployment C3. (These depths are obtained by averaging measured pressures and adding the distance between the sensor and the sea bed).
The depth in deployment A2 is very different from the depth in deployment A3. This is caused by the fact that the instrument was not reinstalled on exactly the same location after retrieving the data of deployment A2. This is not unlikely, as a handheld GPS was used during this operation (Arthur D. Little, 1999). After observing the survey maps, the depths as registered in deployment A2 seem more representative and reliable for location A-CM than the depths registered in deployment A3.

Figure 5.9. Comparison of depths from various sources



The inconsistency, as observed in Figure 5.8, does not seem to be caused by a local variation from the average depth in the grid cell. As stated earlier, the inconsistency can be caused by an error in the definition of the SWL period (1.1 meters above CD, as was deduced from Figure 2.8) or by an error in the definition of the reference level in the bathymetric map. The measurements of the SWL (Figure 2.8) appear more trustworthy than the reference level of the bathymetric map (knowing how much trouble was gone through to distil this bathymetric map from old Russian marine maps (see Appendix III) and realising how difficult it would be to make such a bathymetric map, compensating for the rapid changes in sea level due to surges, seasonal variations and long term variations). Based on the comparison in Figure 5.9, it was decided to reduce all depths of the bathymetric map with 70 centimetres (change highlighted in Figure 5.10).

Figure 5.10. Depths after change in bathymetric map



The surges had to be recalculated, due to the changes to the bathymetric map. The autocalibration of the Delft3D model, using PEST, actually reached a better match with the measured water levels (in terms of the Root Mean Square Errors). This increased confidence that the old map might have been incorrect.

It is decided to calibrate SWAN for one of these locations, as the measured wave spectra in A-CM and C-CM do not differ much. Location C-CM is chosen. The measured depth at this location best matches the bathymetric map. Furthermore this instrument was not moved during the campaign, making this dataset more consistent.

5.6 Numerical issues

5.6.1 Frequency domain

The computational frequency domain has to comply with two rules:

$$1. \frac{\Delta f}{f} = \left(\frac{f_{high}}{f_{low}} \right)^{\frac{1}{msc}} \leq 1.1 \quad 5.3$$

Van Thiel de Vries (2003) applied the following frequency domain:

- $f_{high} = 1$
- $f_{low} = 0.15$
- $msc = 30$ (number of frequency bins)

Therefore $\frac{\Delta f}{f} = 1.0653$. This rule is complied with.

$$2. f_{high} \cdot T_p > 1.5 \quad 5.4$$

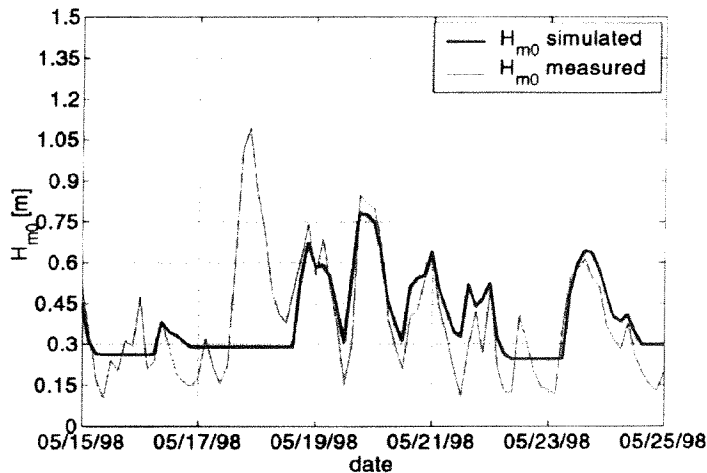
T_p during the calibration time series was never smaller than 2 seconds. Therefore this rule also is complied with.

More about the sensitivity to changes in the frequency domain can be found in Section 7.3.4.

5.6.2 Convergence of the matrix solver

A run of SWAN with default options shows a problem already recognised by Van Thiel de Vries (2003) (Figure 5.11). A lower limit of the significant wave height is observed. This was caused by the non-convergence of the matrix solver in SWAN. The spectrum of the preceding time step then is repeated as output for the next timestep. This problem was solved by setting the tolerance variable `eps1` of the BiCGSTAB solver to 0 instead of the default value `1e-6`. This was set in the SWAN command `NUMERIC`.

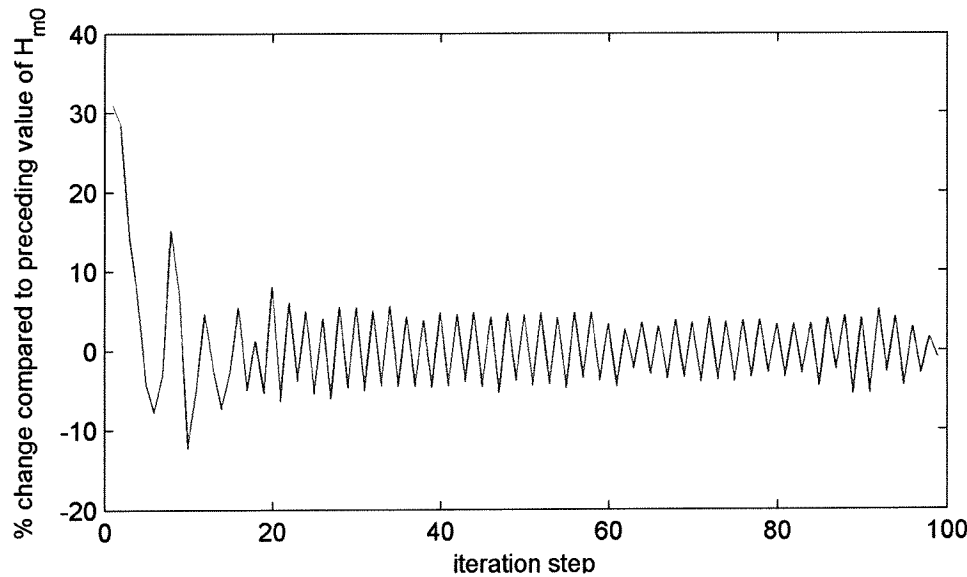
Figure 5.11. No convergence in solver causing minimum H_{m0} (Van Thiel de Vries, 2003)



5.6.3 Wiggles in convergence behaviour

With default options SWAN needs a lot of iteration steps for every time step (often equal to the maximum number of iterations allowed), in particular in cases with relatively small wave heights. For this reason the convergence behaviour of SWAN was studied by plotting the development of H_{m0} against the iteration number (Figure 5.12). It can be observed that when SWAN converges, it keeps on wiggling for some time. The convergence criteria (set in the SWAN command NUMERIC) seem to be too strict (default: $drel = dH = dT = 0.02$), because the wiggles are of an order 5 %. By changing the convergence criteria to $drel = dH = dT = 0.05$, the simulations are broken off sooner, without influencing the results significantly.

Figure 5.12. Convergence behaviour



The sensitivity of SWAN's output to changes in this setting will be discussed in Section 7.

5.7 Summary

The SWAN model of the Caspian Sea, formulated by Van Thiel de Vries (2003), has been used as a base model for this project. The same computational domain, frequency domain, and time domain were applied.

An attempt was made to use the NCEP wind data as wind input for a default configured SWAN model. The resulting simulated significant wave heights were very different from the measured significant wave heights. The uncertainty around the NCEP wind data appears to be greater than what is acceptable for a calibration of the SWAN model. The NCEP wind data is rejected, thereby also rejecting a great part of the available wave measurements, as the alternative ADL wind dataset does not contain simultaneous wind measurements for every available measured wave spectrum.

Spatially defined wind-driven surges were calculated with a Delft3D model, which was auto-calibrated on locally measured surges. After a test run with SWAN, an inconsistency was found. The total depths at Kashagan East and Aktote, as calculated by SWAN through the addition of surge levels and the depths, as defined in the bathymetric map, were very different from the total depths measured with the pressure transducers. A comparison with the available survey data resulted in the decision to raise the bathymetric map by 70 cm. The fact that this new bathymetric map resulted in a better auto-calibration of the Delft3D model increased confidence in this new map.

Finally, two numerical settings were changed:

- 1 The lower tolerance variable applied by the BiCGSTAB matrix solver was set to 0, in order to make sure that the matrix solver always converges.
- 2 The convergence criteria of the SWAN model were relaxed. The presence of strong wiggles in the convergence behaviour prevented the convergence criteria to be met, although the model was already acceptably converged. This resulted in unacceptably large computational times.

6 CALIBRATION AND VALIDATION OF THE SWAN MODEL

6.1 Introduction

In this Section the configuration of the SWAN model of the Caspian Sea is sought which best reproduces the wave spectra measured in the northern part of the Caspian Sea. First a calibration strategy is defined. Then, time series of wave measurements are selected containing characteristic wave conditions. The calibration comprises of the choice for certain source term expressions and their coefficients. Finally, the calibration is validated by inter-comparing model results and observations.

6.2 Calibration method

6.2.1 Limiting factors on the calibration strategy

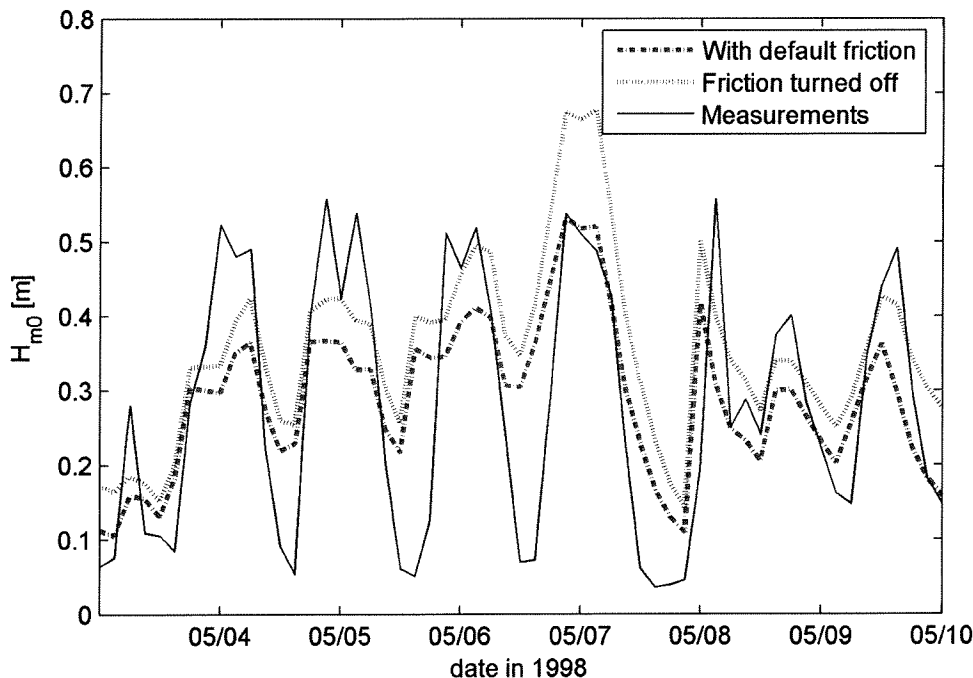
The calibration of the SWAN model involves the tuning of the six source terms. An ideal path of calibration was developed at the start of this study. This ideal path however appeared to be impossible to follow, as the measurements do not contain time series with the needed characteristics:

- a Swell can have a strong influence on whitecapping (Alkyon, 2002; Booij and Holthuijsen, 2002). The measurements, however, do not contain swell waves (proven in Section 4.3). Therefore the model cannot be calibrated to predict the influence of swell on whitecapping.
- b An ideal method to calibrate for whitecapping would use a time series characterised by deep water conditions and no wind, but with an initial wave energy content. The use of an exact quadruplets method would then imply that a calibration on the energy contents of the spectrum would be solely dependent on the tuning of the whitecapping source terms. A numerical aspect, however, causes this strategy to be impossible. Quadruplets cannot be calculated for situations without wind. When calculating quadruplets, a limiter is active. This limiter causes a decrease of the total amount of energy, which is not justified by a physical process, but caused by a numerical cause. The effect of this limiter is acceptable, when the wind input source term is active simultaneously.
- c Deep water source terms can best be calibrated on time series with deep water conditions, as the shallow water source terms do not play an important role in these time series. Deep water conditions can be scanned for by searching for measurements with d/L_{op} greater than 0.5. The plots in Appendix IV show that no measured time series exists with prevailing deep water conditions. Figure 6.1 shows two SWAN hindcasts of a time series with as deep as available conditions: one hindcast with default bottom friction and one with friction turned off. The results of these runs would have been equal, if the time series would have been sufficiently deep for the purpose of calibration of deep water source terms without the influence of shallow water source terms.
- d Triads only play a role, if the Ursell number (expression 6.1) is smaller than 0.02. Measurements with Ursell numbers smaller than 0.02, however, are almost non-existent. This can be observed in Appendix III. Triads therefore do not play an important role on the Caspian Sea and can not be calibrated for.

$$Ursell = \frac{g}{8\sqrt{2}\pi^2} \frac{H_s \bar{T}^2}{d^2} \quad 6.1$$

- e The maximum fraction of breaking waves observed in the measurements is very small (8.6e-5; calculated in Section 4.3). This is expected to be insufficient for a calibration of the source terms for depth-induced wave breaking.

Figure 6.1. Comparison calculations with and without friction for "deep" water conditions



6.2.2 Selection of timeseries

The used calibration strategy needed the selection of two time series. These were selected, using the plots of Appendix IV. The plots in Appendix IV, however, were created using the NCEP wind data. As the NCEP wind data was rejected for usage in the calibration phase (Section 5), only plots IV.1 and IV.2 could be used. The ADL wind dataset does not contain wind measurements for the period of July to September 1998. The following two time series were selected:

- Deep water time series:
The first time series contains records of the wave spectra measured between 4 May 1998 0:00 and 10 May 1998 0:00. During this period the wave heights did not reach very high values (the maximum H_{m0} was 0.6 m). d/L_{0p} did not reach values smaller than 0.36 and Ursell did not reach values greater than 0.02. As such this time series represents relatively deep water conditions.
- Shallow water time series:
The second time series contains records of the wave spectra measured between 15 May 1998 0:00 and 21 May 1998 0:00. During this time series the spectra contain more wave energy. This time series thus represents the more shallow conditions.

These time series have a length of six days, because:

- A simulation period of six days results in a sufficient amount of wave spectra, usable for comparison with the measured spectra.
- The model is expected to have a spin-up time, which is sufficiently small compared to the length of the simulated timeframe. Of the first day of the time series no output was generated. This first day is expected to cover the spin-up behaviour of the model.
- Longer time series would result in unacceptably large computational times per calibration run.
- A sufficient amount of measurements should be left over for the validation of the model.

6.2.3 The calibration procedure

The source terms were calibrated in the following order, so that a good configuration could be obtained with a small number of SWAN runs:

- Wind input

The addition by wind of wave energy to the wave spectra is important during both deep water and shallow water conditions. SWAN runs with various wind formulations have been performed for both the shallow and the deep water time series. Shallow situations need to be modelled most accurately, as the focus of the study is on the more extreme conditions with higher waves. Therefore an optimal setting for the shallow water conditions is preferred, in case the optimum setting for wind differs for deep and shallow water conditions.
- Bottom friction

Bottom friction is configured next, as it already plays a small role in the deep water time series (see Figure 6.1). Bottom friction is in practice a closure term during calibration of SWAN models and is used to get the total energy in the spectra at the correct level. Therefore the comparison is mostly focussed on the significant wave heights H_{m0} . Runs for both the deep water and the shallow water time series were made. The result for the shallow water time series was again considered most important.
- Whitecapping and quadruplet interactions

The remaining deep water source terms, whitecapping and the quadruplet interactions, are configured next. These also are calibrated with both the shallow water time series and the deep water time series.
- Depth induced wave breaking

If at all, depth induced wave breaking will only play a role in the shallow water time series.
- Triads

Triads are expected not to play a significant role. As discussed in Section 6.2.1, the Ursell numbers (expression 6.1) in the measurements mostly stay below 0.02. By default triads are turned off in SWAN. When turned on, they are only calculated if the Ursell number is between 0.1 and 10. A SWAN run was made to test whether triads are relevant in this study.

6.2.4 Definition of spectral moments

The measurements taken at A-CM and C-CM are directionally-integrated (1D) spectra. These spectra and their moments will be used for comparison with the results of the SWAN hindcasts, which are directional (2D) spectra and should therefore be integrated over the directional domain.

Spectral shapes can be described by spectral moments, defined as

$$m_n = \int_0^{\infty} f^n E(f) df \quad 6.2$$

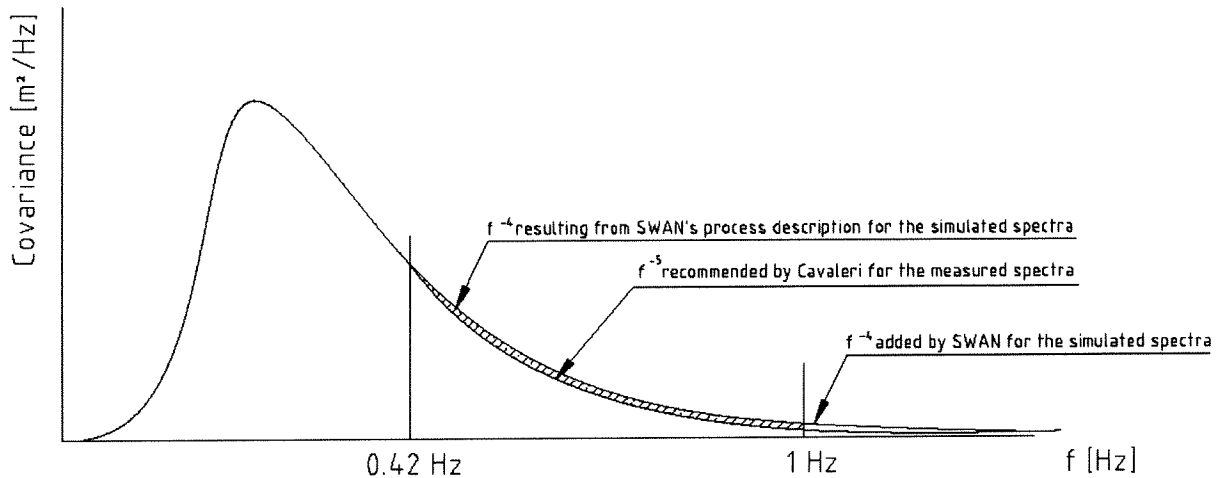
Spectral moments m_{-4} , m_{-3} , m_{-2} and m_{-1} are mostly influenced by the shape of the low frequency side of the spectra; spectral moments m_1 , m_2 , m_3 and m_4 by the high frequency side of the spectrum. m_0 is a measure for the total amount of wave energy in a spectrum. These spectral moments are valuable parameters for a comparison.

The following issues played a role when deciding how to calculate the spectral moments (illustrated in Figure 6.2):

- 1 In Section 3, the burst pressure measurements have been converted by means of a Fourier Analysis to a pressure variations spectrum. This pressure spectrum had to be converted to a wave spectrum through a multiplication with a gain correction factor. This gain correction factor was cut-off at a frequency of 0.42 Hz, as at higher frequencies the signal-to-noise ratio becomes too great. Therefore, the measured spectra were only truly based on the burst pressure measurements for frequencies between 0 and 0.42 Hz.
- 2 A f^5 tail was added to these measured spectra, starting from 0.42 Hz. Some controversy exists on, whether a f^4 tail or a f^5 tail should be added (McKee, 2002; Cavaleri, 1980). However, in a personal communication Cavaleri (2004) recommended to use a f^5 tail for this particular case.
- 3 The computational frequency domain, used in SWAN, had an upper limit of 1 Hz. Spectral output of SWAN was therefore not obtained for frequencies higher than 1 Hz.

- 4 The physical process descriptions in SWAN have been defined such that the high frequency tail of the spectrum approaches a f^{-4} tail.
- 5 SWAN adds a theoretical f^{-4} tail to the high frequency side of the upper limit of the computational frequency domain (1 Hz in this particular case), when calculating integral wave parameters.
- 6 For the calculation of spectral moments it is decided to apply a domain of 0 to 1 Hz. At frequencies higher than 1 Hz both SWAN and the measurements use an assumed parametric tail. The difference in wave energy under these tails (at frequencies greater than 1 Hz) is small. However, in particular, when calculating higher order spectral moments, the multiplication by f^n might result in significant differences for frequencies greater than 1 Hz, as a result of these assumptions.
- 7 The differences, related to the difference in spectral tail shape for the frequencies between 0.42 Hz and 1 Hz, form an insignificant contribution to the computed spectral moments (hatched area in Figure 6.2) and are therefore not expected to influence the calibration process.
- 8 A frequency domain of 0 to 0.42 Hz for the calculation of the spectral moments (in which the measured spectra are fully defined by the burst pressure measurements) is too small and would result in a poor comparison.

Figure 6.2. Conflicting definitions of the spectral tail



Considering the argumentation stated above, it was decided to define the spectral moments up to the cut-off frequency of 1 Hz:

$$m_n = \int_0^1 f^n E(f) df \quad 6.3$$

6.2.5 Calibration criteria

The quality of a given calibration was assessed by evaluating the following output:

1 Graphs of the development in time of H_{m0} and T_{m01}

These parameters are frequently used in design formulae of constructions, such as breakwaters. A correct prediction of these parameters is important to Witteveen+Bos. The graphs will be used for visual inspection.

2 Scatterplots of the calculated spectral moments compared to the spectral moments of the measurements

Such plots are useful for a visual inspection of the accuracy of the calculated spectral moments. They can also show unexpected trends.

3 Tables of Root Mean Square Errors (RMSE) and biases of the spectral moments

The bias is the average difference between the measured (x) and the calculated (y) spectral moment, analytically described as:

$$BIAS = \frac{\sum (x - y)}{n} \quad 6.4$$

The RMSE is the root of the mean square of the difference between the measured (x) and the

calculated (y) spectral moments:

$$RMSE = \sqrt{\frac{\sum (x - y)^2}{n}} \quad 6.5$$

With these tables the performance of SWAN can be quantified and compared.

It is stated that if a SWAN run performs best for m_0 , it also performs best for H_{m0} , as these are related through. $H_{m0} = 4\sqrt{m_0}$

4 Plots of the 1D wave spectra and 1D source terms per time step (and as animations)

The 1D spectra and source terms, integrated over the wave directions, were plotted. Only 1D spectra were measured and can be compared with calculated 1D spectra. Source terms were not directly measured, but it is interesting to study the simulated source terms as they can give an indication of sources of uncertainty.

Plots of spectra on a double logarithmic scale give a better indication of SWAN's performance in describing the spectral shape, because these:

- result in less grassy shapes
- give a better representation of small amounts of energy
- clearly show the exponential decay in the spectral tail.

In the Appendices Report the spectra and source terms of some characteristic moments in the time series have been added.

5 Plots of the 2D-wave spectra and 2D source terms per time step (and as animations)

It can be interesting to study these plots, although 2D spectra and 2D source terms are not available as measurements. They give an indication of whether the results of the SWAN calculations are realistic. Furthermore the directional spreading of the calculated spectra is known to be a good indicator of SWAN's performance (the smaller the better).

In the Appendices Report the spectra and source terms of some characteristic moments in the time series have been added.

6 Plots of the development in time of the variance density at certain frequencies

Such plots can give an interesting insight in the performance of the SWAN model at certain frequencies of the spectrum. These plots will be used for a visual inspection.

In practice the choice was mostly based on the RMSEs and biases per spectral moment, combined with a visual inspection of the source terms and wave spectra.

6.2.6 Calibration runs

The following calibration scheme was used to calibrate SWAN for the northern part of the Caspian Sea (Table 6.1):

Table 6.1. Calibration scheme

Calibration on	Description of SWAN run	Name of run deep water series	Name of run shallow water series
Wind	Komen wind formulation (cfjon = 0.02) Janssen wind formulation (cfjon = 0.02) Yan wind formulation (cfjon = 0.02)	Som 001 Som 002 Som 003	Som 101 Som 102 Som 103
Bottom friction	cfjon=0.01 cfjon=0.04 cfjon=0.06	Som 004 Som 005 Som 006	Som 104 Som 105 Som 106
Whitecapping and quadruplets	whitecapping: cds2=1e-5; quadruplets: DIA whitecapping: cds2=5e-5; quadruplets: DIA whitecapping: delta=1; quadruplets: DIA whitecapping: delta=0.5; quadruplets: DIA whitecapping: CSM; quadruplets: DIA whitecapping: default; quadruplets: DIA; $\lambda=0.19$ whitecapping: default; quadruplets: MDIA whitecapping: default; quadruplets: XNL	Som 007 Som 008 Som 009 Som 010 Som 011 Som 012 Som 013	Som 107 Som 108 Som 109 Som 110 Som 111 Som 112 Som 113
Depth induced breaking	breaker coefficient = 0.6 breaker coefficient = 0.8 breaker coefficient = 0.9		Som 114 Som 115 Som 116 Som 117
Triads	Triads turned on		Som 118

Appendix V contains an example of an input file of the SWAN calculations (of a validation run; Som 201).

In the following subsections the calibration of the SWAN model will further be discussed per source term.

6.3 Calibration process

6.3.1 Generation by wind

The generation of wave energy by wind is described by the following formula:

$$S_{wind}(\sigma, \theta) = A + BE(\sigma, \theta) \quad 6.7$$

A is the linear growth term; B is the exponential growth term:

- A represents the wave growth caused by the shear stress, caused by wind blowing over the surface. This term only depends on the wind speed and therefore is linear.
- B is caused by the fact that the presence of waves results in over- and underpressures, when the wind blows over the surface. This term therefore depends on both the wind speed and the present wave heights (i.e. wave spectrum) and is exponential.

SWAN 40.31 contains three formulations for the wind source term. The differences lie in the description of growth rate B in the exponential growth term:

1. Komen et al 1984)	$B \sim \frac{U_*}{c_{ph}}$	6.8
2. Janssen (1991)	$B \sim \left(\frac{U_*}{c_{ph}} \right)^2$	6.9
3. Yan (1987)	$B \sim \frac{U_*}{c_{ph}}$ for low values of $\frac{U_*}{c_{ph}}$; $B \sim \left(\frac{U_*}{c_{ph}} \right)^2$ for high values of $\frac{U_*}{c_{ph}}$	6.10

The term by Yan is still under development at Delft University of Technology, but was included because it was expected to show improvement to the Komen formulation.

The Janssen formulation had some stability problems while being applied by Van Thiel de Vries (2003). In SWAN version 40.31 these problems have not been solved yet. As found by Van Thiel de Vries (2003) quite an effort had to be made in order to find water level files for the first two time steps of the runs, that would lead to stable simulations. This effort was successful, but the reason why these resulting water levels were stable while others were not, is still unclear. Clarification of this discrepancy is beyond the scope of this project.

During the calibration of the wind term all source terms were kept at their default formulations, except for the bottom friction source term. Bottom friction coefficient c_f was set to 0.02, as this is the value Van Thiel de Vries (2003) had chosen as the best value for the northern part of the Caspian Sea. This is much lower than default (0.06), but not completely unrealistic, because the bottom material of the North Caspian Sea is very fine ($D_{50} = 50 \mu\text{m}$) and no significant bed forms exist.

Six swan runs were made, in order to be able to choose one of these formulations (see Table 6.1). It was decided to focus on a comparison of H_{m0} of the SWAN runs and the measurements. Appendix VI and VII contain the relevant plots made for this comparison. From these plots the following conclusions were drawn:

- VI.1 Komen gives much better results for H_{m0} than Janssen for the deep water time series.
- VI.2 Komen and Yan perform similarly for the deep water time series.
- VII.1 On average Komen seems to perform better in hindcasting H_{m0} than Janssen for the shallow water time series (except for the last two days of the simulation).
- VII.2 For the shallow water time series Yan shows slightly greater values for H_{m0} than Komen. The Komen formulation resulted in the best fit.

The improvement to the Komen expression, introduced by Yan, did not lead to a better performance. Therefore the Yan formulation is not further analysed. It can be observed that the Komen formulation describes the wave heights better than the Janssen formulation for the deep water time series. For the shallow water time series, however, their performance is of a more comparable quality. Therefore a closer look is also given to the spectral moments. In Table 6.2 the biases and RMSEs of the spectral moments of the simulations compared with those of the measurements are presented. The best performing run for every spectral moment is highlighted. It can be observed that the biases and RMSEs for the runs using Komen's expression are smallest.

It is decided to use the Komen formulation to further calibrate the model. Both for the shallow as the deep water time series the Komen formulation gave the best results.

Table 6.2. bias and RMSE; calibration of S_{wind} (best results are highlighted)

		Deep water time series		Shallow water time series	
		Som 001: Komen	Som 002: Janssen	Som 101: Komen	Som 102: Janssen
bias	m_0	1.28E-03	5.11E-03	-2.70E-03	5.11E-03
	m_1	1.00E-05	1.85E-03	-1.49E-03	1.88E-03
	m_2	-3.40E-04	6.63E-04	-1.05E-03	6.67E-04
	m_3	-4.03E-04	2.22E-04	-8.37E-04	2.04E-04
	m_4	-3.85E-04	5.27E-05	-6.99E-04	2.22E-05
	m_{-1}	5.36E-03	1.43E-02	-6.92E-03	1.40E-02
	m_{-2}	1.80E-02	4.07E-02	-2.31E-02	3.97E-02
	m_{-3}	5.67E-02	1.18E-01	-8.64E-02	1.17E-01
	m_{-4}	1.75E-01	3.49E-01	-3.34E-01	3.64E-01
RMSE	m_0	6.19E-05	1.08E-04	9.16E-05	1.32E-04
	m_1	7.91E-06	1.50E-05	1.27E-05	1.32E-05
	m_2	1.42E-06	2.30E-06	3.23E-06	1.78E-06
	m_3	4.98E-07	4.05E-07	1.31E-06	3.20E-07
	m_4	2.69E-07	8.88E-08	7.35E-07	8.94E-08
	m_{-1}	5.33E-04	8.50E-04	1.10E-03	1.70E-03
	m_{-2}	4.84E-03	7.18E-03	1.70E-02	2.65E-02
	m_{-3}	4.64E-02	6.48E-02	3.00E-01	4.64E-01
	m_{-4}	4.67E-01	6.21E-01	5.71E+00	8.69E+00

Two other interesting conclusions can be drawn, when studying the plots and tables:

- 1 These calculations result in a different choice than made by Van Thiel de Vries (2003). He chose to use the Janssen source term. According to Van Thiel de Vries the Komen formulation overestimates the wind growth.
- 2 It is well known that SWAN estimates period measures inaccurately. This is suspected to be caused by the description of the quadruplet interactions by SWAN. The DIA (discrete interaction approximation) is not an exact solution of the three dimensional Boltzmann integral (see Section 6.3.3), which describes the physics of the quadruplets. However, where Van Thiel de Vries (2003) observed an error of approximately one second between the measured and simulated T_m , the plots resulting from these SWAN runs show a much smaller error.

Both these phenomena can be explained, by studying the gain correction factor. The wave parameters used by Van Thiel de Vries for his calibration were obtained using the ADL method (Section 3.3). In this method the wave spectra were obtained by multiplying the covariance spectra of the pressure variations with a gain correction factor, shaped as shown in Figure 3.3. All wave energy with a frequency greater than 0.42 Hz is reduced to zero, when using this method. This explains both phenomena:

- 1 The wave energy at frequencies greater than 0.42 Hz was not taken into account in the wave parameters used by Van Thiel de Vries. In practice this wave energy is not negligible. The true H_{mo} was greater. The Komen formulation therefore did not overestimate the wave heights, but the measured wave heights were underestimated.
- 2 If the wave energy at frequencies greater than 0.42 Hz had been taken account, the mean wave frequency f_m would have been greater and the mean wave period T_m would have been smaller. This implies that SWAN did not underestimate the mean wave periods, but that the inaccurate conversion method used by ADL had produced too great mean wave periods of the measured spectra.

It is emphasised that the wave periods calculated by SWAN still are not accurate. The problem is being actively researched at present. The quadruplet interactions influence the shape of the wave spectra, therefore influencing the mean wave periods.

6.3.2 Dissipation by bottom friction

The bottom friction coefficient c_{fj0} was $0.02 \text{ m}^2/\text{s}^3$ during the calibration runs for the wind source term. The default values are $0.06 \text{ m}^2/\text{s}^3$ for sea waves and $0.038 \text{ m}^2/\text{s}^3$ for swell waves. More SWAN runs were made using the Komen wind formulation and various bottom friction coefficients, in order to determine whether $0.02 \text{ m}^2/\text{s}^3$ is the best value. These runs were compared with the results of Som 001 and Som 101, where c_{fj0} was $0.02 \text{ m}^2/\text{s}^3$. The calibration of the bottom friction coefficient was used as a way to get the total amount of energy in the spectrum at a correct level. The influence of bottom friction is most felt by higher waves. The comparison was therefore mostly focussed on the amount of wave energy in the spectrum (H_{m0} and m_0) during the shallow water time series. The other spectral moments are of less importance for this comparison.

Appendix VIII and IX contain relevant plots made for this calibration step. From these plots the following conclusions can be drawn:

- VIII.1,2,3 The calibration on the deep water time series would suggest a slight preference for a c_{fj0} of $0.01 \text{ m}^2/\text{s}^3$. It must be stated however that the differences are very small and that it was decided to base the decision mostly on the shallow water time series.
- IX.1,2,3 On average the calibration run with a c_{fj0} of $0.04 \text{ m}^2/\text{s}^3$ seems to give the best results. For the last two days of the time series the energy levels seem best represented by a run with a c_{fj0} of $0.06 \text{ m}^2/\text{s}^3$. A lower value than $0.06 \text{ m}^2/\text{s}^3$ (default value) is, however, expected based on the fact that the sea bed material is very fine $D_{50} = 50 \mu\text{m}$) and that no significant bed forms exist.

In Table 6.3 the biases and RMSEs of the simulated spectral moments compared with the measured spectral moments are presented. The choice for a certain value of c_{fj0} was based on the comparison of the biases and RMSEs of m_0 for the shallow water time series.

Table 6.3. bias and RMSE; calibration of S_{fric} (best results for m_0 are highlighted)

		Deep water time series				Shallow water time series			
		Som 001: c_{fj0} 0.02	Som 004: c_{fj0} 0.01	Som 005: c_{fj0} 0.04	Som 006: c_{fj0} 0.01	Som 101: c_{fj0} 0.02	Som 104: c_{fj0} 0.01	Som 105: c_{fj0} 0.04	Som 106: c_{fj0} 0.06
bias	m_0	1.28E-03	4.07E-04	2.05E-03	2.59E-03	-2.70E-03	-5.75E-03	6.46E-04	2.62E-03
	m_1	1.00E-05	-3.04E-04	2.85E-04	4.94E-04	-1.49E-03	-2.37E-03	-4.74E-04	1.58E-04
	m_2	-3.40E-04	-4.69E-04	-2.32E-04	-1.44E-04	-1.05E-03	-1.33E-03	-7.08E-04	-4.84E-04
	m_3	-4.03E-04	-4.66E-04	-3.55E-04	-3.12E-04	-8.37E-04	-9.43E-04	-6.96E-04	-6.02E-04
	m_4	-3.85E-04	-4.22E-04	-3.59E-04	-3.34E-04	-6.99E-04	-7.51E-04	-6.27E-04	-5.80E-04
	m_{-1}	5.36E-03	2.77E-03	7.63E-03	9.16E-03	-6.92E-03	-1.83E-02	4.84E-03	1.14E-02
	m_{-2}	1.80E-02	9.95E-03	2.50E-02	2.94E-02	-2.31E-02	-6.71E-02	1.99E-02	4.26E-02
	m_{-3}	5.67E-02	3.08E-02	7.85E-02	9.17E-02	-8.64E-02	-2.62E-01	7.56E-02	1.56E-01
	m_{-4}	1.75E-01	9.03E-02	2.45E-01	2.85E-01	-3.34E-01	-1.05E+00	2.90E-01	5.84E-01
RMSE	m_0	6.19E-05	5.75E-05	6.83E-05	7.33E-05	9.16E-05	1.54E-04	1.15E-04	1.64E-04
	m_1	7.91E-06	7.84E-06	8.38E-06	8.86E-06	1.27E-05	1.98E-05	9.44E-06	1.10E-05
	m_2	1.42E-06	1.57E-06	1.37E-06	1.36E-06	3.23E-06	4.34E-06	2.20E-06	1.72E-06
	m_3	4.98E-07	5.69E-07	4.53E-07	4.27E-07	1.31E-06	1.58E-06	1.02E-06	8.41E-07
	m_4	2.69E-07	3.04E-07	2.46E-07	2.32E-07	7.35E-07	8.29E-07	6.18E-07	5.45E-07
	m_{-1}	5.33E-04	4.83E-04	5.97E-04	6.42E-04	1.10E-03	1.79E-03	1.88E-03	2.69E-03
	m_{-2}	4.84E-03	4.34E-03	5.47E-03	5.87E-03	1.70E-02	2.60E-02	3.32E-02	4.66E-02
	m_{-3}	4.64E-02	4.12E-02	5.25E-02	5.60E-02	3.00E-01	4.20E-01	6.16E-01	8.44E-01
	m_{-4}	4.67E-01	4.13E-01	5.28E-01	5.60E-01	5.71E+00	7.22E+00	1.19E+01	1.59E+01

The bias of m_0 would lead to a choice for a value of c_{fj0} of 0.04. The RMSE of m_0 would result in a choice for a c_{fj0} of $0.02 \text{ m}^2/\text{s}^3$, but the difference with the RMSE of the run with c_{fj0} of $0.04 \text{ m}^2/\text{s}^3$ is very small. Combined with the visual inspection of the plots of H_{m0} in time and keeping in mind the fine sea bed material and the absence of significant bed forms, it is decided to choose a c_{fj0} of $0.04 \text{ m}^2/\text{s}^3$.

6.3.3 Quadruplet interactions and dissipation by whitecapping

Quadruplets and whitecapping are the remaining deep water sources terms that need to be calibrated. They were configured simultaneously, because the influence of these source terms needs to be well balanced.

quadruplet interactions are resonant interactions between four waves. Wave energy is redistributed within the spectrum, transferring energy from the spectral peak towards the lower and the higher frequencies, without energy loss. Quadruplets can be described with the Boltzmann integral (Hasselmann, 1962):

$$\frac{\partial \eta_1}{\partial t} = \iiint G(\vec{k}_1, \vec{k}_2, \vec{k}_3, \vec{k}_4) \times \delta(\omega_1 + \omega_2 - \omega_3 - \omega_4) \times \delta(\vec{k}_1 + \vec{k}_2 - \vec{k}_3 - \vec{k}_4) \times [n_1 n_3 (n_4 - n_2) + n_2 n_4 (n_3 - n_1)] d\vec{k}_1 d\vec{k}_2 d\vec{k}_3 \quad 6.11$$

With:

- $n_i = n(\vec{k}_i)$ n is the action density at wave number k_i
- G G is a complicated coupling coefficient
- δ the delta functions ensure that the contributions to the integral only occur for quadruplets that satisfy the resonance conditions

Four methods have been developed to calculate this integral:

1 DIA	Discrete Interactions Approximation (Hasselmann and Hasselmann, 1981) Not accurate, but relatively inexpensive in CPU time (3 hours per calibration run in this project)
2 MDIA	Multiple Discrete Interaction Approximation (Hashimoto et al 2003) Not accurate, a little more expensive in CPU time than DIA
3 XNL	Developed by Van Vledder and Bottema (2003) Accurate, but required 150 times the CPU time of a DIA run
4 FD-RIAM	Developed by Hashimoto et al (2003) Accurate, but is said to require 1000 times the CPU time of a DIA run (not tested)

The XNL and FD-RIAM require such great amounts of CPU time that the final model should not make use of these methods. The added value of the model to Witteveen+Bos would then be reduced to a minimum. However, results using exact quadruplet calculations could be of interest when estimating the accuracy of a calibrated model using the DIA.

The **Whitecapping** source term is not very well understood. The formulation used in SWAN is based on the Hasselmann (1974) pulse-based model. The following expression, due to Günther et al (1972) is used:

$$S_{wcap}(\sigma, \theta) = C_{ds2} \left[(1 - \delta) + \delta \left(\frac{k}{\tilde{k}} \right)^n \left(\frac{\tilde{s}}{\tilde{s}_{PM}} \right)^p \times \tilde{\sigma} \frac{k}{\tilde{k}} E(\sigma, \theta) \right] \quad 6.12$$

The default configuration is:

C_{ds2}	= 2.36e-5
\tilde{S}_{PM}	= 3.02e-3 (average steepness of a Pierson Moskowitz spectrum)
δ	= 0
n	= 1
p	= 2

An alternative is the Cumulative Wave Steepness method (CSM) (Hurdle and Van Vledder, 2004). This method features an adaptation to expression 6.12 to yield better results for cases with swell. This method is not expected to increase SWAN's performance during this project, as swell is hardly present in the North of the Caspian Sea.

calibration of whitecapping

The total strength of the whitecapping source term is set with $cds2$ coefficient and will be tuned. The default value of exponent m of 2 is quite well accepted and will not be tuned. Delta will be tuned. Rogers et all (2002) found that they obtained rather accurate results by setting delta to 0.5. Furthermore they found that in some cases a value of delta = 1 can result in an even better performance of the model. More wave energy would then be dissipated at the high frequency end of the spectrum, resulting in a lower value of the peak wave frequency. Although physically incorrect this might compensate for the error introduced by the use of the DIA, as the DIA tends to produce too high peak frequencies.

calibration of quadruplets

The only parameter amenable to tuning in the DIA is λ . This coefficient describes how the wave frequencies of the interacting waves relate to each other. Hashimoto et al (2003) has expressed a preference for a value of $\lambda = 0.19$ instead of the default value $\lambda = 0.25$. Changes in the value of λ influence both the directional spreading and the strength of the energy transfers.

Also the MDIA (multiple DIA) is tested. This method, also developed by Hashimoto et al (2003), calculates with an increased number of interacting wave numbers (6 instead of 4). Finally also a run using the XNL method was made. In Table 6.1 the runs, used to configure whitecapping and the quadruplet interactions, are listed (Som 007 to 013 and Som 107 to 113).

results

The calibration of quadruplets and whitecapping is in a way a calibration of the spectral shape. The spectral shape can quantitatively be described by means of the higher order spectral moments. Therefore the tables of the biases and RMSEs of the simulated spectral moments compared with the measured spectral moments played a significant role in the decision making process.

Table 6.4 and Table 6.5 contain the biases and RMSEs of the spectral moments of the SWAN calibration runs. The top three values per spectral moment are highlighted. The XNL run was not included in Table 6.5, as will be discussed later.

From these tables the following conclusions were drawn:

- For the deep water time series Som 009 (delta =1) and Som 010 (delta =0.5) give the best results in terms of small biases and RMSEs of the spectral moments.
- For the shallow water time series Som 009 (delta = 1) and Som 111 (CSM) give the best results in terms of small biases and RMSEs of the spectral moments.
- The Cumulative Steepness Method obtained good results for the shallow water time series. For cases without swell, however, the CSM is supposed to yield results comparable to Komen et al (1984).
- The setting of delta = 1 is the only calibration run which performs well for both the shallow (Som 109) and the deep (Som 009) water time series. Based on these tables, a decision for delta = 1 would be most acceptable.

Table 6.4. bias and RMSE; calibration of S_{nl4} and S_{wcap} for the deep water time series
 (top three results are highlighted for every spectral moment)

		Deep water time series								
		Som 005: default	Som 007: cds2=1e-5	Som 008: cds2=5e-5	Som 009: delta=1	Som 010: delta=0.5	Som 011: CSM	Som 012: labda=0.19	Som 013: MDIA	
bias	m_0	2.04E-03	3.74E-03	6.76E-03	1.76E-03	1.73E-03	2.70E-03	3.58E-03	2.08E-03	
	m_1	2.85E-04	1.00E-03	2.45E-03	4.50E-04	3.22E-04	6.87E-04	7.76E-04	2.58E-04	
	m_2	-2.32E-04	1.06E-04	8.69E-04	2.10E-05	-1.08E-04	2.80E-05	-1.09E-04	-2.69E-04	
	m_3	-3.55E-04	-1.73E-04	2.72E-04	-1.11E-04	-2.22E-04	-1.75E-04	-3.58E-04	-3.89E-04	
	m_4	-3.59E-04	-2.46E-04	4.35E-05	-1.44E-04	-2.37E-04	-2.25E-04	-4.03E-04	-3.88E-04	
	m_{-1}	7.63E-03	1.20E-02	1.87E-02	5.69E-03	6.13E-03	8.73E-03	1.21E-02	7.95E-03	
	m_{-2}	2.50E-02	3.66E-02	5.25E-02	1.74E-02	1.96E-02	2.68E-02	3.79E-02	2.63E-02	
	m_{-3}	7.85E-02	1.11E-01	1.50E-01	5.28E-02	6.10E-02	8.12E-02	1.16E-01	8.36E-02	
	m_{-4}	2.45E-01	3.39E-01	4.38E-01	1.60E-01	1.89E-01	2.47E-01	3.53E-01	2.63E-01	
RMSE	m_0	6.83E-05	8.87E-05	1.49E-04	6.67E-05	6.62E-05	7.71E-05	8.58E-05	6.82E-05	
	m_1	8.38E-06	1.08E-05	2.05E-05	8.90E-06	8.56E-06	9.85E-06	9.83E-06	8.13E-06	
	m_2	1.37E-06	1.42E-06	3.01E-06	1.40E-06	1.36E-06	1.48E-06	1.35E-06	1.26E-06	
	m_3	4.53E-07	3.00E-07	4.73E-07	3.09E-07	3.49E-07	3.62E-07	4.68E-07	4.42E-07	
	m_4	2.46E-07	1.46E-07	8.53E-08	1.11E-07	1.52E-07	1.68E-07	3.02E-07	2.56E-07	
	m_{-1}	5.97E-04	7.54E-04	1.16E-03	5.53E-04	5.61E-04	6.49E-04	7.62E-04	6.04E-04	
	m_{-2}	5.47E-03	6.70E-03	9.57E-03	4.96E-03	5.08E-03	5.81E-03	6.92E-03	5.57E-03	
	m_{-3}	5.25E-02	6.24E-02	8.38E-02	4.74E-02	4.87E-02	5.49E-02	6.52E-02	5.38E-02	
	m_{-4}	5.28E-01	6.10E-01	7.77E-01	4.79E-01	4.93E-01	5.47E-01	6.41E-01	5.44E-01	

Table 6.5. bias and RMSE; calibration of S_{nl4} and S_{wcap} for the shallow water time series
 (top three results are highlighted for every spectral moment)

		Shallow water time series								
		Som 105: default	Som 107: cds2=1e-5	Som 108: cds2=5e-5	Som 109: delta=1	Som 110: delta=0.5	Som 111: CSM	Som 112: labda =0.19	Som 113: MDIA	
bias	m_0	6.46E-04	7.88E-03	1.32E-02	-4.24E-04	-8.59E-03	6.53E-04	4.76E-03	1.92E-03	
	m_1	-4.74E-04	2.31E-03	4.62E-03	1.29E-05	-3.31E-03	-2.48E-04	6.84E-04	-7.70E-05	
	m_2	-7.08E-04	5.23E-04	1.64E-03	-3.06E-06	-1.53E-03	-5.00E-04	-4.30E-04	-5.71E-04	
	m_3	-6.96E-04	-5.25E-05	5.63E-04	-5.76E-05	-8.65E-04	-5.35E-04	-6.75E-04	-6.40E-04	
	m_4	-6.27E-04	-2.31E-04	1.57E-04	-8.93E-05	-5.79E-04	-5.04E-04	-6.77E-04	-5.99E-04	
	m_{-1}	4.84E-03	2.57E-02	3.91E-02	-3.30E-03	-2.55E-02	3.43E-03	1.89E-02	9.22E-03	
	m_{-2}	1.99E-02	8.44E-02	1.20E-01	-1.71E-02	-8.26E-02	1.19E-02	6.80E-02	3.55E-02	
	m_{-3}	7.56E-02	2.85E-01	3.84E-01	-7.55E-02	-2.83E-01	3.87E-02	2.41E-01	1.32E-01	
	m_{-4}	2.90E-01	9.95E-01	1.28E+00	-3.09E-01	-1.01E+00	1.33E-01	8.70E-01	5.02E-01	
RMSE	m_0	1.15E-04	3.79E-04	6.16E-04	1.04E-04	3.77E-04	1.13E-04	1.94E-04	1.42E-04	
	m_1	9.44E-06	3.22E-05	6.14E-05	1.09E-05	4.93E-05	9.96E-06	1.13E-05	9.36E-06	
	m_2	2.20E-06	3.18E-06	7.43E-06	1.75E-06	8.59E-06	1.95E-06	1.51E-06	1.60E-06	
	m_3	1.02E-06	4.15E-07	1.09E-06	4.34E-07	2.12E-06	8.15E-07	9.78E-07	8.37E-07	
	m_4	6.18E-07	1.61E-07	1.93E-07	1.52E-07	7.45E-07	4.81E-07	7.16E-07	5.49E-07	
	m_{-1}	1.88E-03	5.10E-03	7.40E-03	1.35E-03	3.60E-03	1.70E-03	3.27E-03	2.38E-03	
	m_{-2}	3.32E-02	7.70E-02	1.02E-01	2.10E-02	4.05E-02	2.86E-02	5.66E-02	4.19E-02	
	m_{-3}	6.16E-01	1.26E+00	1.57E+00	3.68E-01	5.11E-01	5.18E-01	1.01E+00	7.71E-01	
	m_{-4}	1.19E+01	2.20E+01	2.61E+01	6.94E+00	7.04E+00	9.89E+00	1.87E+01	1.47E+01	

It was decided to further analyse the runs which used the following settings:

- 1 Som 009 and Som 109: delta =1.
- 2 Som 010 and Som 110: delta = 0.5.
- 3 Som 011 and Som 111: CSM.
- 3 Som 114: XNL.

Appendices X (deep water time series) and XI (shallow water time series) contain the plots, as used for the decision making process, of these four types of runs. From these plots the following conclusions were drawn:

- X.1,2,3 The differences between the runs, concerning the simulation of H_{m0} , are very small. With respect to T_{m01} , however, a decision to choose Som 009 (delta = 1) would be best.
- X.4,5,6 These plots show the variations in time of the amounts of wave energy at certain frequencies. Som 009 results in the best match with the measurements.
- X.7 to 12 These plots show the 2D-wave spectra, 1D spectra and 1D source terms. Again Som 009 gives the best results. More conclusions can be drawn on these figures:
 - Som 009 results in the smallest directional spreading, which often is described as a good indicator for the performance of a setting;
 - in the plots of the 1D spectra it can clearly be seen that the simulated spectra have a different shape of the spectral tail than the measured spectra. This was expected. The process descriptions in SWAN are programmed to approach a f^4 tail, while during the conversion of burst pressure measurements to wave spectra, a f^5 tail was added, as recommended by Cavalieri. More about this can be found in Section 6.2.4;
 - in plots X.7, 9 and 11 it can be seen that a small amount of wave energy is present at a direction, much different from the average direction of the spectrum. This can be explained by the fact that the wind direction had probably changed, relative to the preceding time step. Calculations, using smaller time steps, are expected not to show such results. The amount of wave energy, however, in this direction was very small and is not expected to have influenced the calibration process (proven in Section 7).
- X1.1,2,3 Again the differences regarding the simulation of H_{m0} are very small. With respect to T_{m01} Som 109 seems to give an overprediction on part of the time series. On average, however, the results are good.
- X.4 The XNL, which was expected to give good results being an exact method for quadruplets, didn't perform well at all.
- X.5 to 8 The results of these plots shows a smaller accuracy than the same plots for the deep water time series. No reliable decision to choose one setting above the other could be made, based on these plots.
- X.9 to 14 The plotted spectra for the time steps chosen to plot would result in a decision for Som 109 (delta = 1).
- X.15 to 18 The XNL resulted in a completely erratic directional distribution of energy. The 2D source terms were plotted to analyse these results. The XNL seems to spread wave energy to all directions. The spectrum therefore also contains energy in all directions. This triggers white-capping in every direction as well.

Summarising and concluding, the following can be stated:

- It is not needed to change the default value of $cds2 = 2.35e-5$ to another value. Both an increase and a decrease of this value decreased the model's performance.
- The Cumulative Steepness Method gave rather accurate results for the shallow water time series.
- A decrease of λ from 0.25 to 0.19, as suggested by Hashimoto et al (2003), did not increase the accuracy of the model.
- The XNL resulted in an unrealistic directional spreading. The plots of the 2D-quadruplets source term in Appendices X.15 to X.18 illustrate this. It is beyond the scope of this project to further investigate the causes of these errors.
- An increase of delta from 0 to 1 increases the model's performance. Rogers et al (2002) also observed this. With this configuration more wave energy is dissipated at higher frequencies, resulting

in an increased accuracy of SWAN's results for T_m . Whether this is a compensation of the malperformance of the DIA or in true correspondence with what physically occurs, could not be concluded.

- SWAN is designed to result in a high frequency tail of f^4 , while during the conversion of burst pressure measurements to wave spectra a f^5 tail was added, as recommended by Cavalieri in a personal communication (2004). Therefore the results of the simulations don't seem very good for higher frequencies, but such a conclusion can not be justified.

Based on the tables and plots, it was decided to choose the following settings:

- Whitecapping: default, except that $\delta = 1$;
- Quadruplets: default DIA.

6.3.4 Depth induced wave breaking

In the measurements no values of H_{m0}/d are found greater than 0.36. This value corresponded with a very small breaker fraction Q_b (8.6e-5). It was expected to be difficult to calibrate SWAN for this source term, as the most extreme conditions represented in the measurements are not very extreme at all.

SWAN runs were made with breaker parameter ($\gamma = H_{max}/d$) values of 0.6, 0.8 and 0.9 (Som 115, Som 116 and Som 118, runs for the shallow water time series only). The default values is 0.73. The differences between these SWAN runs are very small (Table 6.6). In Appendix XII a plot was added of a rare example of a time step in which the variation of the breaker coefficient made a difference (S_{surf} is the source term of depth-induced wave breaking). The error bandwidth around the hindcasted values (caused by the many uncertainties and schematisations in the model and the error bandwidth of the measurements) is greater than the differences between these calibration runs. A deviation from the default configuration of this source term ($\gamma = 0.73$) cannot be justified. In a personal communication Smale (2004) suggested that this default value actually should be higher. The uncertainty of this parameter is more extensively treated in Section 7.

Table 6.6. bias and RMSE; calibration of S_{surf} (best results are highlighted)

		Shallow water time series			
		Som 109: ($\gamma = 0.73$)	Som 115: ($\gamma = 0.6$)	Som 116: ($\gamma = 0.8$)	Som 117: ($\gamma = 0.9$)
bias	m_0	-4,24E-04	-4,57E-04	-4,20E-04	-5,12E-04
	m_1	1,29E-05	-2,57E-06	1,18E-05	-1,34E-05
	m_2	-3,06E-06	-9,92E-06	-4,56E-06	-1,22E-05
	m_3	-5,76E-05	-6,05E-05	-5,87E-05	-6,13E-05
	m_4	-8,93E-05	-9,05E-05	-9,00E-05	-9,12E-05
	m_{-1}	-3,30E-03	-3,37E-03	-3,28E-03	-3,63E-03
	m_{-2}	-1,71E-02	-1,72E-02	-1,70E-02	-1,84E-02
	m_{-3}	-7,55E-02	-7,57E-02	-7,52E-02	-8,10E-02
	m_{-4}	-3,09E-01	-3,09E-01	-3,07E-01	-3,32E-01
RMSE	m_0	1,04E-04	1,05E-04	1,06E-04	1,02E-04
	m_1	1,09E-05	1,10E-05	1,10E-05	1,08E-05
	m_2	1,75E-06	1,77E-06	1,77E-06	1,75E-06
	m_3	4,34E-07	4,41E-07	4,37E-07	4,41E-07
	m_4	1,52E-07	1,55E-07	1,52E-07	1,55E-07
	m_{-1}	1,35E-03	1,36E-03	1,36E-03	1,29E-03
	m_{-2}	2,10E-02	2,11E-02	2,12E-02	1,99E-02
	m_{-3}	3,68E-01	3,69E-01	3,70E-01	3,44E-01
	m_{-4}	6,94E+00	6,95E+00	6,96E+00	6,45E+00

6.3.5 Triads

By default, triads are turned off in SWAN. At the project site triads are not expected to play a significant role. This can be illustrated by the fact that the measured Ursell number (expression 6.1) rarely exceeded a value of 0.02 (Appendix IV). A SWAN run with triads turned on was made, to verify this assumption.

It can be seen that triads remain inactive during the whole run, when observing the triads source term of the SWAN run with triads turned on (Snl3 in Appendix XIII.2). The calculated spectra do not differ from the SWAN run with triads turned off. Therefore, triads may remain turned off in the final SWAN model of the northern part of the Caspian Sea. This is very fortunate, as triads are known to be not very well modelled by SWAN.

It is expected that also during extreme events triads will not play a significant role. These extreme events are characterised by greater depths, as these enable greater wave heights (waves are expected to be depth limited in design conditions). Although the wave heights and periods will increase, the Ursell number is not expected to be significantly greater, as the depths will be greater as well.

6.3.6 Final settings

The final settings obtained during the calibration process do not deviate much from the default SWAN settings. The deviations are:

- Bottom friction coefficient cfj0n was set to $0.04 \text{ m}^2/\text{s}^3$.
- Whitecapping coefficient delta was set to 1.

6.4 Validation

The model created in the preceding Section was calibrated on two time series. The deep water time series contained the measurements taken from 5 to 10 May 2004. The shallow water time series contained the measurements taken from 16 to 21 May 2004. To validate the model two validation runs were made on two other time series:

- Som 201: 22 May to 2 June 1998;
- Som 202: 2 June to 17 June 1998.

Both time series contain mixed deep and shallow water conditions. They were split for reasons of efficiency.

Table 6.7 presents the biases and RMSEs of the spectral components of Som 109 (the final calibration) and Som 201 and Som 202 (the validation runs). It appears the validation runs have performed even better than the final calibration run.

Plots were also made to analyse the results. These can be found in Appendices XIV and XV.

XIV.1 and XV.1 these plots show that the wave heights and periods are quite accurately modelled. The wave periods still show a slight underestimation, which is well-known to be caused by the DIA. The effect is, however, compensated relatively well by the setting of delta to 1.

XIV.2 and XV.2 these plots show rather accurate result for the simulation of wave energy at various frequencies through time. The results are significantly more accurate than during the final calibration run.

XIV.3 and XV.3 these scatterplots actually are a visual representation of the values presented in Table 6.7. The scatter is quite acceptable.

XIV.4-7 and XV.4-7 the spectra and source terms shown in these plots also show that the spectra have been rather well calculated. The source terms do not show any surprises.

Table 6.7. bias and RMSE; final calibration run compared with validation run

		Deep water time series		
		Som 109: calibration	Som 201: validation 1	Som 202: validation 2
bias	m_0	-4,24E-04	7,94E-04	5,52E-04
	m_1	1,29E-05	3,99E-05	5,17E-05
	m_2	-3,06E-06	-1,46E-04	-1,04E-04
	m_3	-5,76E-05	-1,76E-04	-1,42E-04
	m_4	-8,93E-05	-1,68E-04	-1,44E-04
	m_{-1}	-3,30E-03	3,61E-03	2,04E-03
	m_{-2}	-1,71E-02	1,40E-02	6,29E-03
	m_{-3}	-7,55E-02	5,29E-02	1,82E-02
	m_{-4}	-3,09E-01	2,02E-01	5,14E-02
RMSE	m_0	1,04E-04	4,89E-05	5,11E-05
	m_1	1,09E-05	6,75E-06	7,23E-06
	m_2	1,75E-06	1,31E-06	1,36E-06
	m_3	4,34E-07	3,63E-07	3,63E-07
	m_4	1,52E-07	1,42E-07	1,36E-07
	m_{-1}	1,35E-03	4,79E-04	4,48E-04
	m_{-2}	2,10E-02	5,86E-03	4,59E-03
	m_{-3}	3,68E-01	8,27E-02	5,28E-02
	m_{-4}	6,94E+00	1,28E+00	6,67E-01

6.5 Summary

A closer look at the available time series of measurements led to the conclusion that the time series are fairly limited. An ideal calibration path proved to be impossible to follow, mainly because all wave measurements represent transitional water depths. Only two time series need to be selected: one with relatively deep water depths and one with relatively shallow water depths.

In this Section the SWAN model of the Caspian Sea has been re-calibrated. The results of the calibration are as follows:

- 1 The Komen expression for wind input should be used. This result is different from that of Van Thiel de Vries (2003). This is mostly caused by the different conversion method, applied to transform the burst pressure measurements to wave spectra.
- 2 The bottom friction coefficient c_{fj0} is set to $0.04 \text{ m}^2/\text{s}^3$.
- 3 Whitecapping and quadruplets interactions were calibrated simultaneously (balanced). It was decided to apply a default configured DIA for quadruplets, combined with a setting of $\delta = 1$ in the whitecapping formulation. The setting of δ to 1 cannot be physically justified, but can be interpreted as a compensational measure for the errors caused by the use of the DIA.
- 4 The measurements did not contain sufficiently extreme events to calibrate the coefficient for depth induced wave breaking.
- 5 Triads were found not to play a role of significance on the Caspian Sea.

7 SENSITIVITY ANALYSIS

7.1 Introduction

The SWAN model of the Caspian Sea has been calibrated and validated to calculate the wave spectra at Kashagan East in the northern part of the Caspian Sea. In this Section an attempt is made to quantify the calibrated model's ability to determine the design values of the wave spectra. A Monte Carlo simulation and a linear regression analysis are used to determine which variables and coefficients cause the existing confidence limits around the SWAN output.

7.1.1 Sources of uncertainty

The flow chart in Figure 2.2, used to determine which data was needed to construct the model, can now be used to illustrate where uncertainties are introduced. The most important causes of uncertainties found in this model are listed below:

1. The measurements used to calibrate SWAN

The SWAN model was calibrated using measurements of wave spectra and wind. The wave spectra were obtained through burst pressure measurements. Uncertainties could be induced through:

a. Pressure measurements

- Uncertainties caused by characteristics of the instruments
- Uncertainties caused by the way the instruments were applied

b. Wind measurements

- Uncertainties caused by characteristics of the instruments
- Uncertainties caused by the way the instruments were applied

c. The conversion method of pressure measurements to wave spectra

— Non-linearities

The used conversion method assumes a linear behaviour of the waves. The measure of non-linearity determines the uncertainty induced through this assumption.

— Choice of conversion method

The various tested conversion methods mostly differ in the definition of the gain correction factor. An example is given by the fact that this study's calibration resulted in different settings than Van Thiel de Vries' project (2003), although the same raw wind data was used, but a different conversion method.

2. Physical input data of SWAN

a. Bathymetry

— Resolution

The used grid spacing of 10 km could induce an uncertainty if the depth variations within these grids are of significant importance to the output of the model.

— Accuracy

The bathymetric maps were once made, based on measurements of depth. Errors in these measurements and physical changes to the bathymetry, which have occurred since these measurements were carried out, can induce uncertainties in the bathymetric input. The fact that in this project the bathymetric map needed to be raised with 70 cm forms a good illustration for this source of uncertainty.

b. Surge data

The surges were calculated with Delft3D. The performance of this model determines the quality of the surge input data to SWAN. The performance of such flow simulations depends on:

- Quality of the local water level measurements, used for calibration of the Delft3D model.
- The accuracy delivered by the Delft3D model.

3. The description of physical processes in SWAN

a. Coefficients in the source term formulations

The formulations for the various source terms all contain certain coefficients, which a certain spreading around the default values. The spreading around the following coefficients is estimated to have the greatest impact on the uncertainty of the Caspian Sea model:

- S_{wind} : agrow
- S_{wcap} : cds2, delta
- S_{nl4} : cnl4
- S_{fric} : cfjon
- S_{surf} : gamma
- S_{nl3} : --

b. The question whether all relevant physical processes are modelled.

4. Numerical aspects of the SWAN model

- a. The computational domain in frequency and direction
- b. The convergence criteria
- c. The spatial resolution of the computational grid
- d. The time step of the non-stationary runs

7.1.2 Approach

This Section quantifies the uncertainties presented above and their impact on the SWAN model's performance when calculating the design waves.

The following strategy is applied:

1. The design storm is defined

Witteveen+Bos is interested in the wave spectra during design conditions. Therefore these design conditions first need to be defined (Section 7.2).

2. The numerical aspects of the SWAN model (no 4. in the list of sources of uncertainty) are studied

By varying certain parameters the sensitivity of the SWAN model to changes in these numerical parameters is studied (Section 7.3).

3. The description of physical processes in SWAN (no 3.) and the physical input data of SWAN (no 2.) are analysed

Probability density functions of various physical coefficients are defined, based on literature and communications with wind-wave experts. The physical input data for SWAN is also defined stochastically. SWAN calculations are then made, in which these physical coefficients are varied by drawing from their distributions. This provides an insight in the spreading of the resulting SWAN output. The relative importance of the various coefficients and their uncertainties are calculated (Section 7.4 and 7.5).

4. The model's performance is quantified

An attempt is made to quantify SWAN's ability to calculate the design wave spectra. The confidence limits of the calibrated model are defined (Section 7.6). The influence of uncertainties in wave or wind measurements (no 1.) on this calibration is discussed.

5. Recommendations for improvements of the model are made

Recommendations are made on how to decrease the confidence limits around the model's output (Section 7.7).

7.2 The design storm and the resulting waves

Witteveen+Bos designs offshore structures for the exploitation of the oil fields at Kashagan East, applying certain design values for the solicitation of the structures. These design values (i.e. of wave heights or wave periods) result from a certain design storm. The design storm, however, has never actually occurred during measuring campaigns of wind and waves. Through some statistical calculations a design storm is constructed. In this Section a study is made of the surges and waves resulting from this design storm. Finally, it is determined, whether the extreme wave spectra resulting from this storm can be modelled by a stationary SWAN run (saving much computational time).

7.2.1 Construction of the storm shape

Theoretically the most extreme wave heights at Kashagan East occur during a storm from the west-southwest (247.5 degrees). This wind direction combines the longest possible fetch with a maximum possible wind-driven surge. Measurements have confirmed this analysis.

The maximum possible wave height during such a storm depends on (amongst others):

- The Still Water Level (SWL)
- Probabilitas (2002) has done extensive research in order to determine the design SWL. During this project a design SWL of CD +2.4 meters is applied. This is derived from the 2043 mean sea Tmaximum wind speed during the storm

The design storm has a maximum wind speed of 30 m/s. This wind speed is expected to occur once every 10 years (Fugro, 2001).
- The development in time of the storm (further referred to as the shape of the storm)

Data on the shape of a design storm is not available. The NCEP database contains some storms, but none is even nearly as strong as the design storm would be. Fugro (2001) however has done extensive research on wind statistics. Tables, containing the monthly total of time in which a certain wind speed is continuously exceeded for at least a certain period of time, are available (Appendix XVI). These tables are summarized in Table 7.1, containing the yearly total of time during which a certain wind speed is continuously exceeded for at least a certain period of time.

Table 7.1. Duration per year of continuous wind speed exceedance during at least a certain time

Wind speed	Duration of continuous wind speed exceedance during at least a certain time											
	max	1	3	5	6	9	12	18	24	36	48	72
30	8760	0.1										
20	8760	21.6	3.1	1.5	1.3	0.5	0.3	0.3	0	0	0	0
15	8760	115.1	33.4	17.5	14.8	8.2	5.6	2.6	1.4	0.5	0	0
10	8760	569.9	165.2	87.4	68.2	38.1	22.4	10.8	6.4	2.2	1.6	0.3
5	8760	2543.6	720.1	376.3	298.2	170.6	108.3	49	27.3	12	6	2.4
												1.1

The column indicated by max contains the total number of hours in one year, which would be the number in every column for a zero wind speed. The row for wind speed 30 m/s was added. This row could be interpreted as follows: an exceedance of 30 m/s for a period of more than one hour occurs 0.1 hours every year (or once every 10 years). Through extrapolation (Figure 7.1) the duration of exceedance of the other wind speeds with a similar probability of occurrence was sought. The results are summarised in Table 7.2.

Figure 7.1. Occurrence of wind speed exceedance; extrapolation was made using this graph

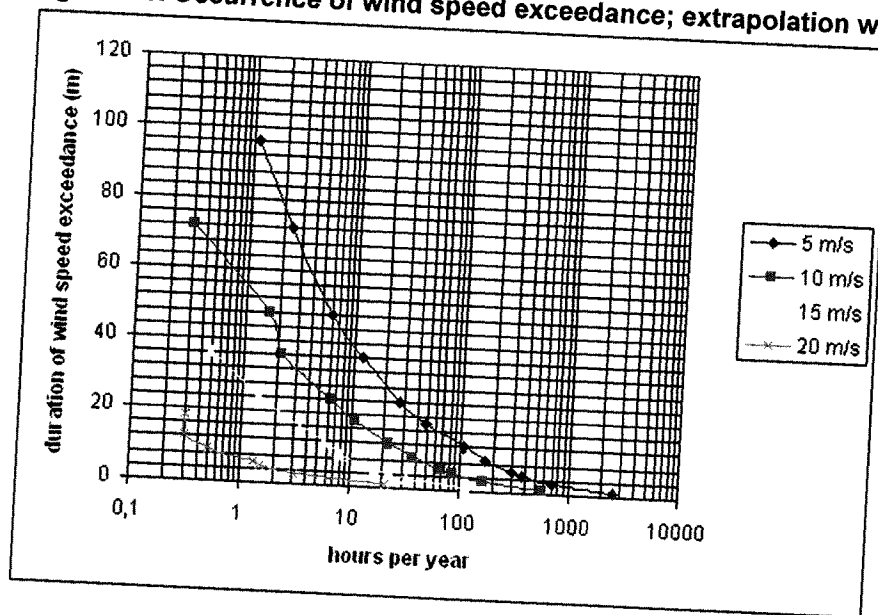
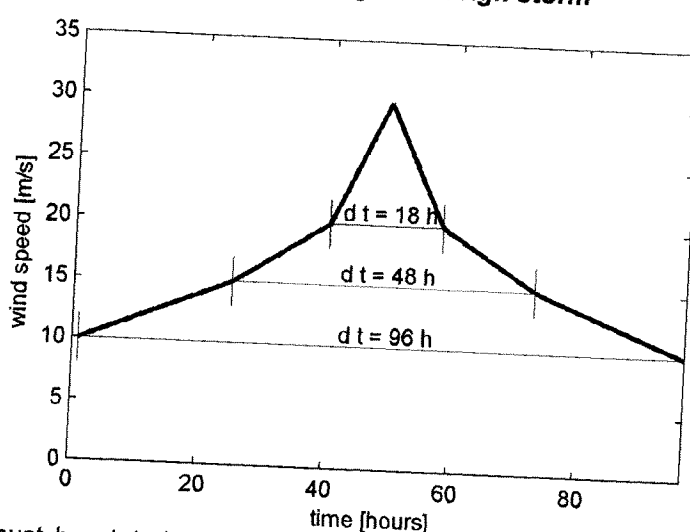


Table 7.2. Duration of continuous exceedance with an occurrence of once every 10 years (result of extrapolation)

Wind speed [m/s]	30	20	15	10
Duration of exceedance [hours]	1	18	48	96

It is assumed that the shape of the storm is symmetrical in time. The shape of the design storm can now be determined and is as is projected in Figure 7.2. The shape approaches a squared cosine shape, which is considered to be a reasonable approximation.

Figure 7.2. Wind speed during the design storm



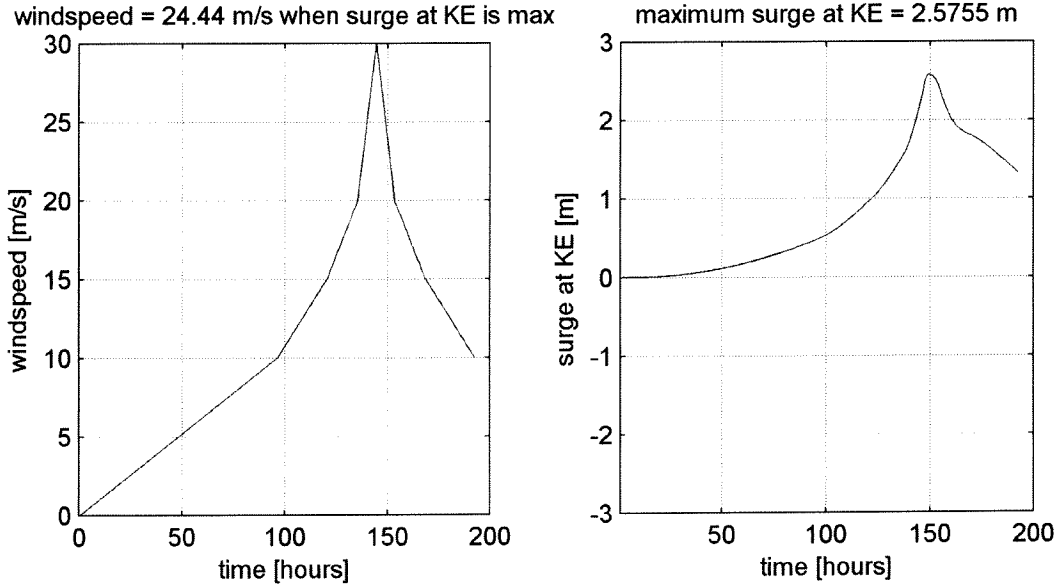
It must be stated that this schematisation is very rough. For the purpose of this study however this schematisation is considered adequate.

7.2.2 The resulting surges

The calibrated Delft3D model was used to determine the surges that will occur during a design storm. A time step of 15 minutes was applied for this calculation, which is smaller than the timescale of the changes of the surges (see Figure 2.3). The SWL was CD +2.4 m.

The resulting surges during the design storm at Kashagan East are plotted in Figure 7.3. The maximum surge at Kashagan East during a design storm is computed at 2.58 m.

Figure 7.3. Wind speeds and the resulting surges at Kashagan East during a design storm from WSW



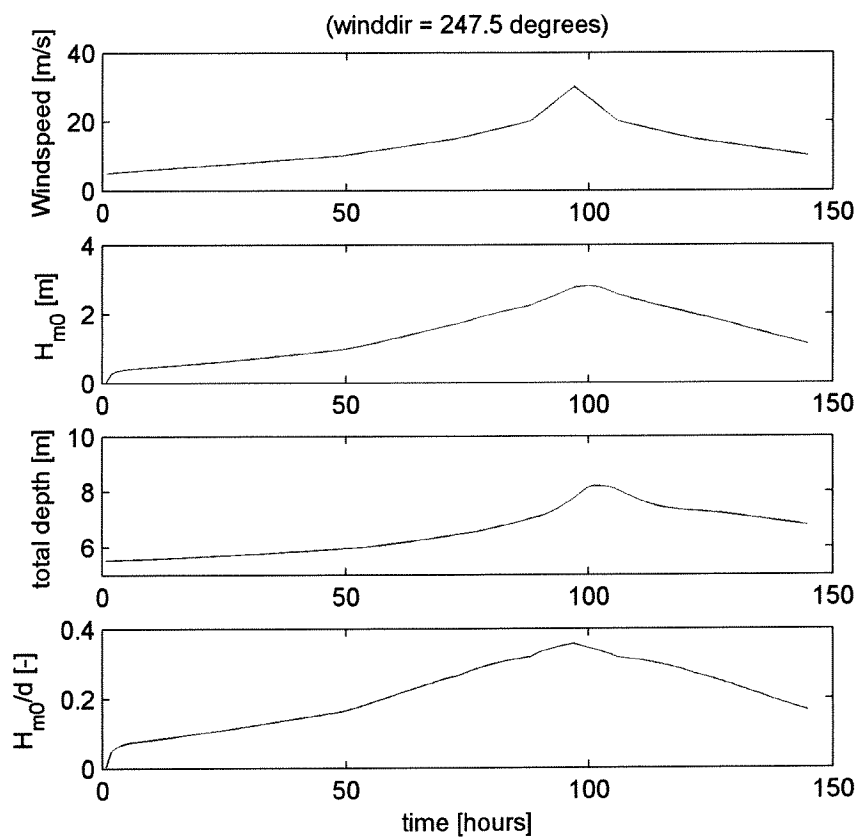
The maximum surge shows a time lag with the maximum wind speed, because surges need some time to react to changes in wind speed. When a certain wind speed has initiated the movement of the water mass, it will keep moving for some time even though the forcing by wind is already decreased.

7.2.3 The resulting waves

Wave heights (and their spectra) react much faster to variations in wind speed than wind-driven surges. Most probably the maximum wave height occurring during a design storm is depth-limited. Therefore it is expected that the greatest wave heights will not occur at the instant when the maximum wind speed occurs, but near the time when the maximum wind-driven surge occurs.

A non-stationary SWAN run, using the calibrated model with very strict convergence criteria and a time step of 1 hour, was made. The surges as calculated with Delft3D and the wind speeds of the design storm were used as input to the SWAN model. The resulting wave heights are presented in Figure 7.4. The maximum wave height occurs at a wind speed of 26.7 m/s, between the moment of maximum wind speed and the moment of maximum surge level. The surge at Kashagan East at that moment is 2.38 m.

Figure 7.4 H_{m0} , wind speed, depth and H_{m0}/d during design storm from WSW



7.2.4 Possibility to schematise as stationary

The situation at the moment when the maximum wave height occurs during a design storm can be modelled as stationary if the waves are depth-limited at that moment. This would very clearly be the case if the H_{m0}/d in Figure 7.4 is exactly horizontal for some time. This cannot sufficiently clearly be observed to draw a conclusion. The maximum value of H_{m0}/d appears to be 0.36 (Figure 7.4). It could not be concluded yet, whether the waves are sufficiently depth-limited.

Brettschneider curve

Brettschneider created a 1D parametric wave growth model. He formulated mathematical relations between dimensionless wind speed, dimensionless fetch and dimensionless significant wave height and peak period. These curves can be applied to simulate fetch-limited situations. Hurdle and Stive (1989) expanded the model to also be usable for the simulation of duration-limited situations. At Kashagan East during a design storm from the west-southwest the situation is much more likely to be duration limited, not fetch limited. The revised Brettschneider curve for duration limited storms can be described as follows:

$$\tilde{H}_s = 0.25 \tanh(0.6\tilde{d}^{0.75}) \sqrt{\tanh\left(\frac{4.3 \cdot 10^{-5} \left(\frac{\tilde{t}}{65.9}\right)^{1.5}}{(\tanh(0.6\tilde{d}^{0.75}))^2}\right)} \quad 7.1$$

with:

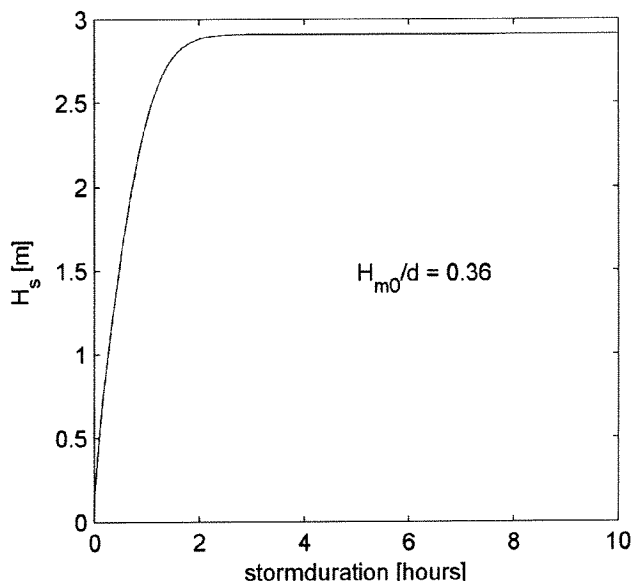
$$\tilde{d} = \frac{g}{U_A^2} d \quad 7.2$$

$$\tilde{t} = \frac{g}{U_A} t \quad 7.3$$

$$\tilde{H}_s = \frac{g}{U_A^2} H_s \quad 7.4$$

$$U_A = 0.71 \cdot (1.1 \cdot U_{10})^{1.23} \quad 7.5$$

Figure 7.5. Revised Brettschneider curve for Kashagan East



A plot of the curve (using the depth and wind speed of a design storm) is presented in Figure 7.5. Two conclusions can be drawn from this plot:

- Waves respond very fast to changes in wind speed
From the Brettschneider curve it can be concluded that waves will be fully grown in about 1.5 hours, if instantaneously a wind speed of 30 m/s blows over the Caspian Sea at Kashagan East. During a design storm the wind speed does not increase instantaneously from 0 m/s to 30 m/s, but increases gradually. Therefore it can be expected that the wave heights will react very quickly to the relatively small changes (compared to this instantaneous increase) during the design storm. This suggests that a stationary model can be used to simulate the maximum wave spectra during the design storm.
- The maximum H_m/d , according to the Brettschneider curve, is 0.36
This approximately equals the value SWAN reaches when simulating the design storm (Figure 7.4).

academic SWAN case: linearly increasing wind speed to 50 m/s

A SWAN run was made in which the wind speed was increased from 5 to 50 m/s at a rate of 1 m/s/hr. It must be noted that it can very well be doubted whether SWAN would still give reliable at high wind speeds for which it has not been calibrated. However, these plots were only made in order to find out at which wind speed waves start to be depth-limited, for which they were very useful. The results were plotted (Figure 7.6).

As from a wind speed of 20 m/s the wave heights appear to be very much depth-limited. H_{m0}/d again reaches value in the order of size of 0.4.

conclusion

It is concluded that the design conditions can be modelled reliably with stationary SWAN runs. The design wave spectrum will be calculated using a wind speed of 26.7 m/s coming from the west-southwest. The surges at this time are taken from the Delft3D simulation of the design storm and are plotted in Figure 7.7.

Figure 7.6. H_{m0} and H_{m0}/d during a linearly increasing storm (5-50 m/s)

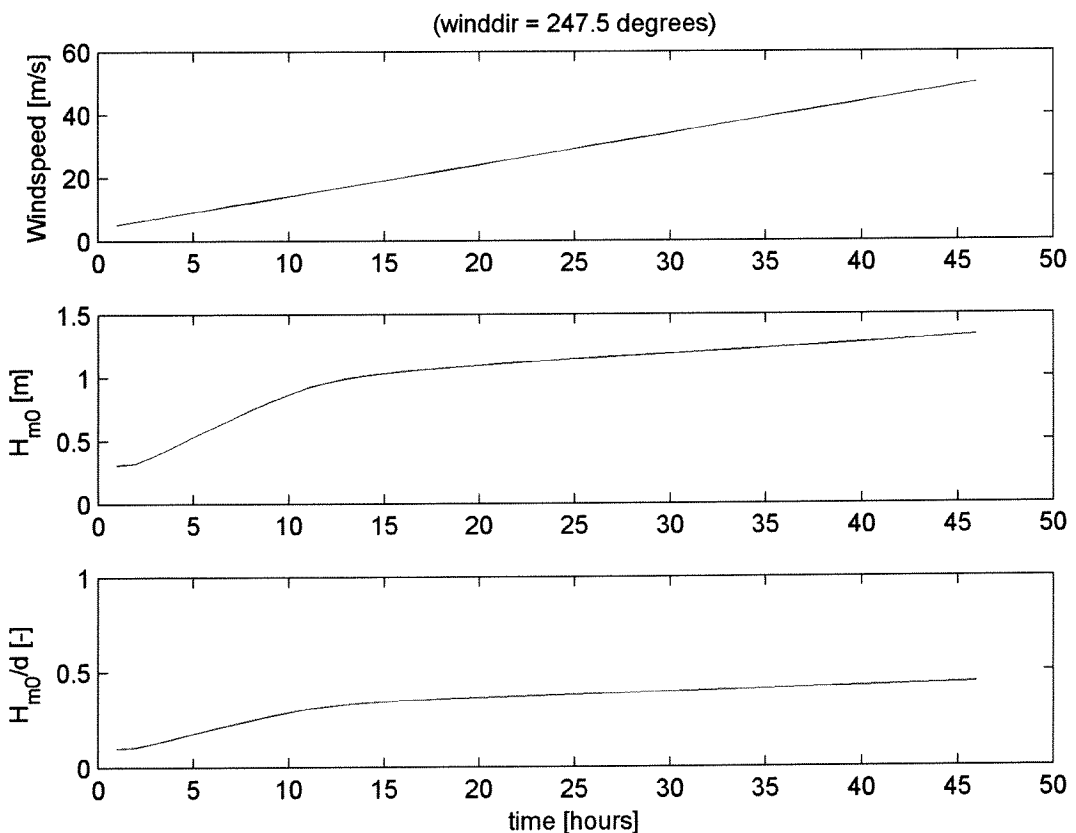


Figure 7.7. Surges during design storm, at the moment when the maximum wave height occurs

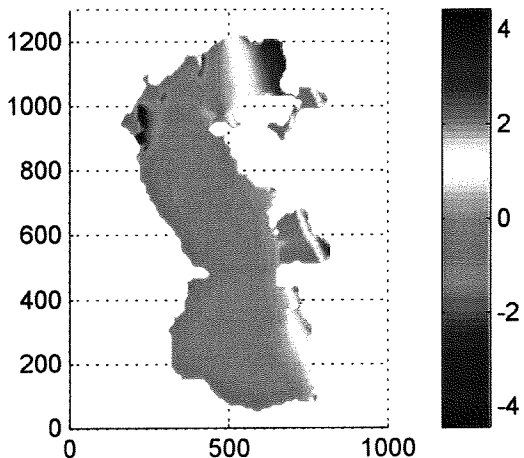
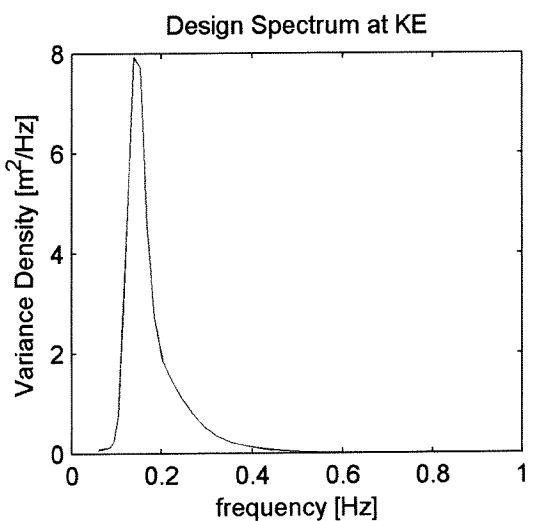


Figure 7.8. The design wave spectrum



7.2.5 Design wave spectrum, as calculated with the validated model

A stationary SWAN run was made with a wind speed of 26.7 m/s coming from the west-southwest and surge levels as presented in Figure 7.7. Very strict convergence criteria were applied, with the objective to reduce the influence of iterative behaviour. This run results in the highest waves occurring during a design storm, according to the validated model.

In Figure 7.8 the design wave spectrum is plotted. Some integral wave parameters interesting for design purposes, corresponding to this spectrum, are as follows:

- H_{m0} = 2.80 m significant wave height
- T_p = 5.46 s peak wave period
- T_{m02} = 5.03 s mean wave period defined as $\sqrt{m_0/m_2}$
- Q_b = 1.24e-4 fraction of broken waves
- L = 34.39 m average wave length

The maximum wave height resulting from this stationary run equals the maximum wave height obtained with the non-stationary run (Figure 7.4). This justifies the decision to apply stationary runs to calculate the design spectrum.

The maximum value of H_{m0}/d is approximately 0.36. During the analysis of the measurements in Section 4 this also was the maximum observed value. However, a timeseries in which such values occur more than once would have been necessary to properly calibrate the model for depth-induced wave breaking.

The confidence limits of these values are analysed in the following Sections.

7.3 Sensitivity to choices regarding numerics

In this Section the numerical settings of the SWAN model are further analysed.

7.3.1 Convergence criteria

The choice for certain convergence criteria during the calibration phase of the project was actually a trade-off between accuracy of the output and computational time. If ever production runs are made with the calibrated model, this consideration can be made again. The convergence criteria can then be set more or less strict. Most important, however, is to establish that the choice for the final calibration would not have been different if more strict convergence criteria would have been used.

Therefore a few calibration runs were performed again, with very strict convergence criteria (forcing 40 iterations for every timestep):

a. The calibration of the wind source term

During the calibration phase the Janssen expression for the wind source term did not perform sufficiently accurately. When using this expression the growth of the simulated spectra appeared to be too slow. During Van Thiel de Vries' study (2003) however this expression performed best. A too relaxed setting of the convergence criteria could have caused this. Therefore this calibration step was repeated with very strict criteria.

b. The calibration of quadruplet interactions and whitecapping

This calibration step influenced the final configuration of the SWAN model most. The choice for a certain configuration of these source terms was based on relatively small differences in the results of these runs. Therefore the four best performing configurations of these source terms, as during the calibration phase, were re-run. It can then be determined whether the same configuration would have been chosen, if very strict convergence criteria were used.

results

a. The calibration of the wind source term

Figure 7.9 shows that the application of more strict criteria does not result in a much better simulation of the wave growth. The decision to use the Komen expression during the rest of the calibration phase would not have been different if stricter convergence criteria were applied.

b. The calibration of quadruplet interactions and whitecapping

The best performing configurations for quadruplet interactions and whitecapping were the following:

1. Som 005 and 105: whitecapping: delta=0; quadruplets: DIA (the default configuration)
2. Som 009 and 109: whitecapping: delta=0.5; quadruplets: DIA
3. Som 010 and 110: whitecapping: delta=1; quadruplets: DIA (the chosen configuration)
4. Som 011 and 111: whitecapping: CSM; quadruplets: DIA

These calibration runs have been repeated with more strict criteria. Table 7.3 shows a comparison of these runs by means of biases and RMSEs. The spectral moments of the spectra, as calculated by SWAN, are compared with the spectral moments of the measured spectra. The comparison confirms that the configuration of Som 009 and 109 gives the best results.

Summarising, it can be stated that with more strict convergence criteria (needing more computational time) the same configuration of SWAN would have been chosen.

Figure 7.9. H_{m0} using Janssen with strict criteria, compared with H_{m0} of calibration run Som 002

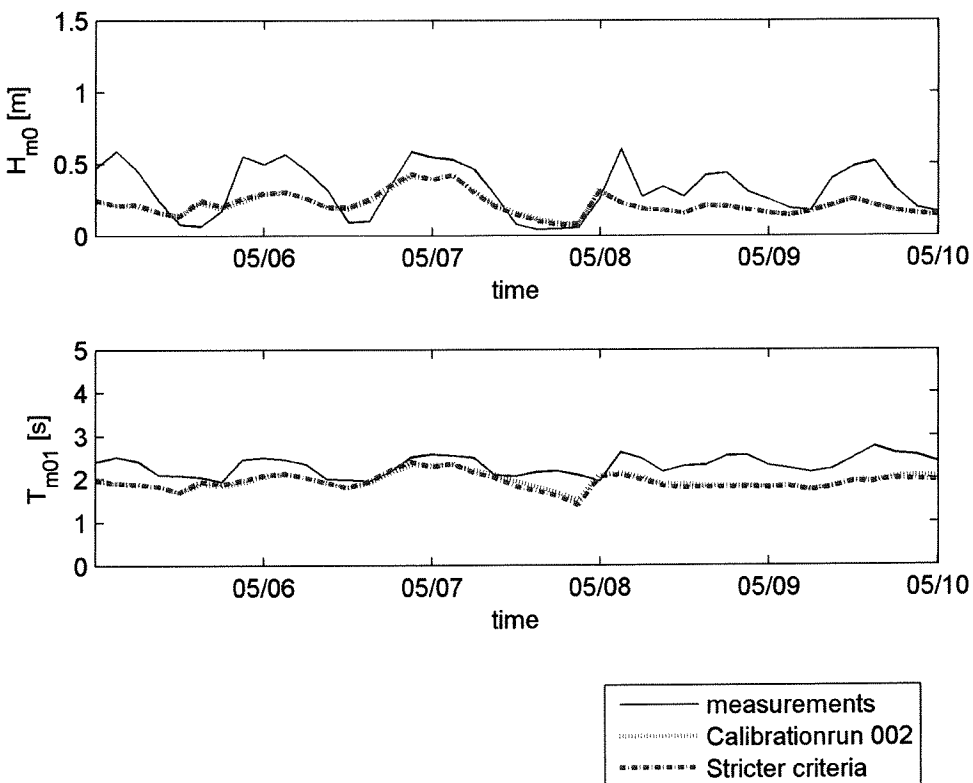


Table 7.3. bias and RMSE; S_{nl4} and S_{wcap} calibration with stricter convergence criteria
Best are highlighted (smallest biases and RMSEs)

		Deep water time series				Shallow water time series			
		Som 005: default	Som 009: Delta = 0.5	Som 010: Delta = 1	Som 011: CSM	Som 105: default	Som 109: Delta = 0.5	Som 110: Delta = 1	Som 111: CSM
bias	m_0	1.91E-03	1.49E-03	1.45E-03	2.48E-03	1.36E-04	-1.90E-03	-1.87E-03	-4.40E-04
	m_1	2.08E-04	3.45E-04	2.06E-04	5.83E-04	-6.71E-04	-3.51E-04	-6.81E-04	-5.88E-04
	m_2	-2.82E-04	-2.58E-05	-1.63E-04	-3.20E-05	-7.99E-04	-9.40E-05	-4.13E-04	-6.35E-04
	m_3	-3.90E-04	-1.35E-04	-2.52E-04	-2.15E-04	-7.47E-04	-7.91E-05	-3.37E-04	-6.06E-04
	m_4	-3.85E-04	-1.59E-04	-2.56E-04	-2.55E-04	-6.61E-04	-9.24E-05	-2.99E-04	-5.51E-04
	m_{-1}	7.35E-03	4.91E-03	5.33E-03	8.19E-03	3.31E-03	-9.44E-03	-7.16E-03	-6.06E-04
	m_{-2}	2.43E-02	1.50E-02	1.72E-02	2.52E-02	1.48E-02	-4.32E-02	-3.01E-02	-4.14E-03
	m_{-3}	7.67E-02	4.47E-02	5.33E-02	7.64E-02	5.67E-02	-1.88E-01	-1.27E-01	-2.69E-02
	m_{-4}	2.39E-01	1.32E-01	1.63E-01	2.32E-01	2.17E-01	-8.05E-01	-5.28E-01	-1.41E-01
	RMSE	6.79E-05	6.55E-05	6.49E-05	7.47E-05	1.05E-04	1.13E-04	1.09E-04	1.06E-04
	m_0	8.56E-06	8.79E-06	8.55E-06	9.54E-06	1.16E-05	1.12E-05	1.18E-05	1.26E-05
	m_1	1.54E-06	1.42E-06	1.45E-06	1.49E-06	3.10E-06	1.93E-06	2.10E-06	2.94E-06
	m_2	5.41E-07	3.30E-07	4.01E-07	4.01E-07	1.37E-06	4.94E-07	5.97E-07	1.19E-06
	m_3	2.93E-07	1.22E-07	1.76E-07	1.97E-07	7.99E-07	1.70E-07	2.53E-07	6.75E-07
	m_4	5.95E-04	5.45E-04	5.51E-04	6.34E-04	1.61E-03	1.73E-03	1.46E-03	1.36E-03
	m_{-1}	5.49E-03	4.92E-03	5.02E-03	5.71E-03	2.82E-02	3.09E-02	2.33E-02	2.11E-02
	m_{-2}	5.30E-02	4.74E-02	4.85E-02	5.43E-02	5.24E-01	5.81E-01	4.06E-01	3.63E-01
	m_{-3}	5.35E-01	4.81E-01	4.92E-01	5.43E-01	1.02E+01	1.12E+01	7.41E+00	6.65E+00
	m_{-4}								

7.3.2 Resolution of the spatial domain

The grid spacing of the computational grid was set at 10 km during the calibration phase. The influence of the size of the computational grid is expected to depend on the fetch length and therefore on the wind direction (Witteveen+Bos, 2004). In particular during northerly winds this grid spacing would imply that Kashagan East would be located at only 4 grid cells from the coast. The sensitivity of the model's output to changes in the size of the computational grid spacing was studied.

Tests were made for both northerly (shortest possible fetch) and west-southwesterly (longest possible fetch) design storms. First the wind speed and surges occurring at the moment, when the highest waves occur during these storms, were calculated (Section 7.2 describes the method). Then stationary SWAN runs were made for computational grid spacings of 1 km, 2 km, 5 km and 10 km.

The resulting H_{m0} , T_p , T_{m02} , Q_b and L were plotted as a function of the grid spacing (Figure 7.10 and Figure 7.11). The differences between the results of a run with grid spacing 10 km and grid spacing 1 km appear to be about 1 %. This is much less than the 10% confidence bounds, related to wave modelling in general. An optimum value in terms of convergence would be 2 km. However the computational time of a run with grid spacing 2 km was 9 times greater than a run with grid spacing 10 km, which in many cases may not be acceptable.

Figure 7.10. H_{m0} , T_p , T_{m02} , Q_b and L as function of computational grid spacing; storm from N

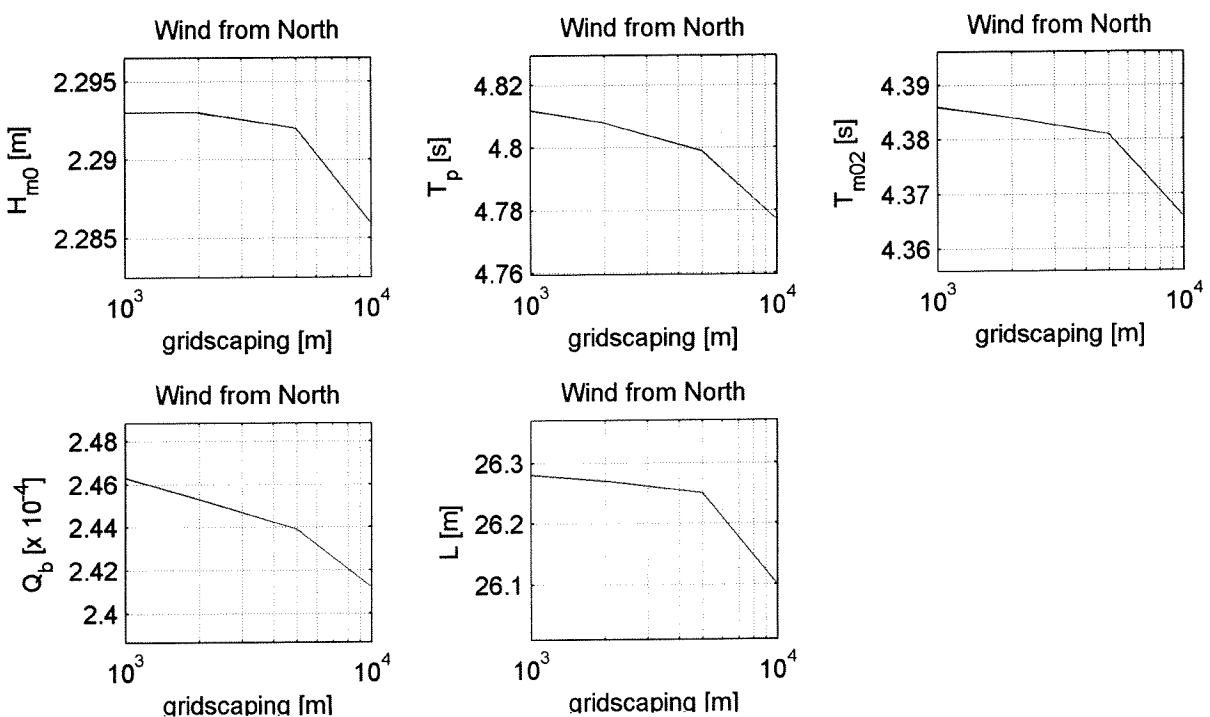
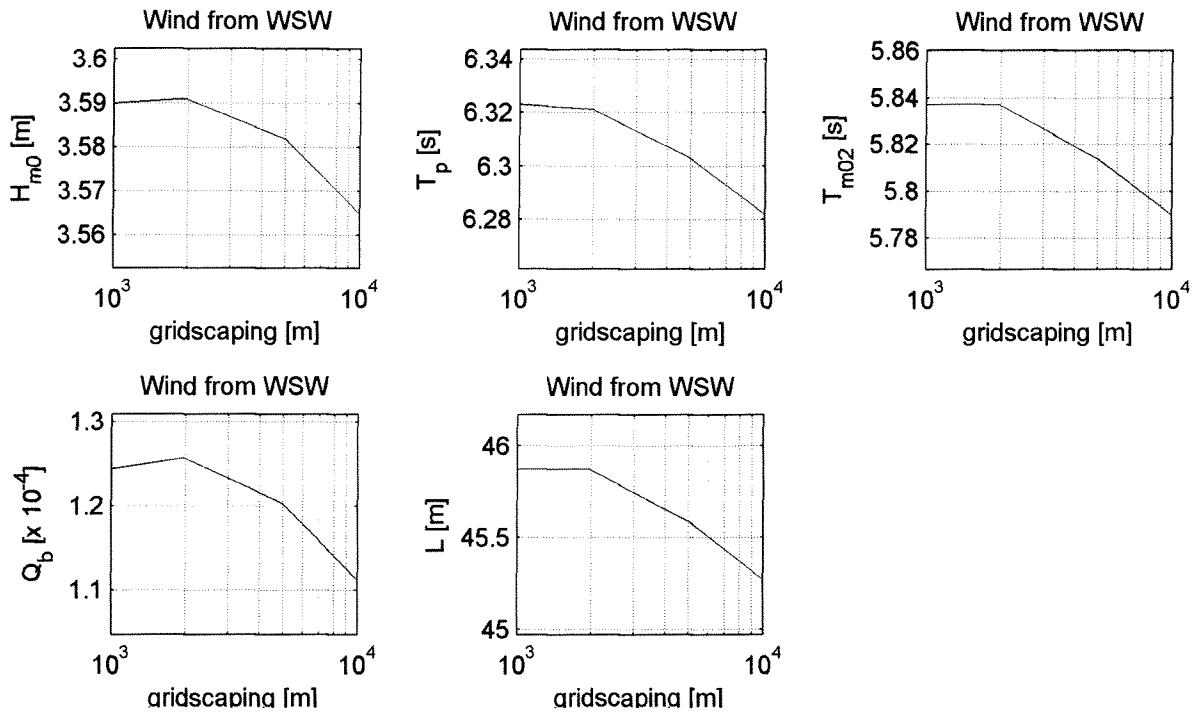


Figure 7.11. H_{m0} , T_p , T_{m02} , Q_b and L as function of computational grid spacing; storm from WSW



For other locations than Kashagan East the differences are greater, particularly in the deeper Southern part of the Caspian Sea. In Appendix XVII plots are presented, which show that in some locations in the Southern part of the Caspian Sea the differences can be up to 10 %, which would not be acceptable, if the model would have been built to calculate design wave heights for those locations.

7.3.3 Resolution of the time domain

The time step applied during the calibration of the SWAN model was 3 hours. It is possible to study the effect of calculating with a smaller timestep, as wind speed measurements are available with an interval of 20 minutes.

Figure 7.12. Comparison of SWAN output of runs with time steps 15 minutes and 3 hours

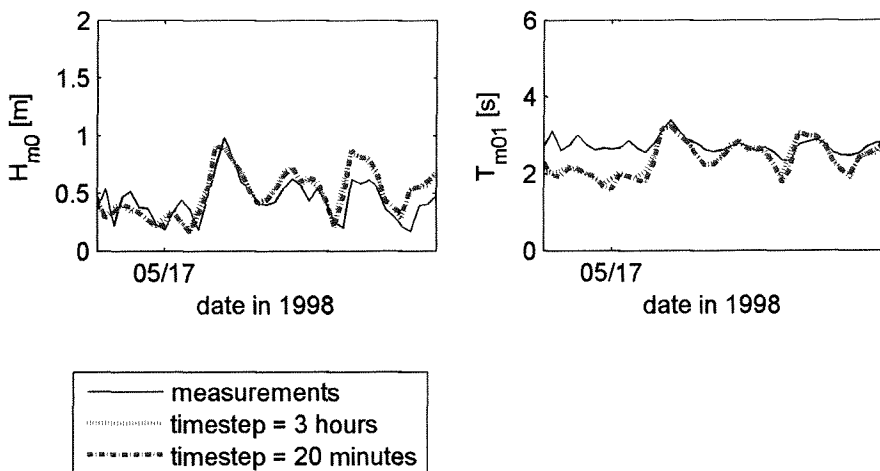


Figure 7.12 shows that a smaller time step results in higher frequency variations in wave height and wave period. According to expectations, the SWAN model now also uses the shorter time scale changes of the wind input. The wave heights and wave periods at those moments, when defined by both runs, do not differ significantly. Therefore it is expected that the time step has not influenced the calibration process.

7.3.4 Resolution of the frequency domain

The frequency domain as applied during the calibration phase was adequate, as calculated in Section 5.6.1. However, when simulating extreme events the low frequency boundary appeared to be too high. The peak frequency reaches values too close to 0.15 Hz (f_{low}). The model's output therefore was sensitive to changes in the lower limit of the frequency domain.

Therefore f_{low} was set to 0.06. This results in the following settings:

- $f_{high} = 1$
 - $f_{low} = 0.06$
 - msc = 30 (number of frequency bins)
- making $\frac{\Delta f}{f} = 1.0983$, which is sufficient

7.3.5 Recommended numerical settings for production runs

The choice for certain numerical settings mainly is a trade-off between computational time and accuracy. A finer resolution of the computational grid, a smaller timestep, smaller frequency bins or directional bins and stricter convergence criteria can all lead to more accurate results. However, significantly more computational time will then be required.

The following recommendations are made for the numerical settings during production runs:

- Convergence criteria

The required accuracy needed during production runs determines which setting should be used. The most accurate results will be reached, when the model is forced to make 40 iterations. Default settings should be applied, when these very strict settings lead to unacceptable computation times.
- Resolution of the computational grid

In terms of convergence of the output a grid spacing of 2 km is optimal. The grid spacing, however, can relatively safely be increased to 10 km, diminishing the required computation time by a factor 9. This would result in an error margin of 1 %.
- Timestep

The choice of the time step depends on the requirements on the high frequency variations of the output. A time step of 3 hours can safely be applied.
- Frequency domain

A safe setting of the frequency domain would be the following:

f_{high}	= 1
f_{low}	= 0.06
msc	= 30 (number of frequency bins)

Such a frequency domain can be applied for both extreme conditions as well as calmer weather.
- Directional domain

No reason has been found to deviate from the default settings.

7.4 Sensitivity to choices regarding physics; one-dimensional analysis

7.4.1 Introduction

In Section 7.1.1 a differentiation was made between two types of sources of uncertainty with a physical background:

1. coefficients in the mathematical expressions for the various source terms
2. physical input data of the SWAN model (bathymetry, surges, wind speeds and directions)

These two items will be dealt with simultaneously in this Section and will be referred to as stochastically defined physical parameters. First probability density functions of these random variables are defined. The influence of the uncertainty of these variables on the model's output will then be calculated.

7.4.2 Probability density functions

The decision, on which variables to include in this analysis, was based on the following:

- whether they are deemed to be uncertain;
- whether they are expected to have a noticeable influence on the results;
- whether a spreading around the default value can result in physically feasible output.

The probability functions of the variables are described below:

agrow

Agrow is the linear wave growth coefficient A in the wind term formulation (expression 6.7). This coefficient has a default value of 0.0015. It was decided to apply a Gaussian distribution with a variation coefficient σ / μ of 0.10. The resulting probability distribution is presented in Figure 7.13.

cds2

Cds2 is a coefficient in the whitecapping formulation (expression 6.12). The default value of this coefficient is 2.36×10^{-5} . The expression was calibrated in order to close the energy balance of waves in idealized wave growth conditions for deep water, both for growing and fully developed wind seas. Komen et al (1984) have tested various values. From his article one can get an idea of the size of a suitable spreading around the mean value. It was decided to apply a Gaussian distribution with 95%-reliability interval with a width of 2×10^{-5} . The resulting probability distribution is presented in Figure 7.13.

delta

Delta is also a whitecapping coefficient (δ in the expression above). Delta has a default value of 0. Research by Rogers et al (2002) has shown that good results can sometimes be obtained by using a value of 0.5. Moreover in some cases a delta of 1 has shown promising results. Any value other than 0 can not be physically justified. A value greater than 1 may not be applied. It was decided to apply a uniform distribution with values between 0 and 1. The resulting probability distribution is presented in Figure 7.13.

cnl4

Cnl4 is a coefficient in the DIA for quadruplet interactions. It determines the strength of the interactions. A change in this factor scales the interactions relative to the frequency-axis, although the expression remains conservative. Varying other coefficients would disturb this energy balance and make the quadruplets interactions a energy-creating or -dissipating process. This would be physically incorrect and will therefore not be executed. Cnl4 has a default value of 3×10^7 . It was decided to apply a Gaussian distribution with a variation coefficient σ / μ of 0.10. The resulting probability distribution is presented in Figure 7.13.

cfjon

Cfjon is the coefficient of the bottom friction source term. The default value of this coefficient is 0.067. Both this study and Van Thiel de Vries (2003), however, found that lower values are needed on the Caspian Sea. This was expected as the sea bed consists of very fine material (50 μm). During the cali-

bration phase values between 0.01 and 0.06 were tested. The result of the calibration phase was a value 0.04. The differences in output, however, were fairly small. This gives an indication of the probability density function of this coefficient. It was decided to work with a Gaussian distribution with an average μ of 0.04 and a 95%-reliability interval with a width of 0.06. The resulting probability distribution is presented in Figure 7.13.

gamma

Gamma is the breaker coefficient in the expression for the source term of depth induced wave breaking. The default value in SWAN is 0.73. Many research projects have however found other values, most of them larger (Smale 2004). Therefore a non-symmetrical distribution should be applied. It was decided to use a triangular distribution. The lower limit of the distribution was defined at 0.55, the upper limit at 1.00. The top value was set at 0.91. The resulting probability distribution is presented in Figure 7.13. The expected value in this distribution is 0.82 (the mean value). The expected value thereby has been set at a higher value than used in the calibrated model. The measurements, however, had not justified a deviation from the default value.

surges

Uncertainties concerning the surges can have many sources, varying from errors in the measured local water levels to the accuracy of the Delft3D model itself. It was estimated that the surges can have errors of up to 5 %. A factor was created by which all values of the spatially defines surges on the Caspian Sea will be multiplied. This factor has a default value 1. Around this value there exists a 95%-reliability interval with a width of 0.1. The resulting probability distribution is presented in Figure 7.13.

bathymetry

The bathymetry also needs to be defined stochastically. In Section 5.5.3 it became obvious that various sources of bathymetric data did not match. The bathymetric map, as used by Van Thiel de Vries (2003), was raised by 70 cm. The resulting map contained depths at A-CM and C-CM which matched the average of the depths measured with the pressure transducers and the survey data. The spreading of the measurements in relation to this average value is used for this sensitivity analysis. The spreading therefore was defined in such a way that the resulting 95%-reliability interval has a width of 0.5 meter. A factor was defined with a Gaussian distribution with an average value μ is 0. During the sensitivity analysis values of this factor are drawn from the probability distribution (shown in Figure 7.13). The value of the factor is then added to all the depths in the bathymetric map.

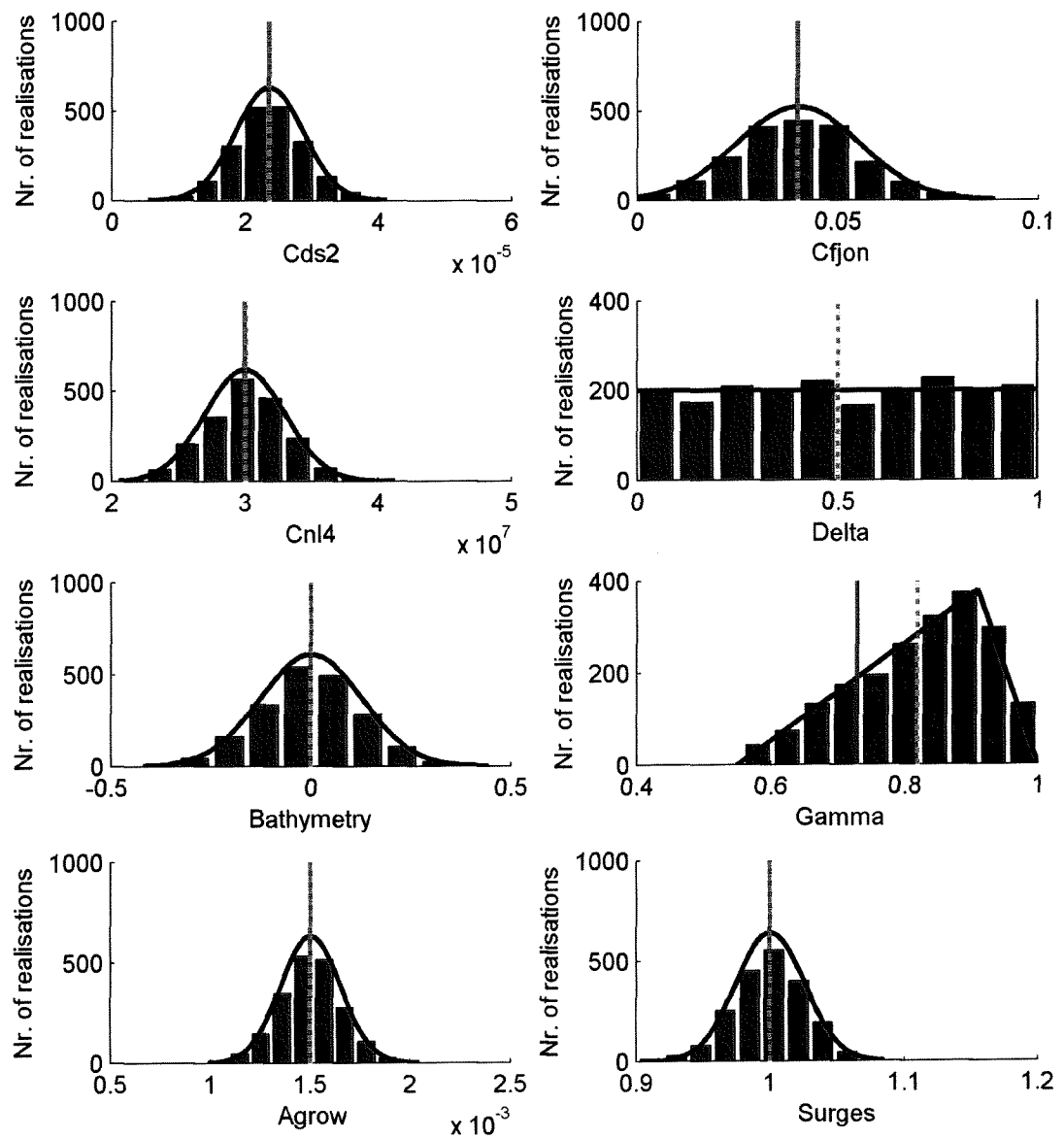
Figure 7.13. Probability density functions of the stochastically defined physical parameters

The black curve represents the probability function.

The red vertical line represents the value, used in the calibrated model.

The green vertical dash-dot line represents the expected value (the mean value of the distribution).

The histograms show the distribution of the 2000 values drawn during the one-dimensional Monte Carlo simulation in Section 7.5.



7.4.3 The one-dimensional Monte Carlo analysis

A first insight into the influence of the uncertainties around the stochastically defined physical parameters on the model's output was needed. Therefore, 50 stationary SWAN runs of the design conditions were made with varying values of one of the stochastically defined physical parameters, while keeping the other parameters at their calibrated value. The spreading of the output parameters was then studied by plotting their histograms. This was done for all of the stochastically defined physical parameters, resulting in 400 SWAN runs.

In order to see whether 50 runs per Monte Carlo simulation were sufficient, plots have been made of the development of the average μ and standard deviation σ with increasing number of simulations. The result is shown in Appendix XVIII. It appears that in all cases the μ and σ have converged sufficiently for this purpose. Only a first insight was wanted into the behaviour of the model. This implies that at least the middle part of the probability distributions (the part which is of most interest for the project's purpose) from which the values were drawn should be well represented by the histograms of the realisations.

7.4.4 Conclusions

In Figure 7.14 the model's output parameters are plotted as a function of the stochastically defined physical parameters. This gives an insight in the linearity of the behaviour. Variations in the random variables appear to have quite a linear effect on the model's output, when calculating the design storm. Therefore, in Section 7.5.3, a linear regression analysis is made, based on the more extensive dataset resulting from the multi-dimensional Monte Carlo analysis, performed in Section 7.5. The linear regression analysis can result in a simplified mathematical model of the SWAN model's output for design storms on the northern part of the Caspian Sea as a linear function of the eight stochastically defined physical parameters.

The resulting spreading of the SWAN output variables H_{m0} , T_p , T_{m02} , Q_b and L is studied (wave length L is actually a function of wave period T , but L was also analysed as L is an important design parameter). The histograms that were made are presented in Appendix XIX. It can be noted that the deviations of the histograms of the input parameters deviate quite much from the probability density functions from which the values were drawn. This can be explained by the relatively small number of realisations (only 50). The mean and standard deviations, however, were proven to be sufficiently converged for the purpose of getting a first insight.

From these plots the following can be concluded:

- The uncertainty in whitecapping coefficient **cds2** mainly influences the uncertainty around the T_p , T_{m02} , Q_b and L . The resulting spreading around H_{m0} is insignificant.
- The uncertainty in bottom friction **cfj0n** has most influence on the uncertainty around the Q_b -output. The other output variables that were studied show a much smaller spreading.
- The influence of the uncertainty around quadruplets' coefficient **cni4** around and linear wind growth coefficient **agrow** is totally insignificant. The small influence of agrow can be explained by the fact that at higher wind speeds the exponential growth term B (in expressions 6.7) is much more influential than linear growth term A (=agrow).
- Deviations from the default value of whitecapping coefficient **delta** (which is 1) have a very small impact on H_{m0} , but lead to a significant decrease in the wave periods, wavelength and Q_b .
- The uncertainty around the **bathymetry** and the **surges** has a relatively small impact on the SWAN-output. The impact was less than expected.
- The uncertainty round breaker parameter **gamma** is by far most responsible for uncertainty around the SWAN-output (for all of the analysed output variables).
- Surges/bathymetry and gamma are of course related. An increase in the surges/depths would lead to more dissipation through breaker parameters gamma. The resulting uncertainty around model output H_{m0} is a function of gamma and the uncertainty around the surges/bathymetry.

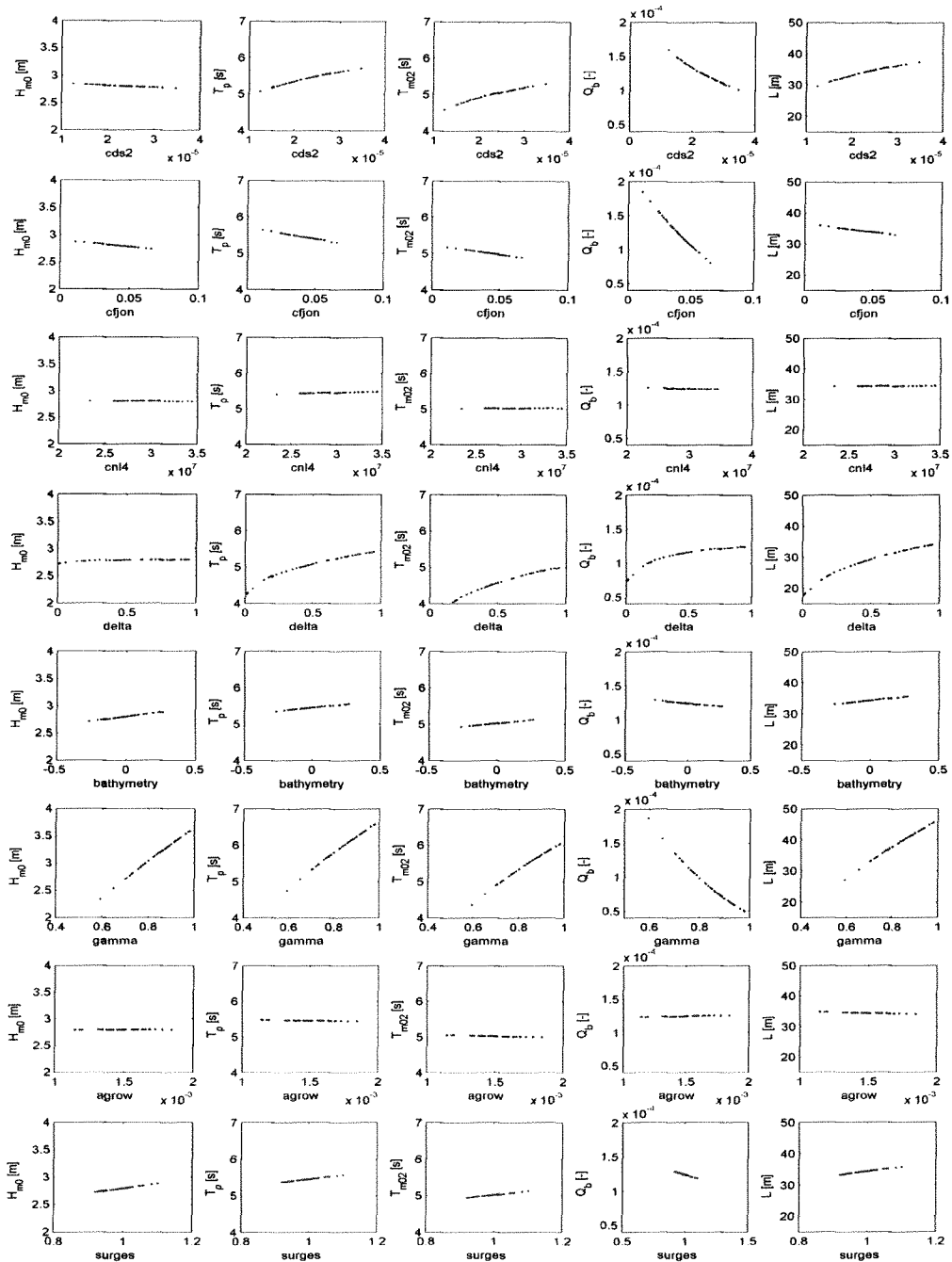
These conclusions can be more quantitatively illustrated with Table 7.4. It can be observed, how the variation coefficients of the input variables influence the variation coefficients of the model's output parameters. The higher the ratio of σ/μ of the output variables divided by σ/μ of the input variables is, the more the uncertainty around the input propagates into uncertainty around the model's output. The importance of the uncertainty around gamma can clearly be observed.

Table 7.4. Ratio of σ/μ of the output parameters to σ/μ of the input parameters
(Low limit 95% = Lower limit of the 95 % reliability interval)

	H _{m0}	T _p	T _{m02}	Q _b	L
Cds	0.027	0.126	0.148	0.486	0.239
Cfjon	0.035	0.047	0.042	0.629	0.065
Cnl4	0.004	0.032	0.010	0.049	0.013
Delta	0.013	0.115	0.168	0.219	0.284
Bathymetry	0.000	0.000	0.000	0.000	0.000
Gamma	0.852	0.645	0.639	3.131	0.971
Agrow	0.003	0.013	0.026	0.052	0.044
Surges	0.313	0.191	0.196	0.465	0.382

A more accurate quantification of the relative contributions of the uncertainties of the physical input parameters on the model's output can be given with a more extensive and multi-dimensional Monte Carlo analysis. Some of the stochastically defined physical parameters are expected not to be completely stochastically independent, requiring a multi-dimensional analysis. This analysis is performed in Section 7.5.

Figure 7.14. Linearity of the model's output as a function of the stochastically defined physical parameters visualised using the results of the one-dimensional Monte Carlo analysis



7.5 Sensitivity to choices regarding physics; multi-dimensional analysis

7.5.1 Introduction

A multi-dimensional Monte Carlo simulation was also made. This can give an increased insight in the confidence limits of the model's output when the uncertainties around the stochastically defined physical parameters are combined. This is expected to be necessary, as these parameters are not expected to be completely stochastically independent.

7.5.2 The multi-dimensional Monte Carlo analysis

A total of 2000 SWAN runs were made. For each SWAN run a value was drawn from the distributions of every stochastically defined physical parameter (the histograms were presented in Figure 7.13). The output of this Monte Carlo simulation is presented in Figure 7.15. In the histograms a vertical line is drawn at the value, resulting from the calibrated model, as described in Section 7.2.5.

By calculating the influence factors α_i (Vrijling and Van Gelder, 2002), the relative importance of the eight random variables in causing the uncertainty of the model's output can be obtained.

$$\alpha_i = \rho_{X_i, Z} = \frac{\text{cov}(X_i, Z)}{\sigma_{X_i} \cdot \sigma_Z} \quad 7.6$$

in this expression:

$\text{cov}(X_i, Z)$ is the covariance between the model's output Z , and the analysed random variable X_i

σ_{X_i} is the standard deviation of random variable X_i

σ_Z is the standard deviation of the model's output Z

$$\text{The relative importance is } \frac{(\alpha_i)^2}{\sum_i (\alpha_i)^2} \quad 7.7$$

The influence factors are presented in Table 7.5. When added, the total per column should be 1. This, however, proved not to be so. A maximum error of about 5 % was observed. This error could have been decreased by increasing the number of SWAN runs, but for the purpose of calculating the relative contributions to the model's uncertainty the error was expected to be acceptable.

Table 7.5. Influence factors α_i resulting from multi-dimensional Monte Carlo simulation

α_i^2	H_{m0}	T_p	T_{m02}	Q_b	L
cds2	0.003	0.061	0.067	0.101	0.067
cfjon	0.035	0.036	0.018	0.348	0.018
cnl4	0.002	0.000	0.002	0.000	0.002
delta	0.002	0.315	0.470	0.046	0.480
bathymetry	0.018	0.008	0.006	0.000	0.008
gamma	0.901	0.535	0.385	0.488	0.370
agrow	0.001	0.000	0.000	0.001	0.000
surges	0.021	0.010	0.008	0.002	0.011

From Figure 7.15 an impression can be obtained of the confidence limits of the model's output. The vertical red line indicates the value of the model's output, when the configuration is used that resulted from the calibration phase. A further quantification of the model's performance, in which the results of these runs are used, and a further interpretation of the influence factors will be given in Section 7.6.

The following striking feature, however, can be observed in the histograms, which should be noted and explained. The values, resulting from the calibrated model, are not the most likely. This is caused by the following two facts:

- 1 In the calibrated model the default value of breaker parameter gamma was applied, as the measurements did not justify a deviation from this default value. While defining the probability function of gamma, however, it was decided that the expected value of this distribution should be higher.
- 2 The mathematical expected value of delta, derived from its uniform distribution ranging from 0 to 1, is 0.5. A value of 1, however, is much more realistic, as long as no good alternative is found for the DIA for the computation of quadruplet interactions.

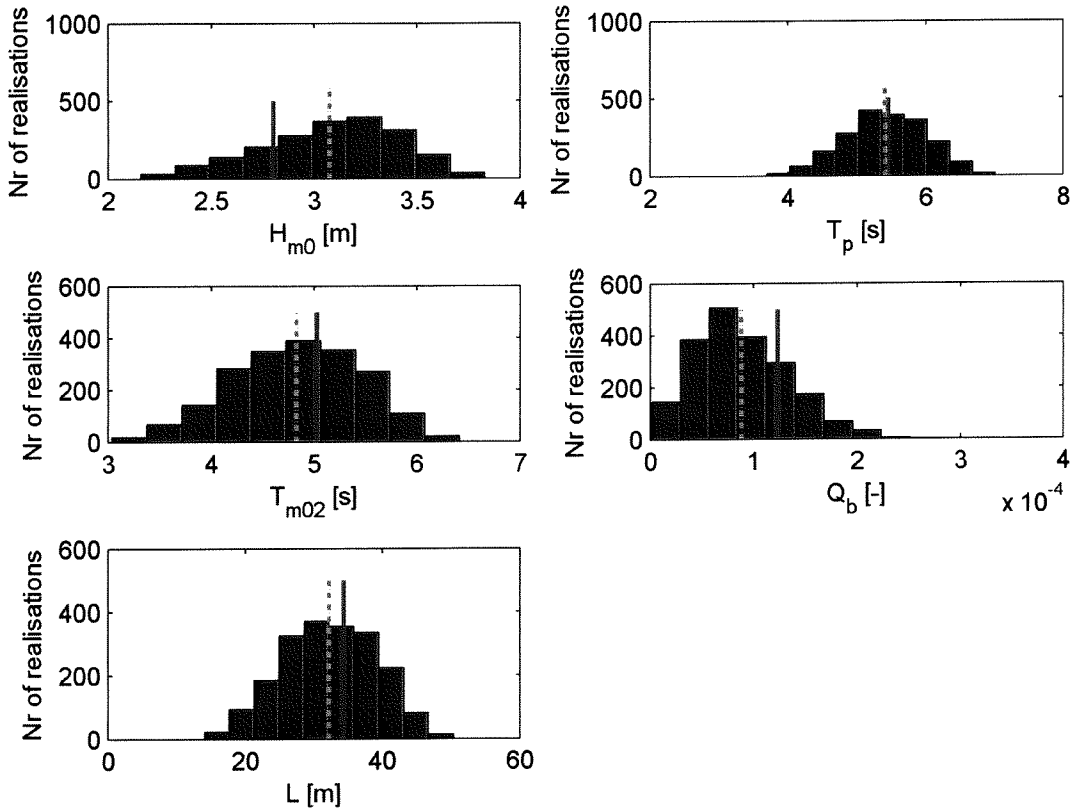
Therefore, it is stated that a small change is needed in the calibration of the model. With the knowledge of the breaker parameter (Smale 2004) and its influence on the model's output, as developed in this project, it is recommended to increase gamma from the default value 0.73 to the most likely (i.e. mean) value 0.82. Delta however will be kept at its calibrated value (calibrated delta is not equal to the mean value of the distribution, but in a uniform distribution one cannot really define a expected value). In the next Section a final design spectrum is presented.

Figure 7.15. Result of multi-dimensional Monte Carlo Simulation

The red vertical line represents the value, obtained with the calibrated model.

The green dash-dot line represents the expected value (the mean value of the distribution).

The histograms show the distribution of the 2000 values obtained with the multi-dimensional Monte Carlo simulation in Section 7.5.



7.5.3 Final design spectrum

A final stationary SWAN run was made to calculate the design spectrum. The calibration that resulted from the calibration phase was applied, with one small change. The breaker parameter gamma was set to 0.82.

In Figure 7.16 the design wave spectrum is plotted. Some integral wave parameters that are interesting for design purposes, corresponding to this spectrum, are as follows:

- $H_{m0} = 3.10 \text{ m}$ significant wave height
- $T_p = 5.89 \text{ s}$ peak wave period
- $T_{m02} = 5.42 \text{ s}$ mean wave period defined as $\sqrt{m_0 / m_2}$
- $Q_b = 0.93e-4$ fraction of broken waves
- $L = 38.70 \text{ m}$ average wave length

The fraction of broken waves may seem very small, however the waves which did break are also the most energetic waves. Therefore the influence on the spectrum is significant. The integrated source term output was studied to prove this. In Figure 7.17 the relative values of the integrated source terms are shown. It is observed that depth-induced wave breaking (S_{surf}) is active and of comparable size to the bottom friction source term.

Note that the integrated value of the quadruplets source terms is not equal to 0, which one would expect as the quadruplets do not generate or dissipate energy. This is caused by the fact that the output was generated by integration over the computational frequency domain. If higher frequencies would have been included in the integration, the result would have been 0. The DIA is conservative.

Figure 7.16. The design spectrum, revised

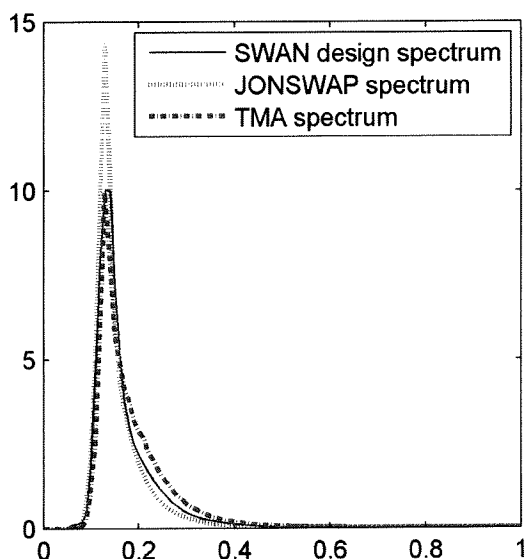
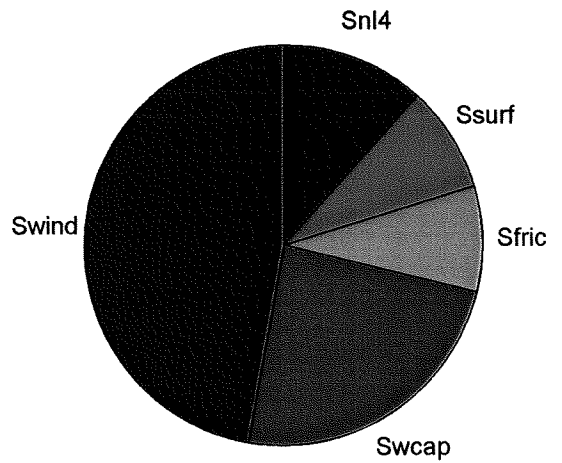


Figure 7.17. Relative integral values of the various source terms during design conditions



In Figure 7.16 the JONSWAP and TMA spectra that correspond to the design spectrum, in terms of total variance and peak period, are also plotted. It is observed that the design spectrum is between a JONSWAP and a TMA spectrum.

7.5.4 Linear regression analysis

A linear regression analysis is made using software package SPSS, in order to analyse how the output variables (Y , being either H_{m0} , T_p , T_{m02} , Q_b or L) can be modelled as a linear function of the input variables. A matrix containing all the realisations (2000) of the eight stochastically defined physical parameters and the resulting SWAN output for H_{m0} , T_p , T_{m02} , Q_b and L was analysed.

The resulting model can be described as follows:

$$Y = \beta_0 + \beta_1 cd2 + \beta_2 cfjon + \beta_3 cnl4 + \beta_4 delta + \beta_5 bathymetry + \beta_6 gamma + \beta_7 agrow + \beta_8 surges$$

SPSS calculated the values of β and their standard deviations. Furthermore SPSS analysed the data using a T-test. The T-test tests whether β_i is significantly different from 0. A random variable can be left out of the model, if Sig is greater than 0.05 (in Appendix XX).

Finally, SPSS also determines a measure of applicability of the linear model, R^2 . In all cases R^2 appeared to be nearly 1.0.

The SPS6 output is presented in Appendix XX. The following conclusions can be drawn:

- **cnl4** and **agrow** have no noticeable effect on the H_{m0} output, when simulating design conditions on the northern part of the Caspian Sea;
- **cnl4** has no significant effect on the Q_b output, when simulating design conditions on the northern part of the Caspian Sea;
- **T_p , T_{m02} and L** are influenced by the effects of uncertainty of all the studies random variables, when simulating design conditions on the northern part of the Caspian Sea.

The signs of the β 's show whether the random variables have a negative or positive influence on the output parameter. No illogical output was found.

It appears the model can be quite well used to get a first insight into the integral wave parameters of the design spectrum at Kashagan East, as long as the input variables are not too widely varied. A general idea of the applicability range of the model can be obtained from Figure 7.14, although this figure is based on the one-dimensional simulation. A quantification of the applicability of the model could not be made sufficiently accurate.

It can be stated, that the linear mathematical model should not be used for more than just a first insight. The dependencies and non-linear characteristics of the input variables are still not sufficiently understood. Furthermore the mathematical model cannot generate spectral wave output.

7.6 The model's performance quantified

The product of this project is a SWAN model of the Caspian Sea, calibrated in such a way that it is able to calculate wave spectra at Kashagan East as accurately as possible. The accuracy of the model depends on three aspects:

- the quality of the configuration
- the choice of numerical settings
- the uncertainty of physical variables

The recommended numerical settings are described in Section 7.3.5. The other two aspects are studied below.

7.6.1 The quality of the calibration

It is not easy to quantify whether the chosen configuration of SWAN actually is the best possible configuration. There is no reason to doubt the quality level of the ADL wind measurements or the ADL burst pressure measurements. The schematisation of the wind field on the Caspian Sea as being uniform proved to be adequate in Appendix II. The measuring interval of wind speeds and wave pressures proved to be sufficiently small (Section 2). The greatest source of uncertainty can probably be found in the conversion method of pressure spectra to wave spectra.

The choice for a different conversion method during this project has resulted into a significant increase of the wave heights and a decrease of the wave periods, compared to those calculated by Arthur D. Little (1999). It can be stated that the error margin was reduced significantly by the thorough study of the conversion methodology during this project. This statement can be illustrated by the fact that the wave spectra, as calculated by a default configured SWAN model, match relatively well with the newly converted wave spectra. The match is much better than with the wave spectra, as calculated using the ADL method. It is difficult to quantify the remaining uncertainty. Another illustration can be given by the fact that the measured spectra match quite well with the spectra, known from theory (Section 4.4). The match is better than that achieved by Van Thiel de Vries (2003).

The configuration that resulted from the calibration phase is not unreasonable. A lower than default friction coefficient was expected and a delta of 1 had appeared to be promising in Rogers et al (2002). Therefore it can be stated that the configuration chosen during the calibration phase of this project, is the best configuration possible of SWAN version 40.31ABCDEFG, considering what was available in terms of measurements.

7.6.2 The error margin of the model's output

One must realise that the output of the SWAN model, when simulating extreme events, has certain confidence limits. On the basis of the multi-dimensional Monte Carlo analysis an insight was obtained into the probability density functions of the model's output of the design spectrum. In Table 7.6 some statistical parameters of the output and the results according to the calibrated model and the revised calibrated model (Section 7.5.3) are presented.

Table 7.6. Design wave parameters, their 95%-reliability interval and shape parameters of their distributions

	H _{m0} [m]	T _p [s]	T _{m02} [s]	Q _b [-]	L [m]
Calibrated model	2.80	5.46	5.03	1.24e-4	34.39
Revised calibrated model	3.10	5.89	5.42	0.93e-4	38.70
Lower limit 95%-rel.interv.	2.37	4.25	3.58	0.17e-4	18.87
Upper limit 95%-rel.interv.	3.64	6.48	5.92	1.88e-4	44.26
Mean	3.08	5.41	4.83	0.88e-4	32.19
Standard deviation	0.33	0.58	0.62	0.45e-4	6.73
Skewness	-0.37	-0.10	-0.17	+0.53	-0.10
Kurtosis	2.54	2.58	2.49	2.88	2.42

The relative contributions of the uncertainties around the eight stochastically defined physical parameters to the model's output are presented in Table 7.7. The percentages are based on the relative values of the influence factors, as presented in Section 7.5.2. This table can also be read as follows. By reducing the uncertainty around (for example) gamma to 0, the spreading around H_{m0} can be reduced with 91.7 %. The relative contributions of the remaining seven random variables to the remaining spreading around H_{m0} will remain the same. The contribution of **cds2** would then (for example) be:
 $0.3 * 100 / (100 - 91.7) = 3.6 \%$.

It is again emphasized that the expected values according to the histograms do not coincide with the revised calibrated model, as during the calibration phase a value for delta of 1 is chosen, while the distribution is uniform from 0 to 1.

Table 7.7. Contribution of the random variables to the uncertainty around the model's output

Random variables	Output variables				
	H_{m0}	T_p	T_{m02}	Q_b	L
cds2	0.3%	6.3%	7.0%	10.3%	7.0%
cfjon	3.6%	3.8%	1.9%	35.3%	1.9%
cnl4	0.2%	0.0%	0.2%	0.0%	0.2%
delta	0.2%	32.7%	49.1%	4.7%	50.2%
bathymetry	1.8%	0.8%	0.6%	0.0%	0.9%
gamma	91.7%	55.5%	40.3%	49.5%	38.7%
agrow	0.1%	0.0%	0.0%	0.1%	0.0%
surges	2.2%	1.1%	0.9%	0.2%	1.2%

In Figure 7.18 the histograms of output parameters H_{m0} , T_p , T_{m02} , Q_b and L are presented. Next to each histogram a circle diagram is presented in which the relative contribution of the various physical parameters on the uncertainty of the output is visualised. From Figure 7.18 it can be concluded that **gamma**, **delta** and **cfjon** contribute most to the spreading of the model's output.

7.7 Recommended activities to increase the model's performance

In the preceding Section it was concluded that in particular the uncertainties around **gamma**, **delta** and **cfjon** determine the uncertainty around the SWAN model's output. Reducing the spreading of these random variables will significantly reduce the error bandwidth of the SWAN output and therefore improve the model's accuracy.

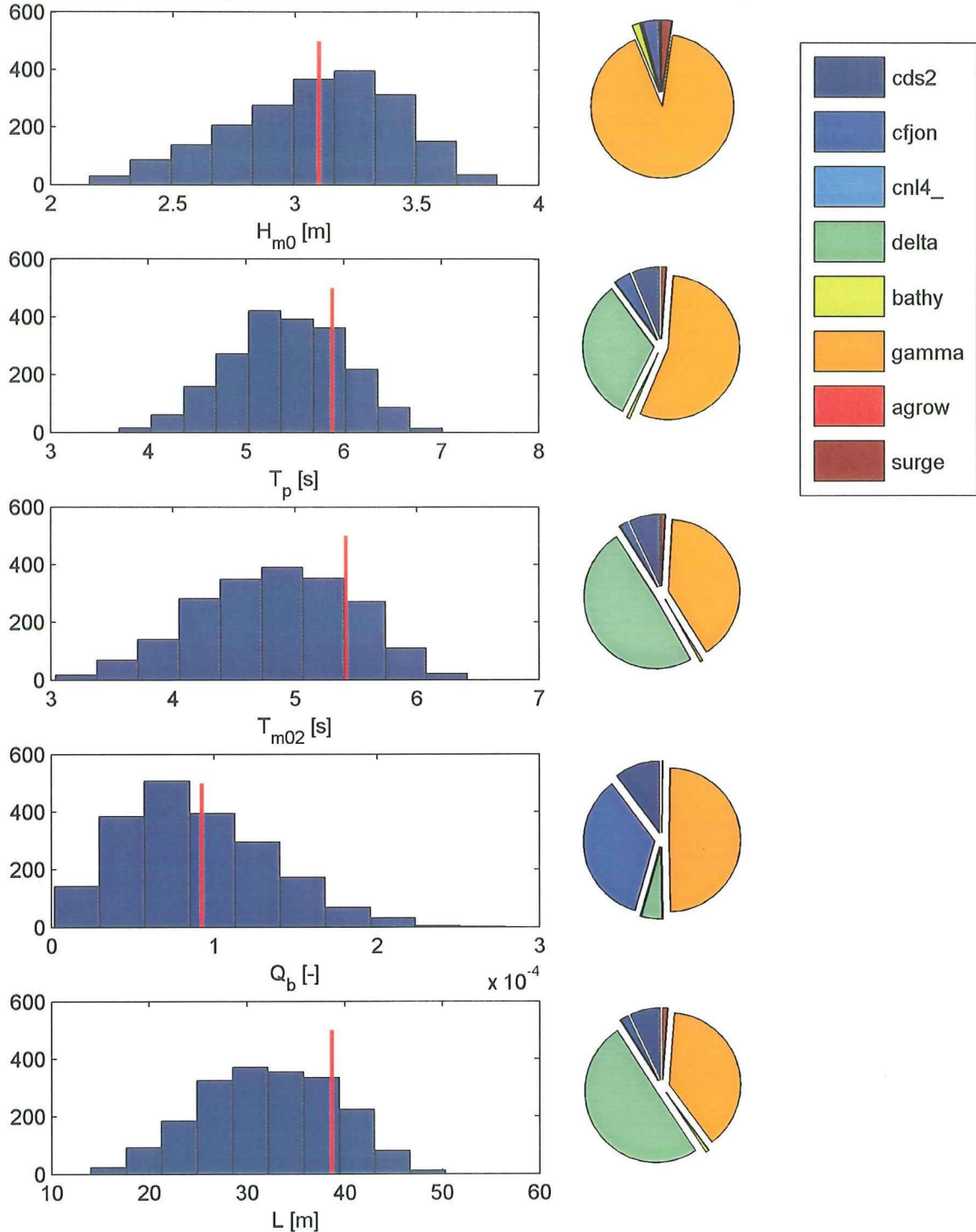
The spreading around H_{m0} can be reduced with a maximum of 91.7 % by calibration of the model on wave spectra, measured during more extreme events with depth-limited wave conditions. **gamma** could then be known with a greater certainty. For this purpose it is very important to keep carrying out measurements at the project sites on the northern part of the Caspian Sea, both of wind and wave spectra.

The spreading around **delta** can be reduced by further research on whitecapping. A reduction of the spreading around the predicted wave length L could be obtained of 50.2 %. Some researchers state that a deviation from the default value delta = 0 only gives such good results, because it compensates the errors created by the use of the DIA. Therefore also research on the quadruplets source term can in the end result in a significant increased accuracy of the model.

The choice for a certain value of **cfjon** will be difficult to make, as long as the other source terms (in particular the quadruplets and whitecapping) still contain such great uncertainties. **Cfjon** in practice is treated as a balancing term. Therefore it can be concluded that more research on quadruplets, whitecapping and depth-induced wave breaking will in the end also result in a more accurate calibration of **cfjon**. This could reduce the uncertainty around Q_b with 35.3 %.

Most interesting is the fact that further analysis of the surges or new measurements of bathymetry (reducing the uncertainty of their values) would not very much contribute to an improvement of the model's performance.

Figure 7.18. Relative contribution of physical coefficients/variables on the model's error margin
 The vertical red line represents the value obtained with the revised calibrated model.



7.8 Summary

The validated model can be used to determine the design wave spectrum. Therefore a design storm had to be defined. A storm was defined on the basis of wind statistics. The SWL was set at CD +2.4 m. It was proven that a stationary SWAN run could be used, as wave conditions during a design storm are depth-limited and therefore time-independent.

The performance of the validated model mainly depends on three factors:

- the quality of the calibration;
- numerical settings;
- the accuracy of physical coefficients and physical input data.

No reasons could be found to doubt the quality of the final calibration. In addition, the numerical setting proved not to have influenced the calibration process.

Monte Carlo simulations have been made to study the uncertainty around the model's output. It appears that gamma, delta and cfjon contribute most to the uncertainty around the model's output.

The following recommendations could therefore be made to improve the SWAN model's accuracy.

- 1 To diminish the uncertainty around gamma, a re-calibration is needed on measurements carried out during more extreme events. Therefore it is strongly recommended to continue measuring wave spectra and wind.
- 2 More research on quadruplets and whitecapping can result in a decrease of the uncertainty around delta.
- 3 The uncertainty around cfjon can only be diminished by a re-calibration, if the uncertainty around the other source terms is diminished. Cfjon, in practice, is a balancing item.

A linear regression analysis was made with the data resulting from the Monte Carlo analysis to study whether a simplified linear model can be made for the SWAN model of design conditions on the northern part of the Caspian Sea. This appeared to be feasible. This model showed that the coefficients agrow and cnl4 are of insignificant importance on the value of H_{m0} and that cnl4 has no significant influence on Q_b (when simulating design waves). The linear mathematical model can be applied to get a first insight in the reaction of the model to changes in certain physical parameters, but should not be applied for more than getting a first insight, as too many uncertainties still exist.

During the sensitivity analysis it became clear that the most probable wave spectrum represented higher waves than the wave spectrum as calculated by the calibrated model. This was caused by the fact that the chosen probability distribution for the breaker parameter gamma has a higher expected value than the default value used in SWAN. On the basis of the available measurements, however, a deviation from the default value of gamma could not be justified. On the basis of the sensitivity analysis it was decided to revise the calibrated model by changing breaker parameter gamma to 0.82.

The final design spectrum and its confidence limits were defined.

8 CONCLUSIONS AND RECOMMENDATIONS

8.1 Conclusions

This Section summarises the conclusions drawn during the project.

From the analysis of the measurements, it was concluded that:

- The NCEP wind database does not contain sufficient information about the higher frequency wind speed variations for the calibration of a SWAN model.
- Wind on the northern part of the Caspian Sea can be modelled as spatially uniform for the purpose of wave and surge modelling, as variations in space of wind speeds and directions do not vary much in this area.
- The conversion of burst pressure measurements to wave spectra needed a revision. Wave heights appeared to be underestimated and wave periods overestimated by Arthur D. Little (1999), as they seem to have applied a conversion method in which all wave energy at frequencies greater than 0.42 Hz is neglected. This has led to a very different calibration of the SWAN model of the Caspian Sea, than the calibration performed by Van Thiel de Vries (2003).
- Parts of the wave spectra measurements appear to be obtained under the influence of nearby ice-coverage. These were not usable for the calibration of the SWAN model.
- Swell does not play a role of importance on the northern part of the Caspian Sea.
- The spectra measured on the Caspian Sea correspond rather well with the theoretical JONSWAP and TMA spectra.
- The bathymetric map, used for the SWAN wave model and the Delft3D surge model, was raised with 70 cm after a comparison with available local water level measurements near Kashagan East. The increased performance of the auto-calibration of the Delft3D model increased trust in this new bathymetric map.
- The burst pressure measurements, carried out at location E-CM, could not be used for the calibration of the model. As these measurements were carried out very near the sea bed and at great depths, pressures caused by waves were hardly felt by the pressure sensor. Multiplication by a gain correction factor introduces a too great uncertainty in the resulting wave spectra for an accurate calibration of the SWAN model.

From the calibration of the model it is concluded that:

- The wind input source term should use the Komen et al (1984) expression, in order to get the best results on the northern part of the Caspian Sea. This conclusion differs from that of Van Thiel de Vries (2003), which was based on an erroneous conversion method applied to derive the wave spectra from the burst pressure measurements.
- The bottom friction coefficient $c_{fj\alpha}$ should be set at a value of $0.04 \text{ m}^2/\text{s}^3$. This value is lower than the default value, due to the fine sea bed material and the fact that no significant bed forms exist.
- The quadruplets should be modelled with the DIA. The XNL method appears not to perform well, as it results in a completely erratic directional spreading. The DIA does not perform without error, as was expected, but the errors are not as great as Van Thiel de Vries (2003) reported. The conversion method for burst pressure measurements to wave spectra used here led to a decrease of the measured wave periods relative to those used by Van Thiel de Vries (2003), leading to a better match of the simulated spectra with the measured spectra.
- Whitecapping was best modelled by increasing delta from the default value 0 to a value of 1. Delta affects the distribution of dissipation by whitecapping over wave numbers. Although a value of 1 cannot be physically justified, the match with the measured wave spectra was best, when using a value of 1. Most probably, an increase of delta to 1 leads to a compensation of the errors caused by the use of the DIA for quadruplets.
- The measurements did not contain a sufficient amount of wave spectra in which depth-induced wave breaking plays an important role. A deviation from the default value of gamma of 0.73 could therefore not be justified.
- Triads appear not to play an important role on the Caspian Sea. This agrees with the finding that the measured Ursell numbers hardly exceed values of 0.05.

From the sensitivity analysis of the model it is concluded that:

- Waves during design conditions appear to be depth-limited. Therefore wave conditions then are time-independent and can be modelled with stationary SWAN runs.
- The improvements regarding the conversion of burst pressure measurements to wave spectra reduced the confidence limits regarding the definition of the measured wave spectra to such a small scale that it is expected that the chosen calibration was not influenced by the conversion method, as it was in Van Thiel de Vries (2003).
- The numerical settings of the model during the calibration phase seem not to have influenced the calibration phase. The resolution in time and space were sufficiently fine. The choice of the frequency domain has not influenced the results. A stricter setting of the convergence criteria would not generate different results.
- Breaker parameter gamma, whitecapping coefficient delta and bottom friction coefficient cfjon contribute most to the model's output.
- A smaller uncertainty regarding the bathymetric map or the computed surges would decrease the SWAN model's accuracy only very little.
- A linear mathematical model can be applied to get a first insight into the influence of variations of the main physical coefficients on the model's output parameters. For more detailed knowledge on such matters SWAN calculations are needed.
- It is expected that breaker parameter gamma needs to be set at a value of 0.82, as this is the expected value in the probability distribution of this parameter (Smale 2004). The default value in SWAN is 0.73.

Some interesting integral wave parameters for design purposes, resulting from the design wave simulation (calculated for a SWL of CD + 2.4 m), are as stated in the boldly printed row, presented in Table 8.1. The confidence limits around this value and some statistical parameters of its probability density function are also given.

Table 8.1. The design wave parameters and their statistical characteristics, resulting from the sensitivity analysis

	H _{m0} [m]	T _p [s]	T _{m02} [s]	Q _b [-]	Average L [m]
Calibrated model	2.80	5.46	5.03	1.24e-4	34.39
Revised calibrated model	3.10	5.89	5.42	0.93e-4	38.70
Lower limit 95%-rel.interv.	2.37	4.25	3.58	0.17e-4	18.87
Upper limit 95%-rel.interv.	3.64	6.48	5.92	1.88e-4	44.26
Mean	3.08	5.41	4.83	0.88e-4	32.19
Standard deviation	0.33	0.58	0.62	0.45e-4	6.73
Skewness	-0.37	-0.10	-0.17	+0.53	-0.10
Kurtosis	2.54	2.58	2.49	2.88	2.42

The relative contributions of the uncertainty around the most important physical coefficients and input data are presented in Table 8.2.

Table 8.2. Relative contributions of the most important physical input variables on the model's output

Random variables	Output variables				
	H _{m0}	T _p	T _{m02}	Q _b	L
cds2	0.3%	6.3%	7.0%	10.3%	7.0%
cfjon	3.6%	3.8%	1.9%	35.3%	1.9%
cnl4	0.2%	0.0%	0.2%	0.0%	0.2%
delta	0.2%	32.7%	49.1%	4.7%	50.2%
bathymetry	1.8%	0.8%	0.6%	0.0%	0.9%
gamma	91.7%	55.5%	40.3%	49.5%	38.7%
agrow	0.1%	0.0%	0.0%	0.1%	0.0%
surges	2.2%	1.1%	0.9%	0.2%	1.2%

Breaker parameter gamma appears to dominate the uncertainty, as this parameter could not be calibrated for due to the absence of wave and wind measurements carried out during extreme conditions. The values in Table 8.2 can also be interpreted as the increase in the confidence in the model that can be gained by decreasing the uncertainty around the corresponding physical input parameters.

8.2 Recommendations

The following recommendations could be made during the project:

Based on the study of the conversion of burst pressure measurements to wave spectra, it is recommended that:

- Measuring wave spectra through burst pressure measurements introduces the need for a conversion. Such conversions can introduce great uncertainties. These can best be reduced by comparing part of the converted spectra with simultaneous directly measured wave spectra (by means of wave buoys). The gain correction factor can be accurately determined.
- If measurements of wave spectra are taken by means of burst pressure measurements, it is recommended to take these measurements at depths below the surface in the order of size of 2 meters. Measuring closer to the sea bed leads to an increase in the needed gain correction factor, introducing a greater uncertainty as the effects of non-linearity then become significant. Furthermore the signal-to-noise ratios will then be smaller.
- A conversion method should be developed, which defines the added high frequency tail of the spectrum as a function of depth.

Based on the study of the model set-up, it is recommended that:

- NCEP wind data should only be used with great care when calibrating wave models. In most cases it is expected that the NCEP wind data will not cover the higher frequency variations in wind speed sufficiently, as needed for this purpose.

Based on the calibration of the SWAN model of the Caspian Sea in particular, it is recommended to:

- Collect more spectral wave measurements and wind measurements on the northern part of the Caspian Sea, also at deeper locations
 - o Measurements carried out during more extreme events would allow a better calibration of the depth-induced wave breaking source term.
 - o Measurements carried during deep water conditions, would allow a calibration of the deep water source terms without the influence of shallow water source terms.
- Re-calibrate the SWAN model of the Caspian Sea, when significant changes are implemented in SWAN.

Based on the calibration of a SWAN model in general, it is recommended that:

- The stability problems in the Janssen (1991) wind formulation should be analysed and solved.
- The causes of the erroneous directional spreading of wave energy generated by the XNL method for quadruplet interactions should be analysed and cured.
- A setting of delta to 1 should also be tested during other calibration studies. The results obtained during this study were most promising. It must however be kept in mind that this setting cannot be physically justified, but is most probably a compensation of the errors caused by the DIA for quadruplets. A better modelling of quadruplets would therefore remove the necessity to set delta to 1 as a compensational measure.

Based on the sensitivity analysis, it is recommended that:

- More spectral wave measurements and wind measurements should be collected. The availability of measurements carried out during more extreme events, would allow a better calibration of the depth-induced wave breaking source term, which could reduce the uncertainty around the model's output significantly.
- Research on the modelling of quadruplets and whitecapping must be a main priority. These source terms cause a significant uncertainty around the model's output. The significant influence of the uncertainty around delta on the uncertainty around the model's output illustrates this.

- The uncertainty around the bottom friction coefficient appeared to have a significant influence on the model's performance. This coefficient in practice is a balancing term. Improvements of the process descriptions of the other source terms are needed, before a better estimate can be made of this coefficient by means of a re-calibration.

REFERENCES

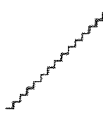
1. Agip KCO, 2001: *Kazakhstan Coordinate Systems – Rev 1*
2. Alkyon, 1999: *Source term investigations SWAN*, report A162-R1r2
3. Alkyon and Delft Hydraulics, 2002: *SWAN fysica plus*, report H3937/A832 (by order of RIKZ/RWS as a part of the project HR-Ontwikkeling)
4. Alkyon and Delft Hydraulics, 2003: *Reliability of SWAN at the Petten Sea Defence*, report H3937 / A832
5. Arthur D. Little, 1999: *MetOcean Data Presentation: northern part of the Caspian Sea. Collection Period October 1997 – September 1998*. Final Report. Reference 34697
6. Battjes, J.A. and Janssen, J.P.F.M., 1978: *Energy loss and set-up due to breaking of random waves*. Proc. 16th Int. Conf. on Coastal Engineering, p569-588
7. Battjes, J.A., 1982: *Windgolven*, handleiding college b78
8. Bishop, C.T. and Donelan, A.D., 1987: *Measuring Waves with Pressure Transducers*. Coastal Engineering, Vol. 11, p309-328
9. Booij, N., Ris, R.C. and Holthuijsen, L.H., 1999: *A third-generation wave model for coastal regions, Part I, Model description and validation*. J. of Geophys. Res. Vol. 104 (C4), p7649-7666
10. Booij, N. and Holthuijsen, L.H., 2002: *The effects of swell and wave steepness on wave growth and depth-induced wave breaking*. Proceedings of the 7th International Workshop on Wave Forecasting and Hindcasting, Banff, Alberta, Canada, 2002.
11. Bottema, M., Waal, J.P. de and Regeling, E.J., 2003: *Some application of the Lake IJssel / Lake Sloten wave data set*, Proc. 28th Int. Conf. on Coastal Eng., ASCE, p413-425
12. Bouws, E., Günther, H., Rosenthal, W. and Vincent, C.L., 1985: *Similarity of the Wind Wave Spectrum in Finite Depth Water 1. Spectral Form*. Journ. of Geoph. Research, Vol. 90, p975-986
13. Bouws, E., 1986: *Provisional results of a wind wave experiment in a shallow lake (Lake Marken, The Netherlands)*. KNMI memorandum 00-86-21
14. Cavaleri, L., 1980: *Wave measurement using pressure transducer*. Oceanologica acta 1980, Vol. 3, N° 3
15. Cavaleri, L., 1987: *Reynolds Stresses under Wind Waves*. J. of Geophysical Research, Vol. 92, N° C4, p3894-3904
16. Cavaleri, L., 2004: Personal communication on conversion of pressure measurements to wave spectra
17. CUR, 2002: *Kansen in de civiele techniek, deel 1: Probabilistisch ontwerpen in theorie*. CUR manual 190.
18. Fugro Global Environmental & Ocean Sciences Ltd, 2001: *Environmental design criteria - Kazakhstan Fields to Coast of Kazakhstan - Final*, Ref Nr.C50171/2422/F1, 15 November 2001.

19. Gaikwad, S.R., Bidwe, P.S. and Tripathi, V.K., 1996: *In situ wave and tide measurements using pressure transducers*. Proc. Int. Conf. Coastal Engineering COE '96, p573-576
20. Gelder, P.H.A.J.M. van, Molenaar, W.F., Bolgov, M.V. and Krasnozhon G.F., 2004: *Statistical analysis of icing event occurrences in the northern Caspian Sea*. paper number: omae2004-51560, the 23rd International Conference on Offshore Mechanics and Arctic Engineering, Vancouver, Canada, 20-25 June 2004.
21. Graham, C., Cardone, V. J., Ceccacci, E. A., Parsons, M.J., Cooper, C. and Stear, J., 2002: *Challenges to wave hindcasting in the Caspian Sea*. Submitted paper at 7th Int. Workshop on Wave hindcasting and forecasting 2002
22. Günther, H., Hasselmann, S. and Janssen, P.A.E.M., 1992: *The WAM model Cycle 4 (revised version)*. Deutsch. Klim. Rechenzentrum, Techn. Rep. No. 4, Hamburg, Germany
23. Hasselmann, K., 1962: *On the non-linear energy transfer in a gravity-wave spectrum. Part 1. General theory*. J. Fluid Mech., Vol.12 (4), p481-500
24. Hasselmann, K. 1974: *On the spectral dissipation of ocean waves due to whitecapping*. Bound.-Layer Meteor., Vol. 6, p107-127
25. Hasselmann, S. and Hasselmann, K., 1981: *A symmetrical method of computing the nonlinear transfer in a gravity wave spectrum*. Hamburger Geophys. Einzelschriften. Reihe A, Heft 52
26. Hashimoto, N., Thurston, S.W., Mitsui, M., 1997: *Surface Wave Recovery from Subsurface Pressure Records on the Basis of Weakly Nonlinear Directional Wave Theory*. Ocean Wave Measurement and Analysis 1997.
27. Hashimoto, N., Haagsma, IJ.G. and Holthuijsen, L.H., 2003: *Four wave interactions in SWAN*, Proc. 28th Int. Conf. Coastal Engineering, p392-404
28. Holthuijsen, L.H., 2002: *Handouts voor college windgolven*
29. Holthuijsen, L.H., Booij, N., Ris, R.C., Haagsma, IJ.G., Kieftenburg, A.T.M.M., Kriezi, E.E., Zijlema, M. and Westhuysen, A.J. van der, 2004: *SWAN Cycle III version 40.31*, User manual
30. Hurdle, D.P. and Stive, R.J.H., 1989: Revision of SPM 1984 wave hindcast model to avoid inconsistencies in engineering applications, Coastal Engineering, Vol. 12, No. 4, p339-351
31. Hurdle, D.P. and Vledder, G. Ph., 2004: *Improved spectral wave modelling of white-capping dissipation in swell sea systems*. Proc. OMAE 2004
32. Janssen, P.A.J.M., 1991: *Quasi-linear theory of wind wave generation applied to wave forecasting*. J. of Phys. Oceanogr. Vol. 21, p1631-1642
33. Komen, G.J., Hasselmann, S. and Hasselman, K., 1984: *On the existence of a fully developed wind-sea spectrum*. J. of Phys. Oceanogr., Vol. 14, p1271-1285
34. Lewis, A.W. and Allos, R.N., 1990: *JONSWAP's parameters: sorting out the inconsistencies*. Coastal Engineering, Vol. 17, No. 4, p409-415
35. McKee Smith, J., 2002: *Wave Pressure Gauge Analysis with Current*. J. of Waterway, Port, Coastal and Ocean Engineering, nov/dec 2002, p271-275.

36. Oelerich, J., Otay, E.N. and Straube, J., 2003: *Pressure and velocity response in random sea approach, measurements and comparisons*. ICCE '92. Proc. 23rd Int. Conf. Coastal Engineering, p509-510
37. Probabilitas, 2002: *Statistical analysis and 40-year forecasting of the Caspian Sea level*. XCASP workshop 2002
38. Rogers, W.E., Hwang, P.A., Wang, D.W., 2002: *Investigation of Wave Growth and Decay in the SWAN Model: Three Regional-Scale Applications*. Journ. of Physical Oceanography, Vol.22, p366-389
39. Roskam, A.P., 2004: Personal communication on conversion of pressure measurements to wave spectra
40. Smale, A.J., 2004: *Applicability of the NCEP database*. Internal Technical Note Witteveen+Bos
41. Smale, A.J., 2004: Personal communication on depth-induced wave breaking parameter gamma
42. Somova, S.M., Gelder, P.H.A.J.M. van, Bolgov, M.V., 2003: *Wind climate analysis of the Caspian Sea*. Proceedings of the World Climate Change Conference WCCC2003, p. 139, Moscow, Sept. 29 to Oct. 3, 2003
43. Tanaka, M., 1986: *The Stability of Solitary Waves*. Phys. Fluids, 29 (3), p650-655.
44. Thiel de Vries, J.S.M. van, 2003: *Wave fields in transitional water depth*, MSC Thesis report. Delft University of Technology
45. Vledder, G.Ph. van, 2000: *Improved Parameterizations of Nonlinear Four Wave Interactions for Application in Operational Wave Prediction Models*
46. Vledder, G. Ph. van and Bottema, M., 2003: *Improved modelling of nonlinear four-wave interactions in shallow water*, Proc. 28th Int. Conf. Coastal Engineering, ASCE, p459-471
47. Vrijling, J.K. and Gelder, P.H.A.J.M. van, 2002: *Probabilistic design in hydraulic engineering*, Lecture notes CT5310
48. Waal, J.P. de, 2001: *Wave growth limit in shallow water*. Proc. 4th Int. Symposium Waves 2001, p560-569
49. Witteveen+Bos, 2004: *Functionality, computational grids and resolution of the wave model SWAN*. Prepared for the Ministry of Transport, Public Works and Water Management, Directorate-General for Public Works and Water Management. Reference code RW1349-1/rijm3/029
50. Wolf, J., 1997: *The analysis of bottom pressure and current data for waves*. 7th Int. Conf. on Electronic Engineering in Oceanography, p165-170
51. Yan, L., 1987: *An improved wind input source term for third generation ocean wave modelling*. Rep. No. 87-8, Royal Dutch Meteor. Inst.
52. Young, I.R. and Verhagen, L.A., 1996: *The growth of fetch limited waves in water of finite depth. Part 2. Spectral evolution*, Coastal Engineering 29 (1996), p79-99

NCEP data:

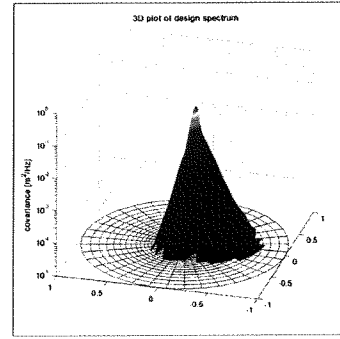
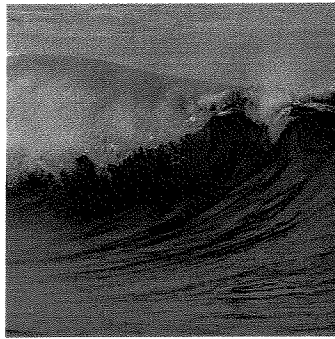
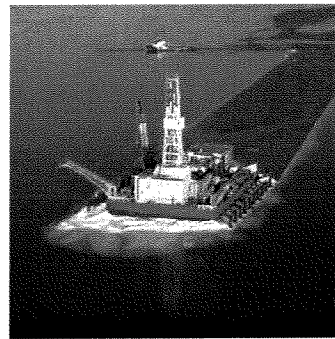
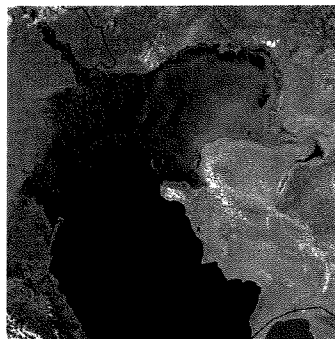
NCEP Reanalysis data provided by the NOAA-CIRES Climate Diagnostics Center, Boulder, Colorado, USA, from their Web site at <http://www.cdc.noaa.gov/>



Analysis and modelling of wave spectra on the Caspian Sea

Appendices

**P.E. Hartgerink, M.Sc. Thesis
9308358**



Analysis and modelling of wave spectra on the Caspian Sea

Appendices
P.E. Hartgerink, M.Sc. Thesis
9308358

our reference	projectcode	status
ZZWI5039/RIJM3/001	ZZWI5039	Final Report
project manager	project director	date
S.C. van der Biezen	H.E. Nieboer	January 24, 2005
authorisation	name	initials
approved	A.J. Smale	(i.o.) DS.



Appendix	Number of Pages
I. ADL measuring campaign information	1
II. Proof that wind on the Northern part of Caspian Sea can be modelled as uniform	1
III. Geometry of the Caspian Sea	1
IV. Plots of the measurements' characteristic parameters in time	5
V. SWAN input file of chosen calibration (validation run)	1
VI. Plots of calibration of Wind input on deep water timeseries	1
VII. Plots of calibration of Wind input on shallow water timeseries	1
VIII. Plots of calibration of Bottom friction on deep water timeseries	2
IX. Plots of calibration of Bottom friction on shallow water timeseries	2
X. Plots of calibration of Whitecapping and Quadruplets on deep water timeseries	11
XI. Plots of calibration of Whitecapping and Quadruplets on shallow water timeseries	16
XII. Plots of calibration of Depth induced breaking on shallow water timeseries	1
XIII. Plots of calibration of Triads on shallow water timeseries	2
XIV. Plots of validation run 201	7
XV. Plots of validation run 202	7
XVI. Wind statistics (by FUGRO)	2
XVII. Influence of grid spacing of computational grid on SWAN output for all grid points	4
XVIII. Proof that linear Monte Carlo simulations converged for μ and σ	8
XIX. Output of linear Monte Carlo simulations	8
XX. SPSS output of the linear regression analysis	7

APPENDIX

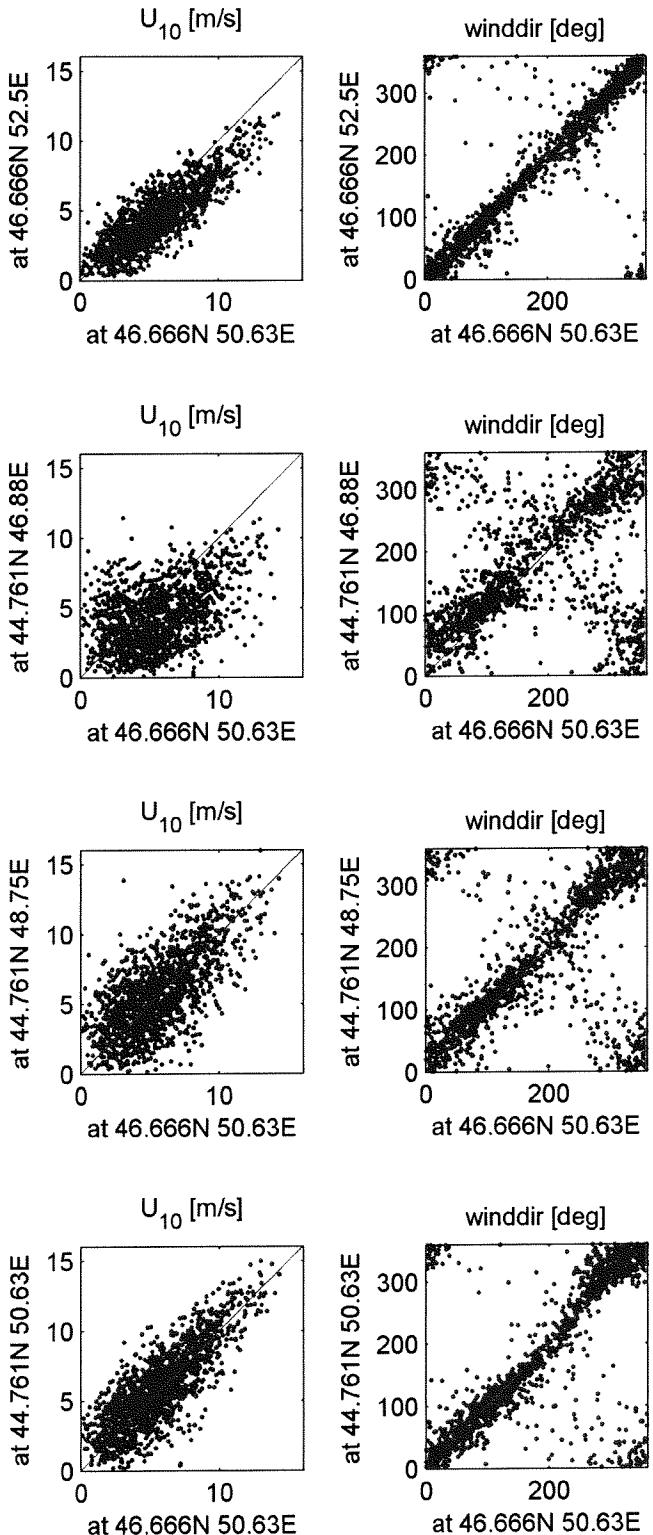
I. ADL measuring campaign information

I.1 Chart wih information on the ADL measuring campaign

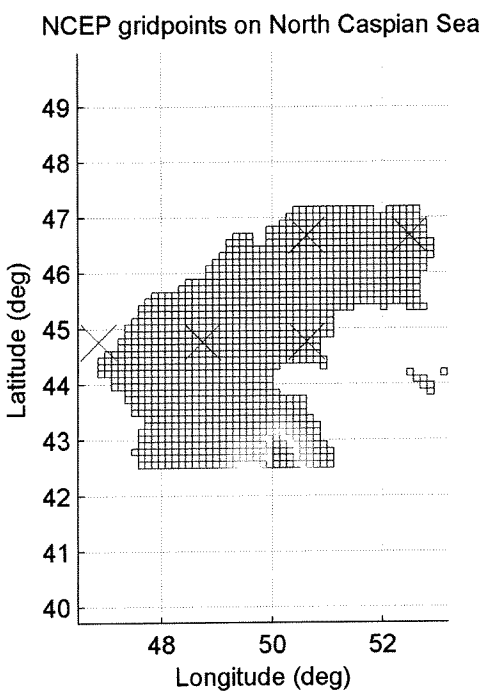
Station	Deployment 1		Deployment 2		Deployment 3							
			Station A-CM North Caspian Sea									
MetOcean Files	A2-CM.TXT, A2-DEEP.TXT, A2-BURST.TXT		A3-CM.TXT, A3-DEEP.TXT, A3-BURST.TXT									
Latitude	46°26'18"N		46°26'29"N									
Longitude	52°17'41"E		52°17'29"E									
Latitude (fraction degrees)	46.4384		46.4413									
Longitude (fraction degrees)	52.2948		52.2915									
Average Station Depth (m)	4,2		3,2									
Type Instrument	CURRENT METER		CURRENT METER									
Instrument	COASTAL MICROSPEC		S4									
Serial Number	10282		5142326									
Manufacture	COASTAL LEASING, INC		INTEROCEAN, INC.									
Data Beginning	1997.10.31.07.15		1998.04.29.08.18									
Data Ending	1998.04.28.09.45		1998.09.24.06.38									
Station												
Station B-CM North Caspian Sea												
MetOcean Files	B1-CM.TXT	B2-CM.TXT, B2-DEEP.TXT	B3-CM.TXT, B3-DEEP.TXT									
Latitude	46°20'37"N	46°20'21"N	46°20'19"N									
Longitude	51°46'27"E	51°46'08"E	51°46'07"E									
Latitude (fraction degrees)	46.3436	46.3391	46.3386									
Longitude (fraction degrees)	51.7742	51.7689	51.7685									
Average Station Depth (m)	7,5	6,8	7									
Type Instrument	ACOUSTIC-DOPPLER-PROFILER ADCP	ACOUSTIC-DOPPLER-PROFILER ADCP	CURRENT METER									
Instrument	RDI WORKHORSE SENTINNEL 1200 kHz	RDI WORKHORSE SENTINNEL 1200 kHz	COASTAL MICROSPEC									
Serial Number	216	216	10253									
Manufacture	RD INSTRUMENTS, INC.	RD INSTRUMENTS, INC.	COASTAL LEASING, INC.									
Data Beginning	1997.10.11.09.03	1997.10.29.11.37	1998.04.29.17.30									
Data Ending	1997.10.29.08.03	1998.04.28.04.07	1998.09.26.04.15									
Station												
Station C-CM North Caspian Sea												
MetOcean Files	C2-CM.TXT, C2-DEEP.TXT, C2-BURST.TXT		C3-CM.TXT, C3-DEEP.TXT, C3-BURST.TXT									
Latitude	46°18'37"N		46°18'38"N									
Longitude	52°28'37"E		52°28'30"E									
Latitude (fraction degrees)	46.3103		46.3106									
Longitude (fraction degrees)	52.4768		52.4749									
Average Station Depth (m)	4		3,9									
Type Instrument	CURRENT METER		CURRENT METER									
Instrument	COASTAL MICROSPEC		COASTAL MICROSPEC									
Serial Number	10253		10282									
Manufacture	COASTAL LEASING, INC.		COASTAL LEASING, INC.									
Data Beginning	1997.10.29.15.00		1998.04.29.03.45									
Data Ending	1998.04.28.13.50		1998.09.25.02.00									
Station												
Station D-CM North Caspian Sea												
MetOcean Files	D1-CM.TXT, D2-DEEP.TXT	D3-CM.TXT, D3-DEEP.TXT										
Latitude	46°10'33"N	46°10'22"N										
Longitude	51°10'25"E	51°10'31"E										
Latitude (fraction degrees)	46.1759	46.1727										
Longitude (fraction degrees)	51.1736	51.1754										
Average Station Depth (m)	9,5	8,3										
Type Instrument	ACOUSTIC-DOPPLER-PROFILER ADCP	ACOUSTIC-DOPPLER-PROFILER ADCP										
Instrument	RDI WORKHORSE SENTINNEL 1200 kHz	RDI WORKHORSE SENTINNEL 1200 kHz										
Serial Number	79	216										
Manufacture	RD INSTRUMENTS, INC.	RD INSTRUMENTS, INC.										
Data Beginning	1997.10.13.03.34	1998.04.30.07.55										
Data Ending	1997.10.28.08.49	1998.09.26.09.25										
Station												
Station E-CM North Caspian Sea												
MetOcean Files	E3-CM.TXT, E3-DEEP.TXT											
Latitude	44°36'11"N		44°36'11"N									
Longitude	49°50'38"E		49°50'38"E									
Latitude (fraction degrees)	44.6031		49.8439									
Longitude (fraction degrees)	49.8439		15,5									
Average Station Depth (m)	15,5		CURRENT METER									
Type Instrument	S4											
Instrument	5142325											
Serial Number	INTEROCEAN, INC.											
Manufacture	1998.05.01.13.57											
Data Beginning	1998.09.27.06.15											
Station												
Station A-MET North Caspian Sea												
MetOcean Files	WIND-1.TXT, METOR-1.TXT	WIND-2.TXT, METOR-2.TXT		WIND-3.TXT, METOR-3.TXT								
Latitude	46°26'24"N	45°01'00"N		46°26'29"N								
Longitude	52°17'15"E	51°41'00"E		52°17'29"E								
Latitude (fraction degrees)	46.4399	45.0167		46.4413								
Longitude (fraction degrees)	52.2875	51.6833		52.2915								
Station Height (m)	4,5	8,5		4,5								
Type Instrument	Meteorological	Meteorological		Meteorological								
Instrument	MicroWind	MicroWind		MicroWind								
Serial Number	10360	10360		10360								
Manufacture	COASTAL LEASING, INC.	COASTAL LEASING, INC.		COASTAL LEASING, INC.								
Data Beginning	1997.10.12.09.00	1997.11.11.14.00		1998.04.29.11.00								
Data Ending	1997.10.30.09.30	1998.04.23.12.00		1998.06.17.14.35								

APPENDIX**II. Proof that wind on the Northern part of Caspian Sea can be modelled as uniform**

II.1 Comparison of wind speeds and directions of various grid point of NCEP on the Northern part of the Caspian Sea



Wind speeds and directions at various grid points of the NCEP dataset, located on the Northern part of the Caspian Sea compared with the wind speeds and directions at the grid point with coordinates 46.666N-50.63E



APPENDIX

**III. Geometry of the Caspian Sea
(taken from MSC thesis by Van Thiel de Vries; paragraph 4.3.1)**

III.1 Paragraph 4.3.1 of Van Thiel de Vries' thesis, dealing with the geometry of the Caspian Sea

The geometry of the model for this study is composed of two sources:

- a Russian Marine chart (nr 31003): The available water depths are from 1989. By adding 0.14 meter, the bottom level in relation to Caspian Datum is found. This map has been digitised for this study.
- A digital map of contour lines of the whole Caspian Sea: This map is downloaded from www.caspianenvironment.org. The underlying data set originates from the Defense Ministry of the USSR in 1987. By adding - 0.86 the bottom level in relation to Caspian Datum is found.

Using the program Coordinate Calculator CC version 4.0, all geographical positions in the maps above were referenced to the Krassovsky 1940 spheroid and all grid positions were referenced to the Gauss Kruger Zone 9 Transverse Mercator projection.

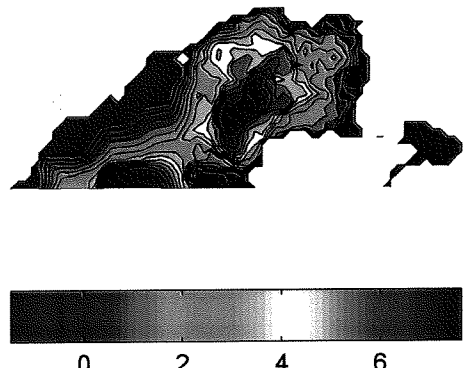
Subsequently the geometry for the model was composed with use of Delft 3D. The depths at the grid points were determined by triangle interpolation. Since in the North Caspian Sea the geometry was determined by two sources (map nr 31003 and the digital map from Caspian Environment) the triangle interpolations resulted in strange gradients in the bottom level that were not likely to be natural. For this reason the less accurate Caspian Environment geometry was not involved to obtain the geometry of the North Caspian Sea.

The resulting geometry is shown in the figures below:

Caspian Sea: depth below CD [m]



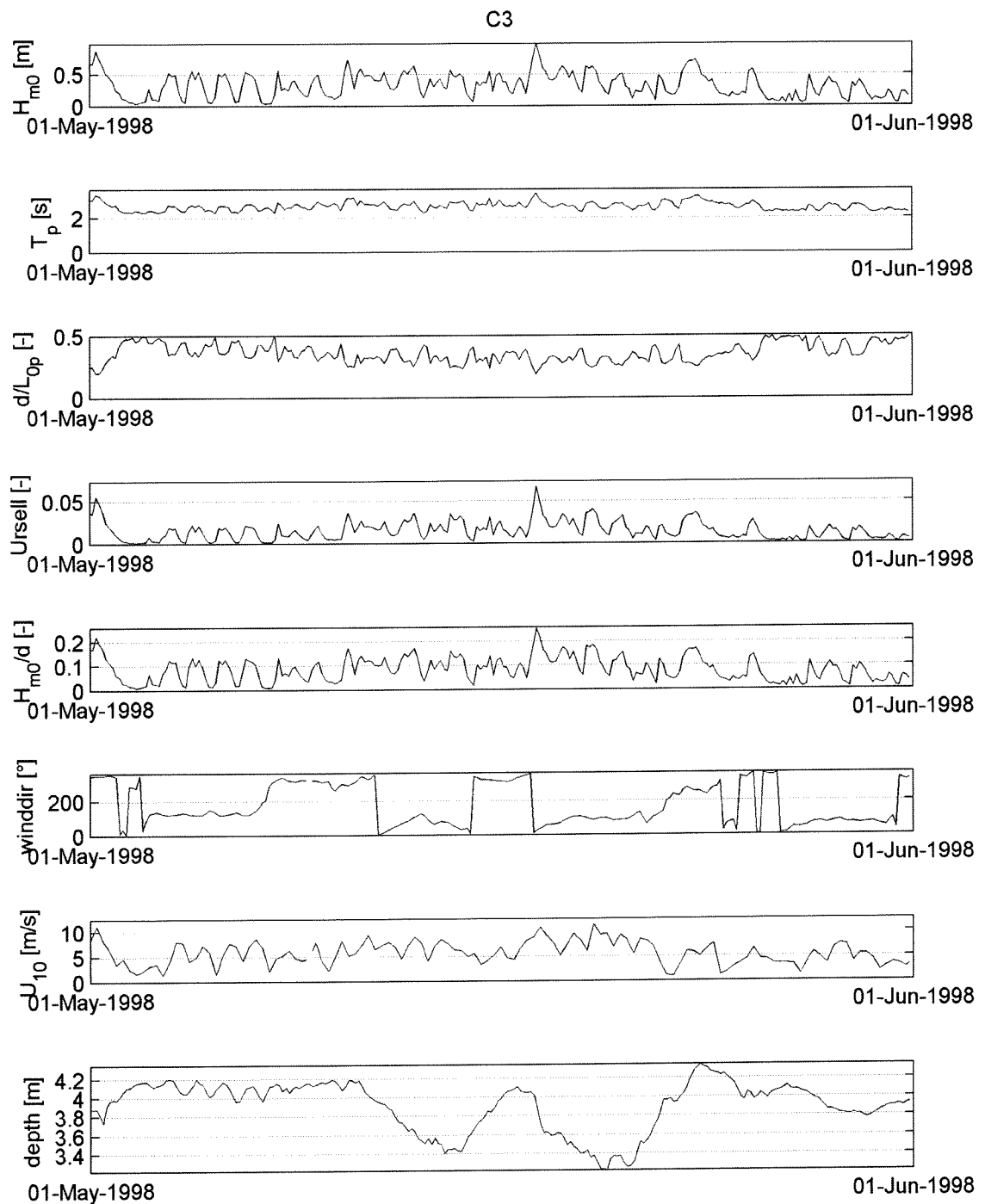
North Caspian Sea: depth below CD [m]



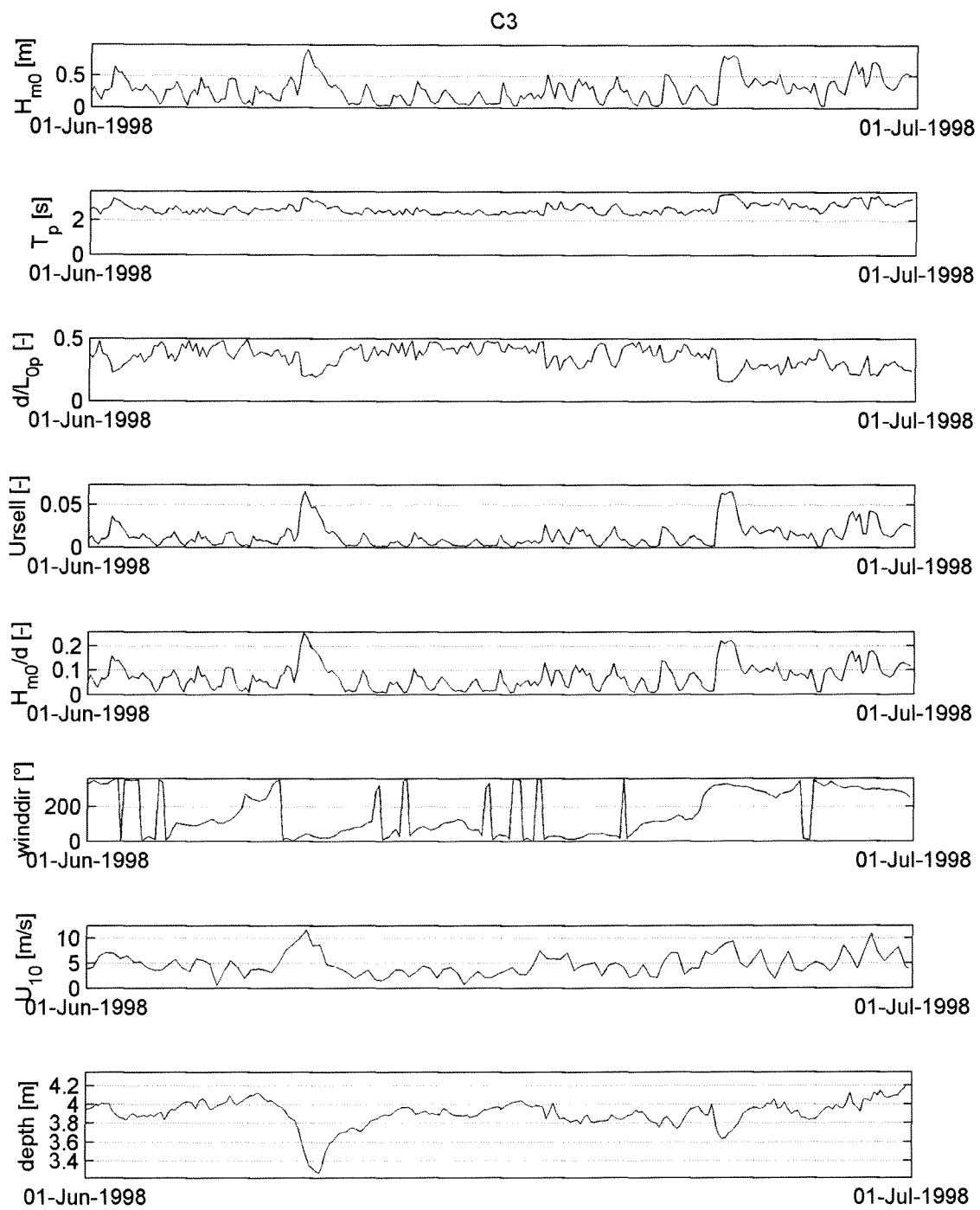
APPENDIX

IV. Plots of the measurements' characteristic parameters in time

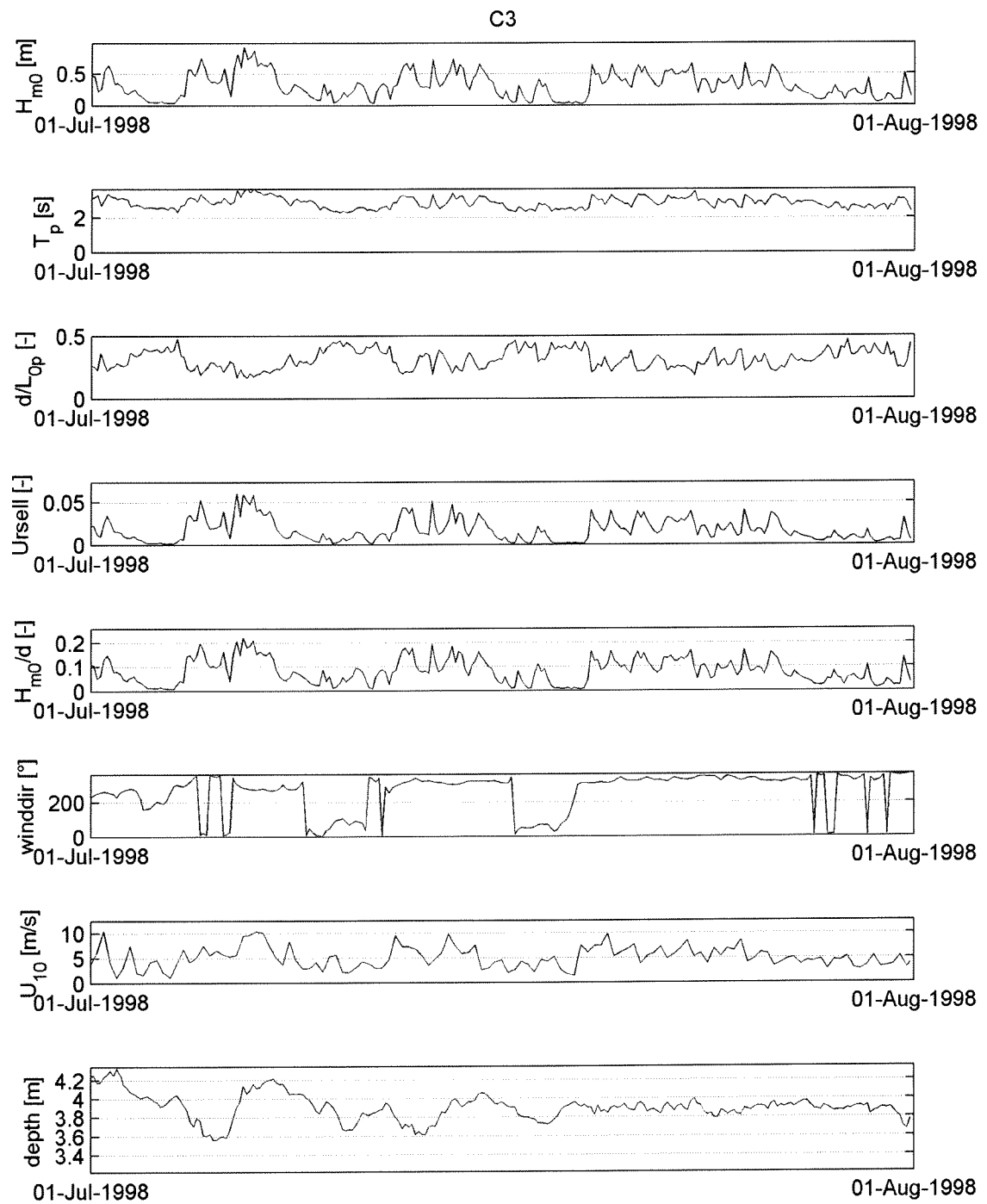
IV.1 Characteristic parameters of the (wave-) climate in May 1998
 Used for the choice of characteristic timeseries needed for the calibration of the model



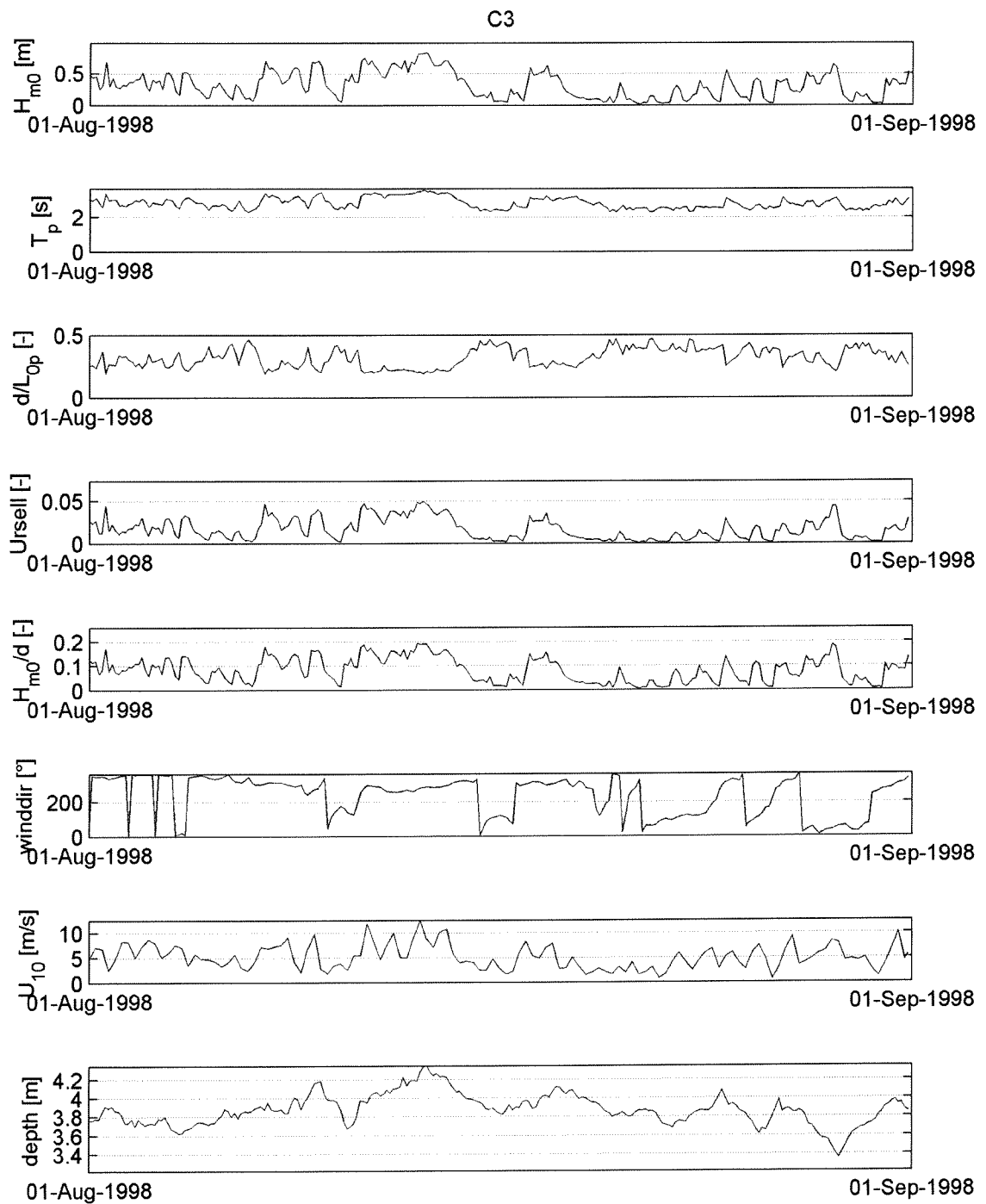
IV.2 Characteristic parameters of the (wave-) climate in June 1998
 Used for the choice of characteristic timeseries needed for the calibration of the model



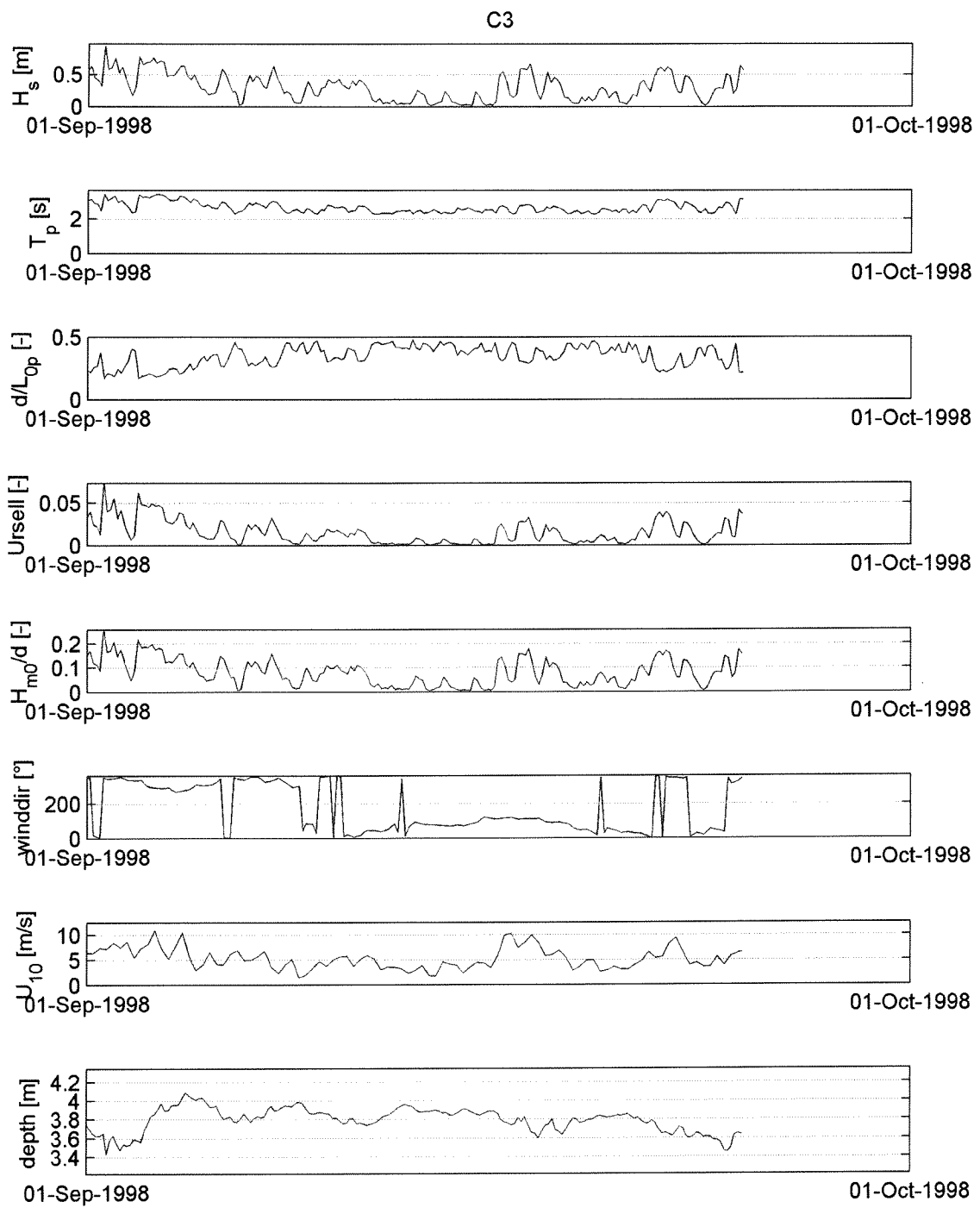
IV.3 Characteristic parameters of the (wave-) climate in July 1998
 Used for the choice of characteristic timeseries needed for the calibration of the model



IV.4 Characteristic parameters of the (wave-) climate in August 1998
 Used for the choice of characteristic timeseries needed for the calibration of the model



IV.5 Characteristic parameters of the (wave-) climate in September 1998
 Used for the choice of characteristic timeseries needed for the calibration of the model



APPENDIX

V. SWAN input file of chosen calibration (validation run)

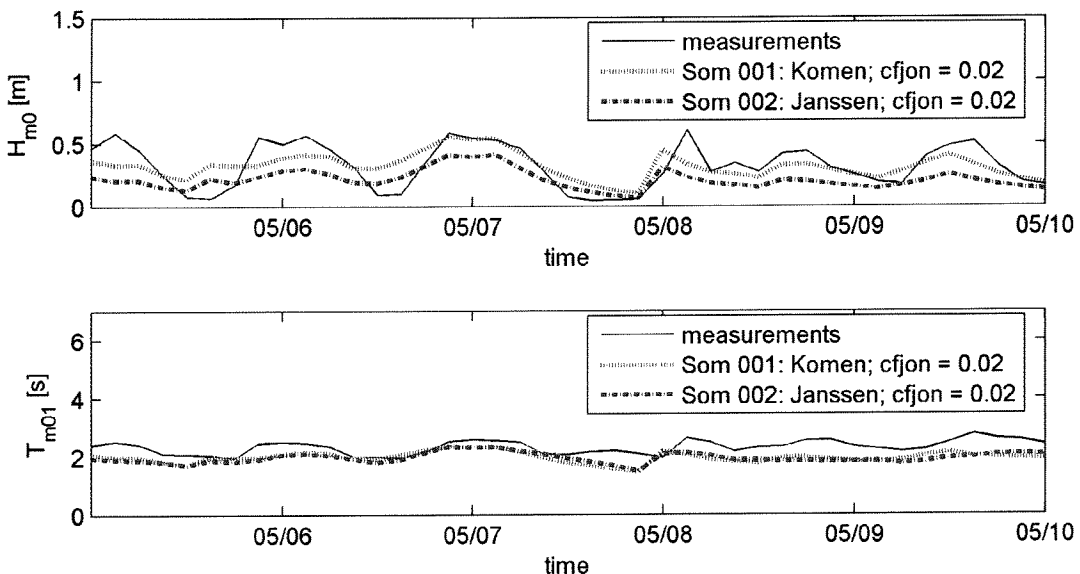
V.1 SWAN input file of Validation run Som 201

```
PROJECT '2-D NS' ''  
SET level=0 NAUTICAL  
SET rho = 1013  
  
MODE NONSTATIONARY TWODIMENSIONAL  
  
COORDINATES CARTESIAN  
  
CGRID REGULAR 0 0 0.00 1000000 1300000 100 130 CIRCLE 36 0.15 1 30  
  
INPGRID BOTTOM REGULAR 0 0 0 100 130 10000 10000 EXCEPTION -999.000  
INPGRID WIND REGULAR 0 0 0 1 1 1000000 1300000 NONSTATIONARY 19980429.110000 20  
MIN 19980617.104000  
INPGRID WLEVEL 5000 5000 0 99 129 10000 10000 EXCEPTION 9.9899990e+002 NONSTA-  
TIONARY 19980429.120000 3 HR 19980617.120000  
  
READINP BOTTOM 1. 'caspian_depth_10k_2.dep' idla=1  
READINP WIND 1 SERIES 'names.wnd' idla=1  
READINP WLEVEL 1 SERIES 'names.wd' idla=3  
  
GEN3 KOMEN AGROW  
WCAP KOM cds2=2.36E-5 stpm=3.02E-3 powst=2 delta=1 powk=1  
FRICTION 0.04  
  
NUMERIC ACCUR drel=0.05 dhoval=0.05 dtoval=0.05 npnts=98 NONST 30 0.1 SIGIMPL 0.5 -3 0  
1e-4 0 20  
  
TEST POINTS XY 613671 1131692 PAR 'Source_terms.plt' S2D 'Source_terms.s2d'  
  
POINTS 'C' 613671 1131692  
  
SPECOUT 'C' SPEC2D ABS '2D_spectrum.s2d' OUTPUT 19980522.000000 3 HR  
  
COMPUTE NONSTATIONARY 19980521.000000 3 HR 19980602.000000  
  
STOP
```

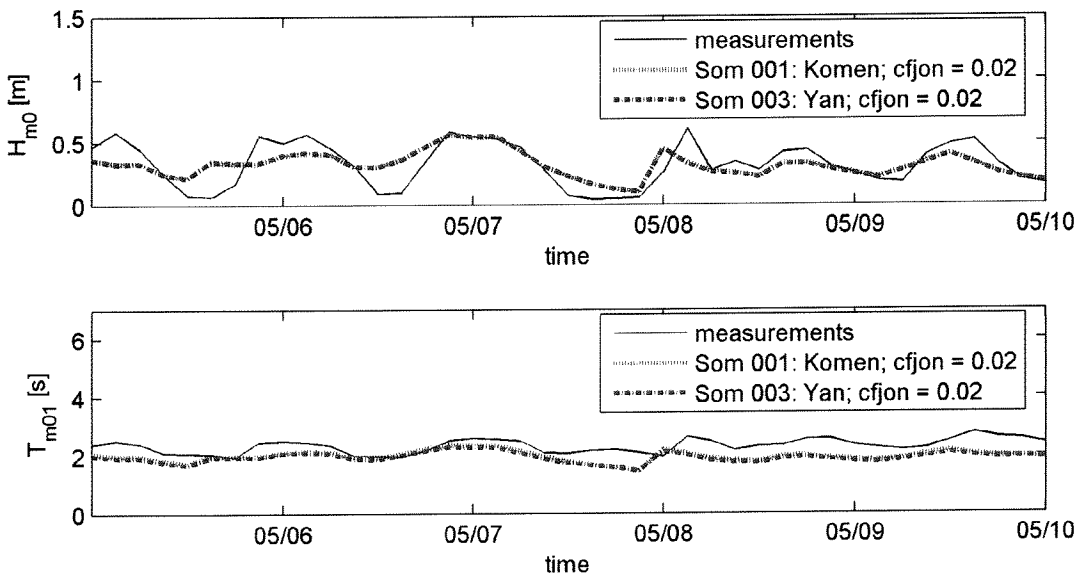
APPENDIX

VI. Plots of calibration of Wind input on deep water timeseries

VI.1 H_{m0} and T_{m01} in time. Comparing Som 001 and Som 002 with the measurements

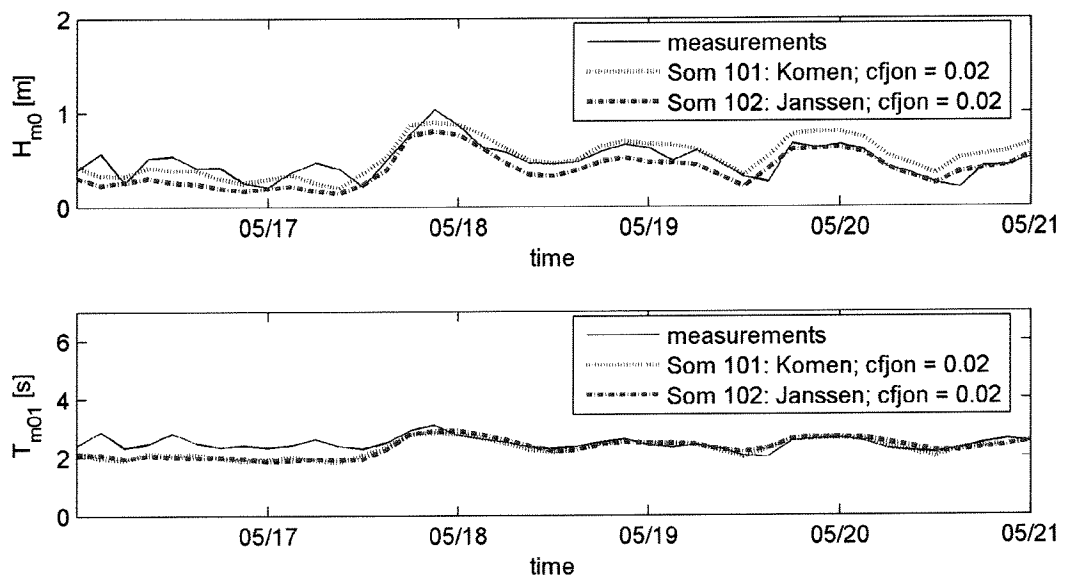


VI.2 H_{m0} and T_{m01} in time. Comparing Som 001 and Som 003 with the measurements

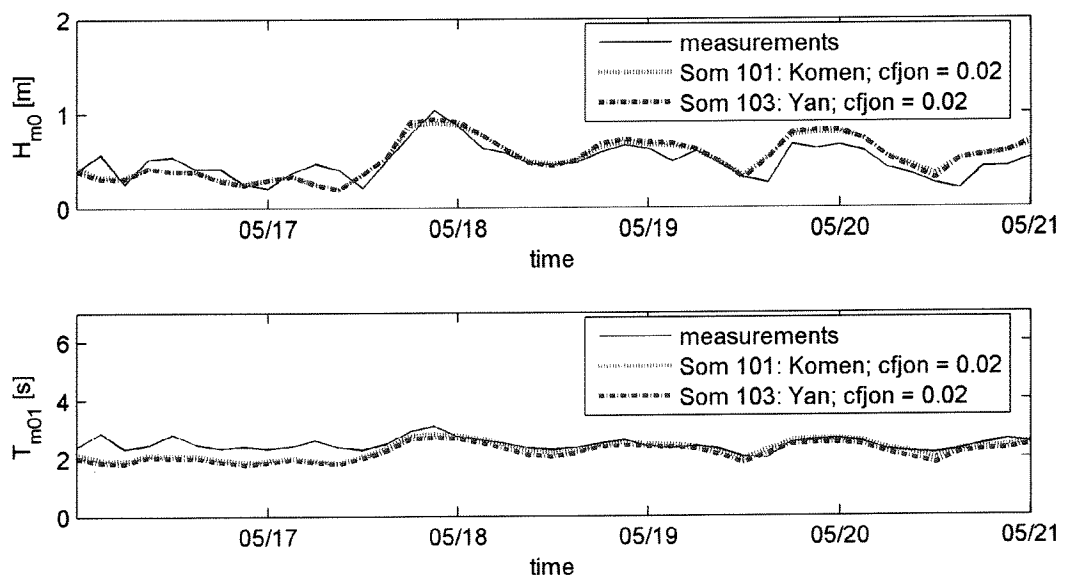


APPENDIX VII. Plots of calibration of Wind input on shallow water timeseries

VII.1 H_{m0} and T_{m01} in time. Comparing Som 101 and Som 102 with the measurements

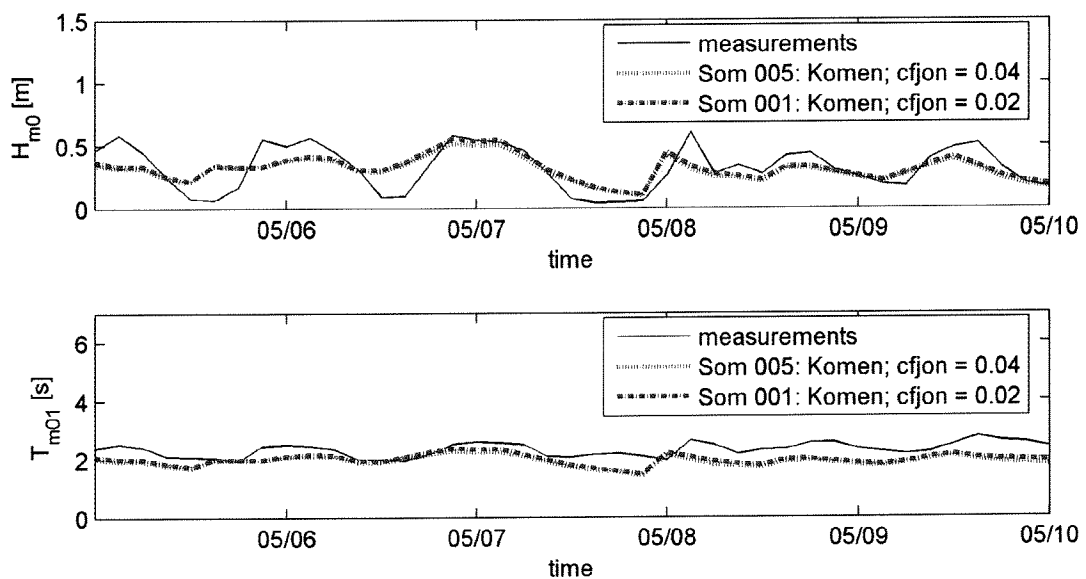


VII.2 H_{m0} and T_{m01} in time. Comparing Som 101 and Som 103 with the measurements

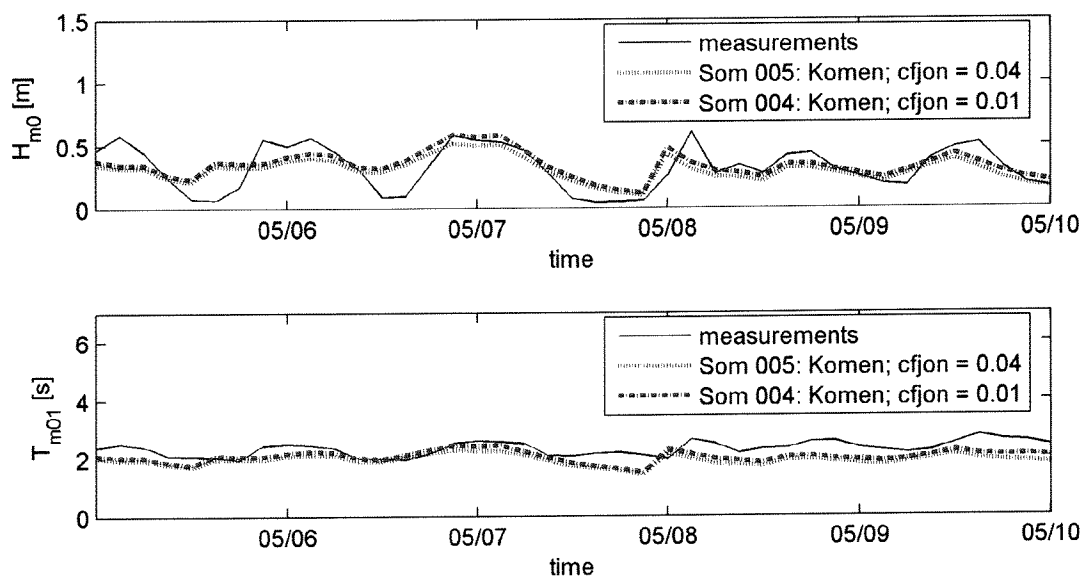


APPENDIX VIII. Plots of calibration of Bottom friction on deep water timeseries

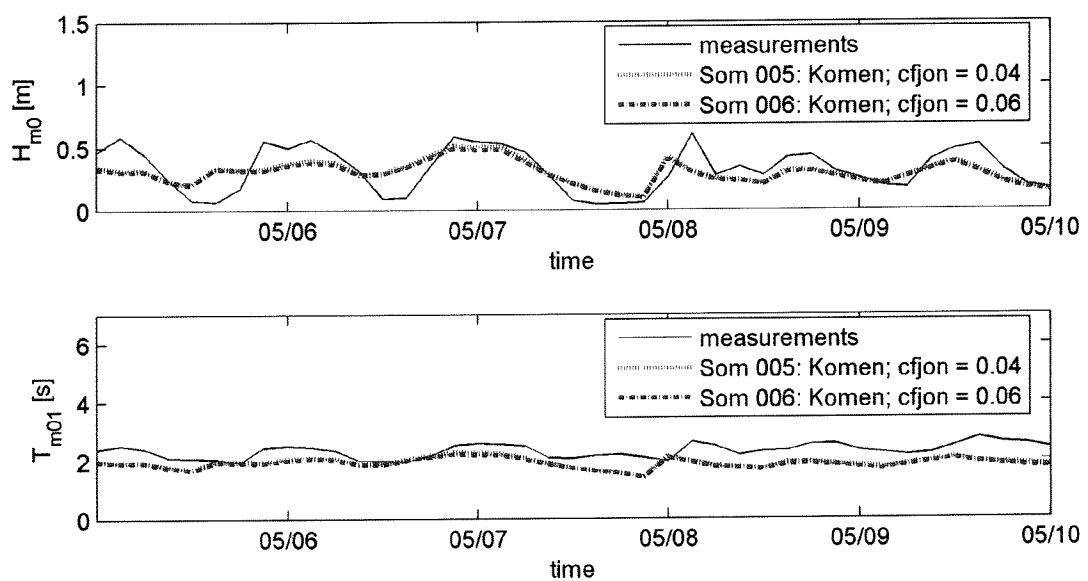
VIII.1 H_{m0} and T_{m01} in time. Comparing Som 005 and Som 001 with the measurements



VIII.2 H_{m0} and T_{m01} in time. Comparing Som 005 and Som 004 with the measurements

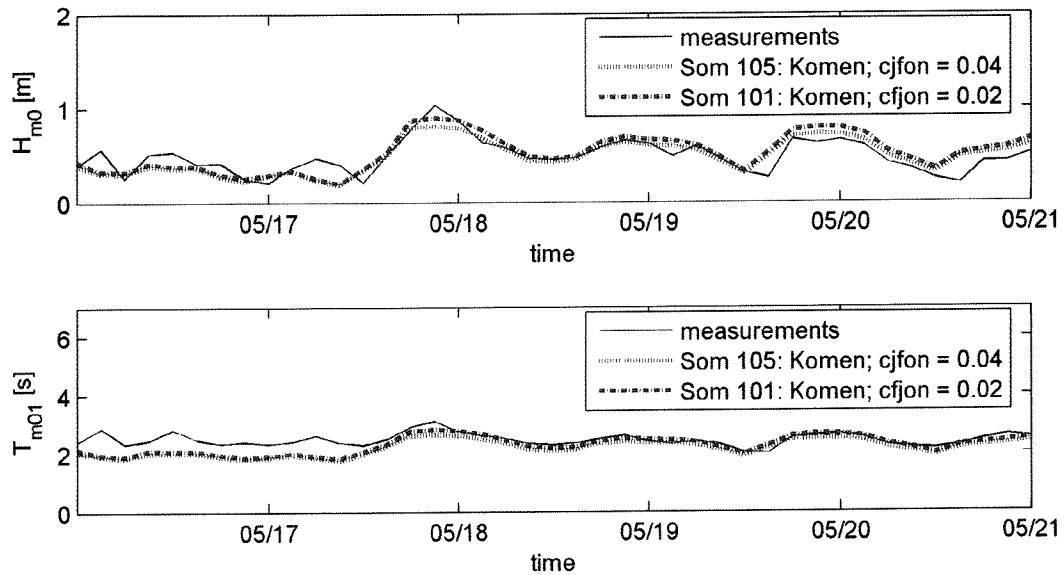


VIII.3 H_{m0} and T_{m01} in time. Comparing Som 005 and Som 006 with the measurements

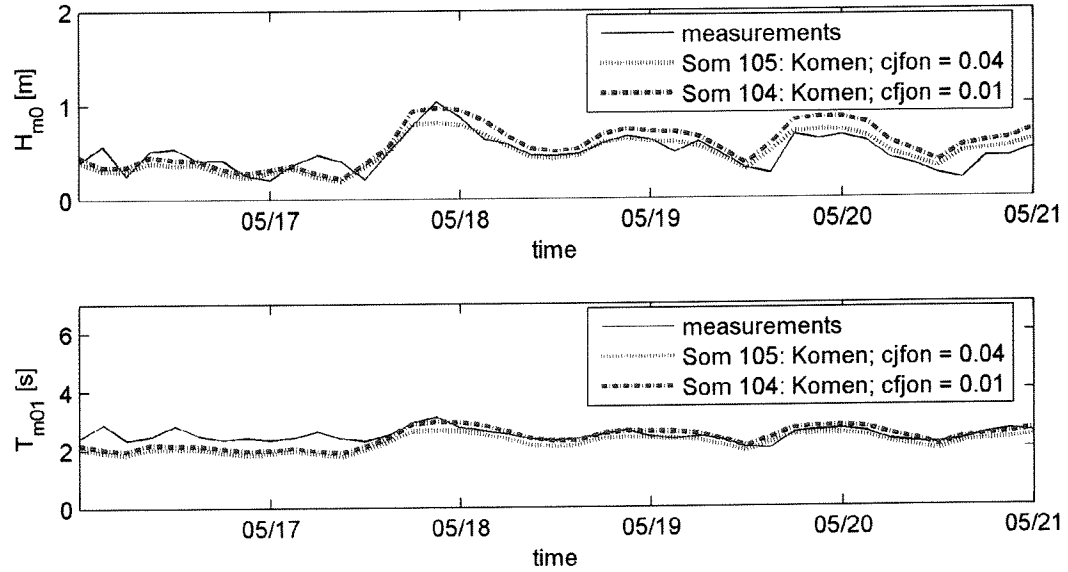


APPENDIX IX. Plots of calibration of Bottom friction on shallow water timeseries

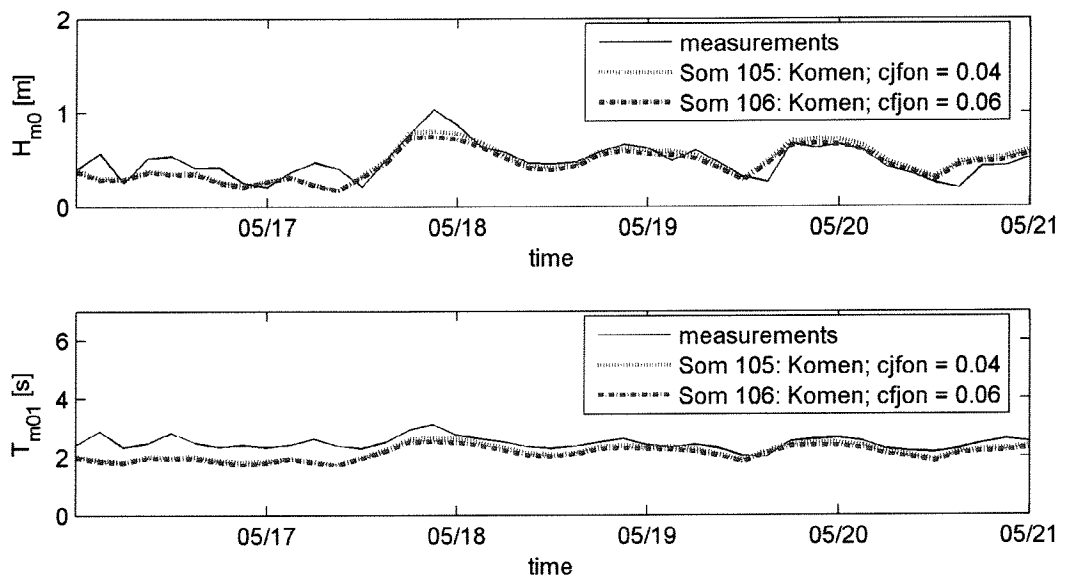
IX.1 H_{m0} and T_{m01} in time. Comparing Som 105 and Som 101 with the measurements



IX.2 H_{m0} and T_{m01} in time. Comparing Som 105 and Som 104 with the measurements



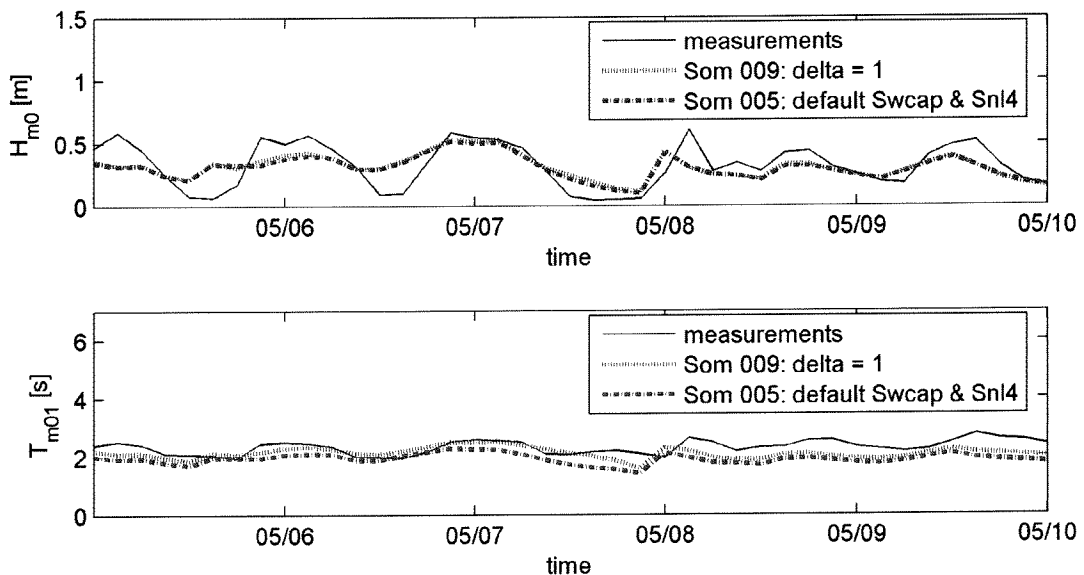
IX.3 H_{m0} and T_{m01} in time. Comparing Som 105 and Som 106 with the measurements



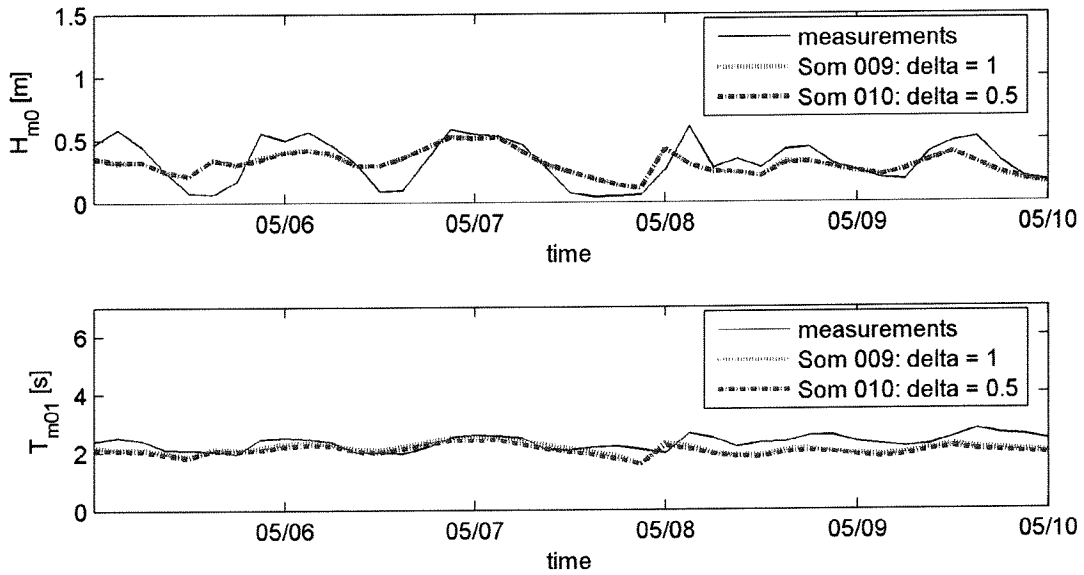
APPENDIX

**X. Plots of calibration of Whitecapping and Quadruplets on deep
water timeseries**

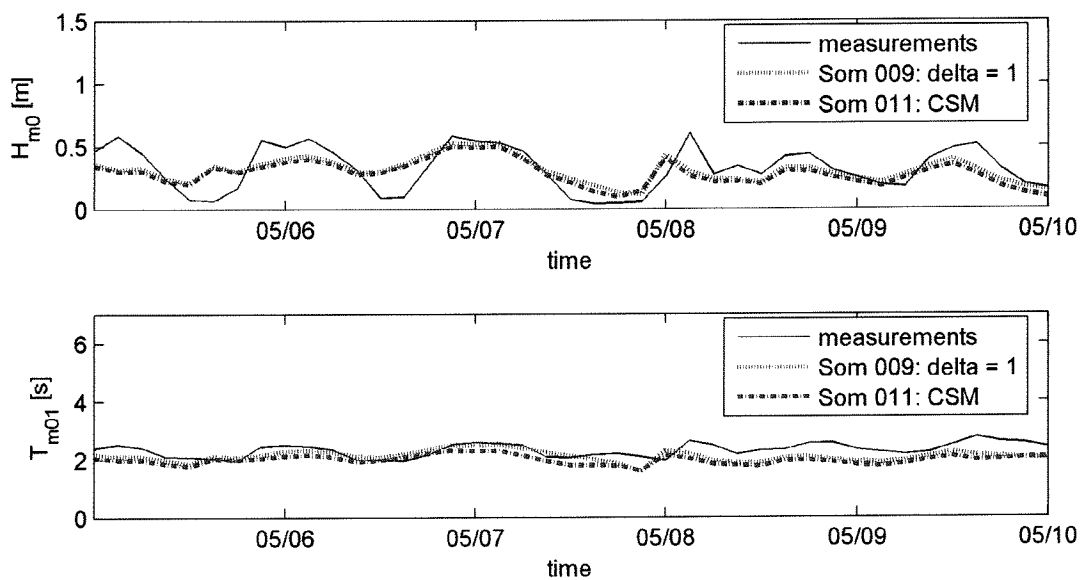
X.1 H_{m0} and T_{m01} in time. Comparing Som 009 and Som 005 with the measurements



X.2 H_{m0} and T_{m01} in time. Comparing Som 009 and Som 010 with the measurements

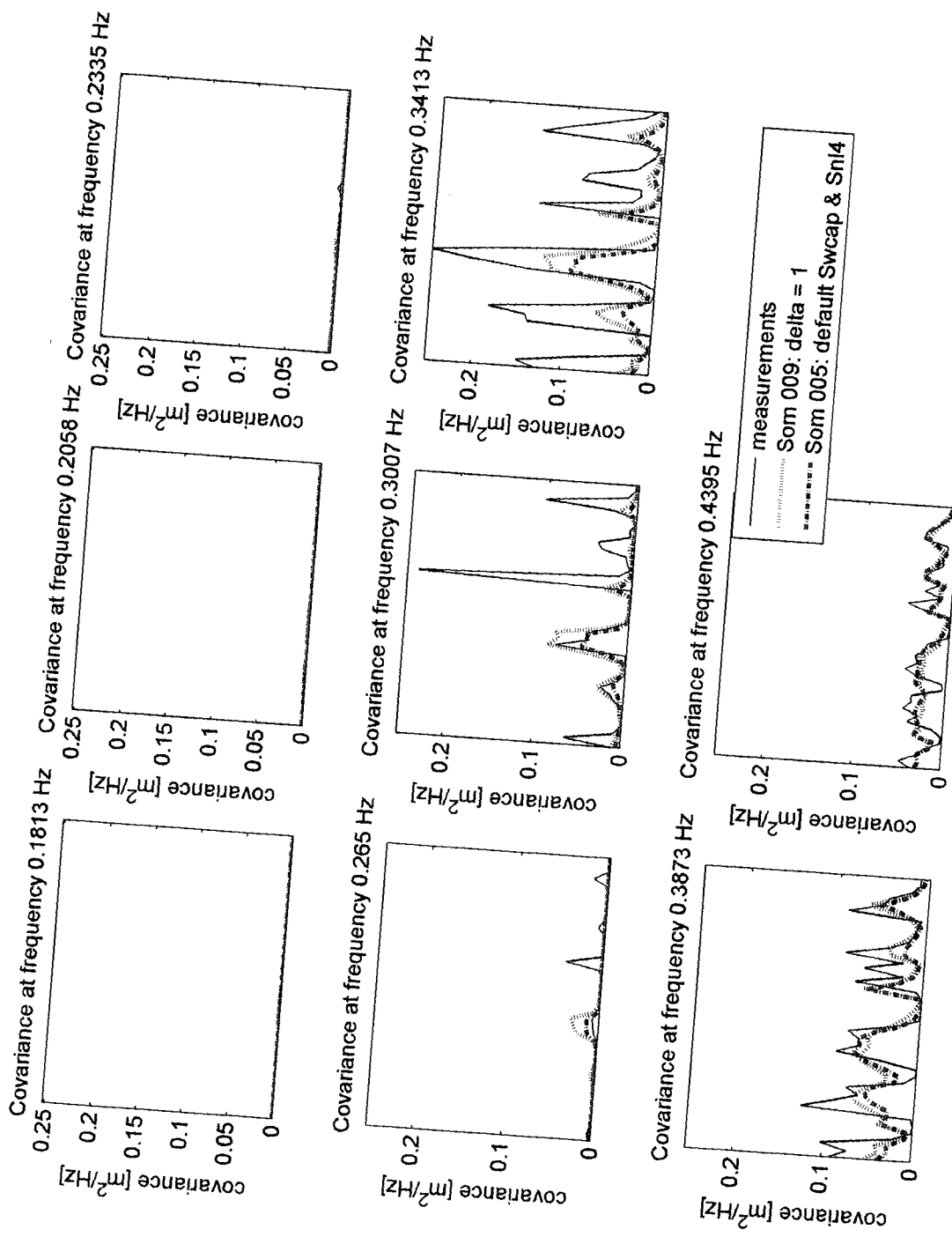


X.3 H_{m0} and T_{m01} in time. Comparing Som 009 and Som 011 with the measurements



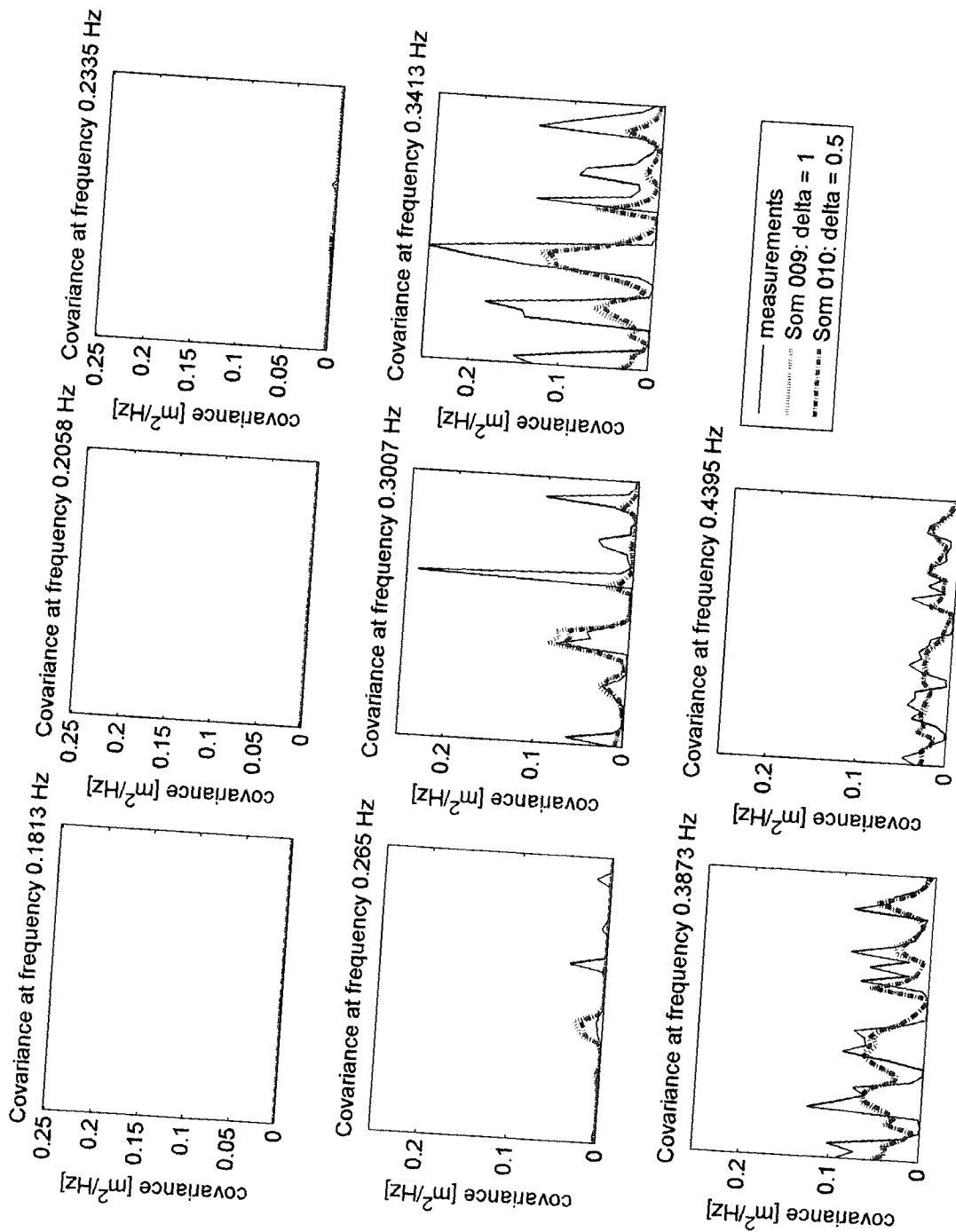
X.4

Covariance at certain wave frequencies of the spectrum, development in time
 Comparing Som 009 and Som 005 with the measurements



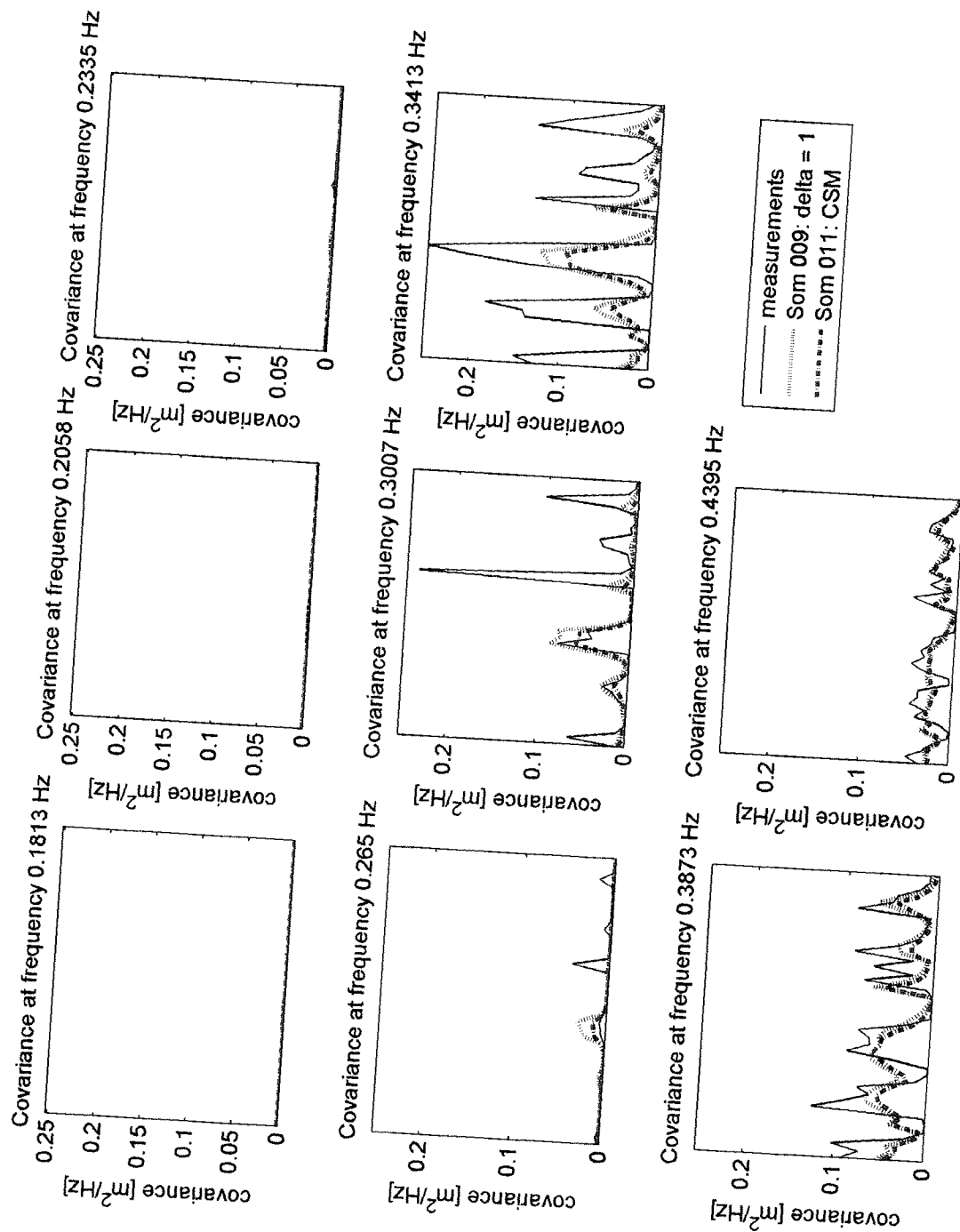
X.5

Covariance at certain wave frequencies of the spectrum, development in time
Comparing Som 009 and Som 010 with the measurements

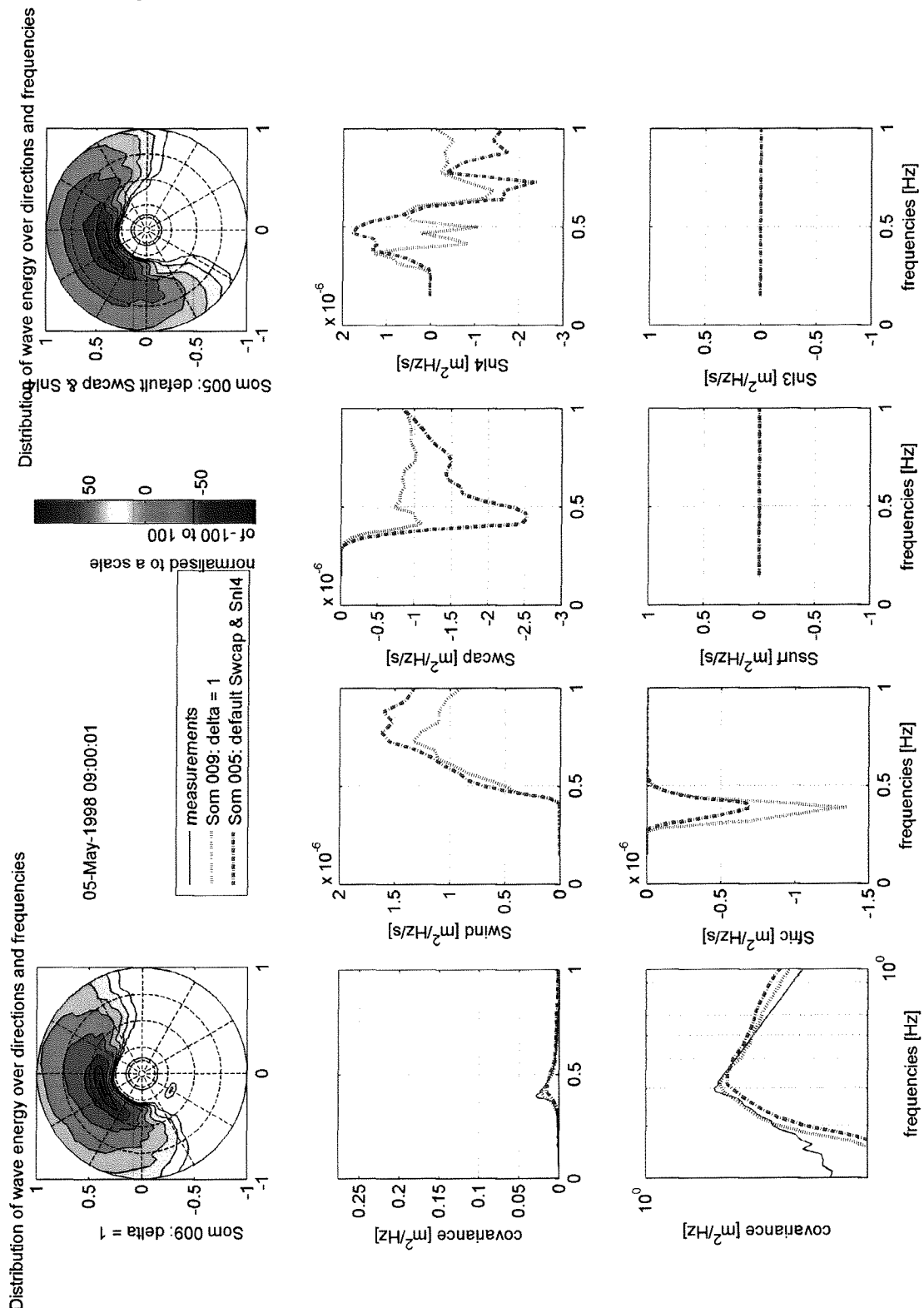


X.6

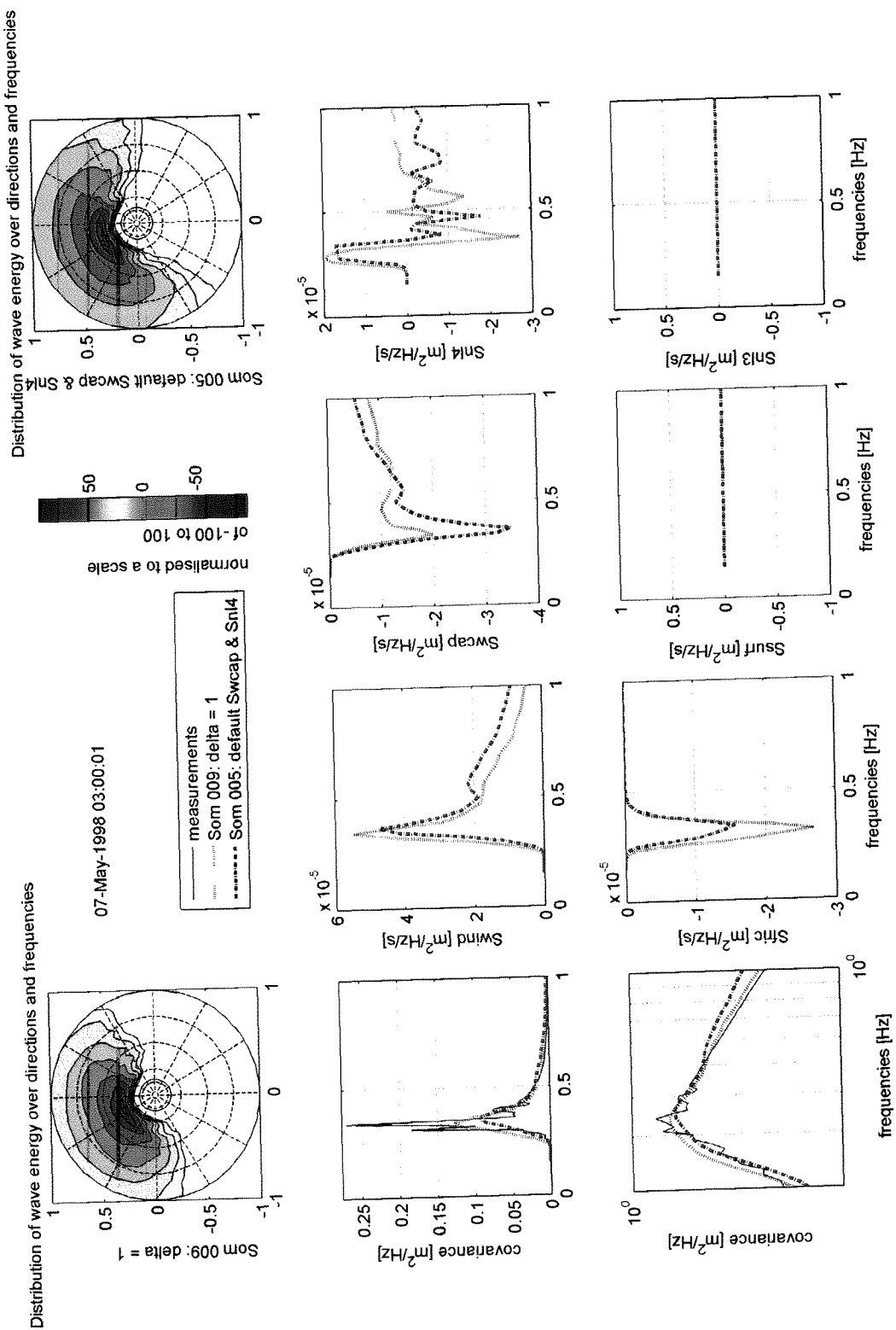
Covariance at certain wave frequencies of the spectrum, development in time
 Comparing Som 009 and Som 011 with the measurements



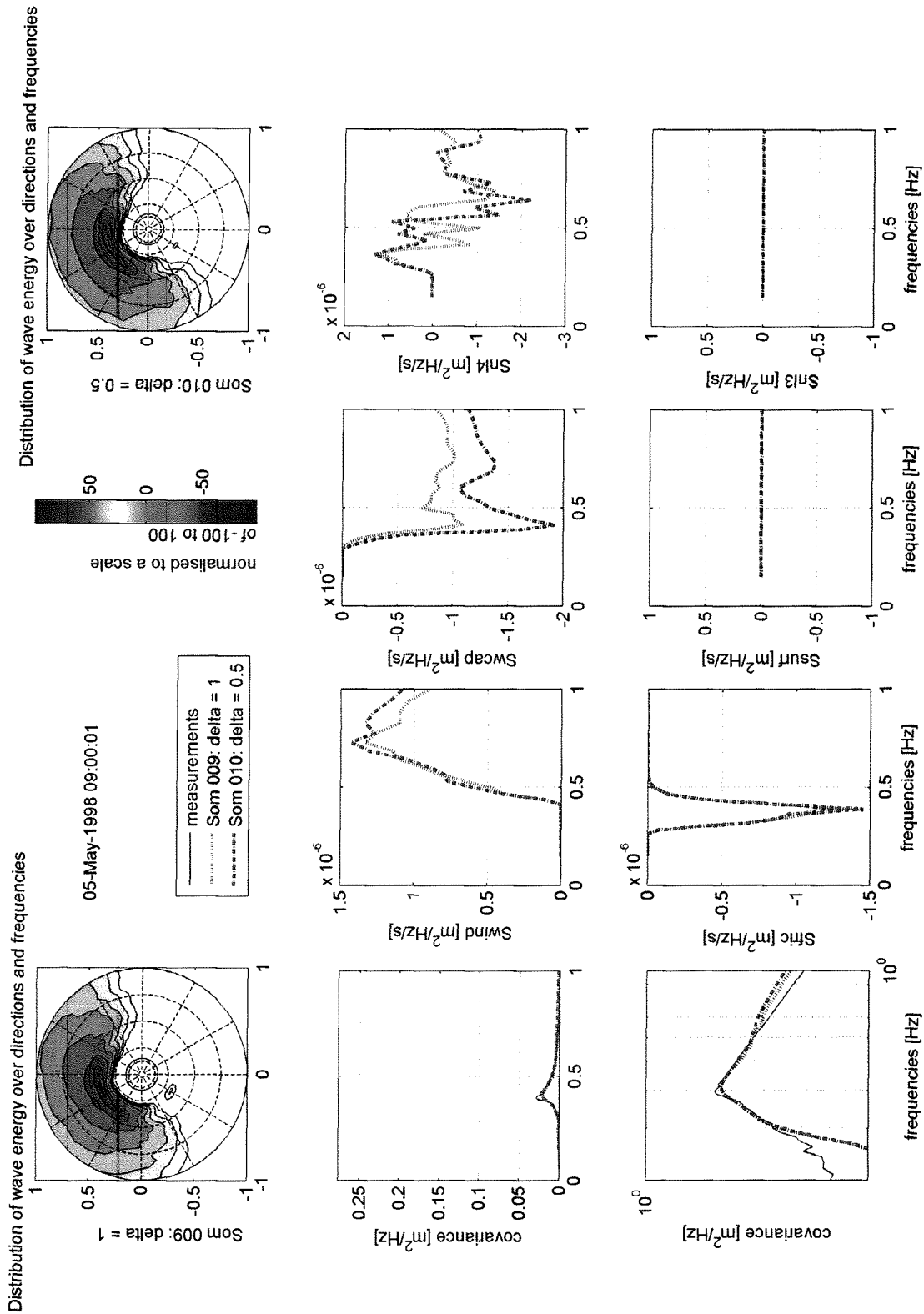
X.7 Wave spectra and source terms at 5 May 1998 09:00
 Comparing Som 009 and Som 005 with the measurements



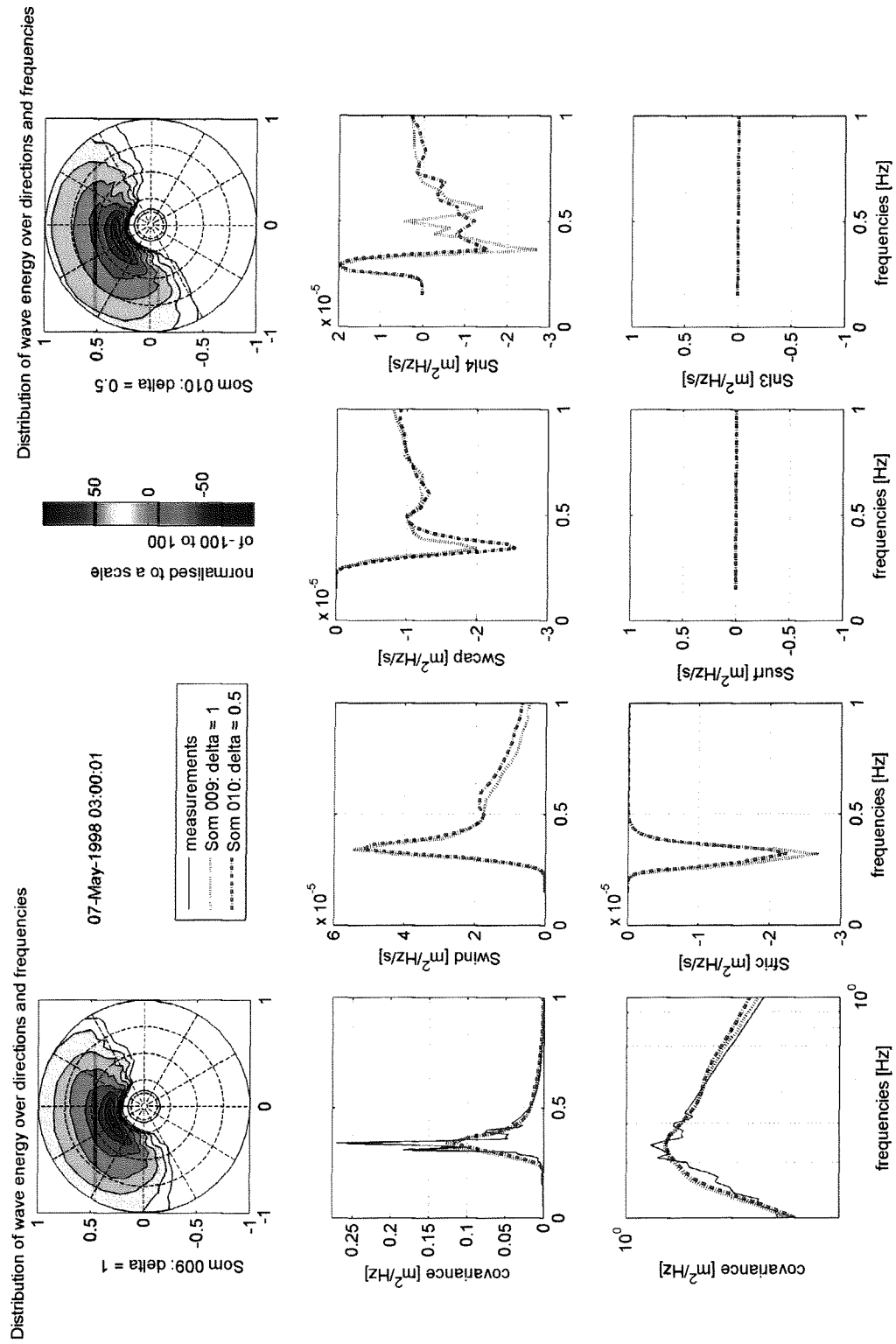
X.8 Wave spectra and source terms at 7 May 1998 03:00
 Comparing Som 009 and Som 005 with the measurements



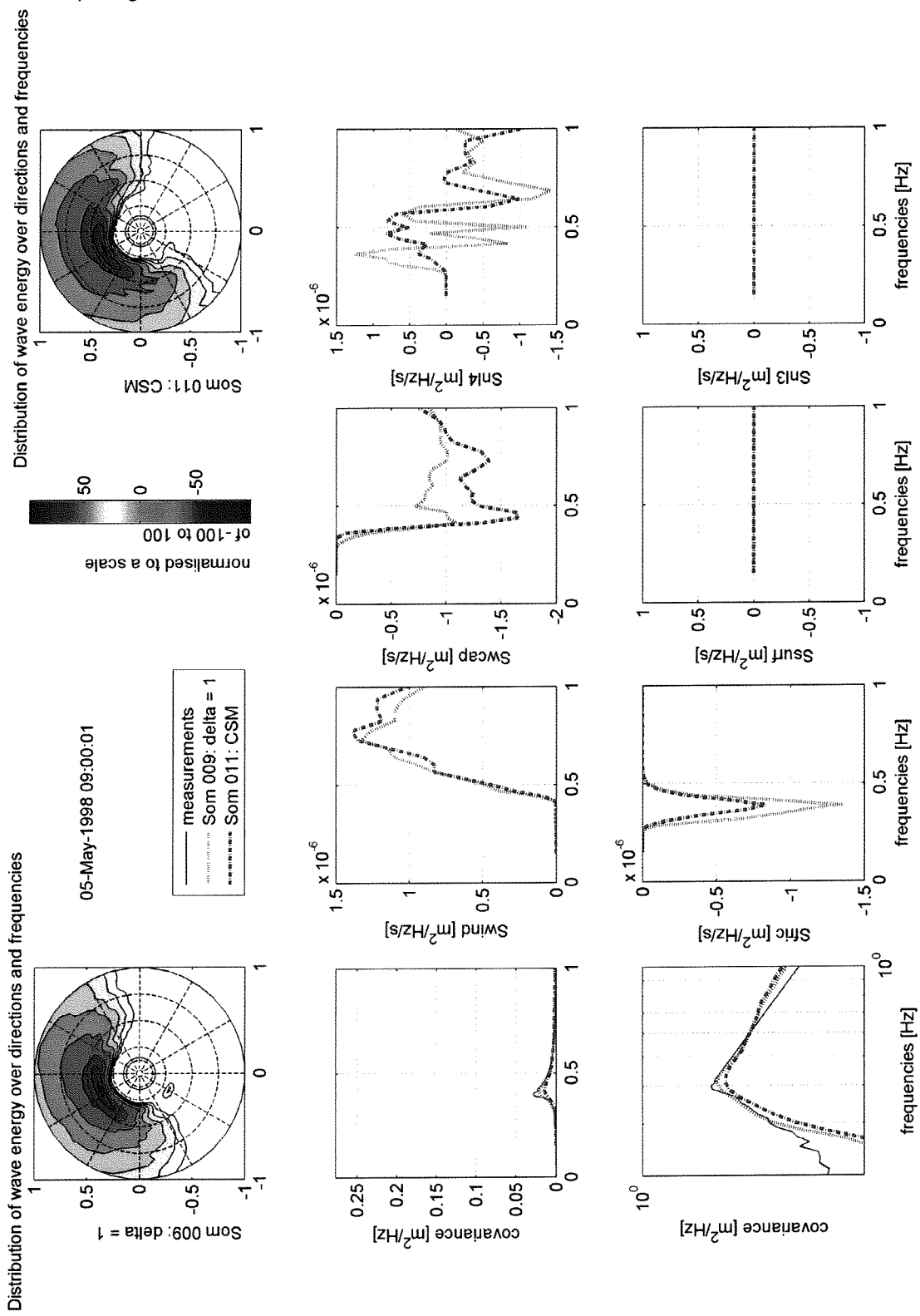
X.9 Wave spectra and source terms at 5 May 1998 09:00
 Comparing Som 009 and Som 010 with the measurements



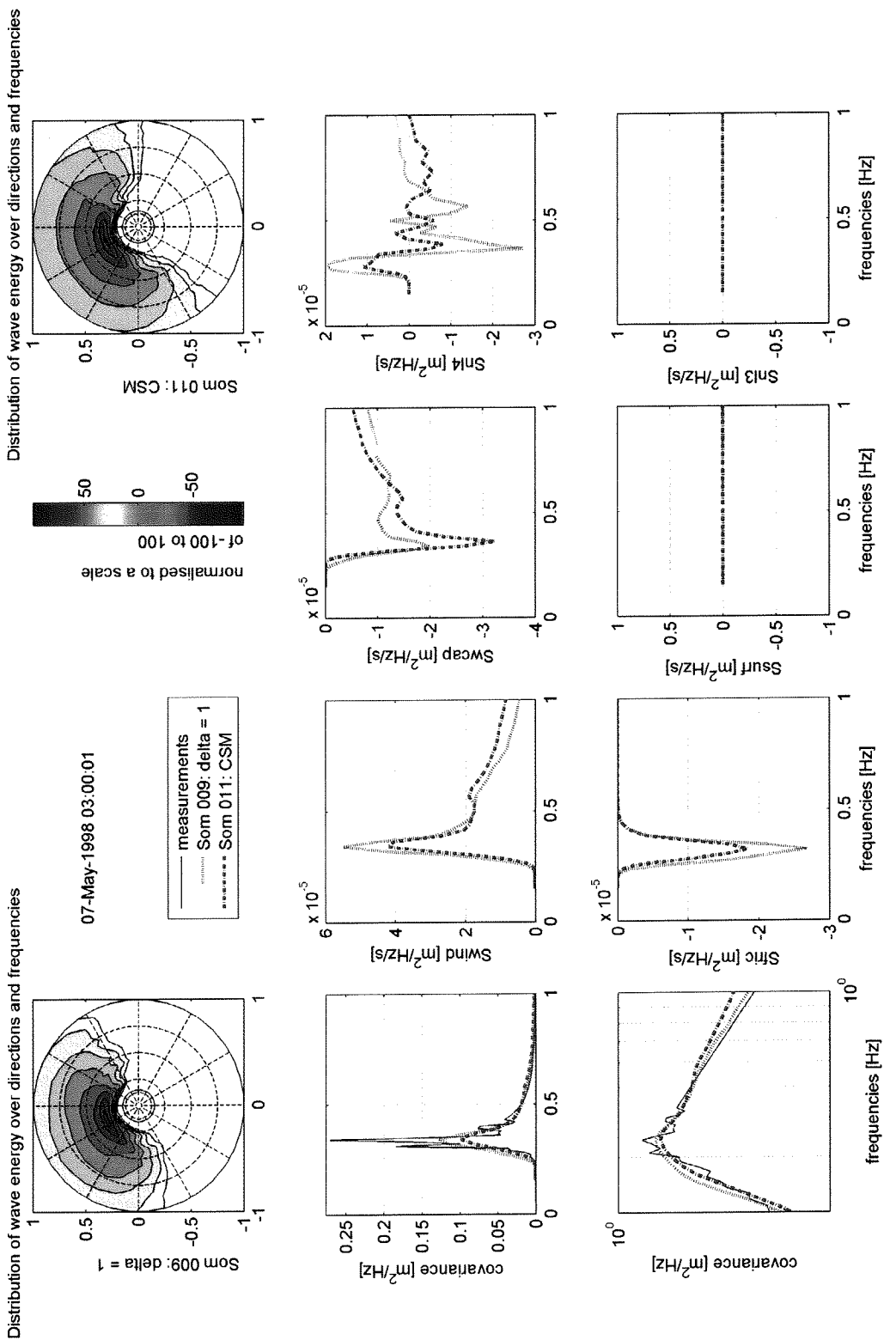
X.10 Wave spectra and source terms at 7 May 1998 03:00
 Comparing Som 009 and Som 010 with the measurements



X.11 Wave spectra and source terms at 5 May 1998 09:00
 Comparing Som 009 and Som 011 with the measurements



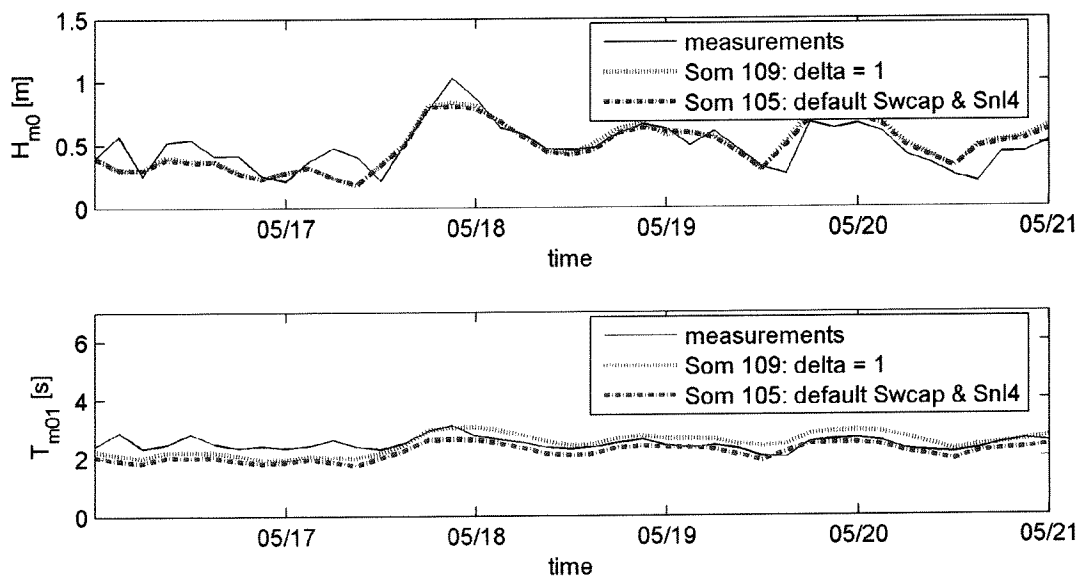
X.12 Wave spectra and source terms at 7 May 1998 03:00
 Comparing Som 009 and Som 011 with the measurements



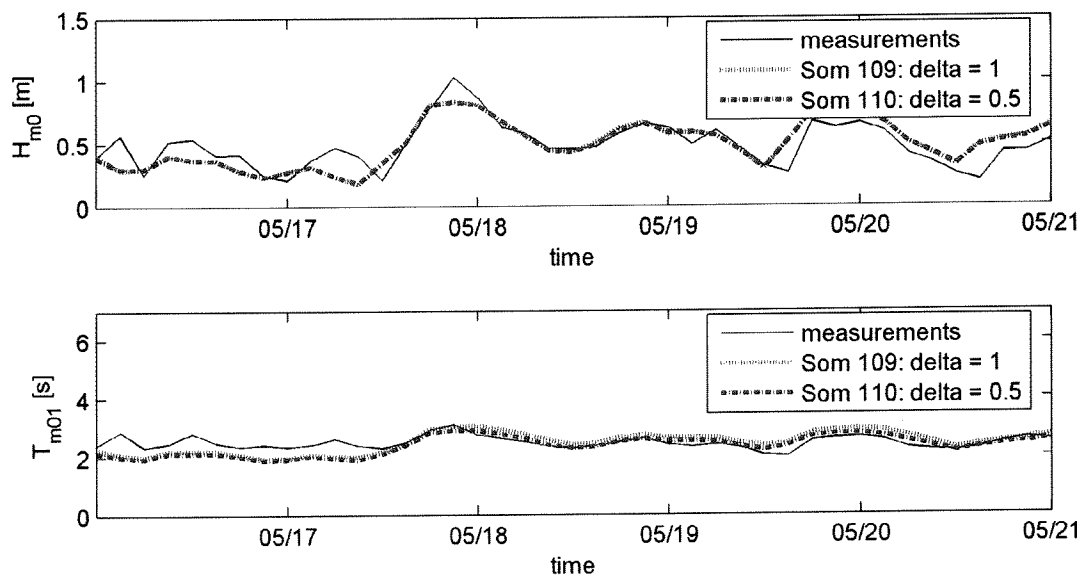
APPENDIX

XI. Plots of calibration of Whitecapping and Quadruplets on shallow water timeseries

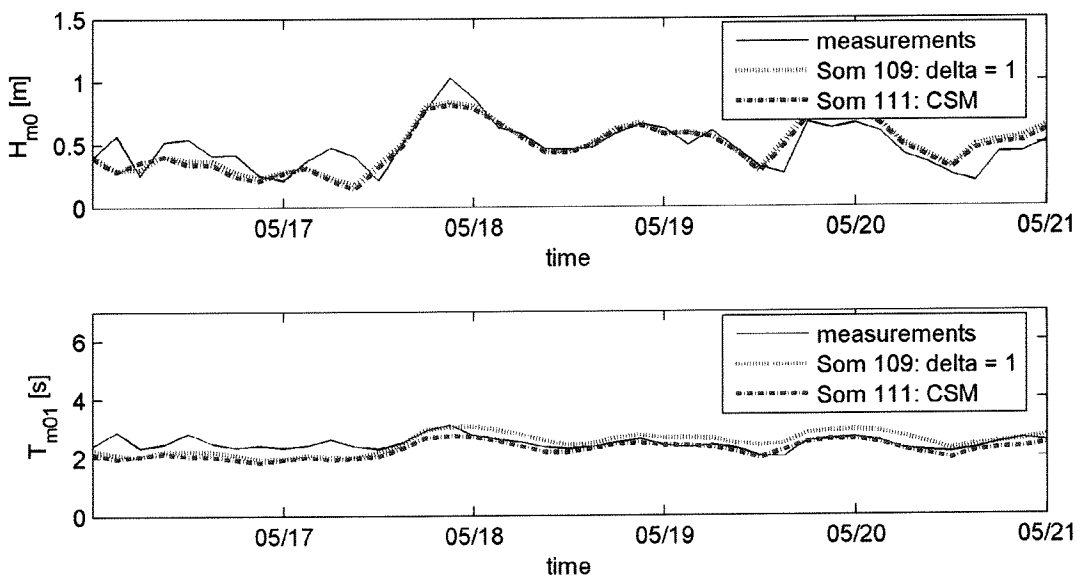
XI.1 H_{m0} and T_{m01} in time. Comparing Som 109 and Som 105 with the measurements



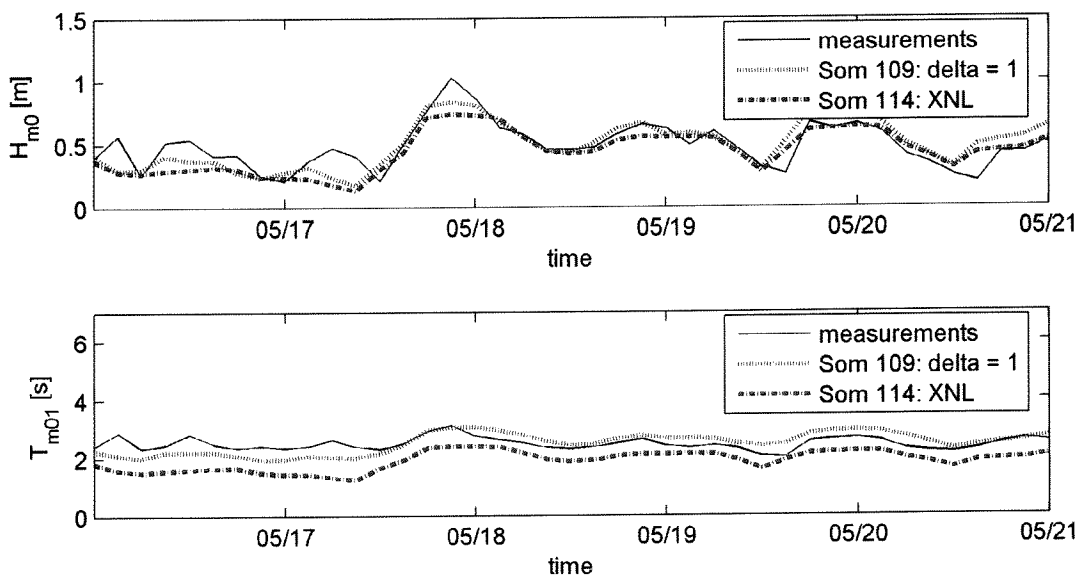
XI.2 H_{m0} and T_{m01} in time. Comparing Som 109 and Som 110 with the measurements



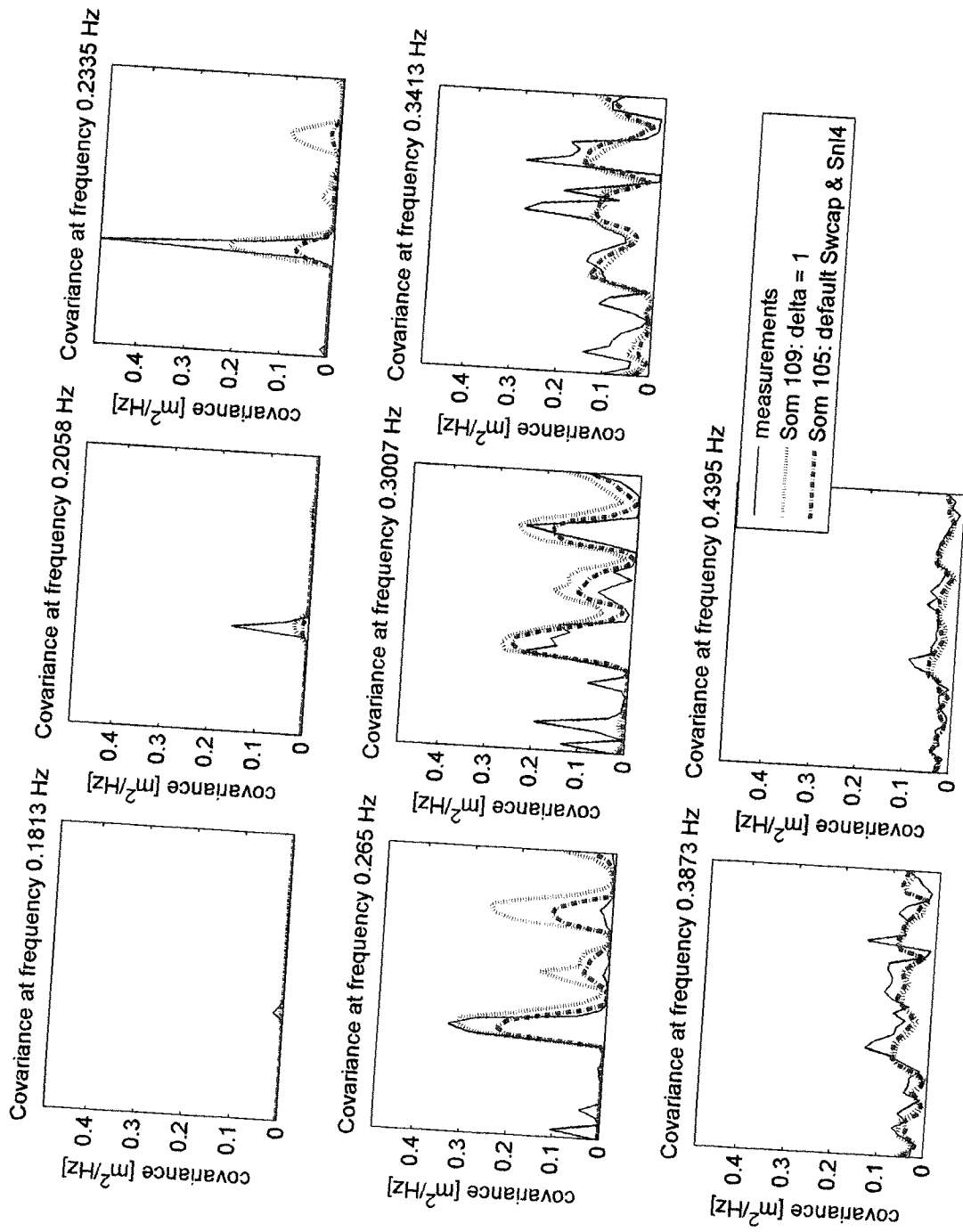
XI.3 H_{m0} and T_{m01} in time. Comparing Som 109 and Som 111 with the measurements



XI.4 H_{m0} and T_{m01} in time. Comparing Som 109 and Som 114 with the measurements

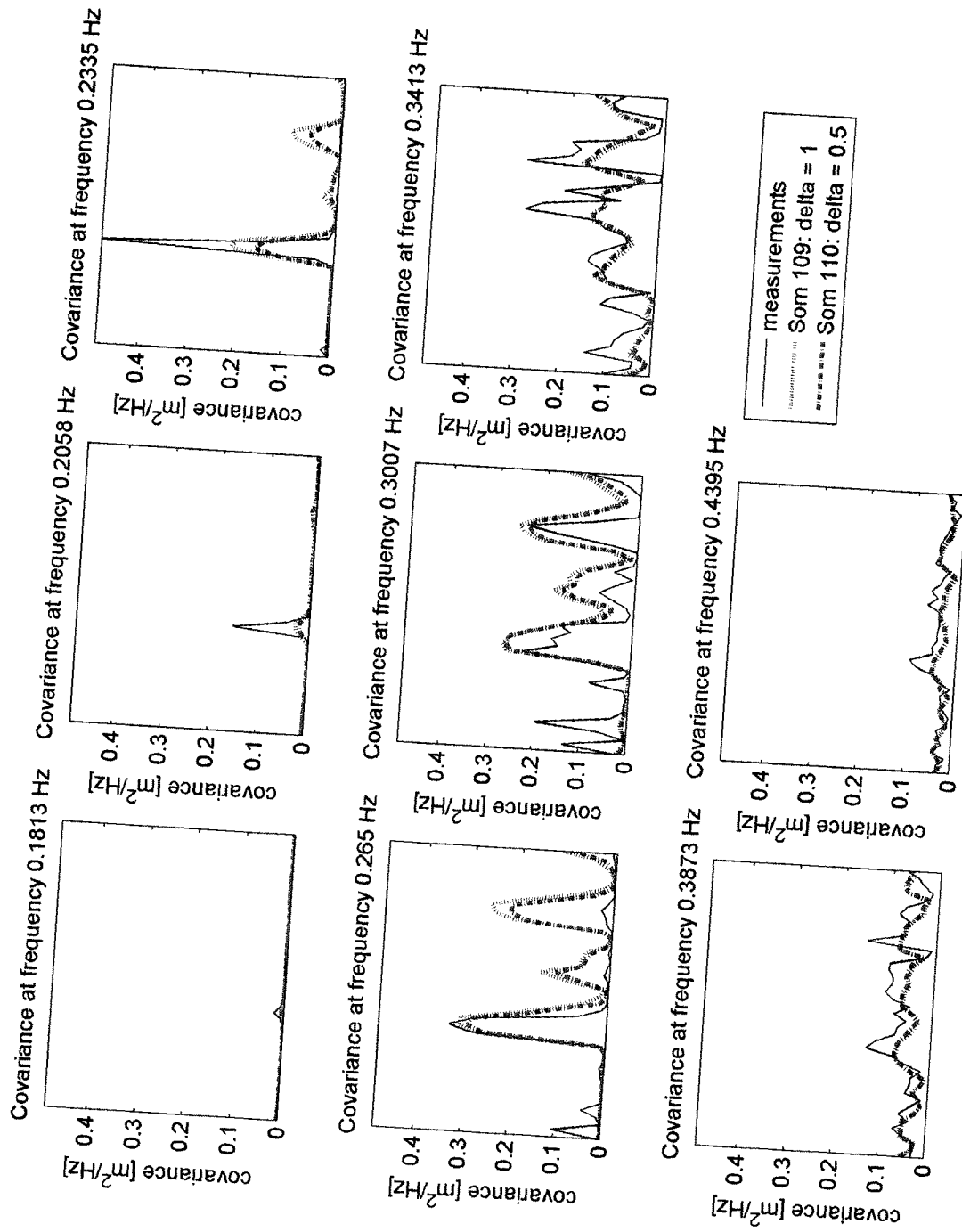


XI.5 Covariance at certain wave frequencies of the spectrum, development in time
 Comparing Som 109 and Som 105 with the measurements

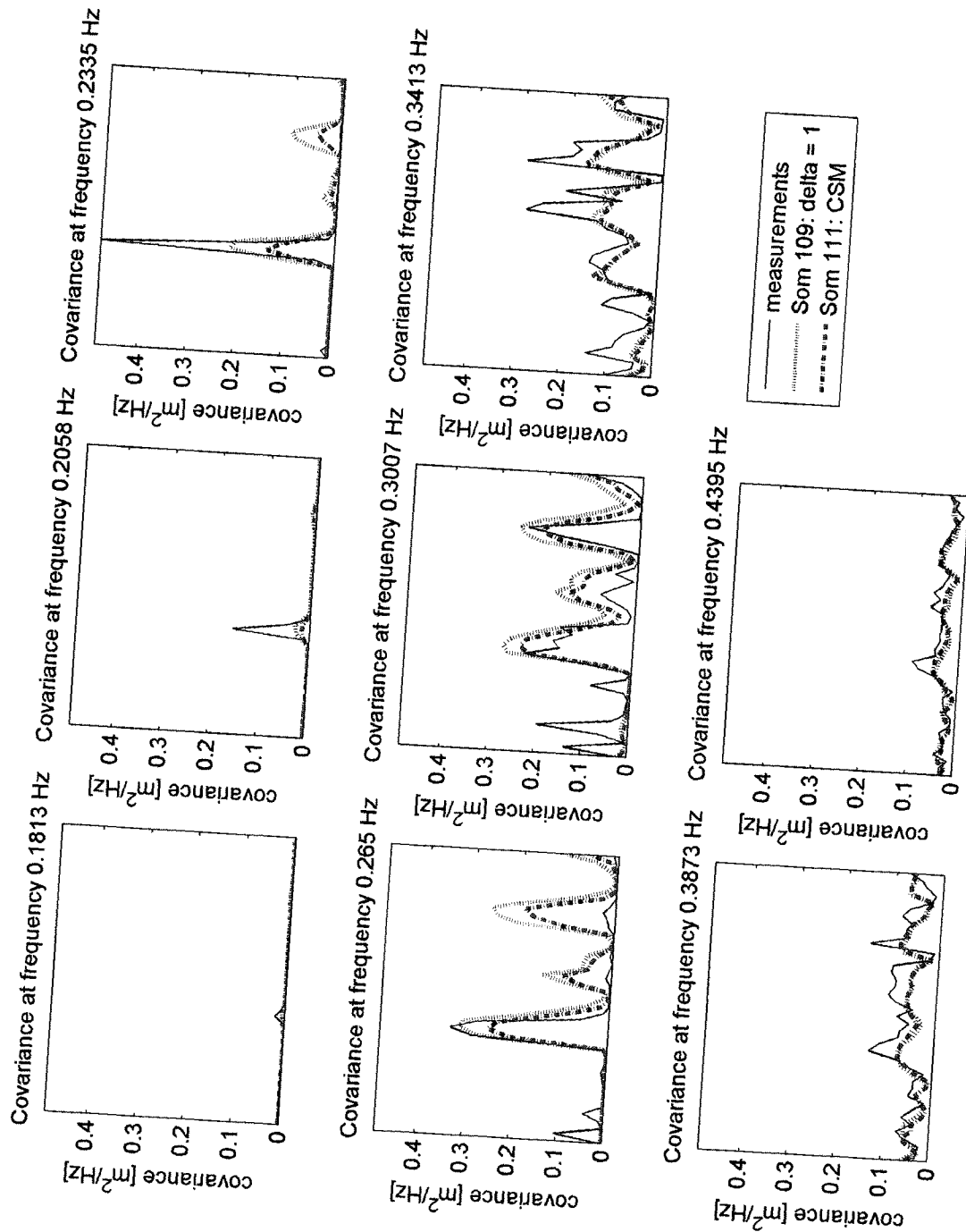


XI.6

Covariance at certain wave frequencies of the spectrum, development in time
 Comparing Som 109 and Som 110 with the measurements

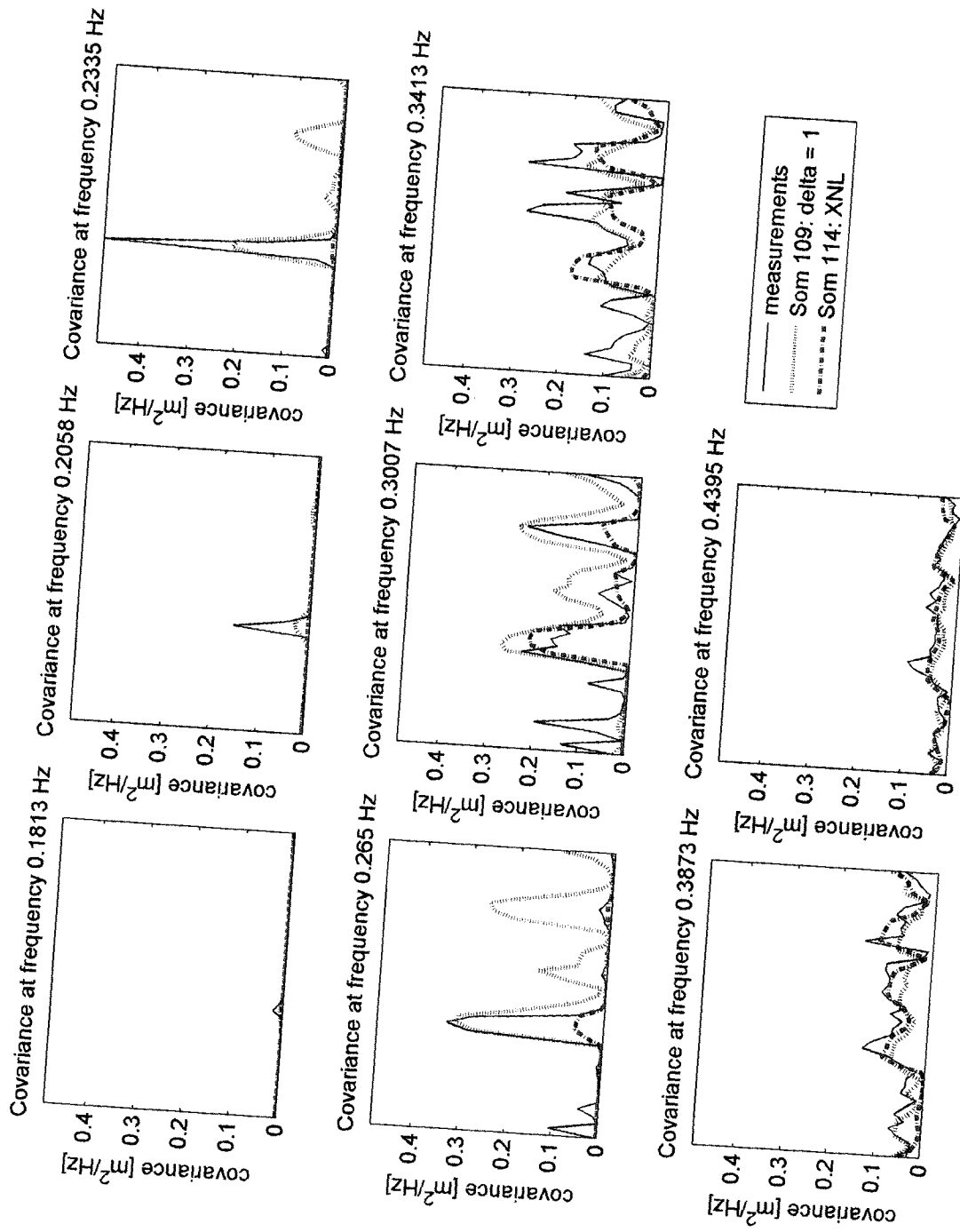


XI.7 Covariance at certain wave frequencies of the spectrum, development in time
 Comparing Som 109 and Som 111 with the measurements

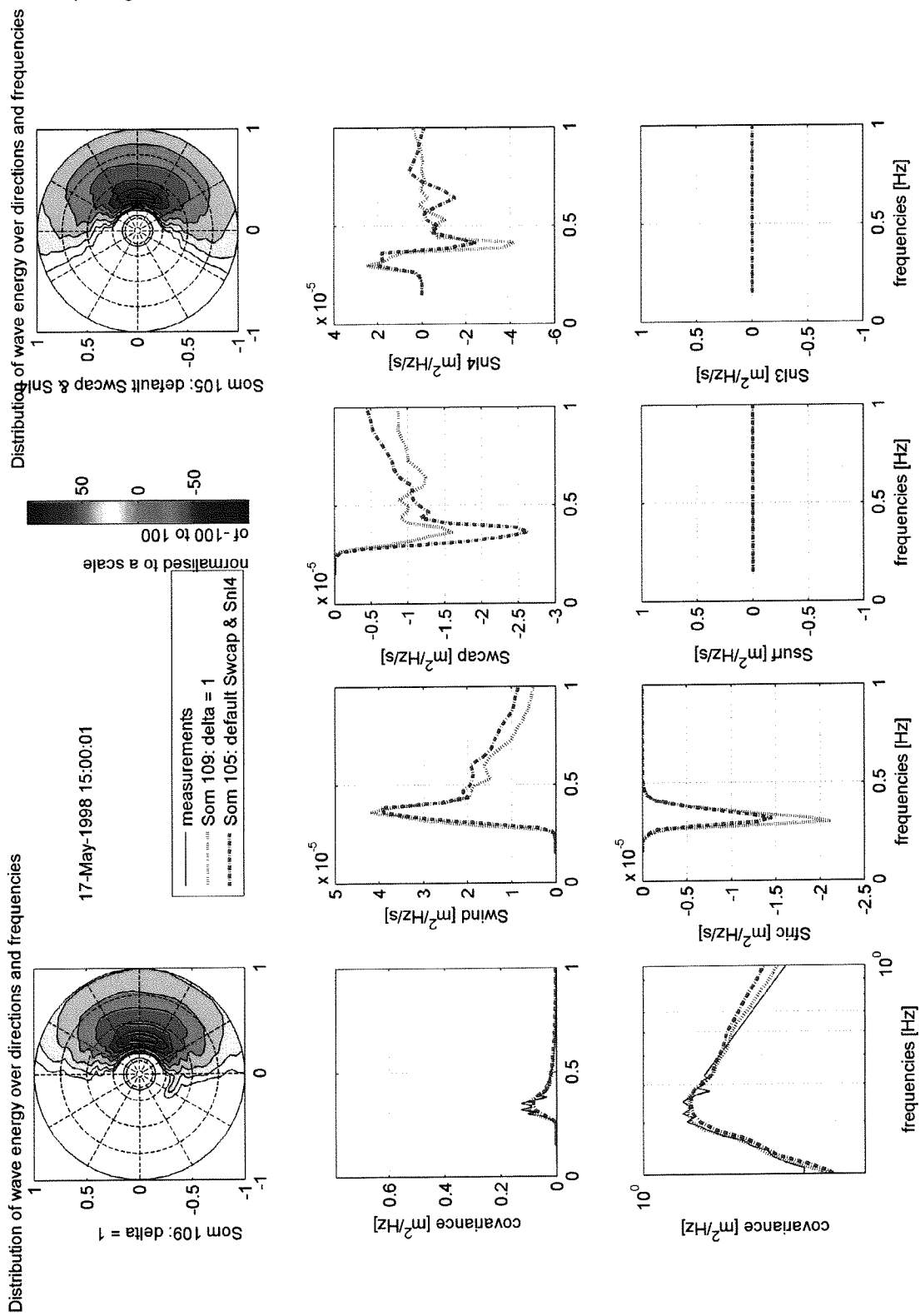


XI.8

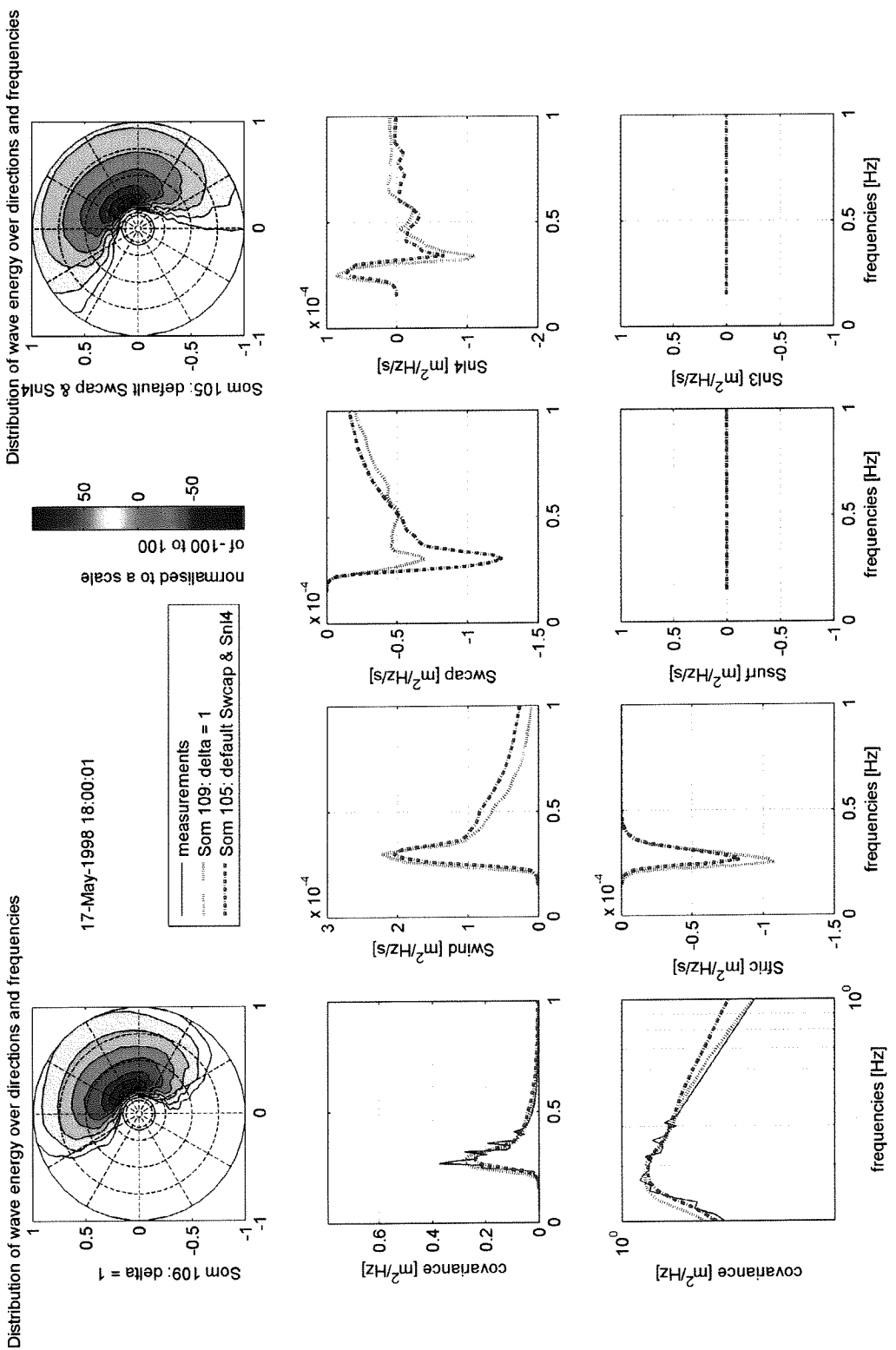
Covariance at certain wave frequencies of the spectrum, development in time
 Comparing Som 109 and Som 114 with the measurements



XI.9 Wave spectra and source terms at 17 May 1998 15:00
 Comparing Som 109 and Som 105 with the measurements

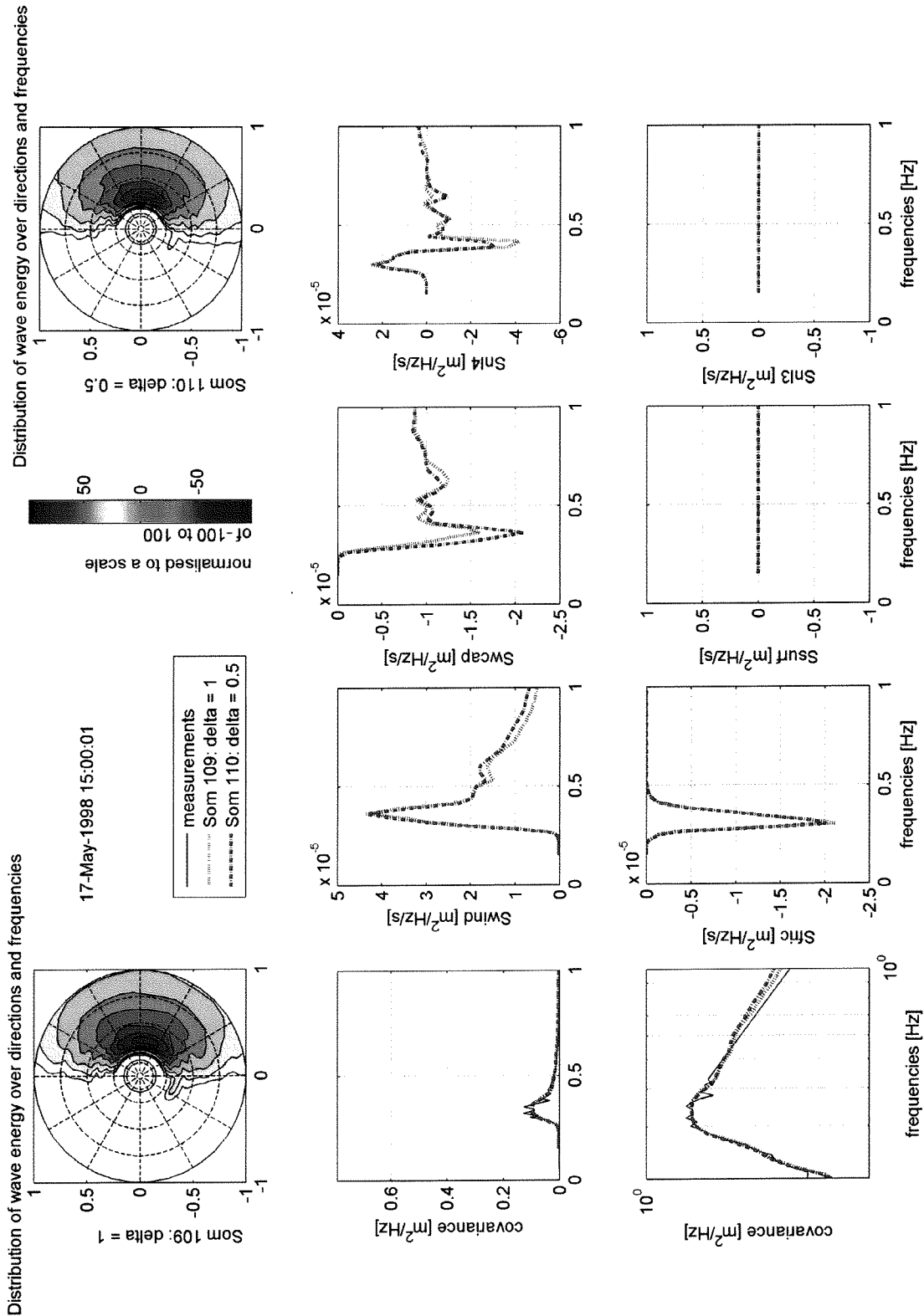


XI.10 Wave spectra and source terms at 17 May 1998 18:00
 Comparing Som 109 and Som 105 with the measurements



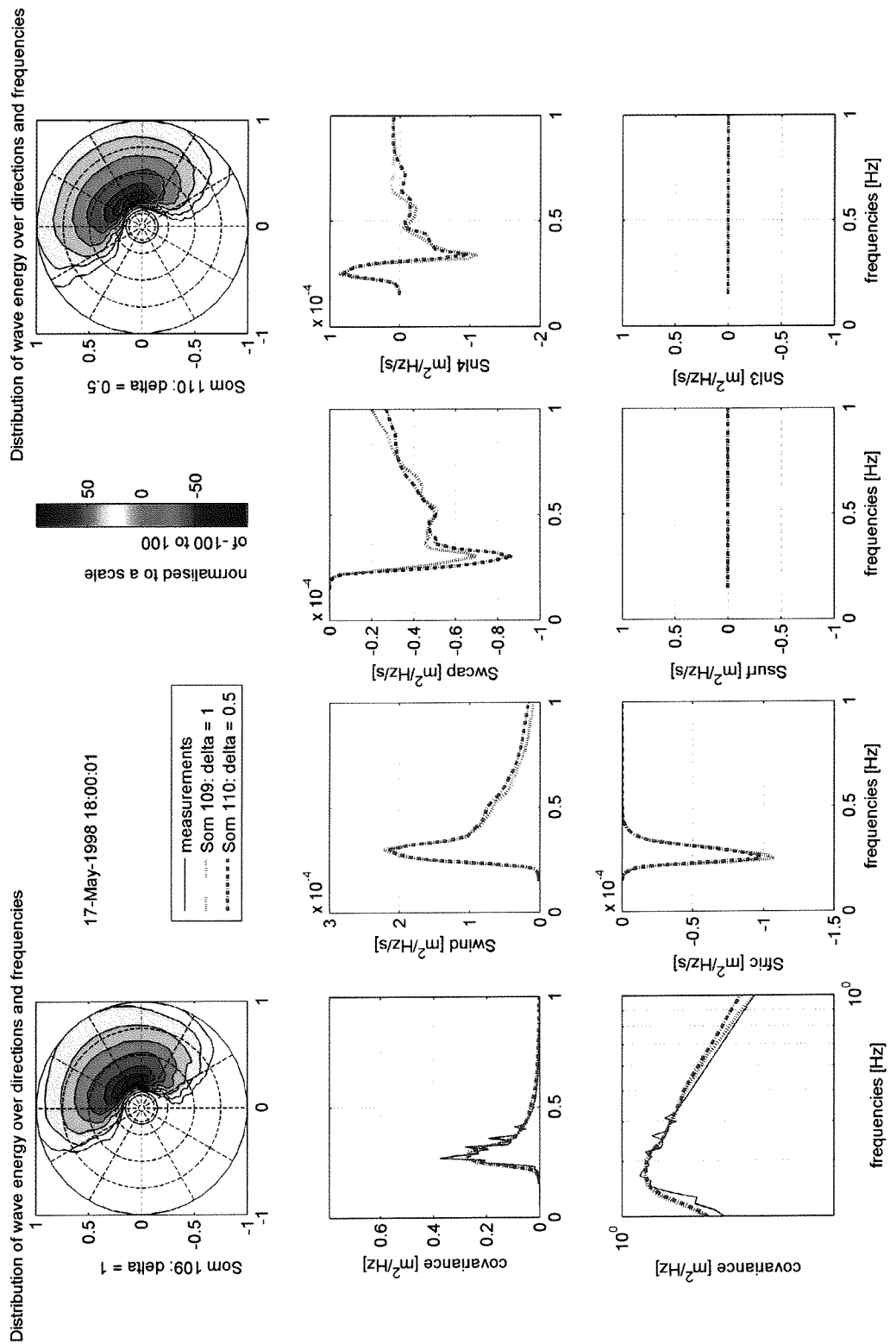
XI.11

Wave spectra and source terms at 17 May 1998 15:00 Comparing Som 109 and Som 110 with the measurements



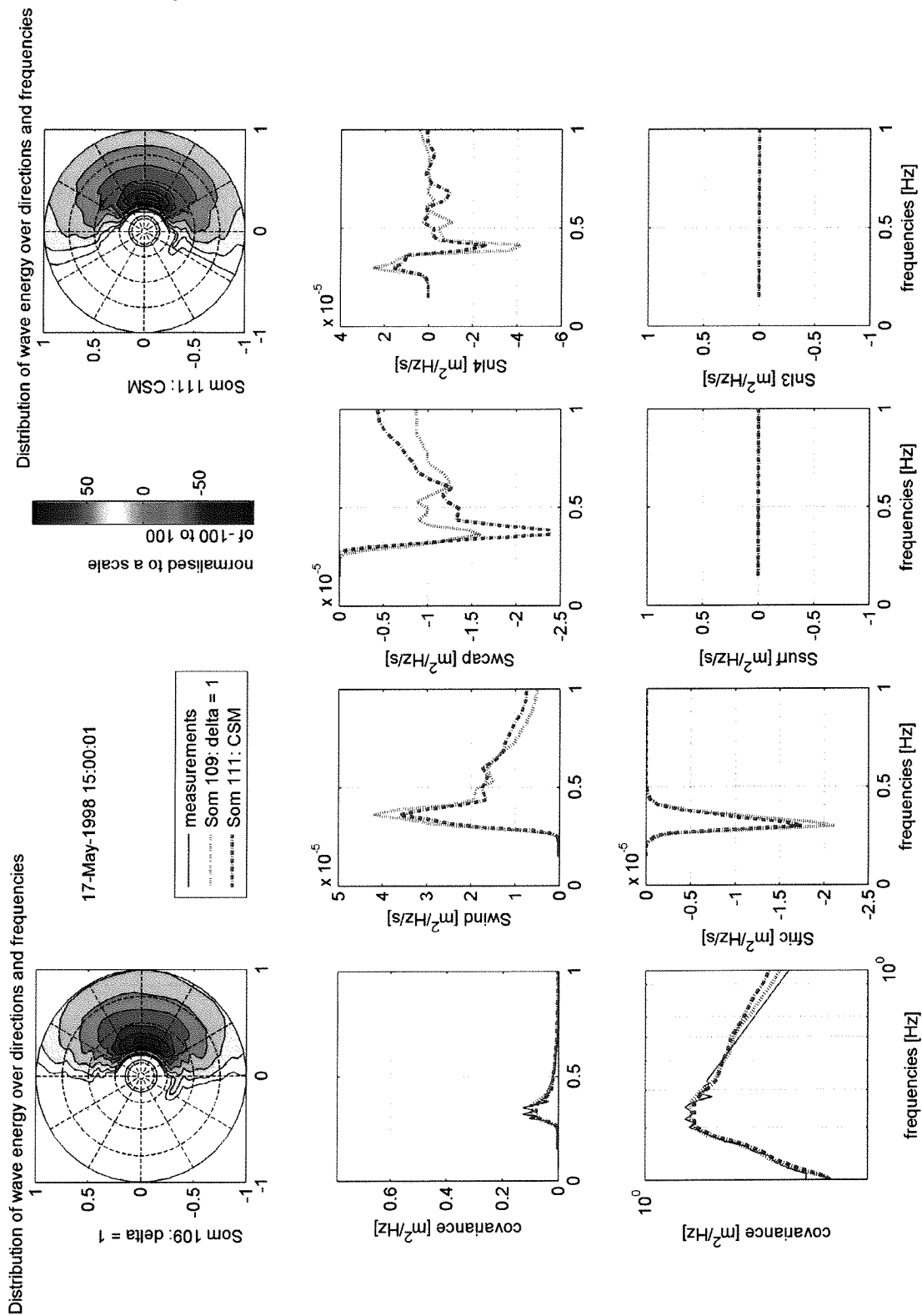
XI.12

Wave spectra and source terms at 17 May 1998 18:00 Comparing Som 109 and Som 110 with the measurements



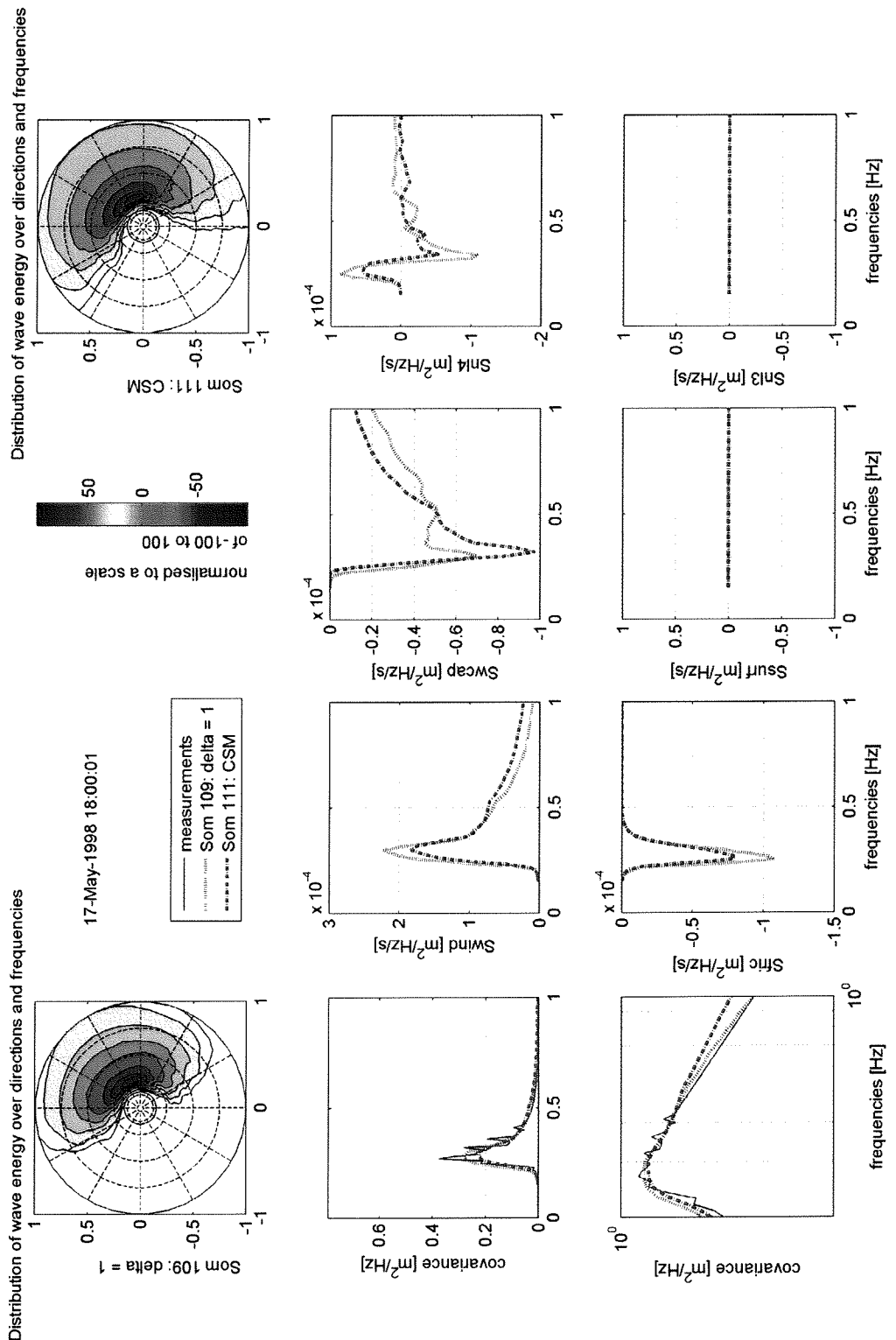
XI.13

Wave spectra and source terms at 17 May 1998 15:00
Comparing Som 109 and Som 111 with the measurements

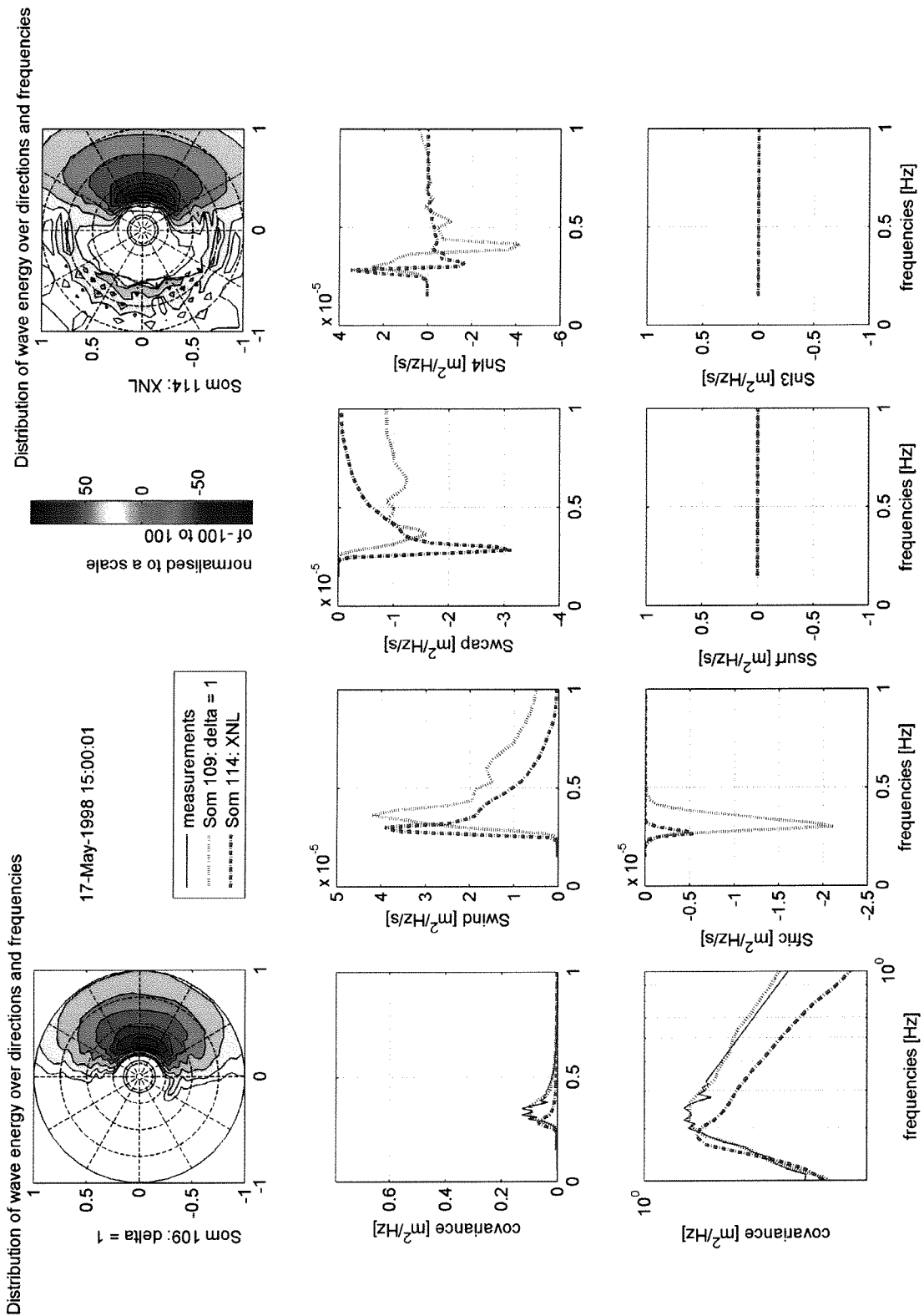


XI.14

Wave spectra and source terms at 17 May 1998 18:00 Comparing Som 109 and Som 111 with the measurements

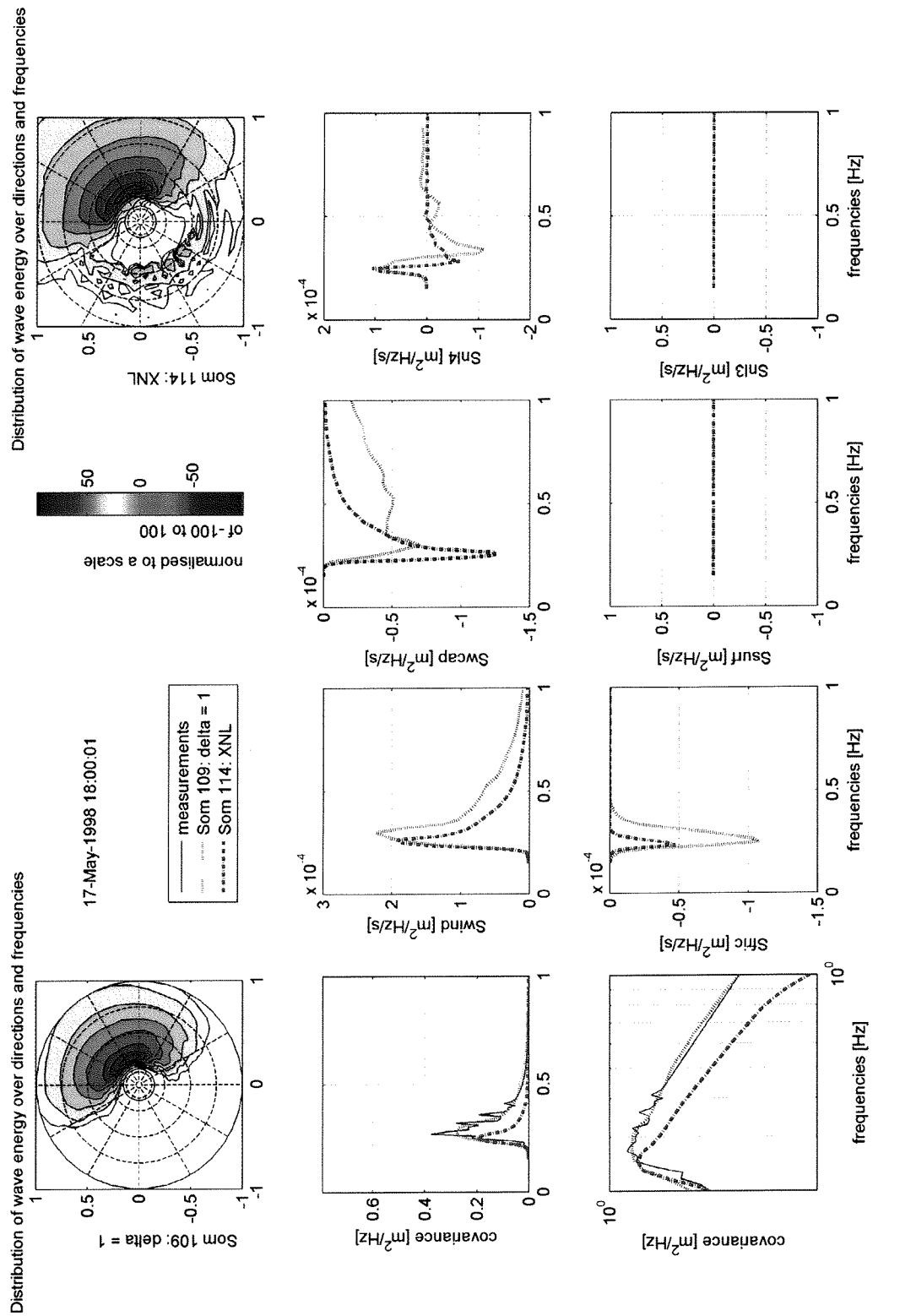


XI.15 Wave spectra and source terms at 17 May 1998 15:00
 Comparing Som 109 and Som 114 with the measurements

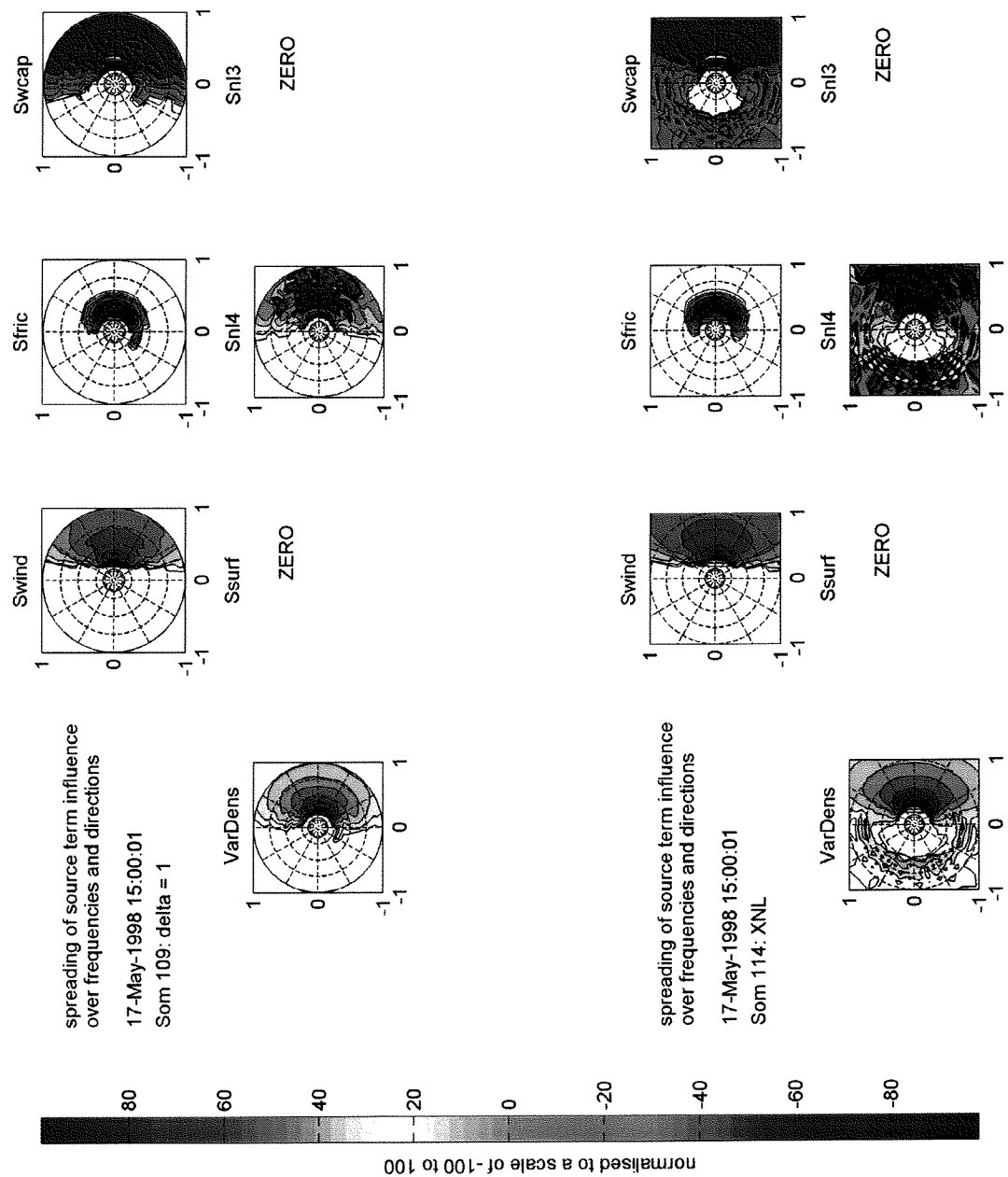


XI.16

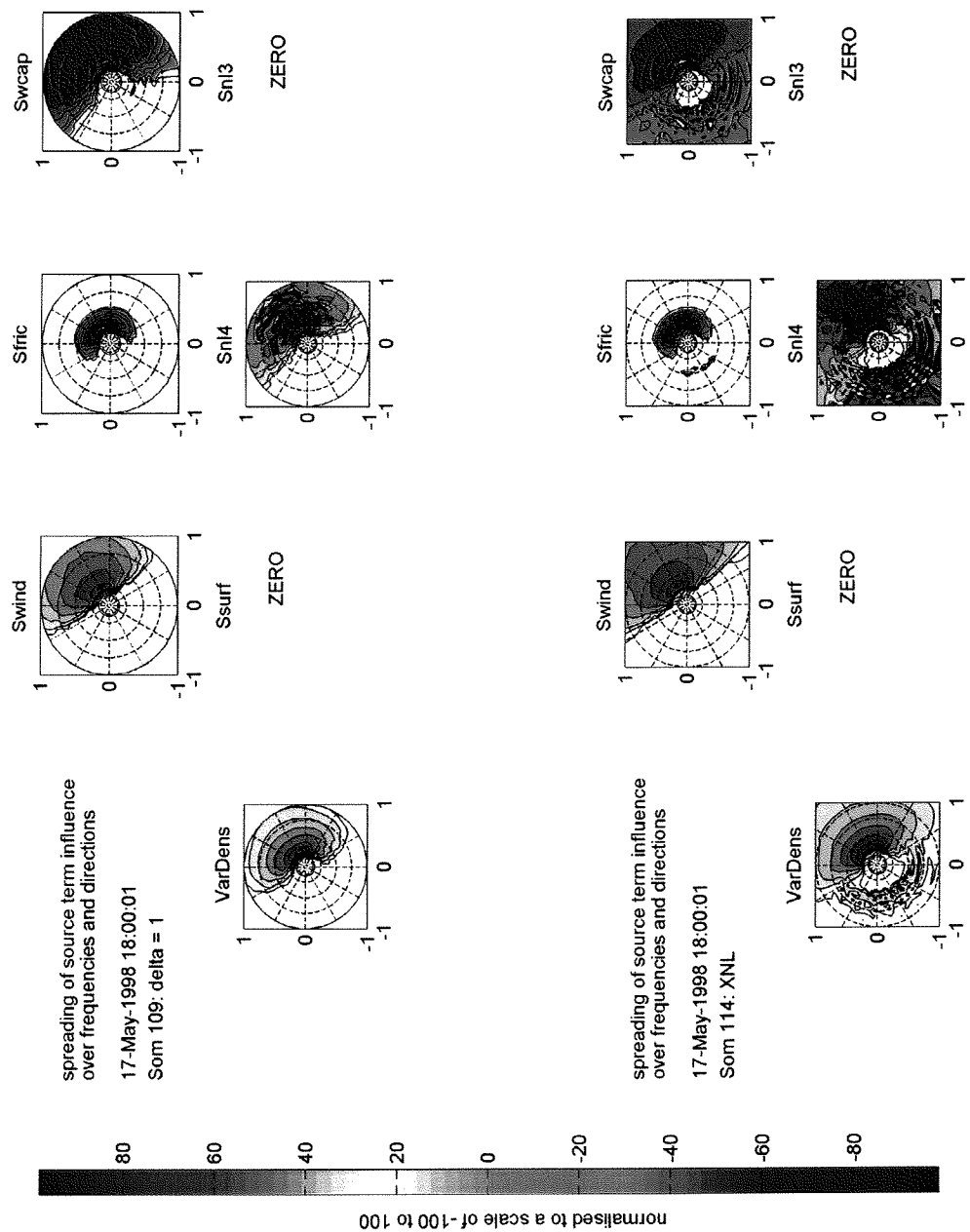
Wave spectra and source terms at 17 May 1998 18:00
Comparing Som 109 and Som 114 with the measurements



XI.17 2D images of source terms at 17 May 1998 15:00 Comparing Som 109 and Som 114

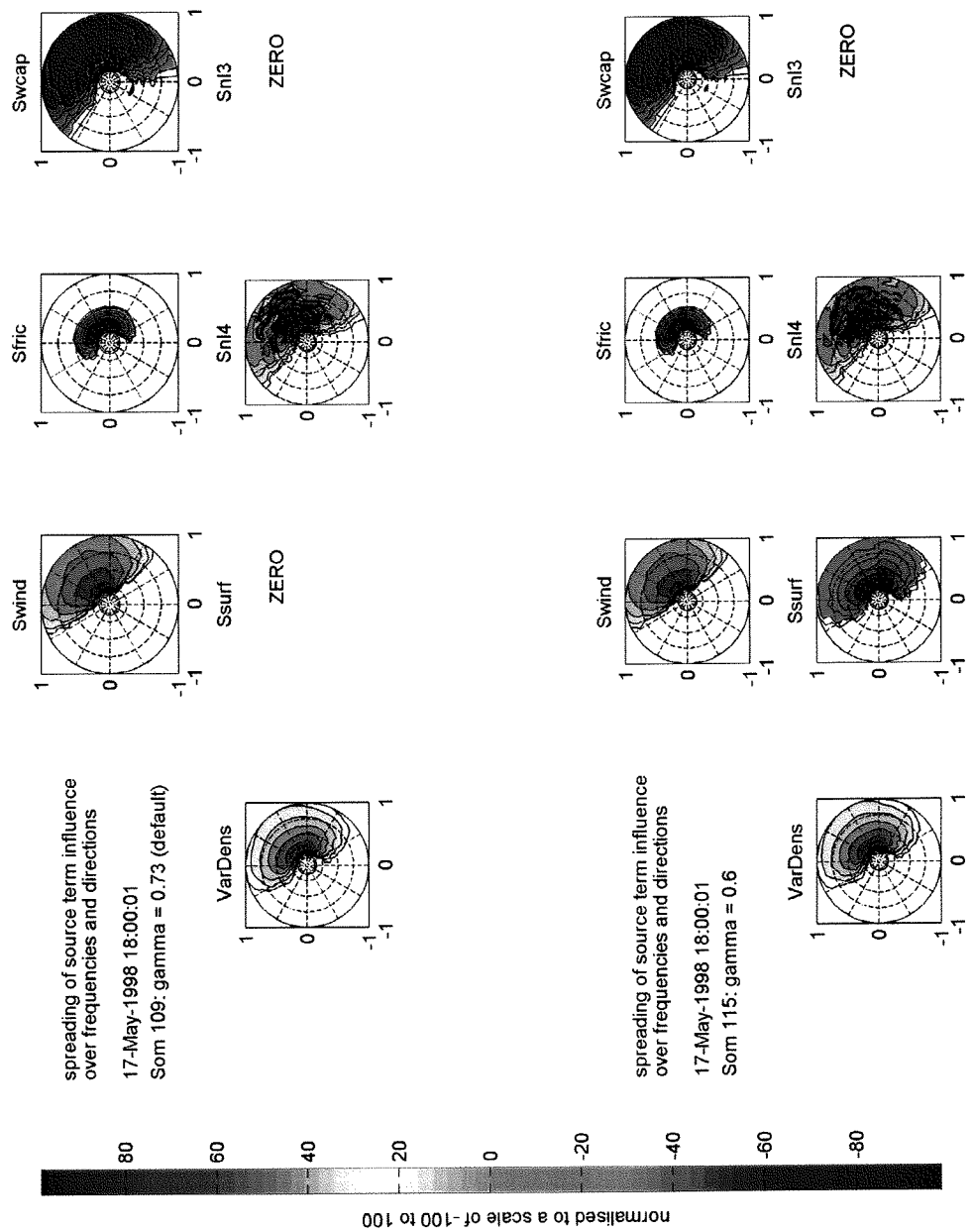


XI.18 2D images of source terms at 17 May 1998 18:00
Comparing Som 109 and Som 114



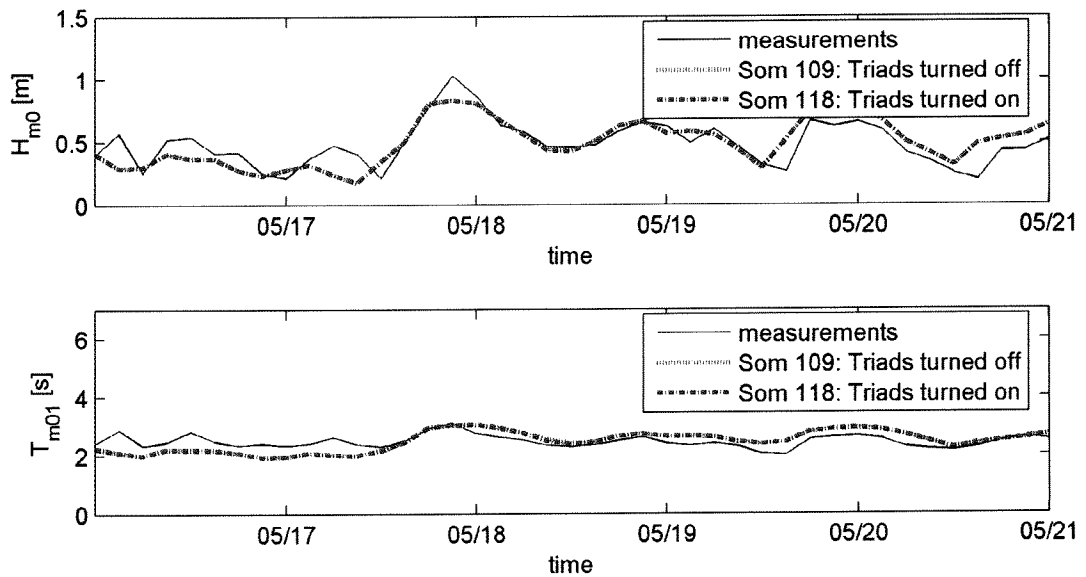
APPENDIX XII. Plots of calibration of Depth induced breaking on shallow water timeseries

XII.1 2D images of source terms at 17 May 1998 18:00
 Rare case in which the change of the setting of gamma makes a difference

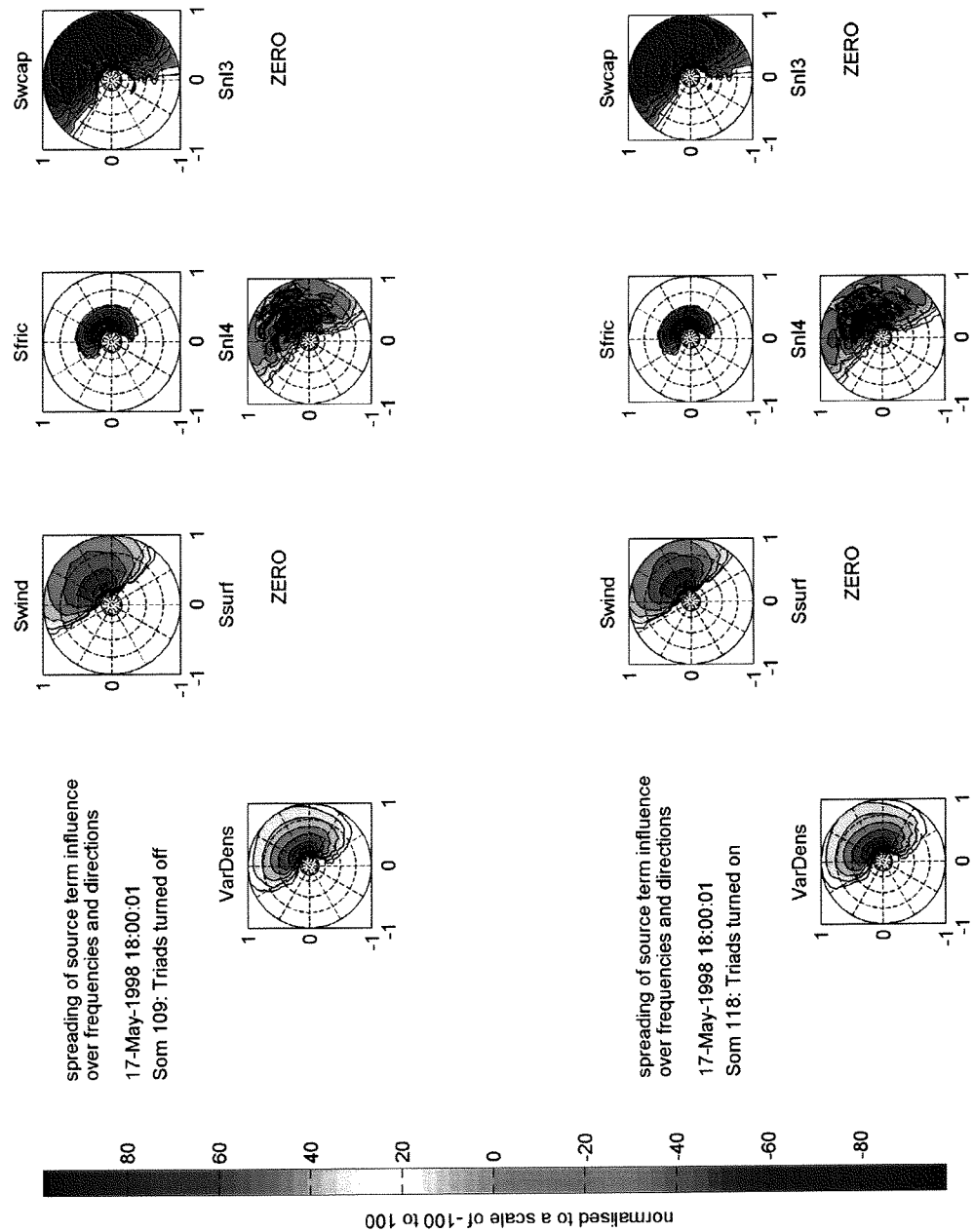


APPENDIX XIII. Plots of calibration of Triads on shallow water timeseries

XIII.1 H_{m0} and T_{m01} in time. Comparing Som 109 and Som 118 with the measurements

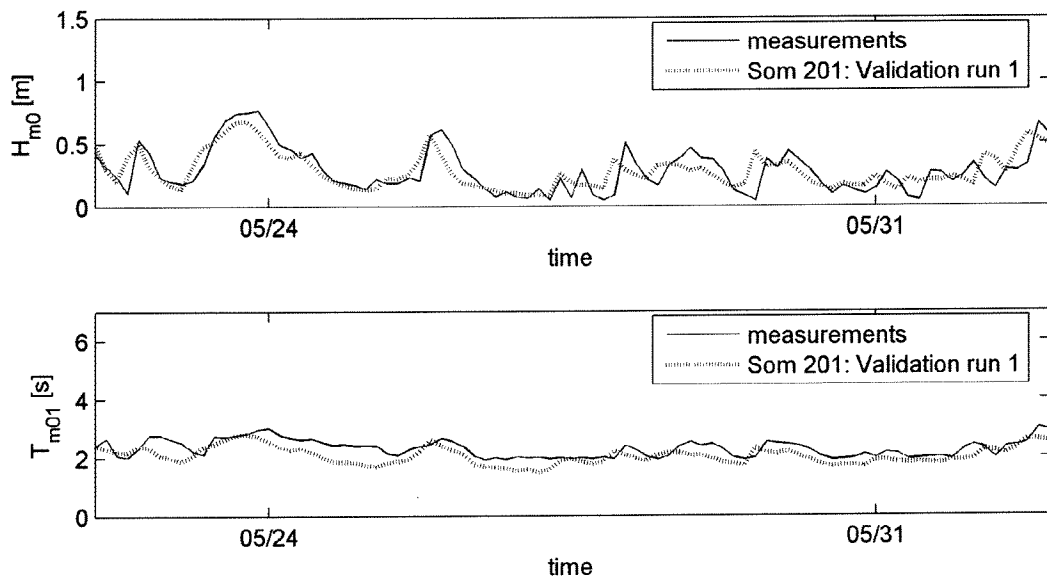


XIII.2 2D images of source terms at 17 May 1998 18:00
 Triads don't play an important role

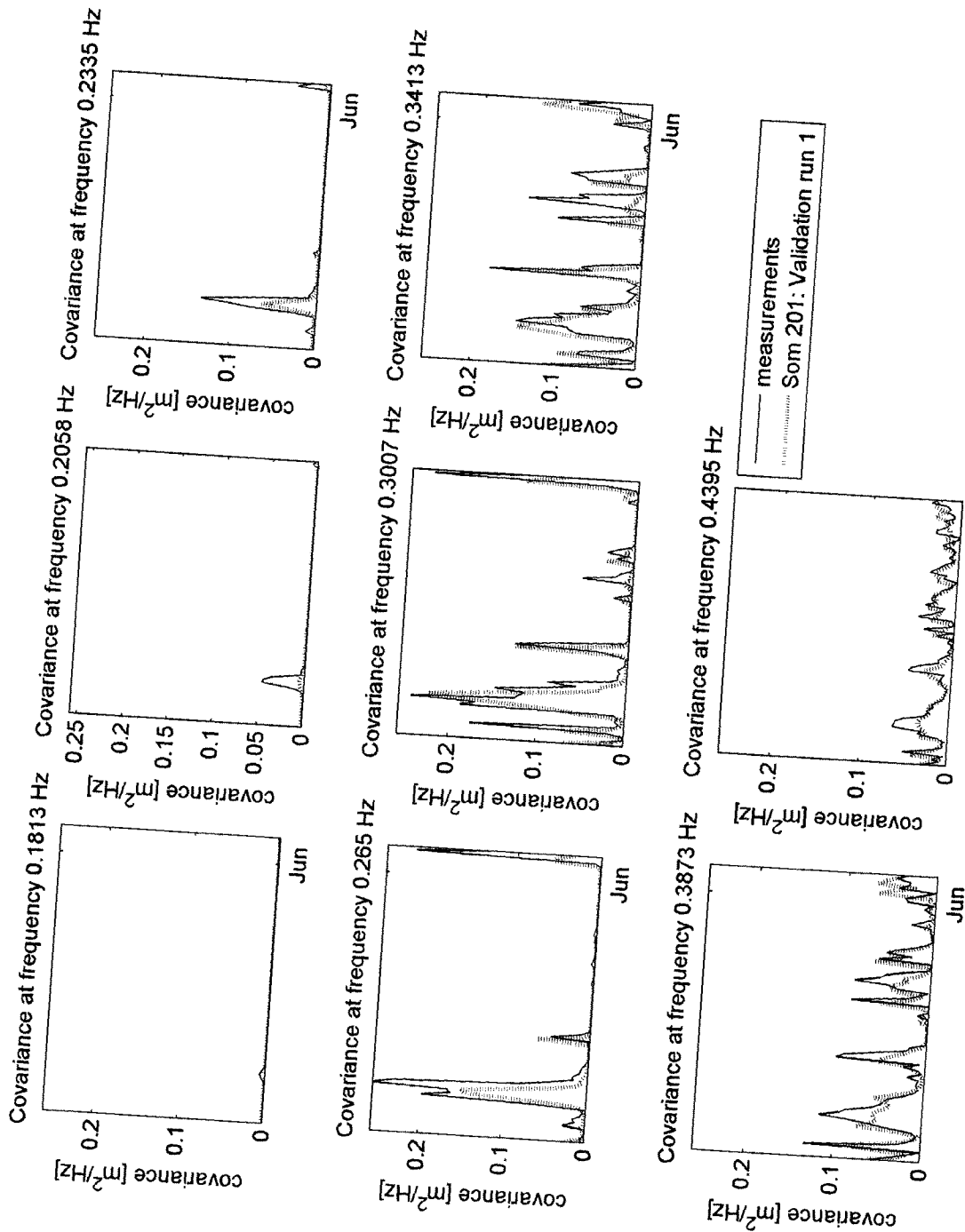


APPENDIX XIV. Plots of validation run 201

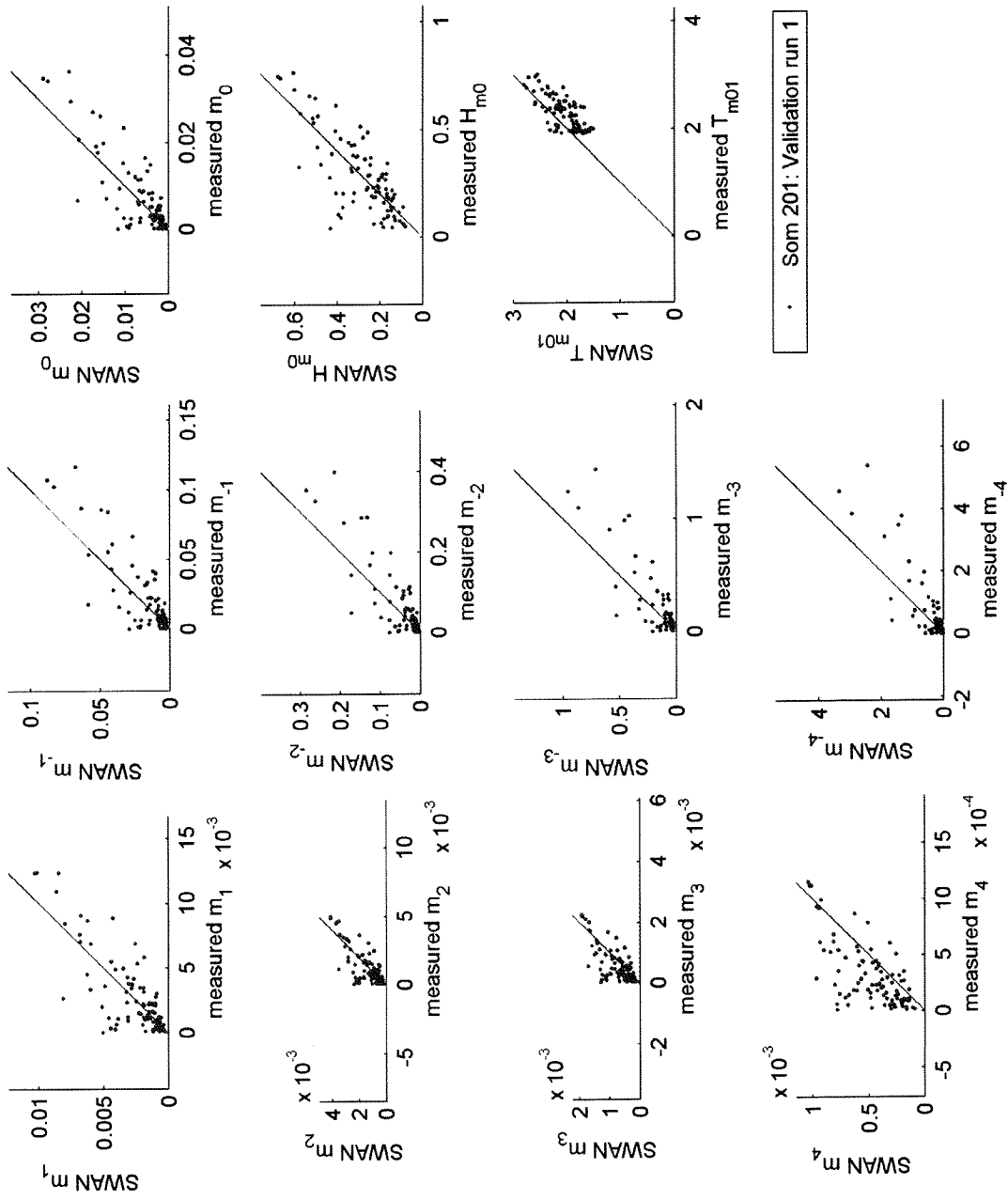
XIV.1 H_{m0} and T_{m01} in time. Comparing Som 201 with the measurements



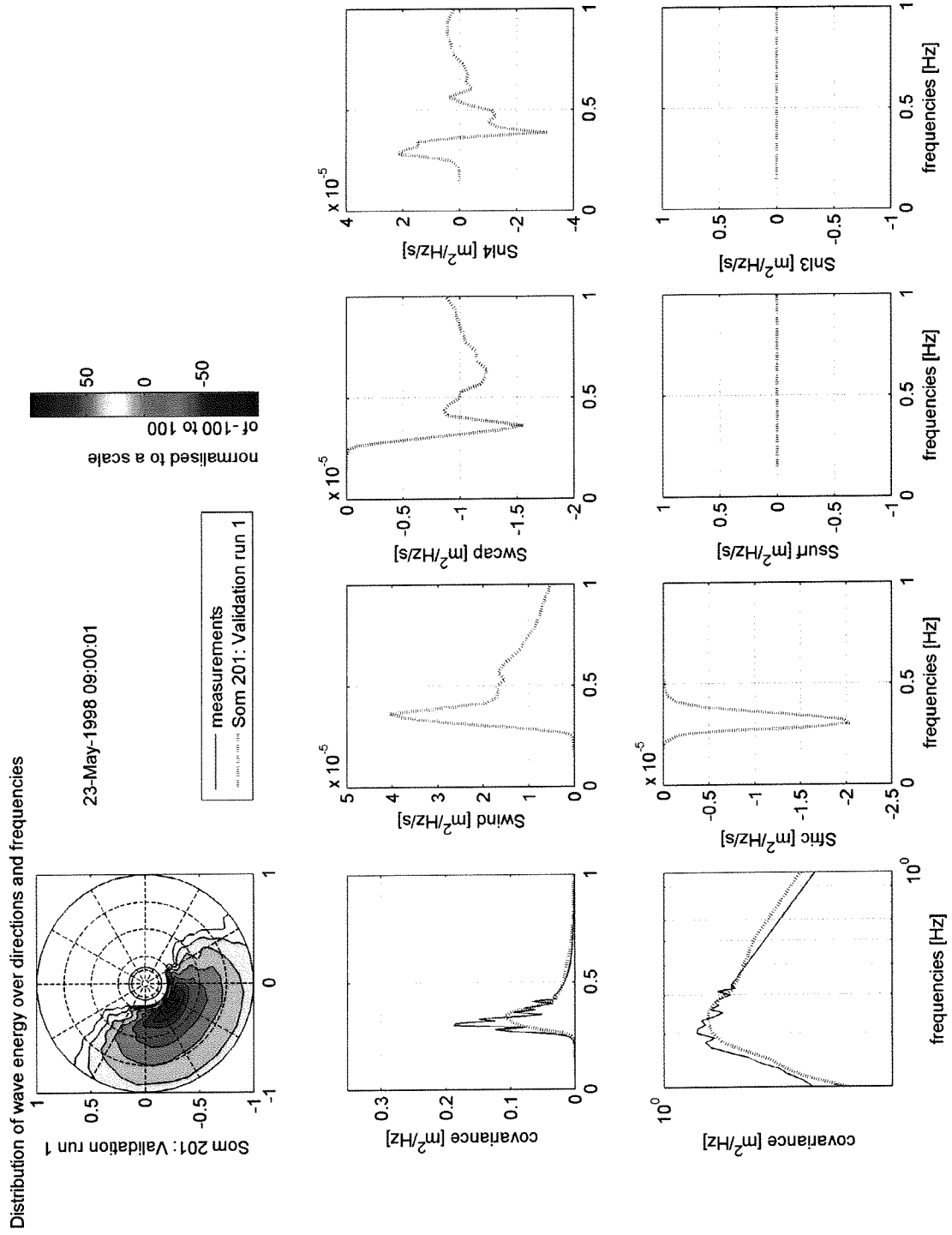
XIV.2 Covariance at certain wave frequencies of the spectrum, development in time
 Comparing Som 201 with the measurements



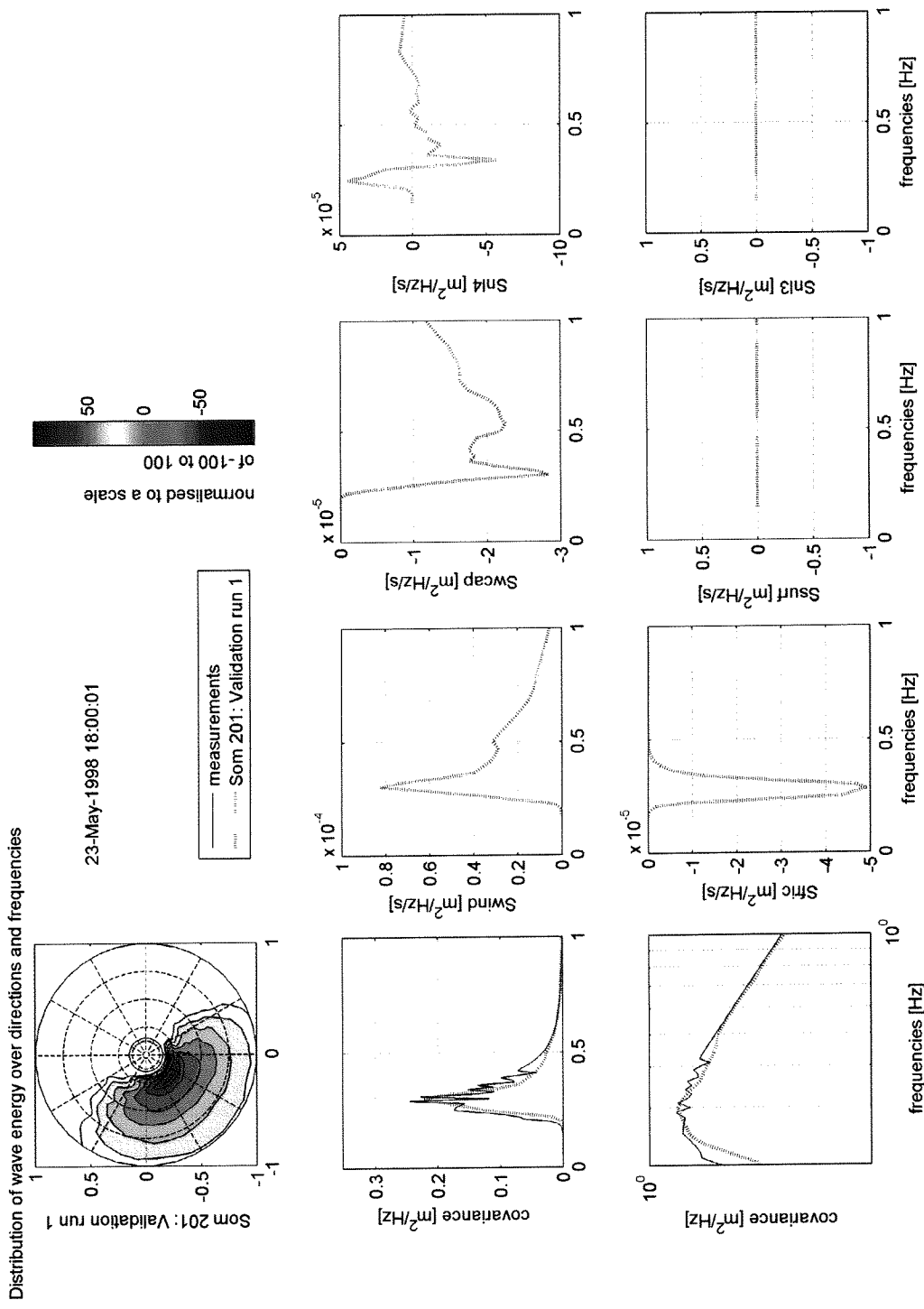
XIV.3 Scatterplots of spectral moments, H_{m0} and T_{m01}
 Comparing Som 201 with the measurements



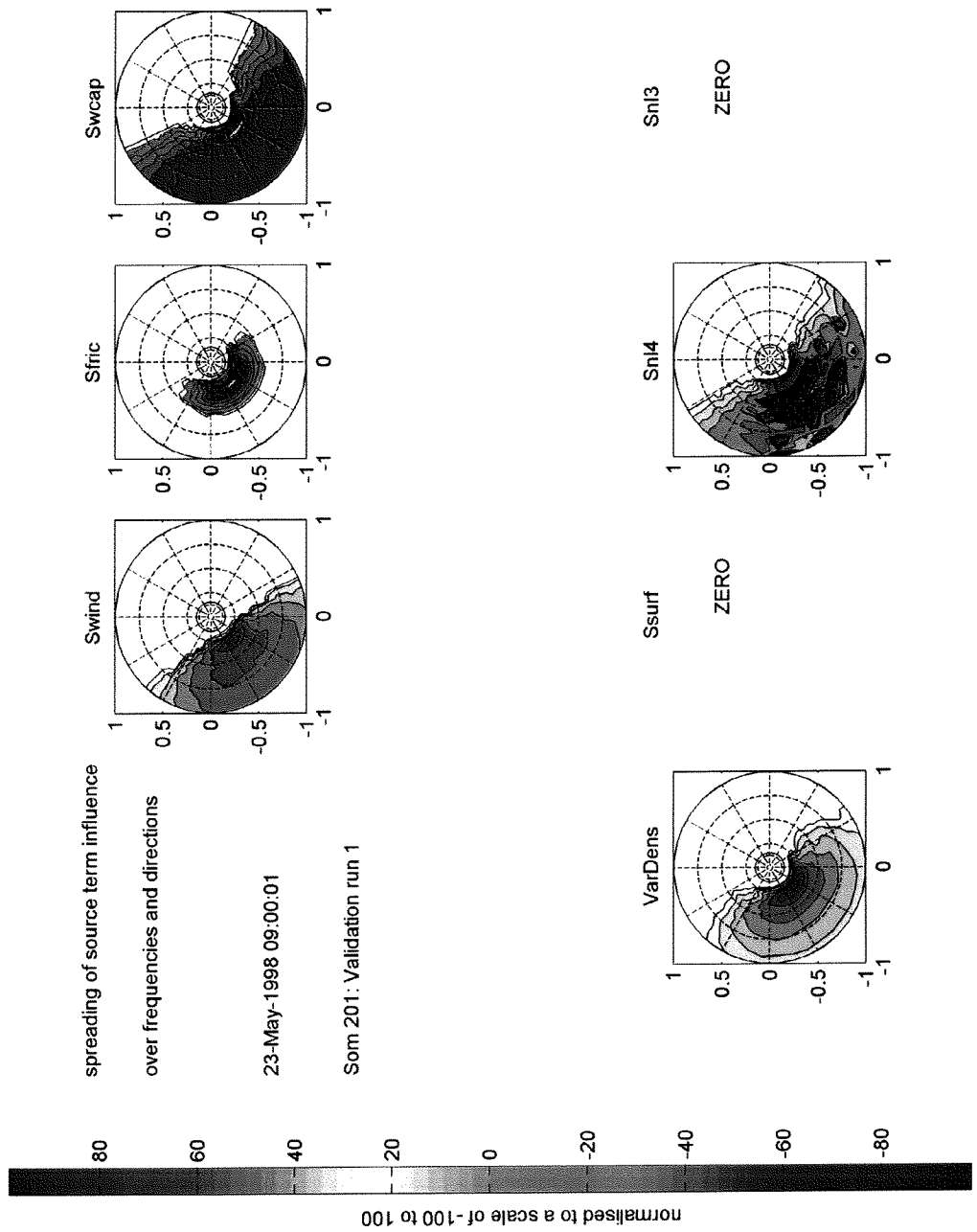
XIV.4 Wave spectra and source terms at 23 May 1998 09:00
 Comparing Som 201 with the measurements



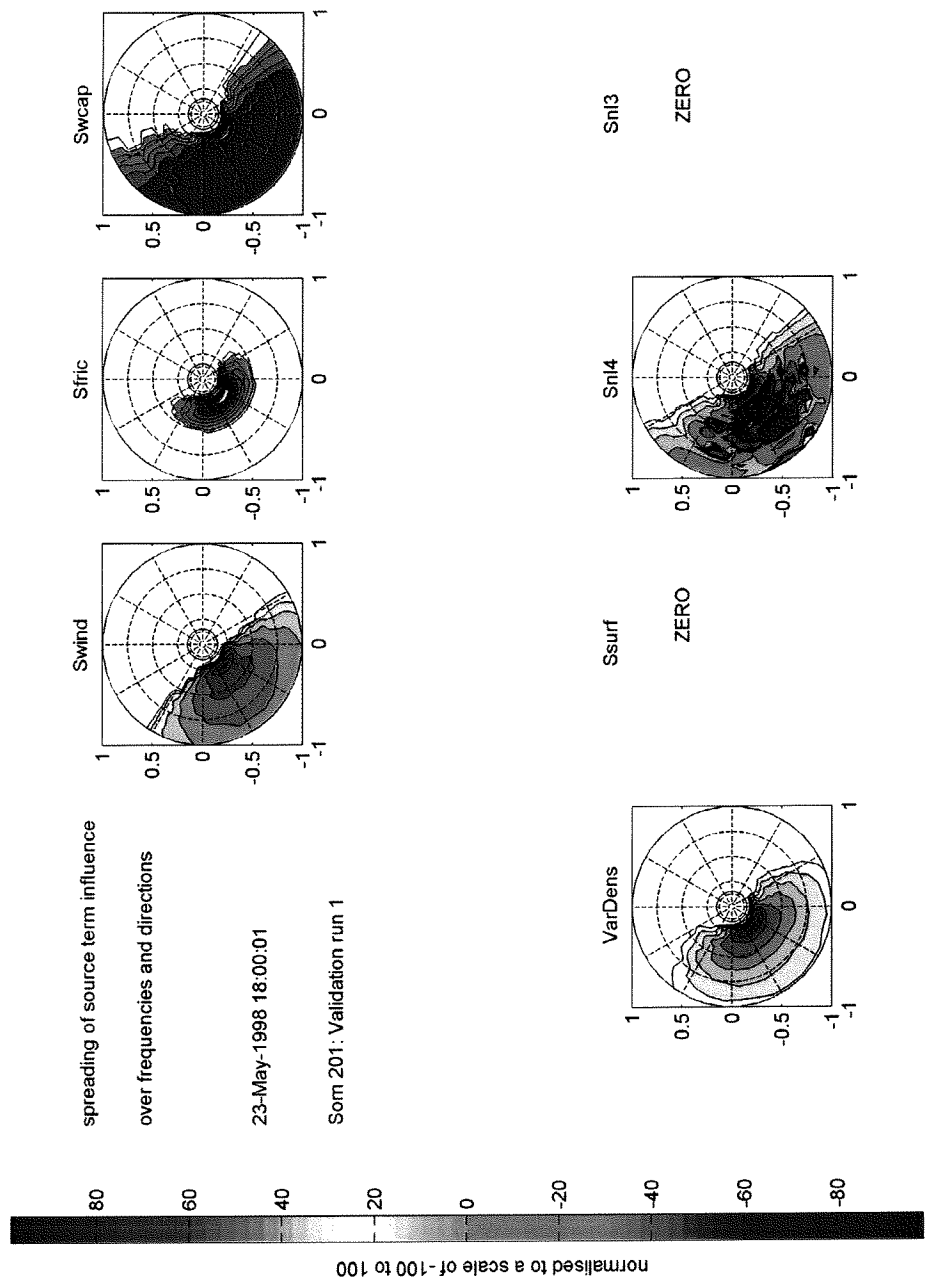
XIV.5 Wave spectra and source terms at 23 May 1998 18:00
 Comparing Som 201 with the measurements



XIV.6 2D images of source terms at 23 May 1998 09:00

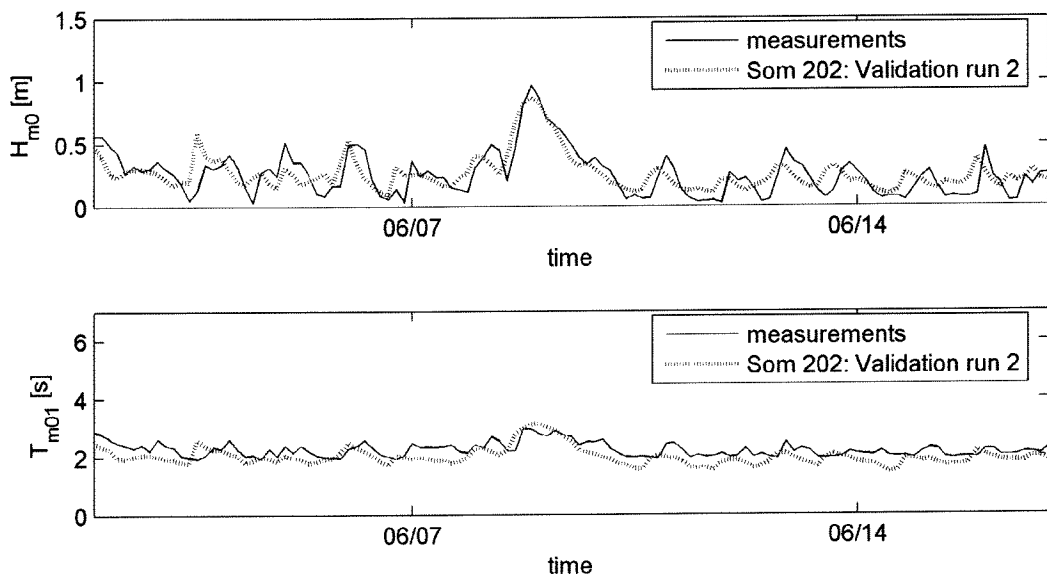


XIV.7 2D images of source terms at 23 May 1998 18:00

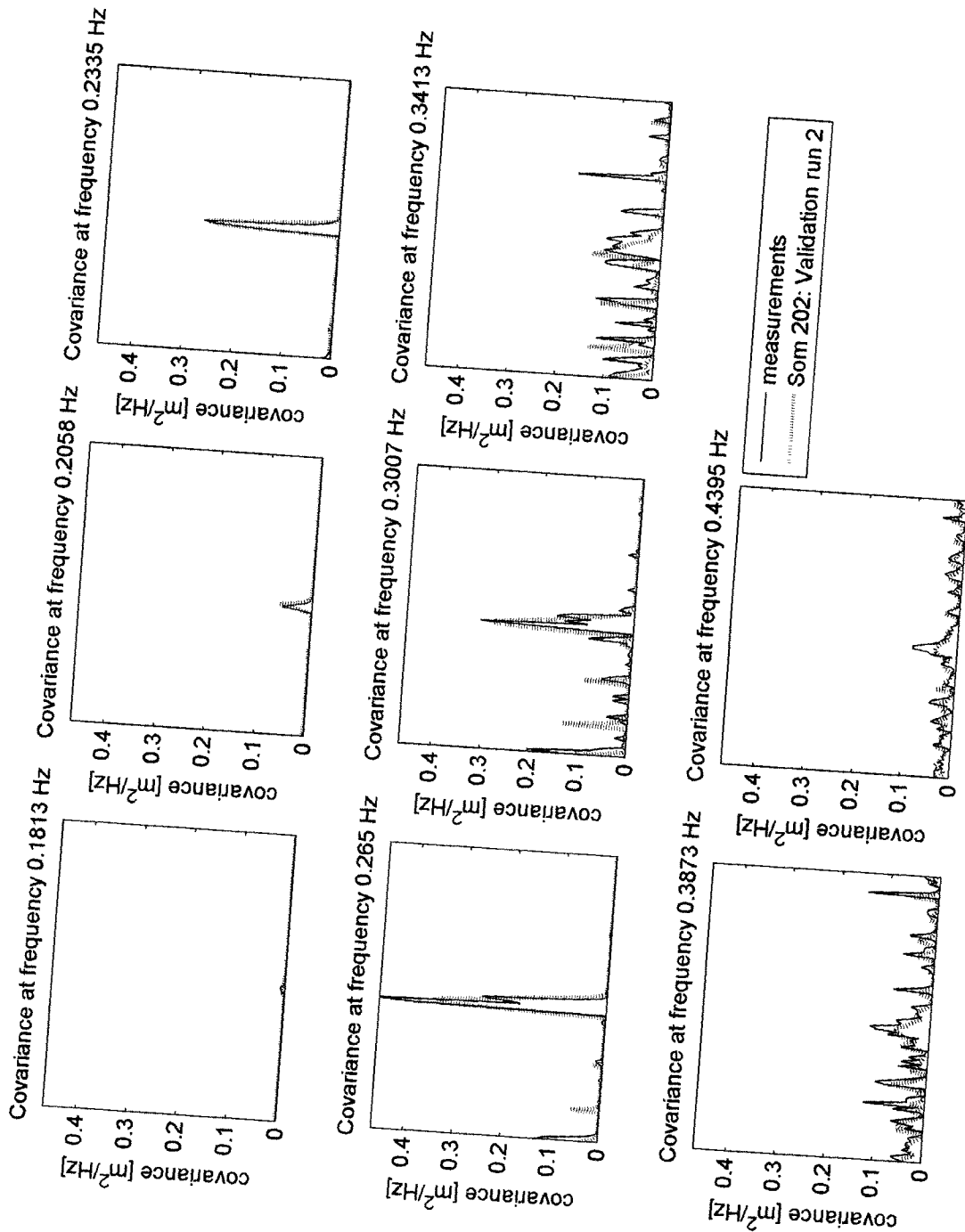


APPENDIX XV. Plots of validation run 202

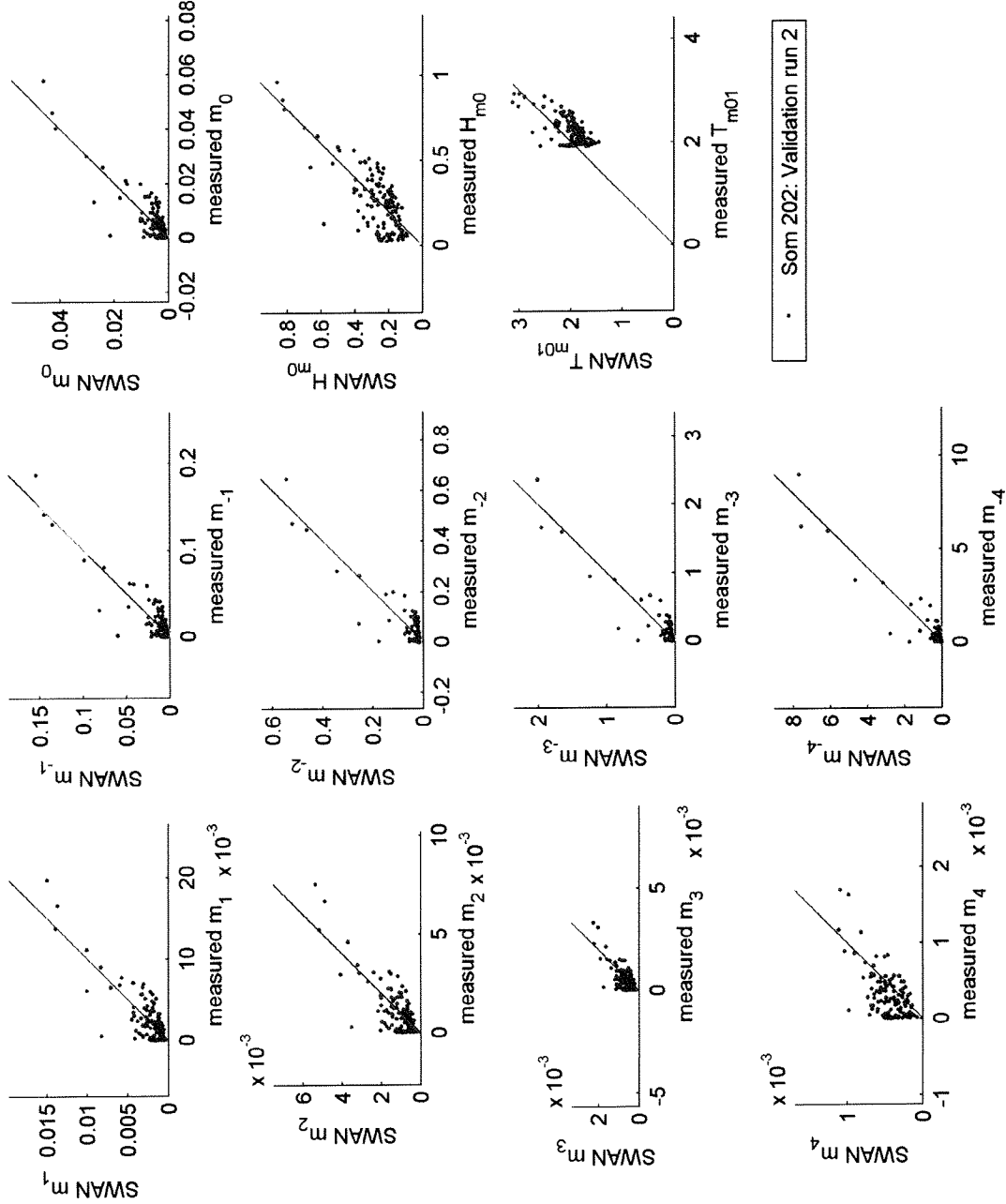
XV.1 H_{m0} and T_{m01} in time. Comparing Som 202 with the measurements



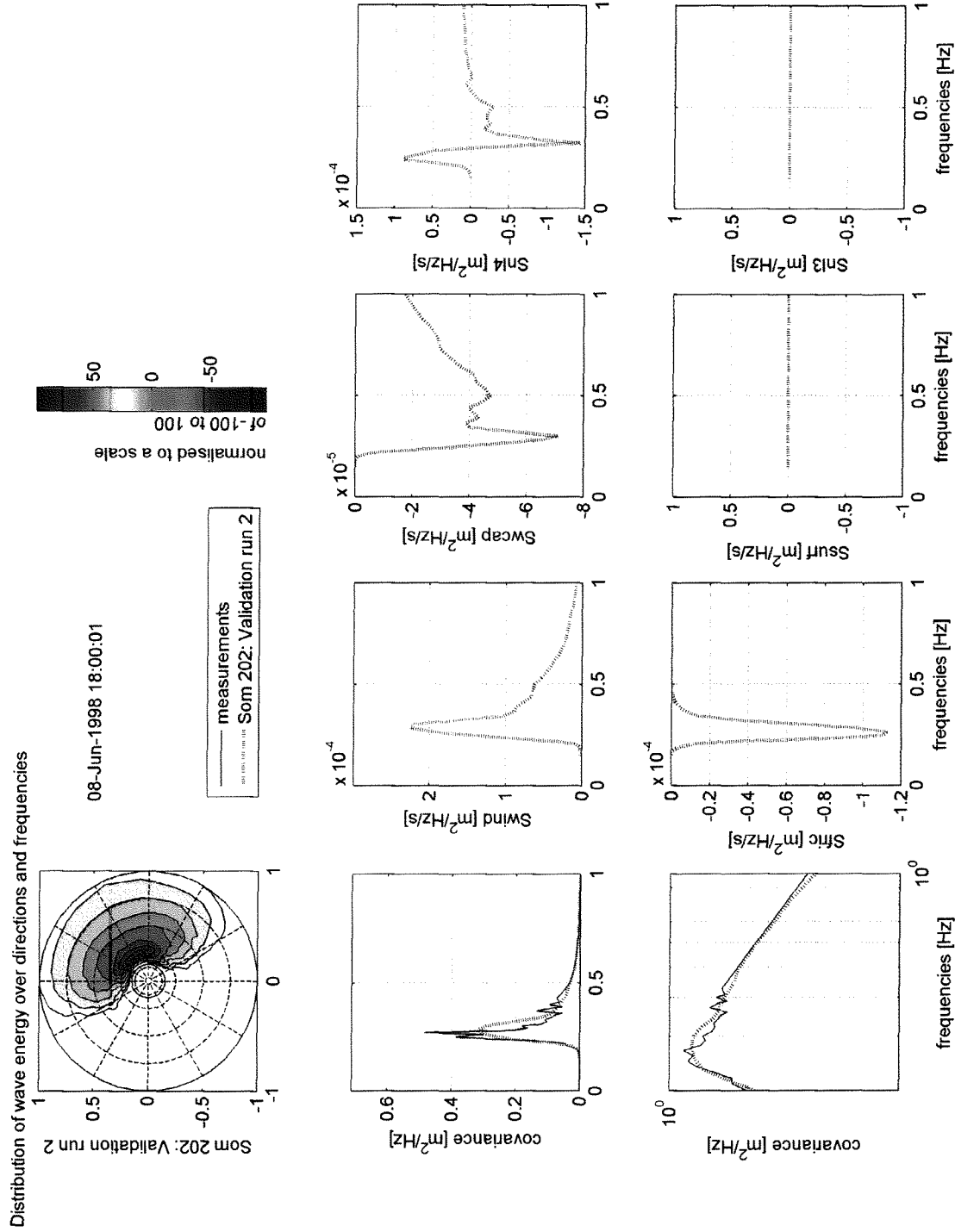
XV.2 Covariance at certain wave frequencies of the spectrum, development in time
 Comparing Som 202 with the measurements



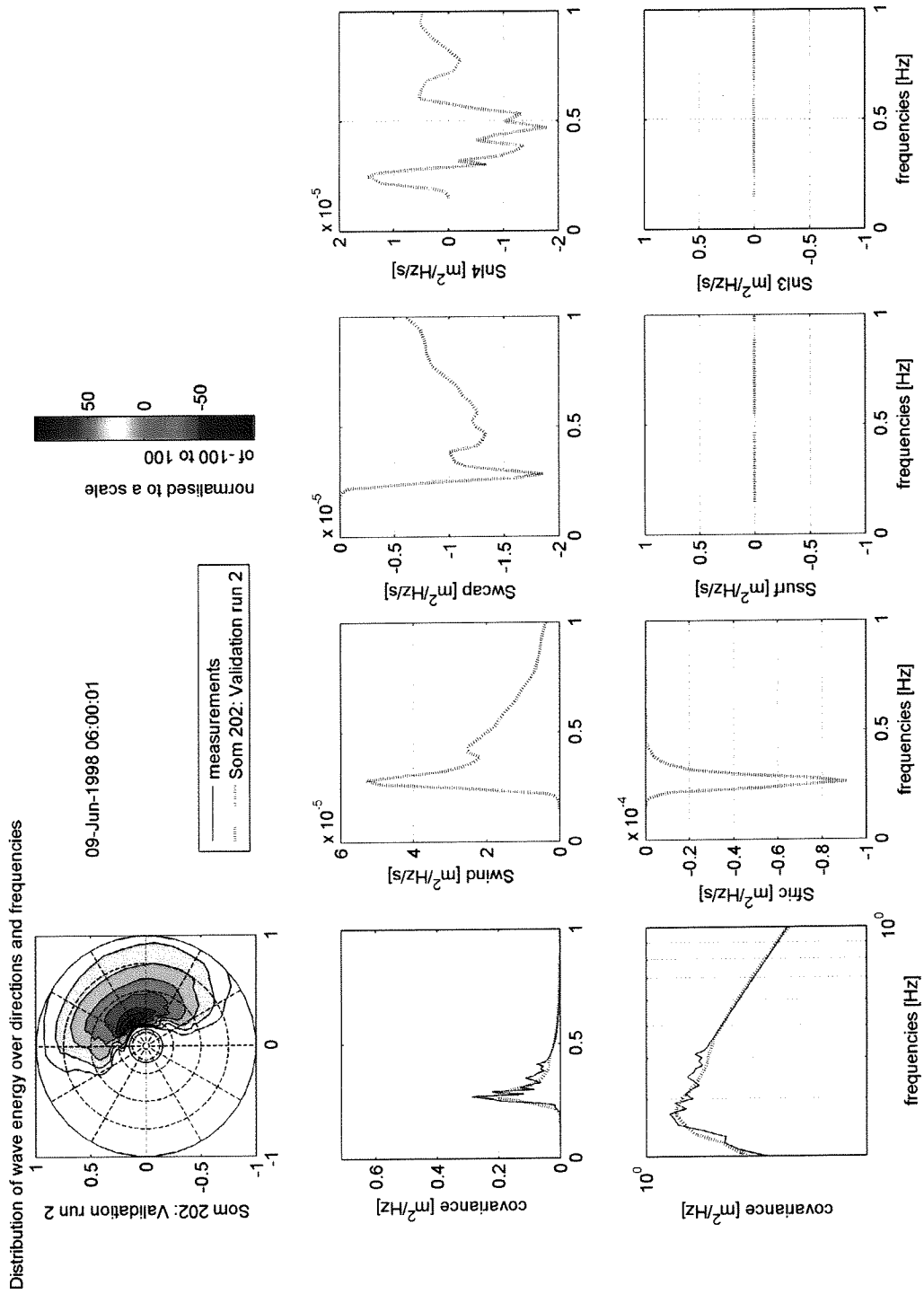
XV.3 Scatterplots of spectral moments, H_{m0} and T_{m01}
 Comparing Som 202 with the measurements



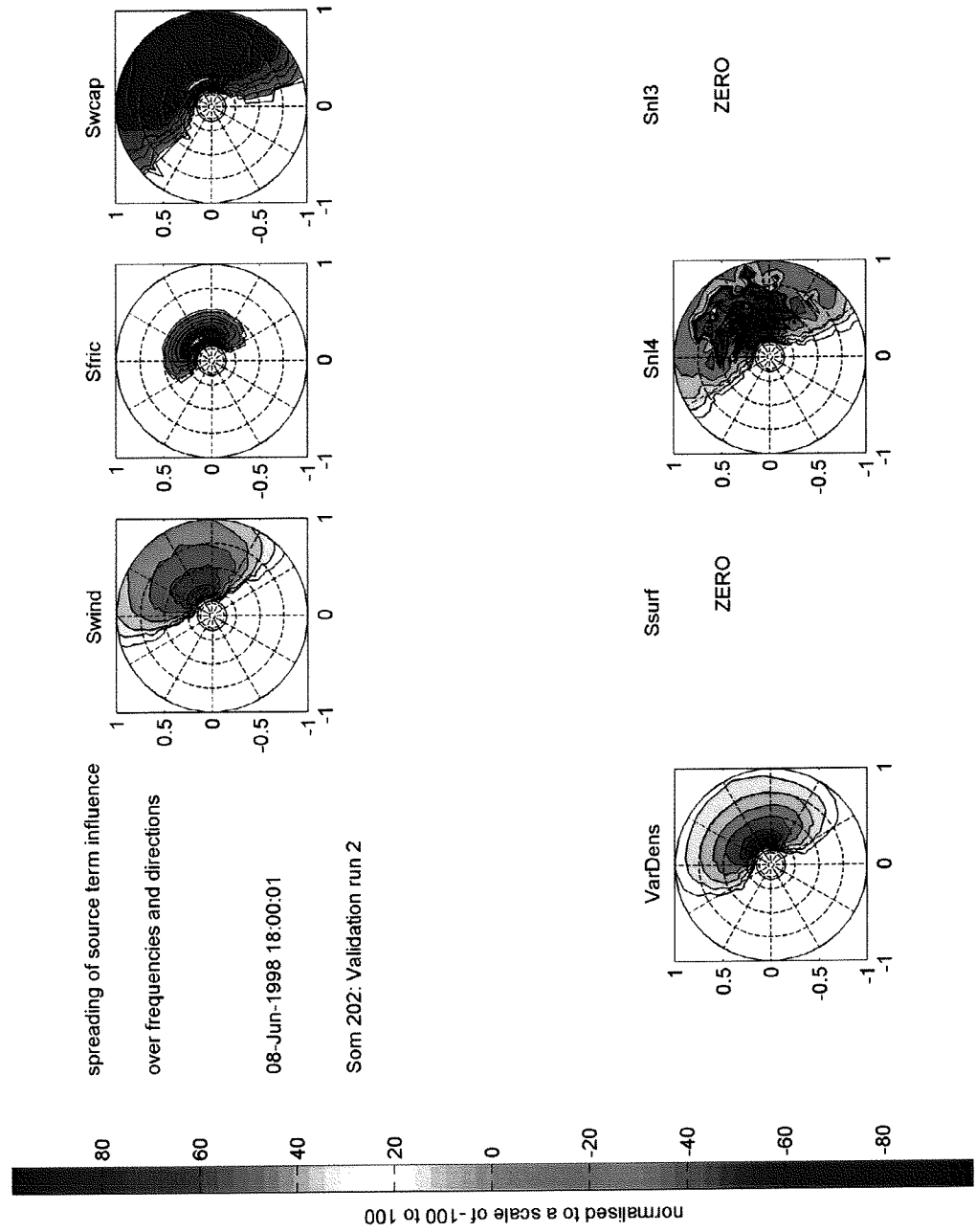
XV.4 Wave spectra and source terms at 8 June 1998 18:00 Comparing Som 202 with the measurements



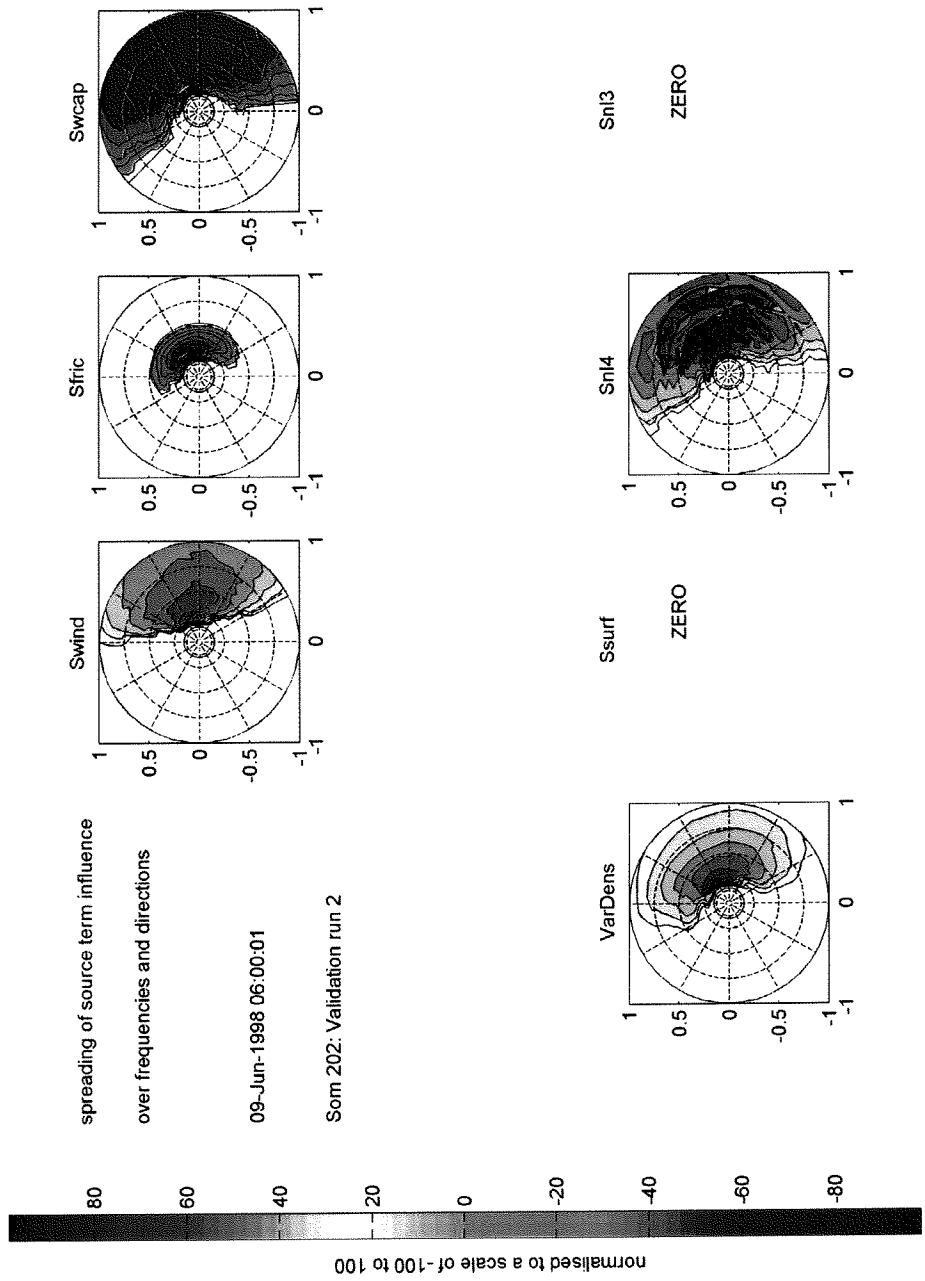
XV.5 Wave spectra and source terms at 9 June 1998 06:00
 Comparing Som 202 with the measurements



XV.6 2D images of source terms at 8 June 1998 18:00



XV.7 2D images of source terms at 9 June 1998 06:00



APPENDIX XVI. Wind statistics (by FUGRO)

XV1.1 Tables of continuous downtime due to wind speed exceedance (by FUGRO)

Wind Speed Greater than 5 m/s													
Duration of Continuous Downtime in Hours													
Month	Max	1	3	5	6	9	12	18	24	36	48	72	96
January	744	179,5	50	25,8	20,3	11,3	7	3	1,8	0,5	0,3	0	0
February	672	258,8	76,5	41,8	33	20	13,3	6,8	4,5	2,3	1,3	0,3	0,3
March	744	286,3	85	45	37	22,5	15,3	7,3	4,5	2	1	0,8	0
April	720	284	84,8	45,5	38,5	22,5	15,3	9	4,5	3,3	1,5	1	0,5
May	744	255,3	73,5	39,3	31,8	16,3	10,8	4,8	3	0,5	0,3	0	0
June	720	199	57,3	29	22,3	13,3	8	3	1,3	0,7	0,3	0	0
July	744	165	45,3	22,3	17,7	10	5,3	1,7	0,7	0,3	0	0	0
August	744	152,7	38,7	18	13	6,7	3,7	1	0	0	0	0	0
September	720	146,3	38,7	21,3	15,3	8	5	1,7	0,7	0,7	0	0	0
October	744	199,7	51,3	26	19,7	11,3	6,3	1,3	1	0	0	0	0
November	720	224,7	65,3	34	27,3	16	10	5,7	3	1,7	1,3	0,3	0,3
December	744	192,3	53,7	28,3	22,3	12,7	8,3	3,7	2,3	0	0	0	0
Total	8760	2543,6	720,1	376,3	298,2	170,6	108,3	49	27,3	12	6	2,4	1,1

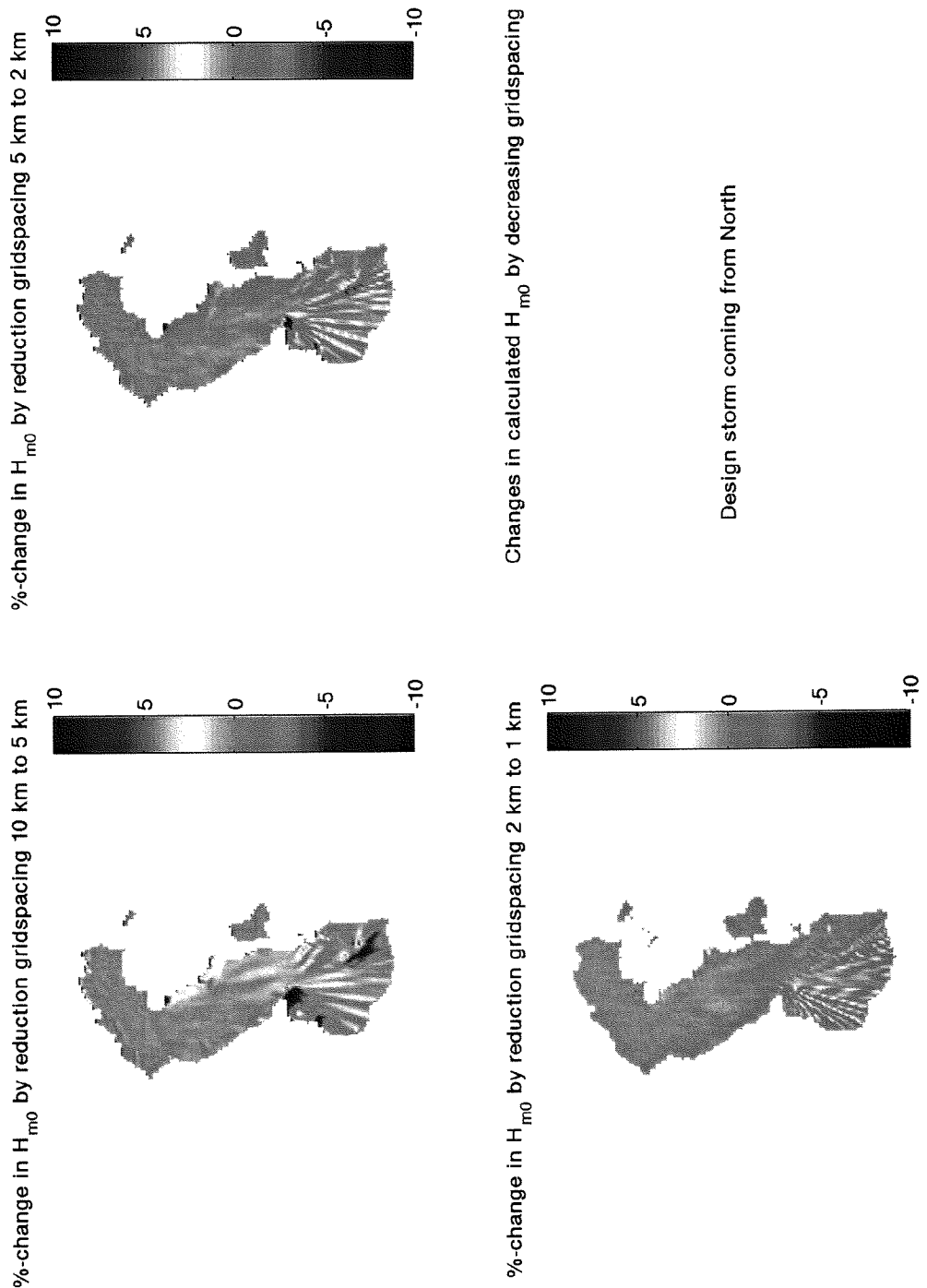
Wind Speed Greater than 10 m/s													
Duration of Continuous Downtime in Hours													
Month	Max	1	3	5	6	9	12	18	24	36	48	72	96
January	744	32,3	9,3	5	3,8	2	1,3	0,5	0	0	0	0	0
February	672	90,5	28	15,5	12,8	7,8	4,3	2	1,3	0,3	0	0	0
March	744	100,3	31	16	13,8	8	5	3	2	0,8	0,5	0,3	0
April	720	100	30,3	17,5	13,5	8	5,8	3	2	0,8	0,8	0	0
May	744	72,3	21,5	10,8	8,8	4,8	2,3	1,3	0,8	0,3	0,3	0	0
June	720	33,7	9	4	3,7	1	1	0	0	0	0	0	0
July	744	24	6	3,3	1,7	0,7	0	0	0	0	0	0	0
August	744	18,7	4,3	2,3	1	0,7	0	0	0	0	0	0	0
September	720	25,7	7,7	4	3	1,7	0,7	0,3	0,3	0	0	0	0
October	744	23,7	5,7	2,7	1,7	1	0,3	0	0	0	0	0	0
November	720	32,7	8,7	4,3	2,7	1,7	1	0,7	0	0	0	0	0
December	744	16	3,7	2	1,7	0,7	0,7	0	0	0	0	0	0
Total	8760	569,9	165,2	87,4	68,2	38,1	22,4	10,8	6,4	2,2	1,6	0,3	0

Month	Wind Speed Greater than 15 m/s												
	Max	1	3	5	6	9	12	18	24	36	48	72	96
January	744	5,8	1,5	1	0,8	0,5	0,3	0,3	0	0	0	0	0
February	672	22,3	6,5	3,5	2,8	1,5	1	0,5	0,3	0	0	0	0
March	744	26,5	7,5	3,8	3,5	2	1,5	0,5	0,3	0	0	0	0
April	720	29,3	9	5	3,8	2,5	1,5	1	0,5	0,5	0	0	0
May	744	16,3	4,8	2,3	2,3	1	1	0,3	0,3	0	0	0	0
June	720	0	0	0	0	0	0	0	0	0	0	0	0
July	744	0,3	0	0	0	0	0	0	0	0	0	0	0
August	744	0	0	0	0	0	0	0	0	0	0	0	0
September	720	3,3	0,7	0,3	0,3	0	0	0	0	0	0	0	0
October	744	0	0	0	0	0	0	0	0	0	0	0	0
November	720	9,3	2,7	1,3	1	0,7	0,3	0	0	0	0	0	0
December	744	2	0,7	0,3	0,3	0	0	0	0	0	0	0	0
Total	8760	115,1	33,4	17,5	14,8	8,2	5,6	2,6	1,4	0,5	0	0	0

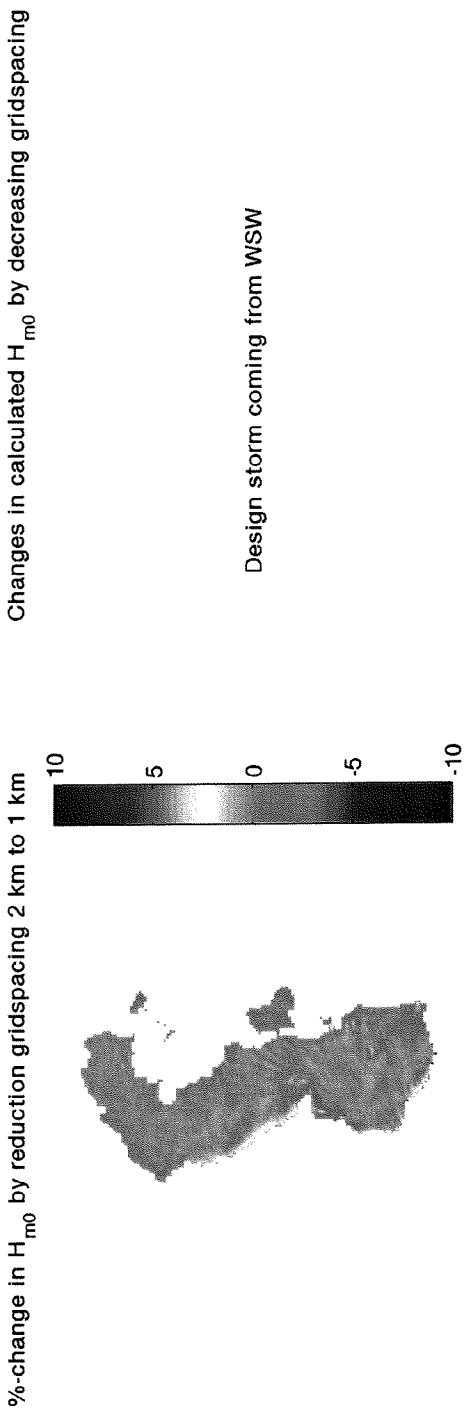
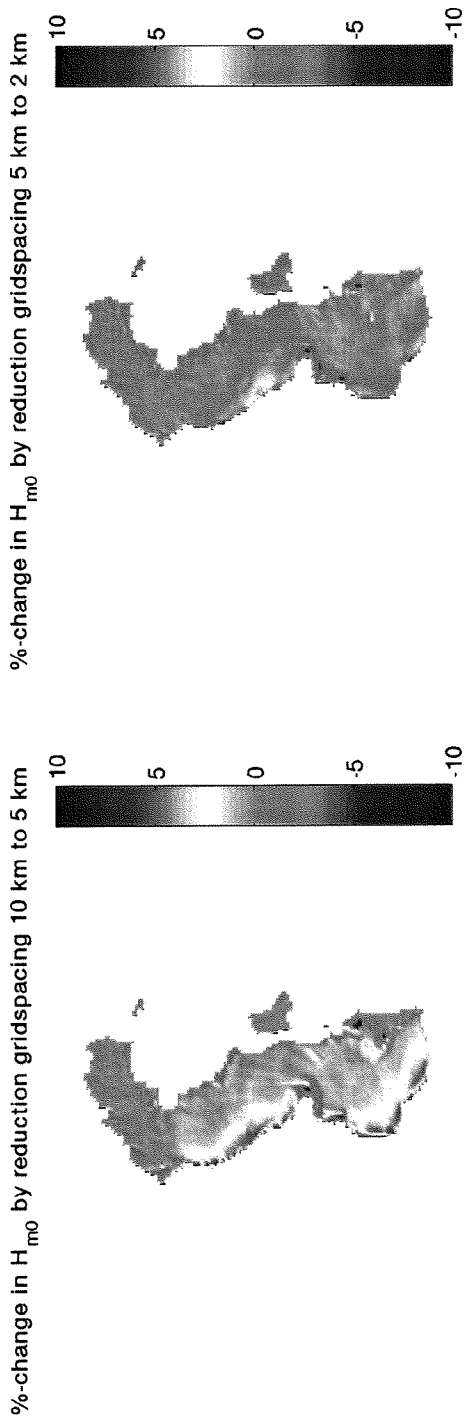
Month	Wind Speed Greater than 20 m/s												
	Max	1	3	5	6	9	12	18	24	36	48	72	96
January	744	2,5	0,3	0	0	0	0	0	0	0	0	0	0
February	672	1,3	0,3	0	0	0	0	0	0	0	0	0	0
March	744	7,5	1,5	1	0,8	0,5	0,3	0,3	0	0	0	0	0
April	720	6,5	1	0,5	0,5	0	0	0	0	0	0	0	0
May	744	3,5	0	0	0	0	0	0	0	0	0	0	0
June	720	0	0	0	0	0	0	0	0	0	0	0	0
July	744	0	0	0	0	0	0	0	0	0	0	0	0
August	744	0	0	0	0	0	0	0	0	0	0	0	0
September	720	0	0	0	0	0	0	0	0	0	0	0	0
October	744	0	0	0	0	0	0	0	0	0	0	0	0
November	720	0,3	0	0	0	0	0	0	0	0	0	0	0
December	744	0	0	0	0	0	0	0	0	0	0	0	0
Total	8760	21,6	3,1	1,5	1,3	0,5	0,3	0,3	0	0	0	0	0

APPENDIX XVII. Influence of grid spacing of computational grid on SWAN output for all grid points

XVII.1 Influence of reduction of grid spacing on H_{m0} output on the complete Caspian Sea during design storm coming from the North

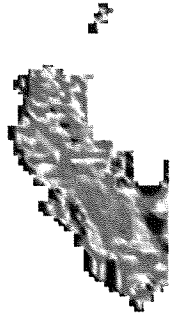


XVII.2 Influence of reduction of grid spacing on H_{m0} output on the complete Caspian Sea during design storm coming from the West Southwest

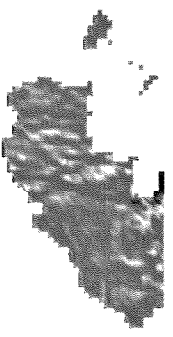


XVII.3 Influence of reduction of grid spacing on H_{m0} output on the Northern part of the Caspian Sea during design storm coming from the North

%-change in H_{m0} by reduction gridspacing 10 km to 5 km



%-change in H_{m0} by reduction gridspacing 2 km to 1 km



%-change in H_{m0} by reduction gridspacing 5 km to 2 km



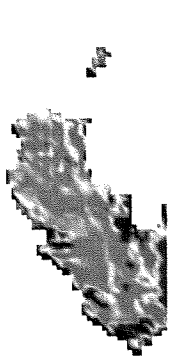
Changes in calculated H_{m0} by decreasing gridspacing

Northern part of the Caspian Sea

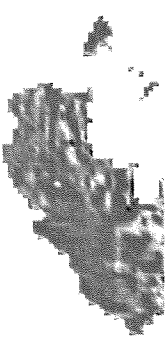
Design storm coming from North

XVII.4 Influence of reduction of grid spacing on H_{m0} output on the Northern part of the Caspian Sea during design storm coming from the West Southwest

%-change in H_{m0} by reduction gridspacing 10 km to 5 km



%-change in H_{m0} by reduction gridspacing 2 km to 1 km



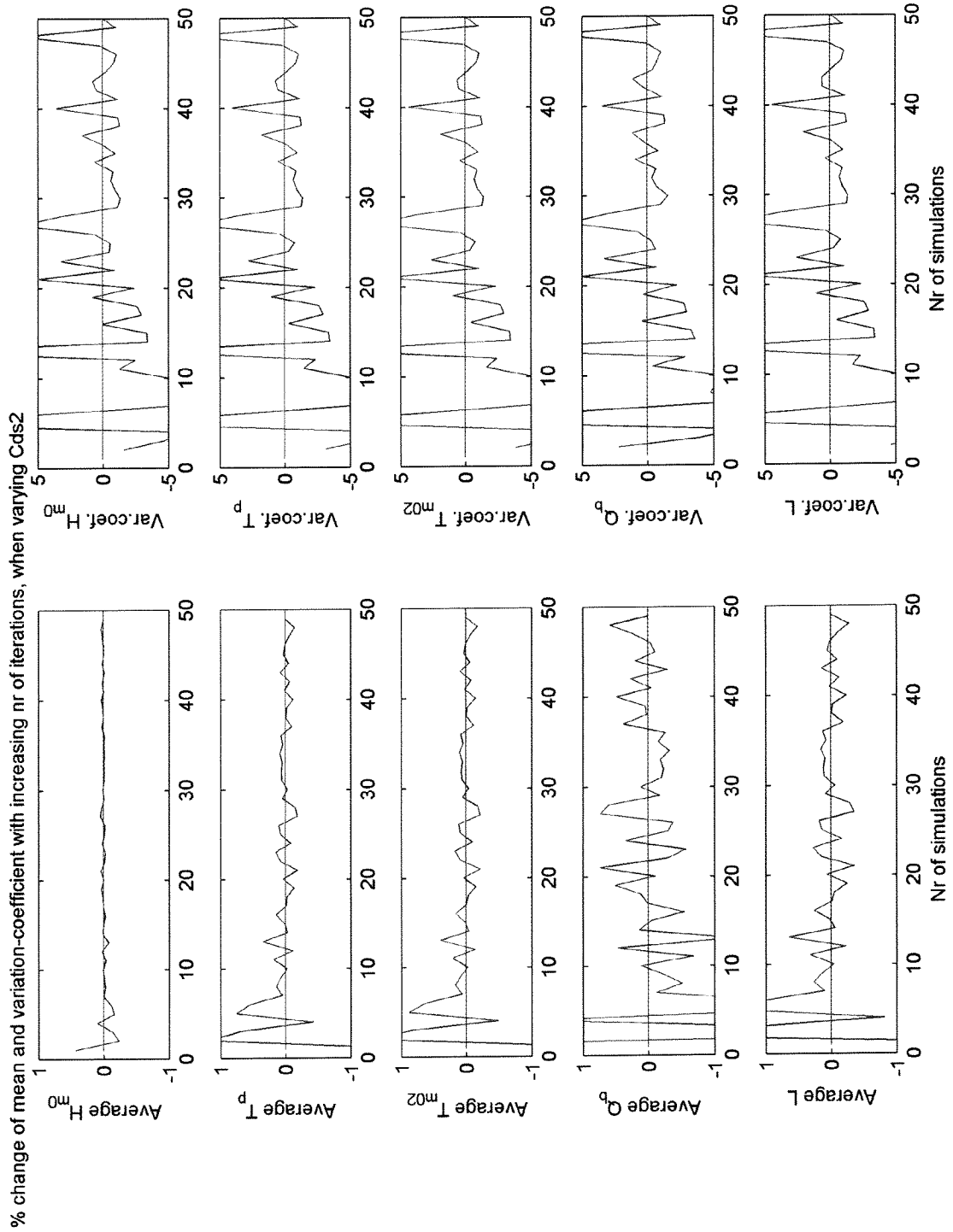
Changes in calculated H_{m0} by decreasing gridspacing

Northern part of the Caspian Sea

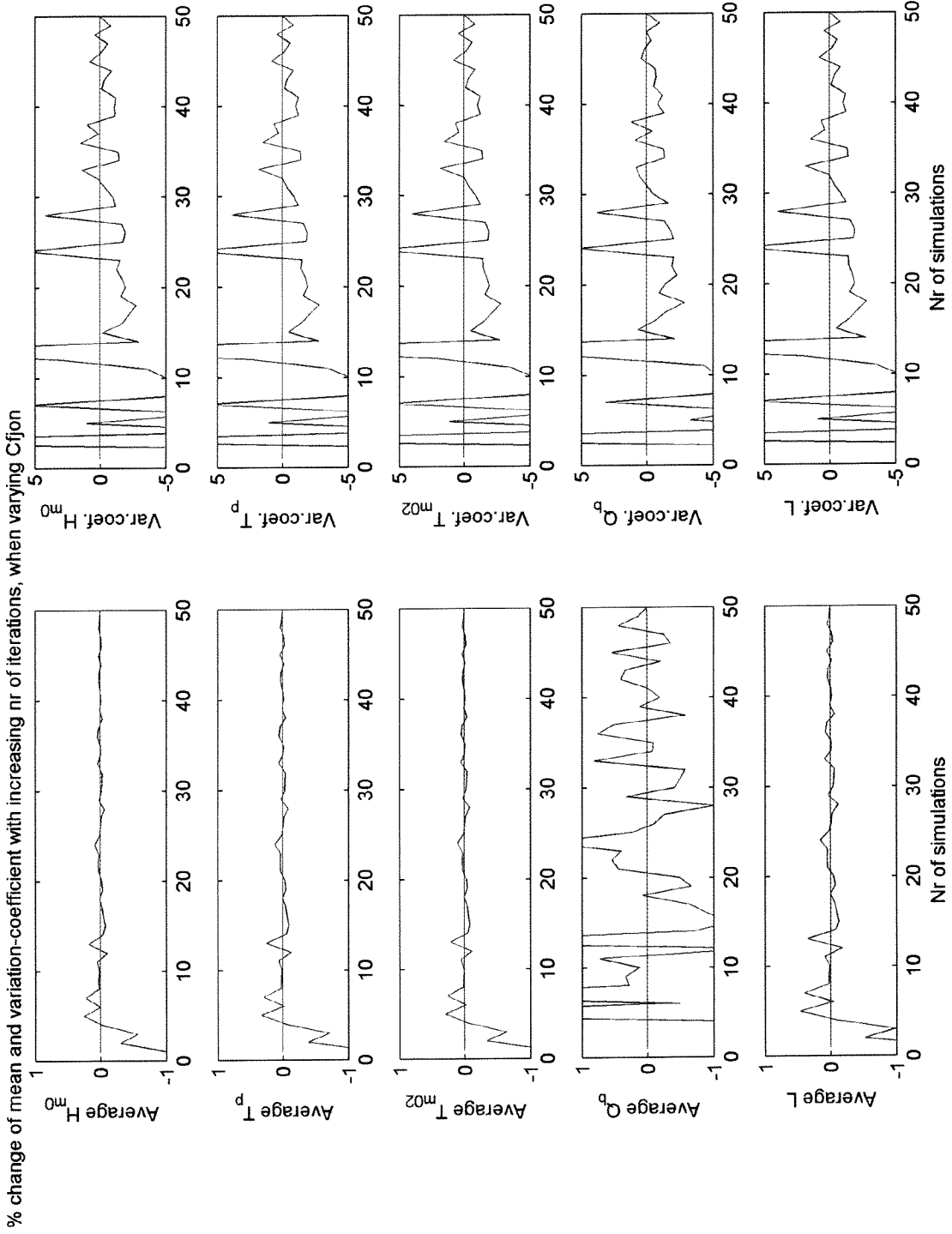
Design storm coming from WSW

APPENDIX XVIII. Proof that linear Monte Carlo simulations converged for μ and σ

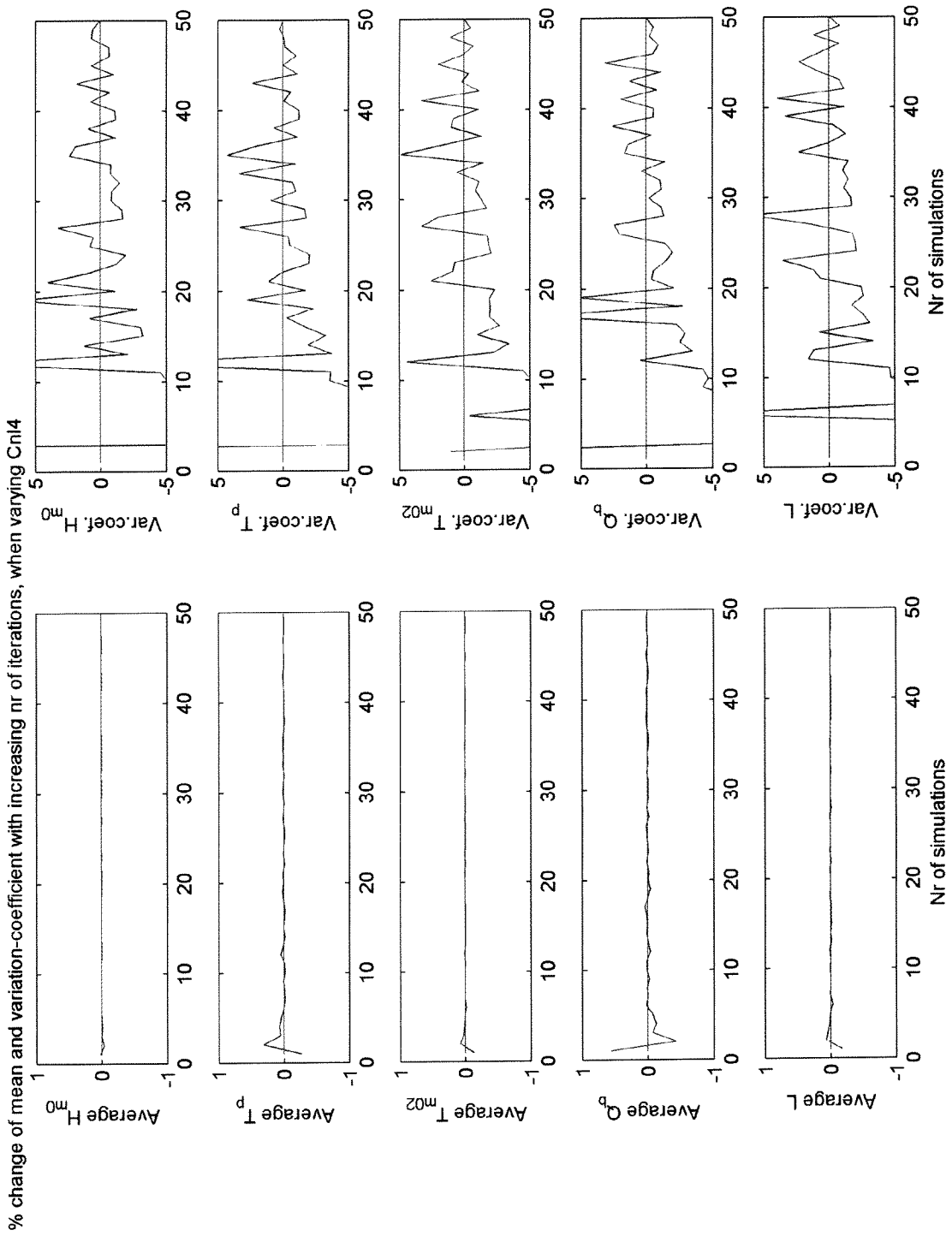
XVIII.1 Convergence of μ and σ , during the linear Monte Carlo simulation when varying cds2



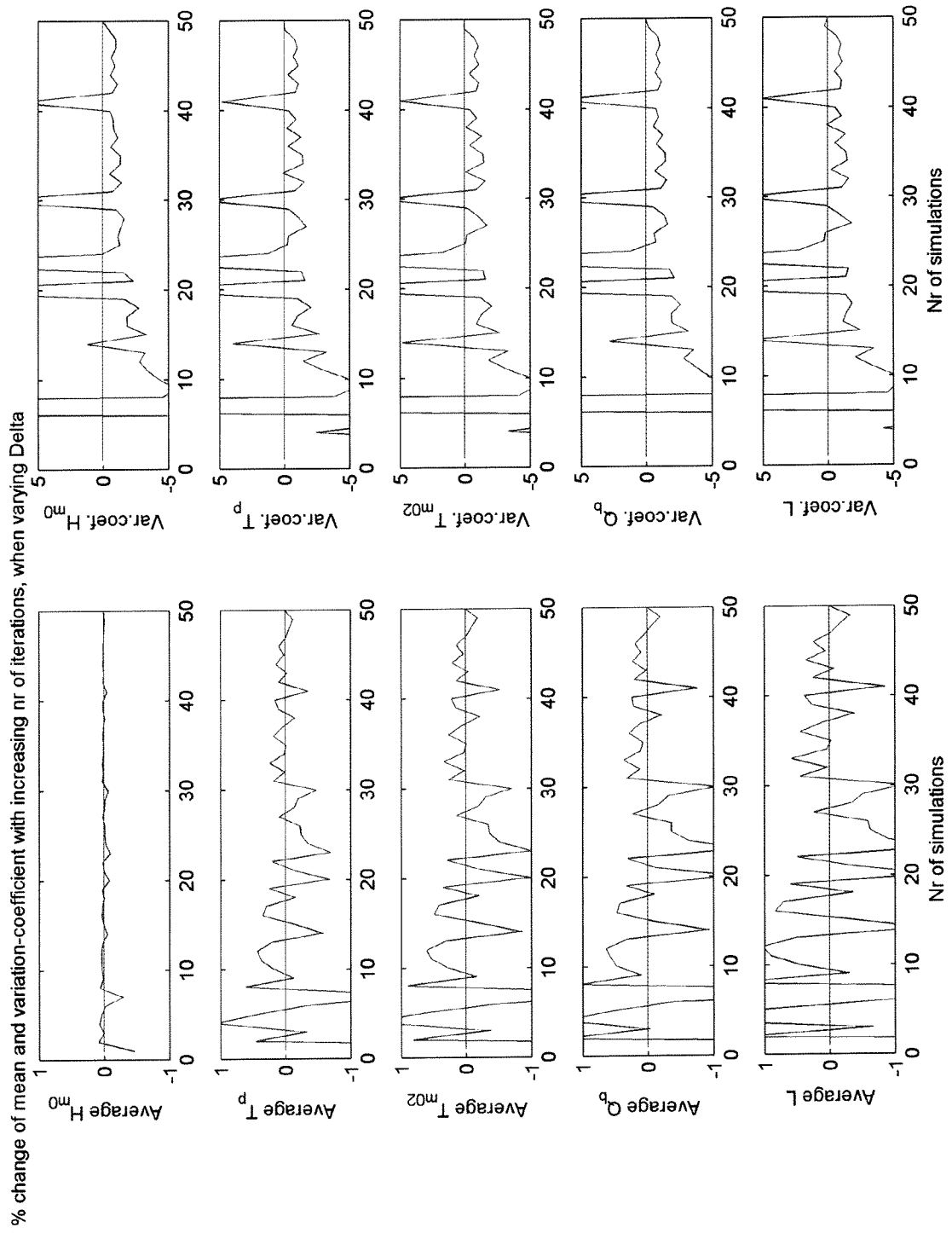
XVIII.2 Convergence of μ and σ , during the linear Monte Carlo simulation when varying C_{fjion}



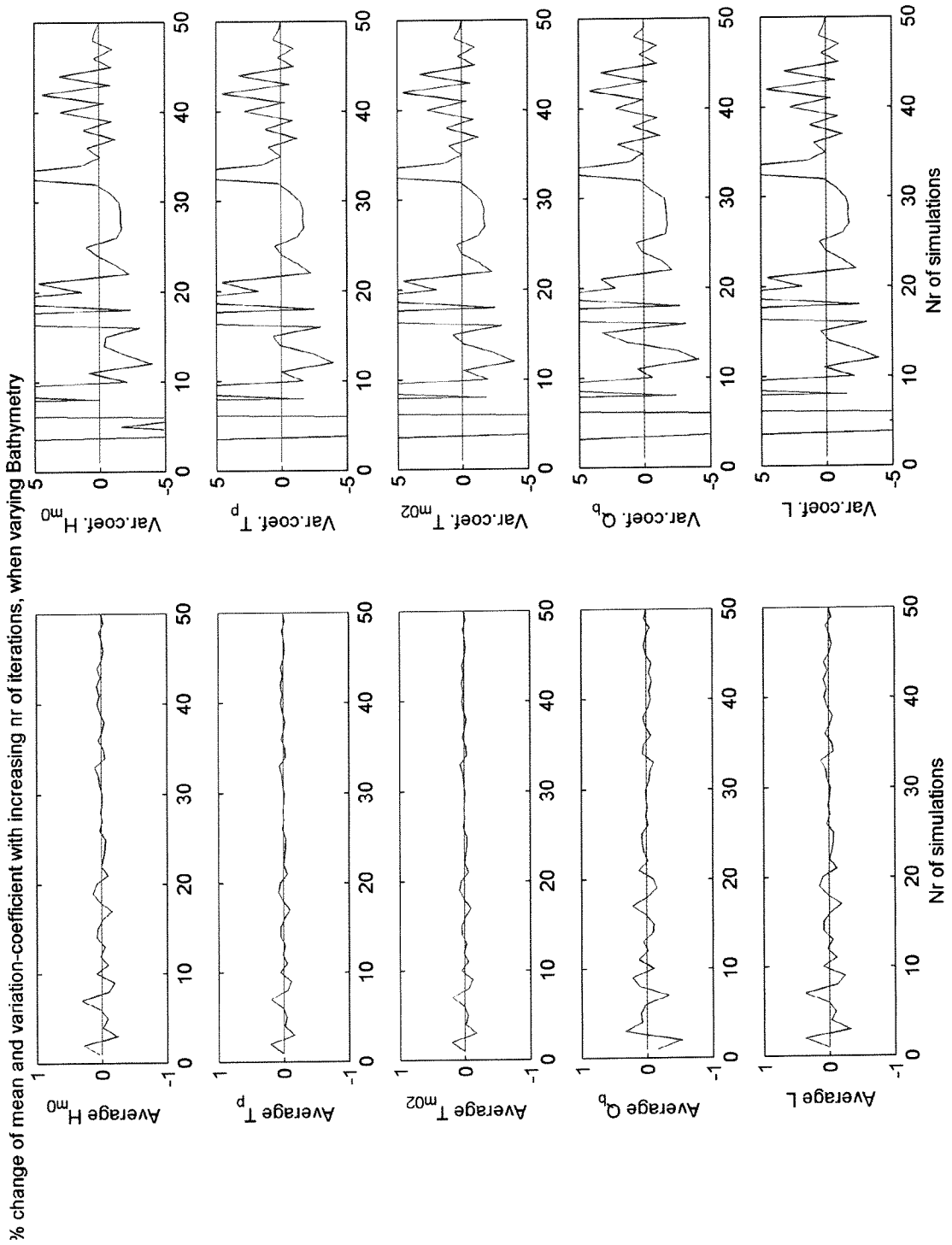
XVIII.3 Convergence of μ and σ , during the linear Monte Carlo simulation when varying cnl4



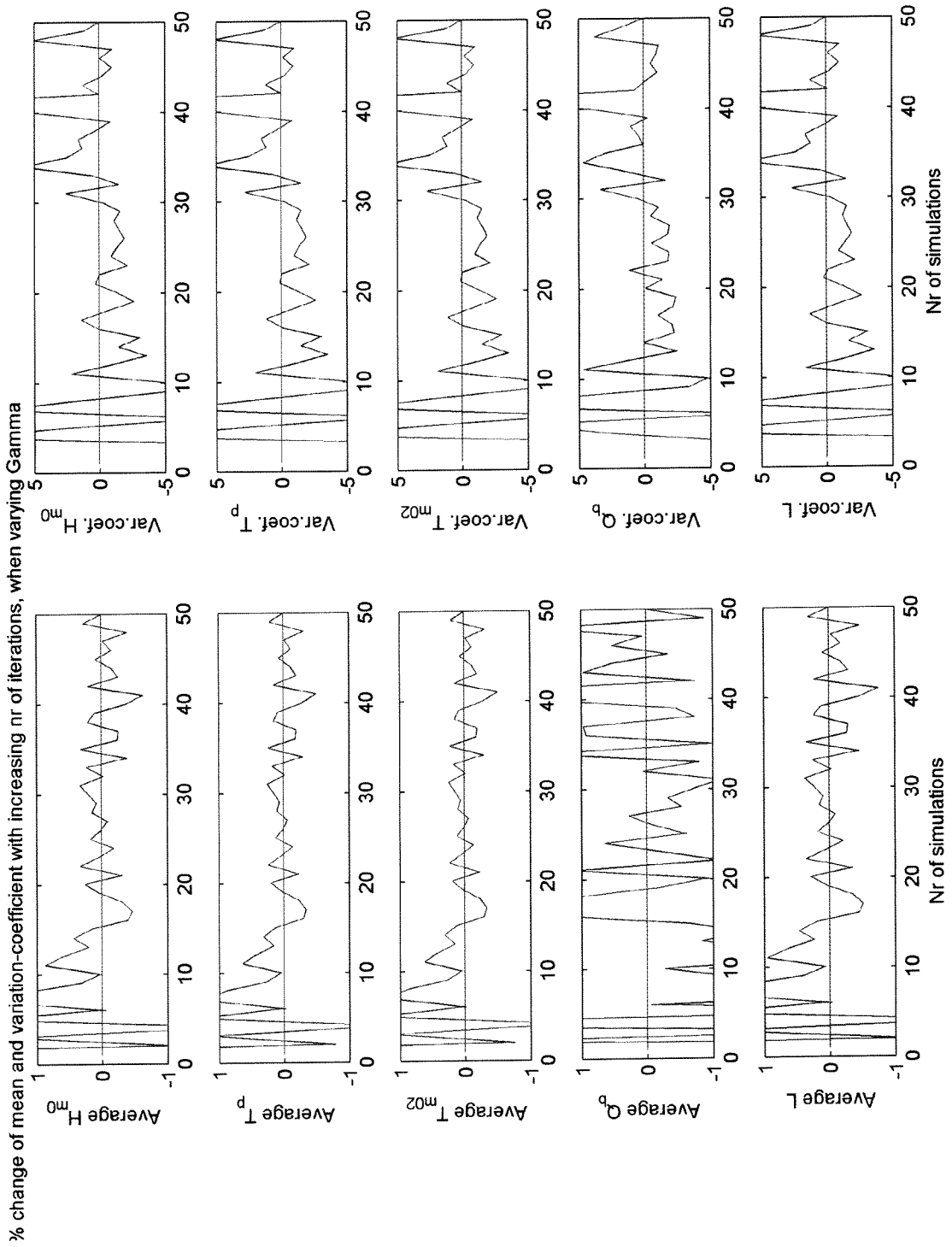
XVIII.4 Convergence of μ and σ , during the linear Monte Carlo simulation when varying delta



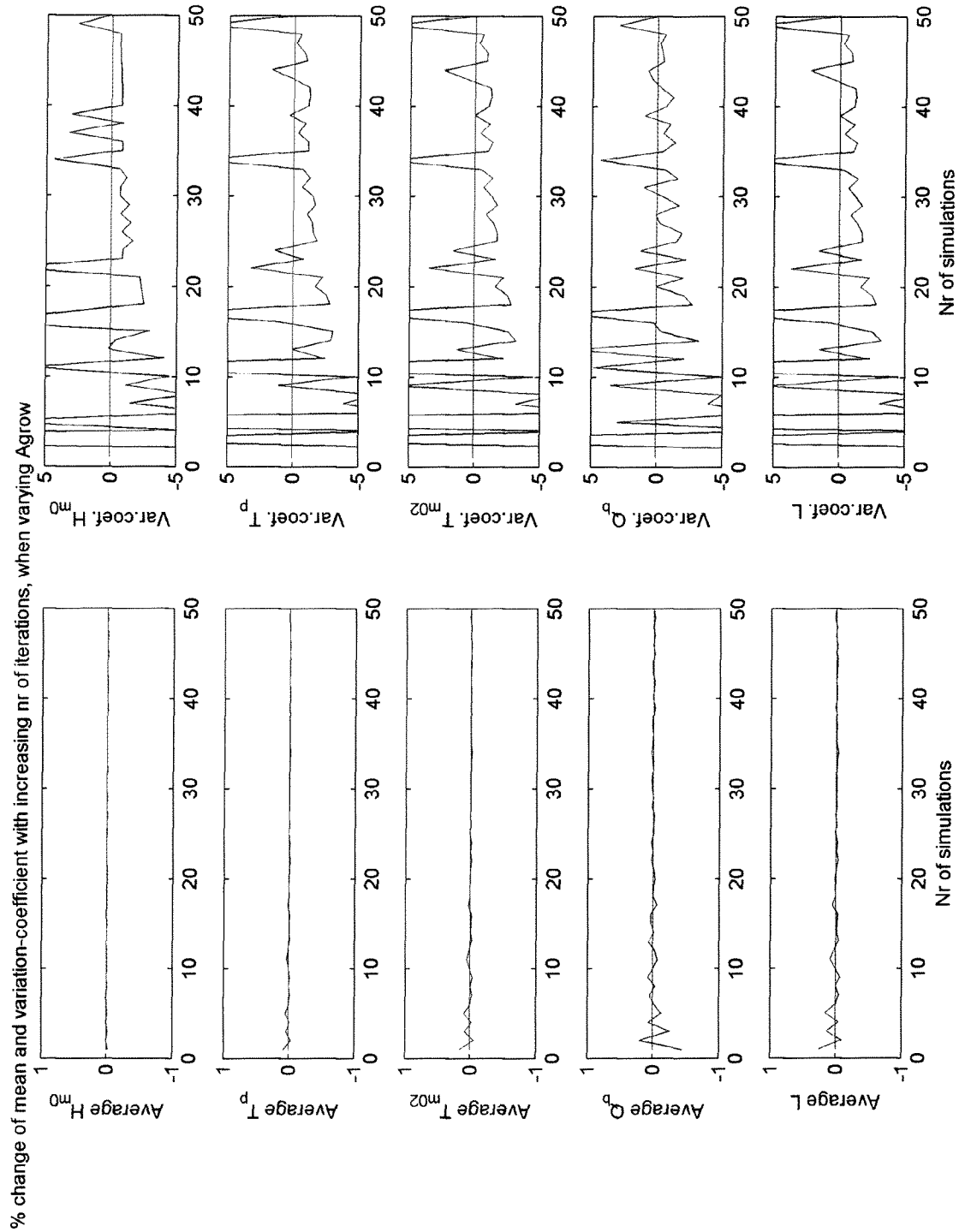
XVIII.5 Convergence of μ and σ , during the linear Monte Carlo simulation when varying bathymetry



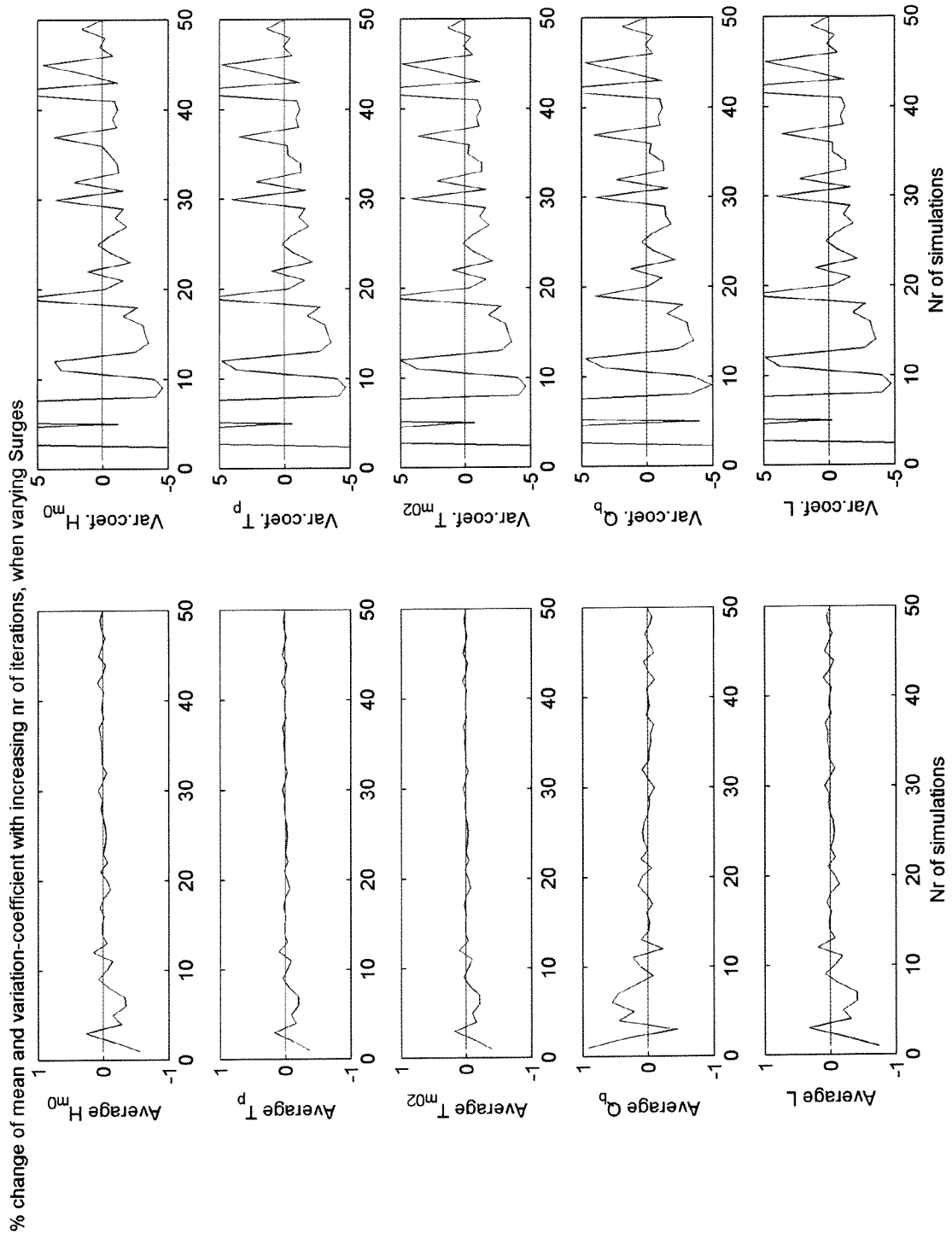
XVIII.6 Convergence of μ and σ , during the linear Monte Carlo simulation when varying gamma



XVIII.7 Convergence of μ and σ , during the linear Monte Carlo simulation when varying agrow



XVIII.8 Convergence of μ and σ , during the linear Monte Carlo simulation when varying surges

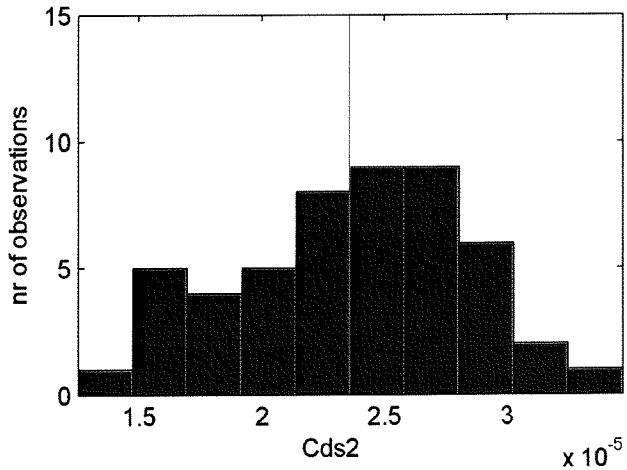


APPENDIX XIX. Output of linear Monte Carlo simulations

XIX.1

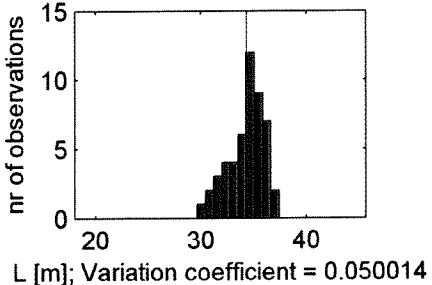
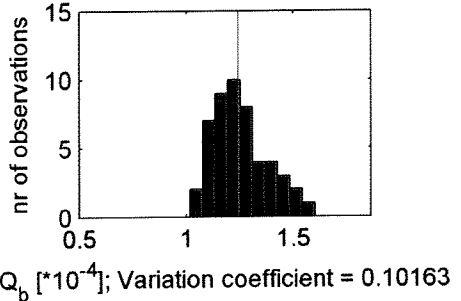
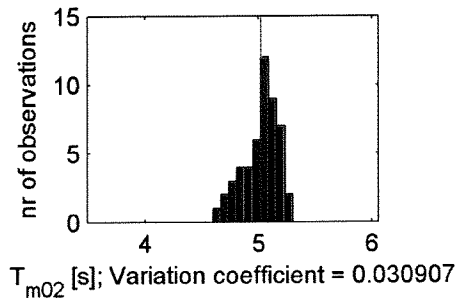
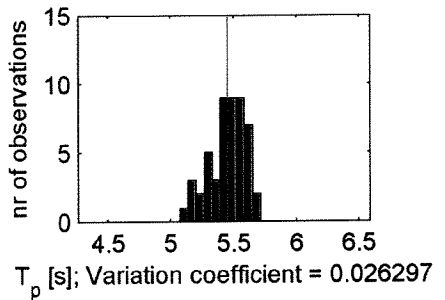
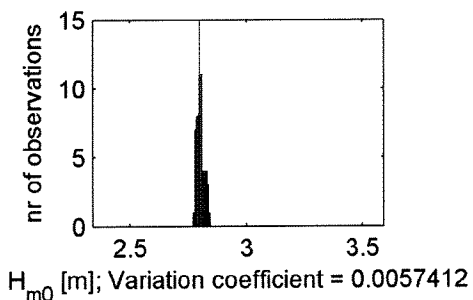
Results on linear Monte Carlo simulation, varying cds2

Red line indicates results when applying validated model settings

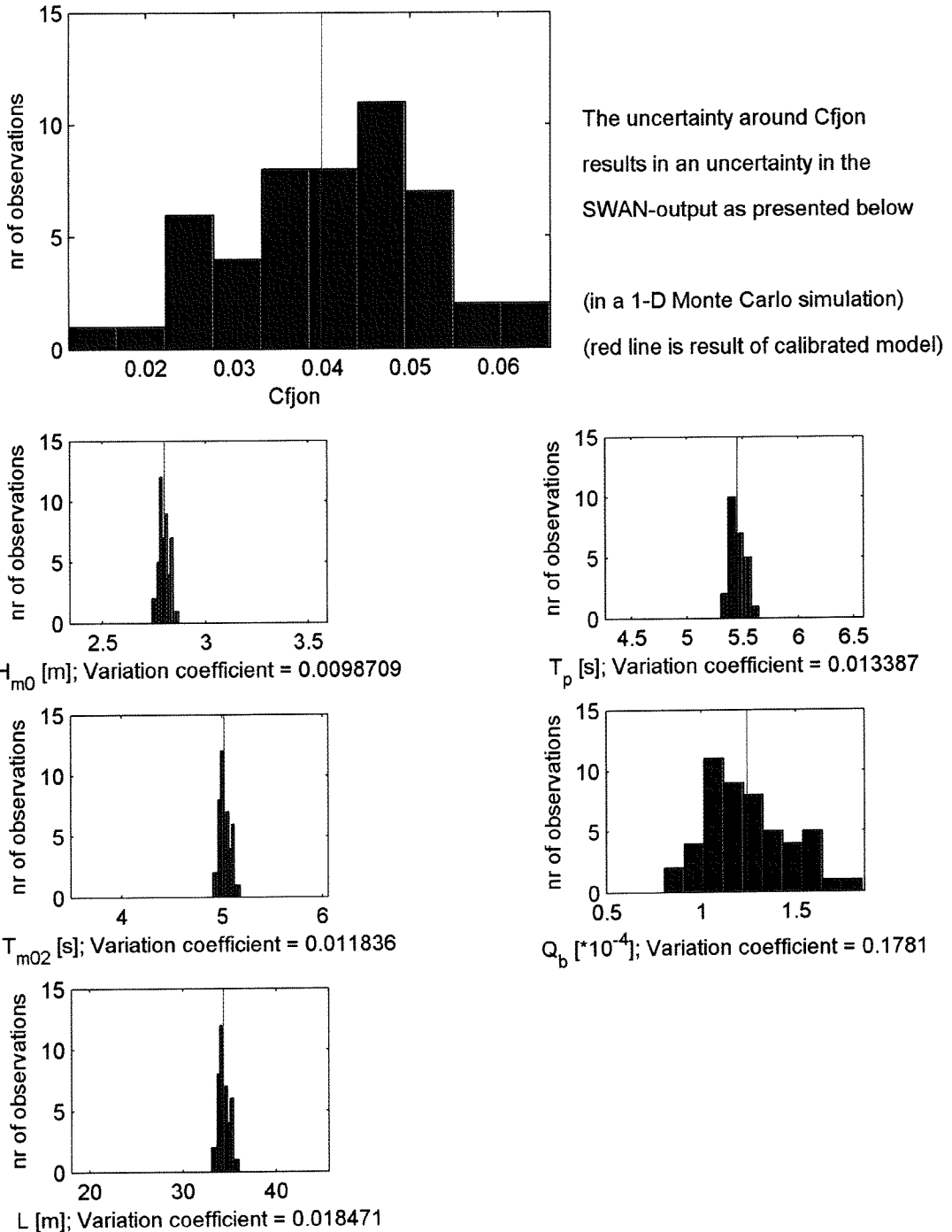


The uncertainty around Cds2 results in an uncertainty in the SWAN-output as presented below

(in a 1-D Monte Carlo simulation)
(red line is result of calibrated model)



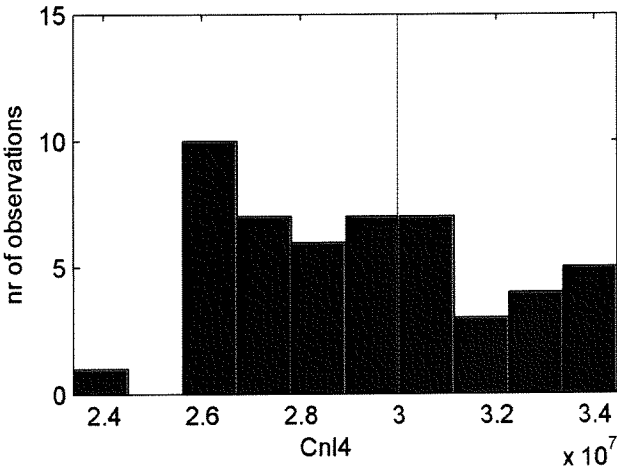
XIX.2 Results on linear Monte Carlo simulation, varying cfjon
 Red line indicates results when applying validated model settings



XIX.3

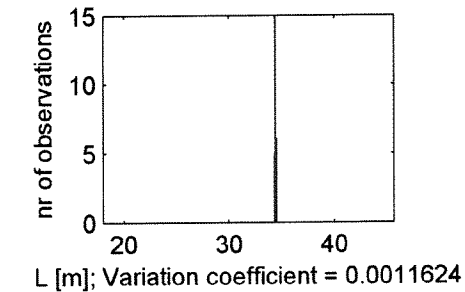
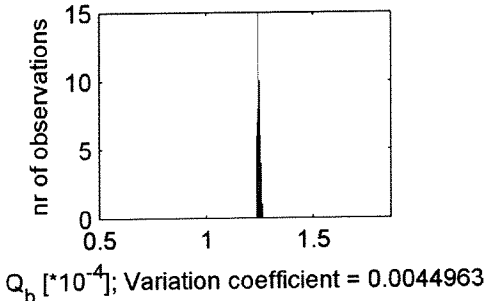
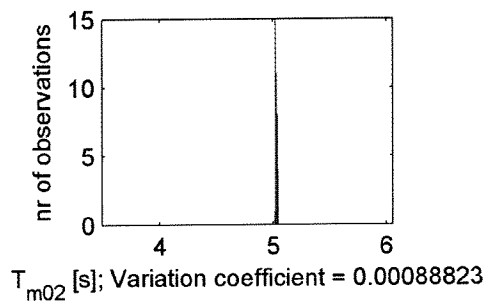
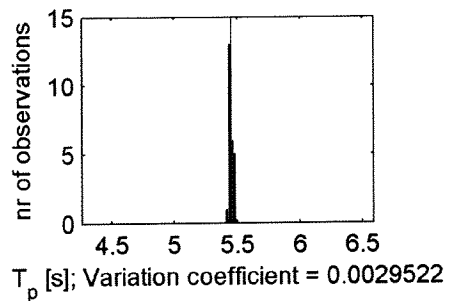
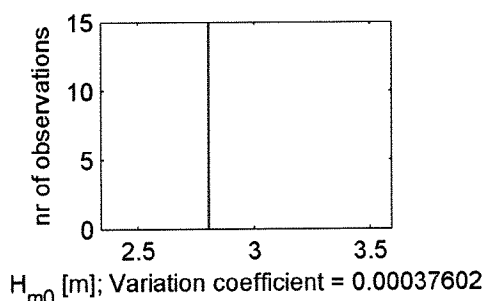
Results on linear Monte Carlo simulation, varying cnl4

Red line indicates results when applying validated model settings

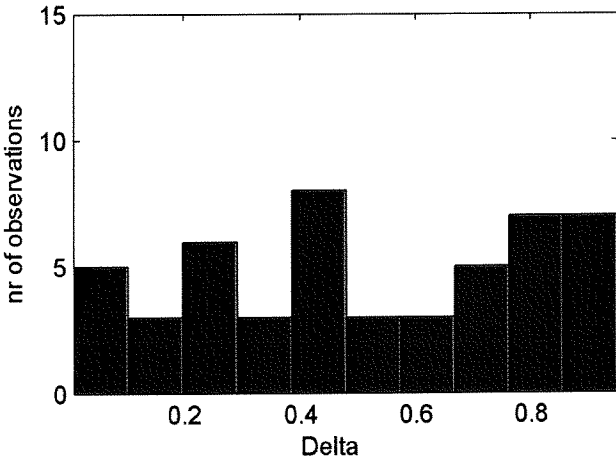


The uncertainty around Cnl4 results in an uncertainty in the SWAN-output as presented below

(in a 1-D Monte Carlo simulation)
(red line is result of calibrated model)

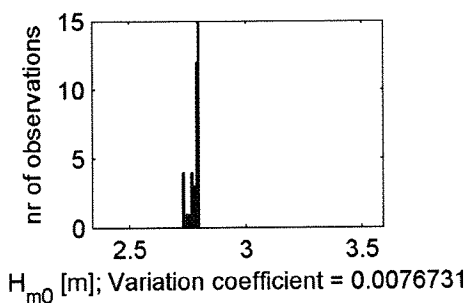


XIX.4 Results on linear Monte Carlo simulation, varying delta
 Red line indicates results when applying validated model settings

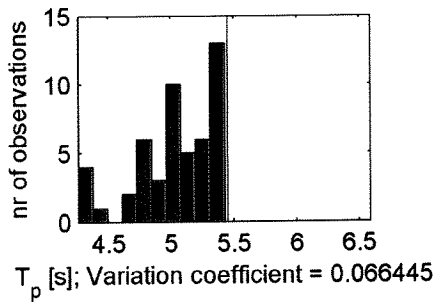


The uncertainty around Delta
 results in an uncertainty in the
 SWAN-output as presented below

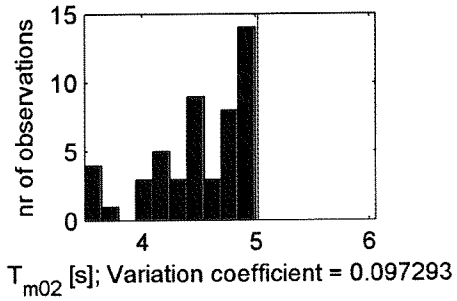
(in a 1-D Monte Carlo simulation)
 (red line is result of calibrated model)



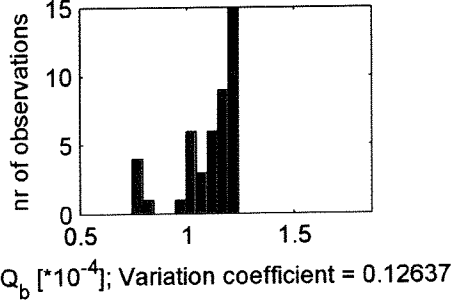
H_{m0} [m]; Variation coefficient = 0.0076731



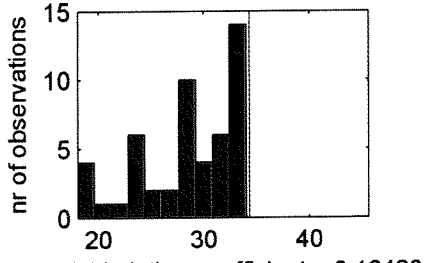
T_p [s]; Variation coefficient = 0.066445



T_{m02} [s]; Variation coefficient = 0.097293

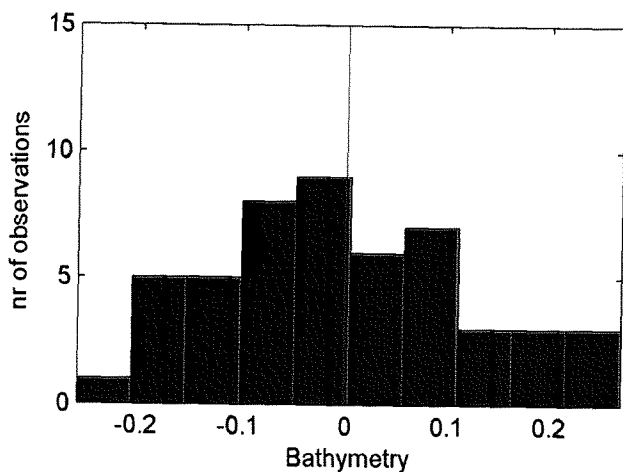


Q_b [$\times 10^{-4}$]; Variation coefficient = 0.12637

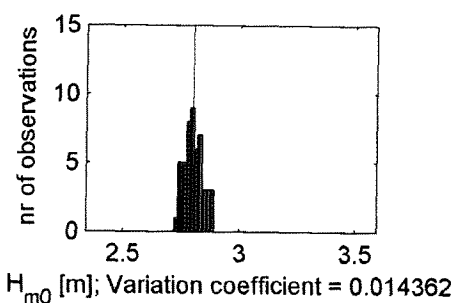


L [m]; Variation coefficient = 0.16423

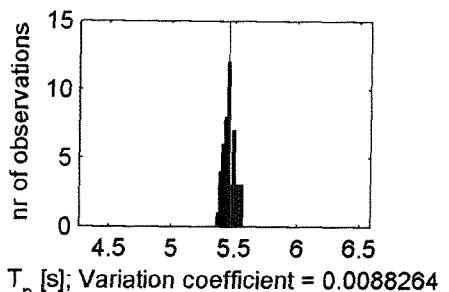
XIX.5 Results on linear Monte Carlo simulation, varying bathymetry
 Red line indicates results when applying validated model settings



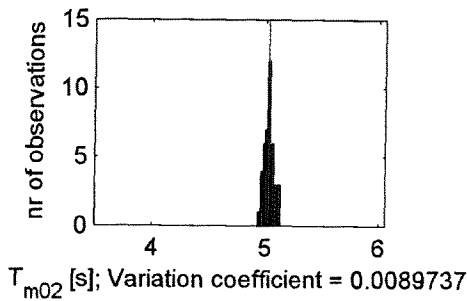
The uncertainty around Bathymetry results in an uncertainty in the SWAN-output as presented below (in a 1-D Monte Carlo simulation) (red line is result of calibrated model)



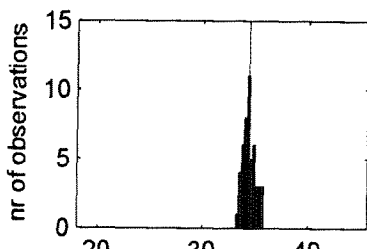
H_{m0} [m]; Variation coefficient = 0.014362



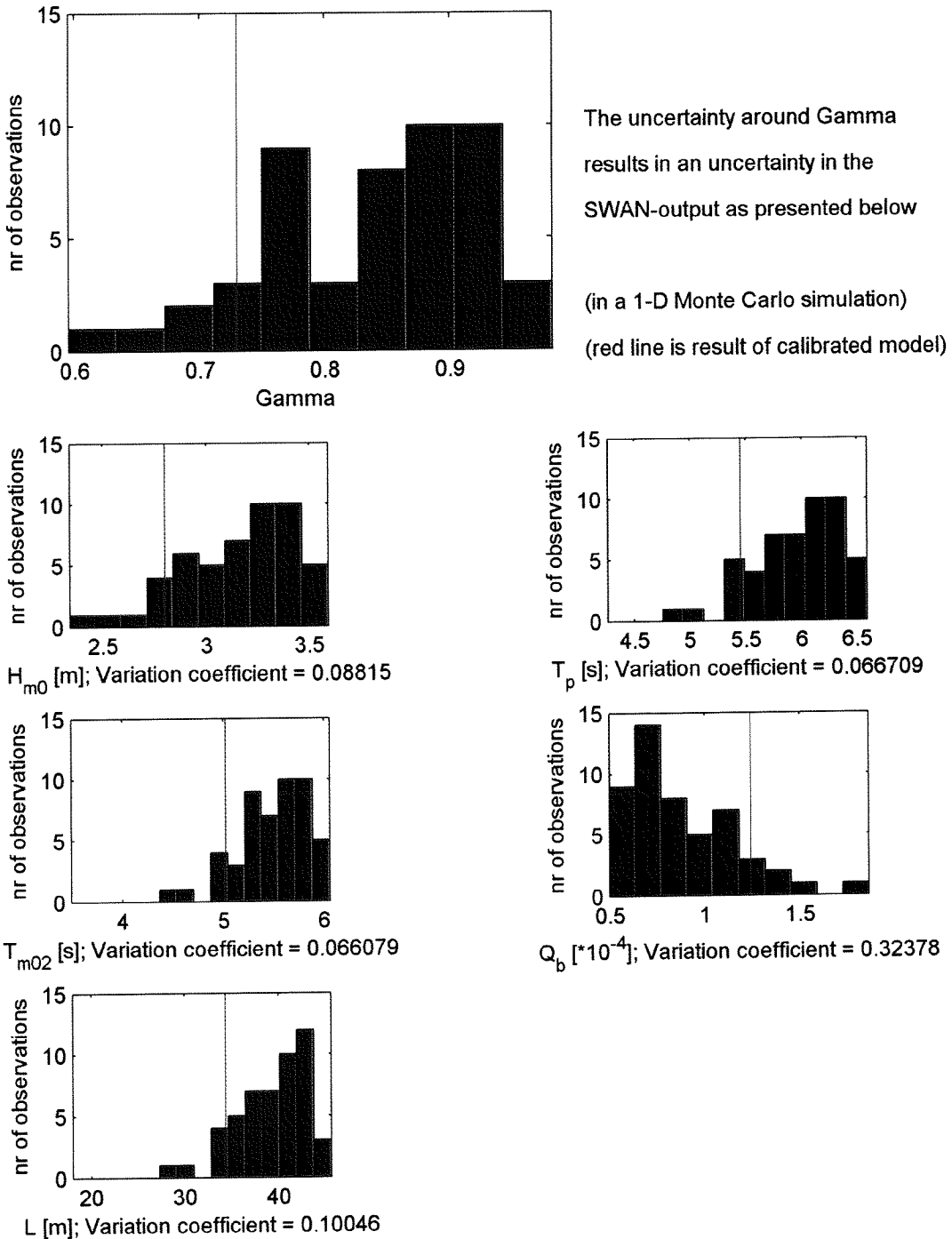
T_p [s]; Variation coefficient = 0.0088264



T_{m02} [s]; Variation coefficient = 0.0089737



XIX.6 Results on linear Monte Carlo simulation, varying gamma
 Red line indicates results when applying validated model settings

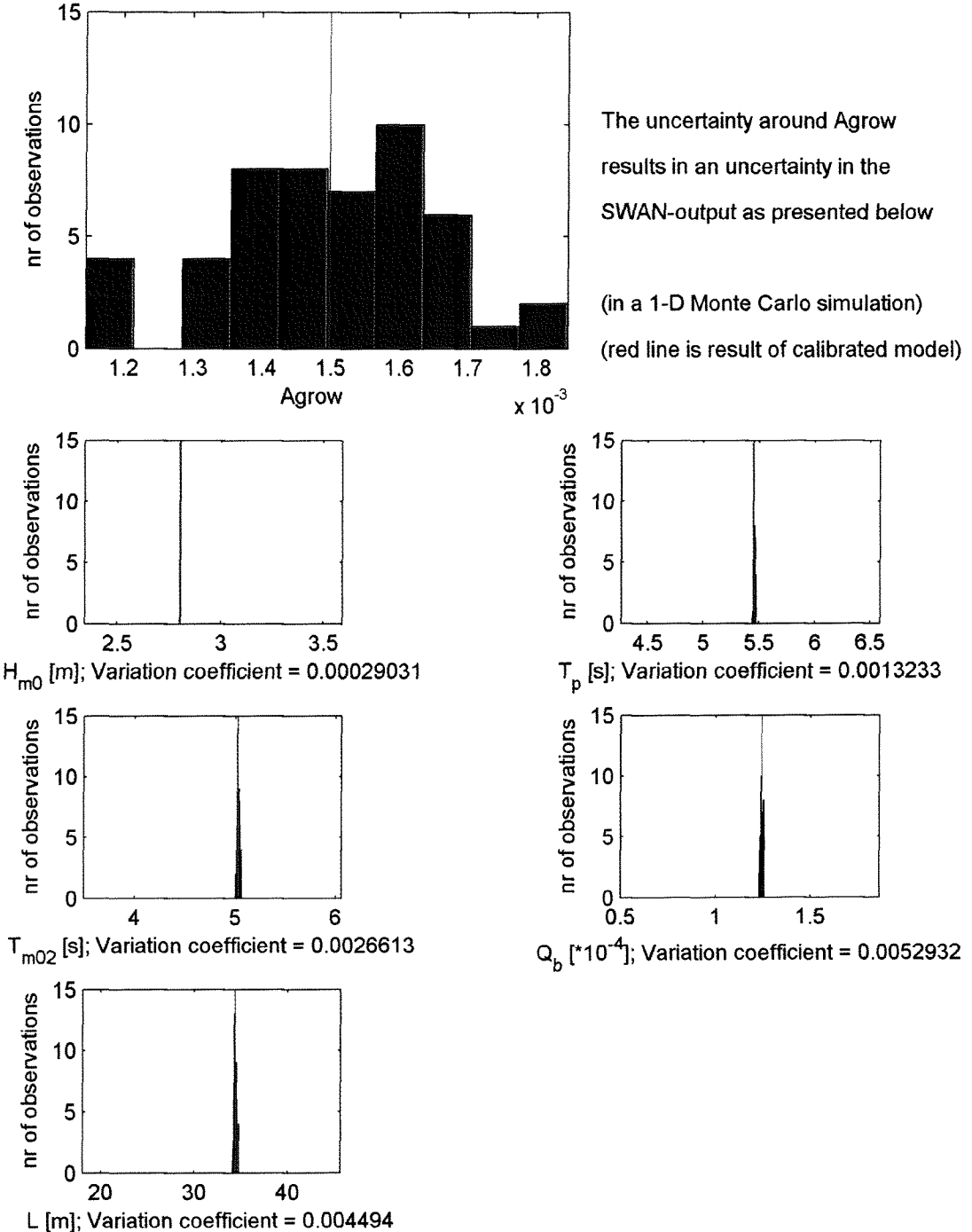


The uncertainty around Gamma results in an uncertainty in the SWAN-output as presented below

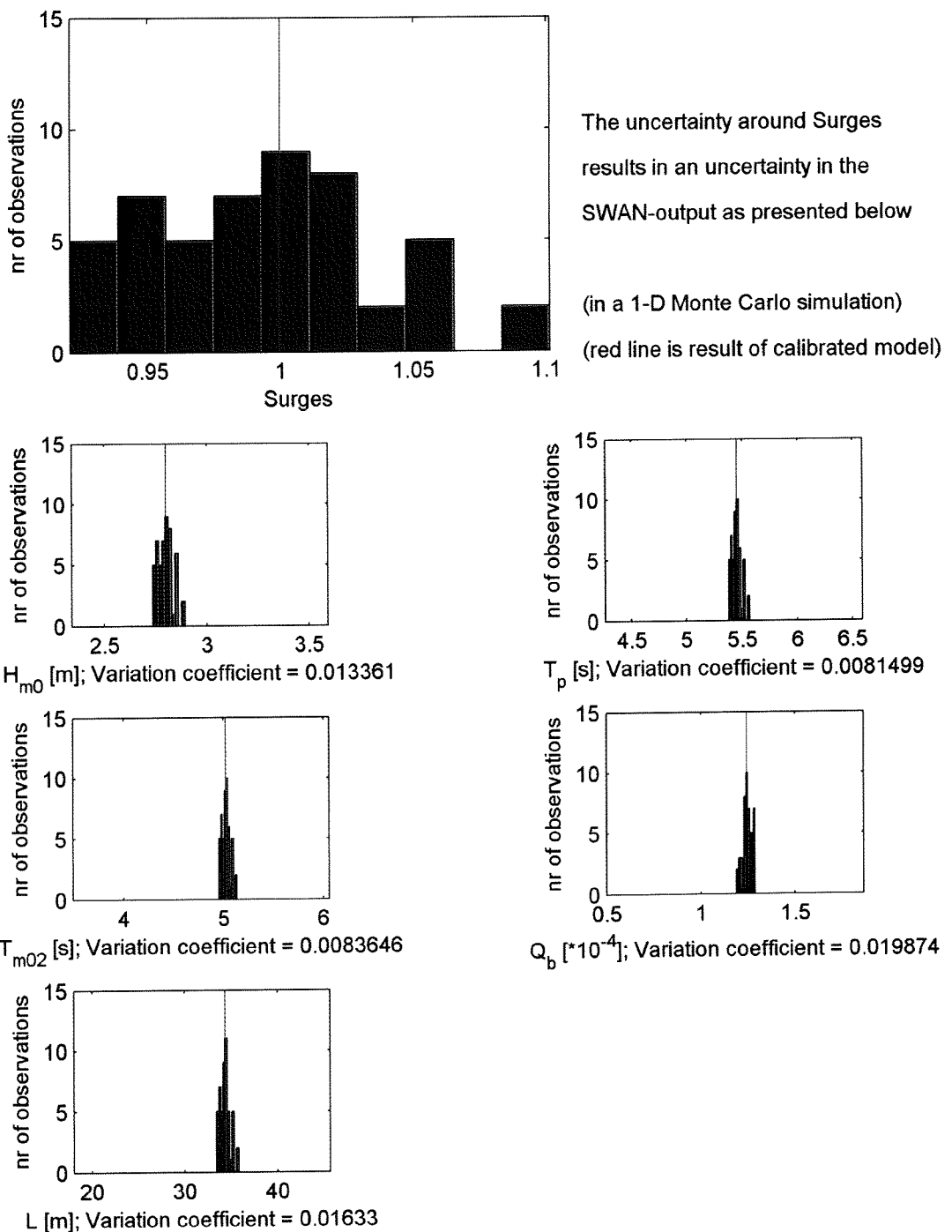
(in a 1-D Monte Carlo simulation)

(red line is result of calibrated model)

XIX.7 Results on linear Monte Carlo simulation, varying agrow
 Red line indicates results when applying validated model settings



XIX.8 Results on linear Monte Carlo simulation, varying surges
 Red line indicates results when applying validated model settings



APPENDIX XX. SPSS output of the linear regression analysis

XX.1 SPSS-output: linear modelling of H_{m0}

SPSS-output: Linear Regression Analysis

Comments:

Hm0 as a function of all 8 stochastically defined physical parameters
 it appears that CNL4 and AGROW should be removed from the linear model
 as Sig. has a value greater than 0.05 (these variables failed the T-test)

entered variables: CDS2, CFJON, CNL4, DELTA, BATHY, GAMMA, AGROW, SURGE
dependent variable: Hm0

Model Summary:

R	R Square	Adjusted R^2	Std. Error of the Estimate
0.995	0.989	0.989	0.034

Coefficients:

	Unstandardized Coefficients		t	Sig.
	beta	Std. Error	Beta	
(Constant)	-1.111	0.033		-33.989 0.000
CDS2	-5456.411	149.055	-0.085	-36.607 0.000
CFJON	-4.078	0.051	-0.184	-79.312 0.000
CNL4	0.000	0.000	0.002	0.830 0.407
DELTA	0.071	0.003	0.062	26.914 0.000
BATHY	0.359	0.006	0.134	57.682 0.000
GAMMA	3.175	0.008	0.957	413.411 0.000
AGROW	3.520	5.080	0.002	0.693 0.488
SURGE	1.819	0.030	0.142	61.564 0.000

XX.2 SPSS-output: linear modelling of H_{m0} , omitting cnl4 and agrow from the model

SPSS-output: Linear Regression Analysis

Comments:

H_{m0} as a function of 6 stochastically defined physical parameters, after removal of CNL4 and AGROW from the linear model!

entered variables:

CDS2
CFJON
DELTA
BATHY
GAMMA
SURGE

dependent variable:

H_{m0}

Model Summary:

R	R Square	Adjusted R^2	Std. Error of the Estimate
0.995	0.989	0.989	0.034

Coefficients:

	Unstandardized Coefficients		Beta	t	Sig.
	beta	Std. Error			
(Constant)	-1.099	0.030		-36.047	0.000
CDS2	-5456.080	148.939	-0.085	-36.633	0.000
CFJON	-4.074	0.051	-0.184	-79.410	0.000
DELTA	0.071	0.003	0.062	26.922	0.000
BATHY	0.359	0.006	0.134	57.766	0.000
GAMMA	3.175	0.008	0.957	414.055	0.000
SURGE	1.818	0.030	0.142	61.576	0.000

XX.3 SPSS-output: linear modelling of T_p

SPSS-output: Linear Regression Analysis

Comments:

T_p as a function of all 8 stochastically defined physical parameters
all of the 8 random variables are significant

entered variables:

CDS2
CFJON
CNL4
DELTA
BATHY
GAMMA
AGROW
SURGE

dependent variable:

T_p

Model Summary:

R	R Square	Adjusted R^2	Std. Error of the Estimate
0.985	0.970	0.970	0.100

Coefficients:

	Unstandardized Coefficients		Beta	t	Sig.
	beta	Std. Error			
(Constant)	-1.182	0.096		-12.348	0.000
CDS2	24564.467	436.418	0.219	56.287	0.000
CFJON	-7.770	0.151	-0.201	-51.621	0.000
CNL4	0.000	0.000	0.042	10.779	0.000
DELTA	1.144	0.008	0.572	147.048	0.000
BATHY	0.430	0.018	0.092	23.597	0.000
GAMMA	4.261	0.022	0.737	189.491	0.000
AGROW	-53.308	14.873	-0.014	-3.584	0.000
SURGE	2.073	0.086	0.093	23.969	0.000

XX.4 SPSS-output: linear modelling of T_{m02}

SPSS-output: Linear Regression Analysis

Comments:

T_{m02} as a function of all 8 stochastically defined physical parameters
all of the 8 random variables are significant

entered variables:

CDS2
CFJON
CNL4
DELTA
BATHY
GAMMA
AGROW
SURGE

dependent variable:

T_{m02}

Model Summary:

R	R Square	Adjusted R^2	Std. Error of the Estimate
0.978	0.956	0.956	0.130

Coefficients:

	Unstandardized Coefficients		Beta	t	Sig.
	beta	Std. Error			
(Constant)	-1.430	0.124		-11.529	0.000
CDS2	27641.005	565.186	0.231	48.906	0.000
CFJON	-6.014	0.195	-0.146	-30.850	0.000
CNL4	0.000	0.000	0.013	2.792	0.005
DELTA	1.479	0.010	0.692	146.831	0.000
BATHY	0.408	0.024	0.082	17.306	0.000
GAMMA	3.866	0.029	0.626	132.746	0.000
AGROW	-90.227	19.261	-0.022	-4.684	0.000
SURGE	1.969	0.112	0.083	17.582	0.000

XX.5 SPSS-output: linear modelling of Q_b

SPSS-output: Linear Regression Analysis

Comments:

Q_b as a function of all 8 stochastically defined physical parameters
 it appears that CNL4 should be removed from the linear model
 as Sig. has a value greater than 0.05 (these variables failed the T-test)

entered variables:

CDS2
 CFJON
 CNL4
 DELTA
 BATHY
 GAMMA
 AGROW
 SURGE

dependent variable:

Q_b

Model Summary:

R	R Square	Adjusted R^2	Std. Error of the Estimate
0.981	0.962	0.961	0.000

Coefficients:

	Unstandardized Coefficients		Beta	t	Sig.
	beta	Std. Error			
(Constant)	0.001	0.000		63.901	0.000
CDS2	-2.462	0.038	-0.284	-64.601	0.000
CFJON	-0.002	0.000	-0.584	-132.427	0.000
CNL4	0.000	0.000	-0.002	-0.453	0.651
DELTA	0.000	0.000	0.216	49.199	0.000
BATHY	0.000	0.000	-0.030	-6.843	0.000
GAMMA	0.000	0.000	-0.685	-155.695	0.000
AGROW	0.004	0.001	0.015	3.417	0.001
SURGE	0.000	0.000	-0.051	-11.669	0.000

XX.6 SPSS-output: linear modelling of Q_b , omitting cnl4 from the model

SPSS-output: Linear Regression Analysis

Comments:

Q_b as a function of 7 stochastically defined physical parameters, after removal of CNL4 from the linear model

entered variables:

CDS2
CFJON
DELTA
BATHY
GAMMA
AGROW
SURGE

dependent variable:

Q_b

Model Summary:

R	R Square	Adjusted R^2	Std. Error of the Estimate
0.981	0.962	0.961	0.000

Coefficients:

	Unstandardized Coefficients		Beta	t	Sig.
	beta	Std. Error			
(Constant)	0.001	0.000		66.188	0.000
CDS2	-2.463	0.038	-0.284	-64.642	0.000
CFJON	-0.002	0.000	-0.584	-132.555	0.000
DELTA	0.000	0.000	0.217	49.282	0.000
BATHY	0.000	0.000	-0.030	-6.851	0.000
GAMMA	0.000	0.000	-0.685	-155.817	0.000
AGROW	0.004	0.001	0.015	3.421	0.001
SURGE	0.000	0.000	-0.051	-11.663	0.000

XX.7 SPSS-output: linear modelling of L

SPSS-output: Linear Regression Analysis

Comments:

L as a function of all 8 stochastically defined physical parameters
all of the 8 random variables are significant

entered variables:

CDS2
CFJON
CNL4
DELTA
BATHY
GAMMA
AGROW
SURGE

dependent variable:

L

Model Summary:

R	R Square	Adjusted R ²	Std. Error of the Estimate
0.978	0.956	0.956	1.414

Coefficients:

	Unstandardized Coefficients		Beta	t	Sig.
	beta	Std. Error			
(Constant)	-38.790	1.348		-28.781	0.000
CDS2	302399.166	6143.262	0.232	49.225	0.000
CFJON	-64.345	2.119	-0.143	-30.367	0.000
CNL4	0.000	0.000	0.011	2.230	0.026
DELTA	16.277	0.109	0.700	148.666	0.000
BATHY	5.174	0.256	0.095	20.175	0.000
GAMMA	41.266	0.317	0.614	130.357	0.000
AGROW	-1020.819	209.354	-0.023	-4.876	0.000
SURGE	24.997	1.218	0.097	20.531	0.000